

**UNIVERSIDADE FEDERAL DE SANTA CATARINA
PROGRAMA DE PÓS-GRADUAÇÃO EM ENGENHARIA
MECÂNICA**

Nury Audrey Nieto Garzón

**MEDIÇÃO E MODELAGEM DA COMBUSTÃO DE MISTURAS
DE ÓLEO DE SOJA *IN NATURA* E ÓLEO DIESEL EM UM
MOTOR DE IGNIÇÃO POR COMPRESSÃO**

Florianópolis
2017

Nury Audrey Nieto Garzón

**MEASUREMENT AND MODELING OF THE COMBUSTION OF
STRAIGHT SOYBEAN OIL AND DIESEL OIL BLENDS IN A
COMPRESSION IGNITION ENGINE**

Tese submetida ao Programa de Pós-graduação em Engenharia Mecânica da Universidade Federal de Santa Catarina para a obtenção do Grau de Doutor em Engenharia Mecânica.

Orientador: Prof. Edson Bazzo, Dr.Eng.

Coorientador: Prof. Amir A. Martins de Oliveira Jr., Ph.D.

Florianópolis
2017

Ficha de identificação da obra elaborada pelo autor,
através do Programa de Geração Automática da Biblioteca Universitária da UFSC.

Garzón, Nury Audrey Nieto

Measurement and modeling of the combustion of
straight soybean oil and diesel oil blends in a
compression ignition engine / Nury Audrey Nieto
Garzón ; orientador, Edson Bazzo, coorientador, Amir
Antônio Martins de Oliveira Jr., 2017.

240 p.

Tese (doutorado) - Universidade Federal de Santa
Catarina, Centro Tecnológico, Programa de Pós
Graduação em Engenharia Mecânica, Florianópolis, 2017.

Inclui referências.

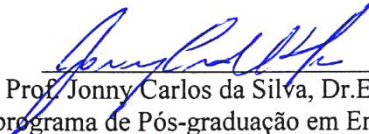
1. Engenharia Mecânica. 2. Modelagem motor
diesel. 3. Biocombustíveis. 4. Óleo de soja in
natura. 5. Taxa de liberação de calor . I. Bazzo,
Edson. II. Oliveira Jr., Amir Antônio Martins de.
III. Universidade Federal de Santa Catarina.
Programa de Pós-Graduação em Engenharia Mecânica. IV.
Título.

Nury Audrey Nieto Garzón

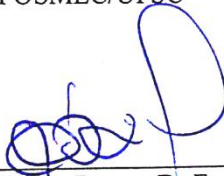
**MEASUREMENT AND MODELING OF THE COMBUSTION OF
STRAIGHT SOYBEAN OIL AND DIESEL OIL BLENDS IN A
COMPRESSION IGNITION ENGINE**

Esta Tese foi julgada adequada para obtenção do Título de “Doutor em Engenharia Mecânica”, e aprovada em sua forma final pelo Programa de Pós-graduação em Engenharia Mecânica.


Florianópolis, 06 de setembro de 2017.



Prof. Jonny Carlos da Silva, Dr.Eng.
Coordenador do programa de Pós-graduação em Engenharia Mecânica –
POSMEC/UFSC




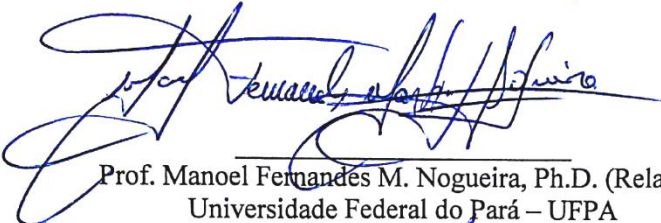
Prof. Edson Bazzo, Dr.Eng.
Orientador
Universidade Federal de Santa Catarina – UFSC

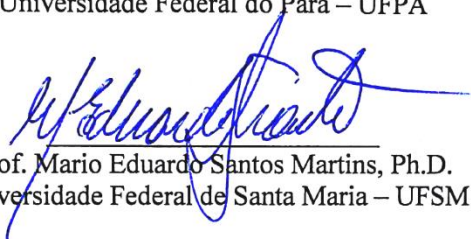



Prof. Amir A. Martins de Oliveira Jr., Ph.D.
Coorientador
Universidade Federal de Santa Catarina – UFSC


Banca Examinadora:



Prof. Amir A. Martins de Oliveira Jr., Ph.D. (Presidente)
Universidade Federal de Santa Catarina – UFSC


Prof. Manoel Fernandes M. Nogueira, Ph.D. (Relator)
Universidade Federal do Pará – UFPA


Prof. Mario Eduardo Santos Martins, Ph.D.
Universidade Federal de Santa Maria – UFSM


Prof. Marcelo Vandresen, Dr.Eng.
Instituto Federal de Santa Catarina – IFSC


Prof. Leonel Rincón Cancino, Dr.Eng.
Universidade Federal de Santa Catarina – UFSC/Joinville


Prof. Jader Riso Barbosa Jr., Ph.D.
Universidade Federal de Santa Catarina – UFSC

I dedicate this thesis to who encouraged me to reach this goal, my husband Juan Pablo and my parents Ismael and Clara.

ACKNOWLEDGEMENTS

I especially thank to Holy Trinity for all blessings at each instant, supporting the different moments to reach this goal. I also thank to Holy Mary for her maternal protection and help.

I am greatly grateful to my husband Juan Pablo for his love, encouragement and support, also to my family, especially, my parents Ismael and Clara and my brothers Wilson and William, for their motivation, prayers and unconditional support.

I would like to thank to my advisors, Prof. Edson Bazzo and Prof. Amir A. de Oliveira for their time, patience and advices to conclude satisfactorily this work. Additionally, I acknowledge them, the opportunity to work in this laboratory.

I would like to thank to the members of the doctoral committee, Prof. Manoel Nogueira, Prof. Mario dos Santos, Prof. Marcelo Vandressen, Prof. Leonel Cancino and Prof. Jader Barbosa, for agreeing to evaluate my thesis and for their suggestions and contributions in order to improve this work.

I acknowledge to CAPES and CNPq for the financial support with the scholarships.

I would also like to thank to POSMEC and LabCET for the technical and financial support for the development of the experimental activities. Additionally, I am grateful for the teachings received and the opportunity to belong to the graduate program and research laboratory.

The gratitude is extended to Gilson Maia for the technical support and the undergraduate students Hugo Meneses Zarza, Borja Gulías Parga, Felipe Schroeder, and particularly Randhy Azevedo dos Santos for their help and contributions regarding the experiments.

I would like to thank to the professors and researchers of the laboratories CERMAT and LMPT at UFSC for the collaboration in some experimental activities.

Special thanks to friends Nathaly, Gonzalo, Yesid, Sandra, Renzo, Marcos Oro, Eduardo Burin, Luis Evelio, Leonel and Nelson for the companionship, support and friendship along these years of my doctorate.

I thank to friends and colleagues of LabCET for their companionship.

Finally, I acknowledge everyone, colleagues, friends and family, that helped me with their technical discussions, camaraderie and stimulus for the conclusion of this project.

Behold, I am instructing you. Be strengthened, and be steadfast. Do not dread, and do not fear. For the Lord your God is with you in all things, wherever you may go.

Joshua 1: 9.

RESUMO

As mudanças climáticas e a forte dependência das economias mundiais do consumo de combustíveis fósseis têm fomentado o estudo de fontes alternativas de energia. Os biocombustíveis, como os óleos vegetais *in natura*, oferecem oportunidades para geração distribuída de eletricidade utilizando motores de ignição por compressão. O presente trabalho enfoca a modelagem e medição do desempenho de um motor monocilíndrico operando com misturas de óleo de soja *in natura* e óleo diesel. Inicialmente, apresenta-se a medição e correlação das propriedades físico-químicas das misturas com frações volumétricas de óleo de soja entre 0 e 100 %. A massa específica, viscosidade dinâmica e tensão superficial das misturas foram correlacionadas com a temperatura e a fração volumétrica do óleo de soja. O desempenho de um motor de ignição por compressão monocilíndrico, com volume de deslocamento 1200 cm³, taxa de compressão 17,3, potência nominal de 14,7 kW/2200 rpm foi medido em um dinamômetro estático para as misturas com 50 % e 80 % v/v de óleo de soja *in natura* em óleo diesel comercial S10. A taxa de liberação de calor foi determinada a partir da medição transiente da pressão no cilindro do motor, utilizando um modelo termodinâmico padrão programado no software MATLAB. Uma função de Wiebe simples foi usada para modelar a fase de combustão pré-misturada e uma função de Wiebe dupla, para as fases de combustão difusiva e residual. Os parâmetros das funções foram obtidos por ajuste às taxas de liberação de calor medidas e correlacionados com o diâmetro médio Sauter, o número de Weber do gás e a fração volumétrica do óleo de soja na mistura. O atraso de ignição foi correlacionado com o diâmetro médio Sauter, o número de Reynolds da gota, a razão de equivalência global, a temperatura do gás, através de um exponencial de Arrhenius, e a fração volumétrica de óleo de soja. As funções obtidas permitiram o desenvolvimento de um modelo zero-dimensional para o ciclo completo do motor, programado no software MATLAB. O modelo foi avaliado através da comparação da previsão da pressão no cilindro, massa de mistura injetada e parâmetros de desempenho com os valores medidos. Finalmente, o modelo foi utilizado em um planejamento fatorial visando estimar o comportamento do motor frente às variações nas suas condições de operação.

Palavras-chave: Óleo vegetal *in natura*. Motor de ignição por compressão. Biocombustíveis. Geração distribuída. Taxa de liberação de calor. Modelagem motor diesel.

RESUMO EXPANDIDO

Introdução

O desenvolvimento da humanidade está fortemente relacionado à disponibilidade de fontes de energia. Desde o século XVIII, combustíveis fósseis como o carvão e o petróleo têm sido as principais fontes de energia. Estes combustíveis não são renováveis, sua exploração e transporte representam ameaças ao meio ambiente e sua queima produz emissões de CO₂ e óxidos de nitrogênio, considerados como gases de efeito estufa, entre outras emissões poluentes. Neste contexto, o câmbio climático global tem motivado o uso de novas fontes de energia, incrementando a atenção em fontes renováveis como a energia solar, a energia eólica e os biocombustíveis. Os óleos vegetais constituem um possível biocombustível para os setores de energia, agricultura, indústria e transporte. Podem ser utilizados puros (*in natura*) ou transformados em biodiesel através do processo químico de transesterificação. Este trabalho centra-se no uso de misturas de óleo de soja *in natura* com óleo diesel como combustível para motores de combustão interna de ignição por compressão, utilizados no setor transporte e na geração distribuída de energia.

Estudos relacionados com o uso de biocombustíveis estão baseados em testes sobre bancada dinamométrica e na análise termodinâmica do motor operando com o combustível alternativo. Diferenças nas propriedades físico-químicas quando comparado com o óleo diesel constituem o principal desafio tecnológico. Os óleos vegetais apresentam tamanho molecular grande e ligações insaturadas que incrementam sua viscosidade e massa específica e reduzem a sua volatilidade, o que influencia significativamente nos processos de atomização e combustão. O aquecimento ou a mistura do óleo vegetal com óleo diesel são as alternativas mais comuns encontradas na literatura para aproximar as propriedades físico-químicas dos óleos vegetais ao óleo diesel. Resultados promissórios e parâmetros de desempenho comparáveis ao óleo diesel têm sido encontrados em testes de motores diesel operando com diferentes óleos vegetais.

Com objetivo de conhecer como acontece a combustão dos óleos vegetais e determinar como pode ser melhorado o processo de combustão foi determinada a taxa de liberação de calor de misturas de óleo de soja, através de uma modelagem zero-dimensional com uso da leitura da pressão da câmara de combustão. A taxa de liberação de calor auxiliou a compressão do processo de combustão das misturas e

suportou o desenvolvimento de um modelo de combustão baseado na função de Wiebe.

Apesar de uma grande quantidade de trabalhos relativos à estimativa das taxas de liberação de calor usando óleos vegetais, existem poucos resultados relacionados aos modelos de combustão de óleos vegetais. Adicionalmente, os parâmetros de combustão para misturas de óleo de soja e óleo diesel não estão disponíveis na literatura. Portanto, este trabalho apresenta um modelo zero-dimensional com uma função Wiebe como modelo de combustão para a operação de um motor diesel de injeção direta alimentado com misturas aquecidas de óleo de soja e óleo diesel. O óleo de soja foi escolhido por sua alta produtividade no Brasil.

Objetivo geral

O principal objetivo da Tese é desenvolver a análise teórica e experimental da combustão de misturas de óleo de soja usadas como combustível em um motor diesel de injeção direta, avaliando a influência das propriedades físico-químicas das misturas sobre o processo de combustão e o desempenho do motor, usando uma modelagem termodinâmica zero-dimensional.

Experimentação

O procedimento experimental consistiu na determinação das propriedades físico-químicas dos combustíveis e nos testes na bancada dinamométrica com medições de pressão no cilindro do motor. O atraso de ignição e a taxa de liberação de calor de cada combustível testado foram obtidos a partir das medições de pressão.

Massa específica, viscosidade dinâmica e tensão superficial foram determinadas a diferentes temperaturas para o óleo diesel e o óleo de soja. As medições permitiram propor correlações para determinar estas propriedades em função da temperatura e da fração volumétrica de óleo de soja na mistura.

A bancada dinamométrica está constituída por um motor de ignição por compressão monocilíndrico, com volume de deslocamento 1200 cm^3 , taxa de compressão 17,3, potência nominal de 14,7 kW/2200 rpm e injeção direta, acoplado a um dinamômetro eletromagnético. Nesta bancada foram testados o óleo diesel e duas misturas, 50/50 % v/v e 80/20 % v/v óleo de soja e óleo diesel. Os combustíveis foram identificados como 100D(25), 50S/50D(25), 50S/50D(85) e 80S/20D(85), indicando a respectiva fração volumétrica de óleo de soja e óleo diesel e a temperatura do combustível na entrada da bomba injetora. Os testes foram realizados na condição de débito máximo da

bomba injetora. Com aplicação de diferentes cargas foram obtidas três rotações de interesse: 1800, 2100 e 2200 rpm. Medições de torque, rotação, vazão de combustível, vazão de ar, temperatura nos gases de exaustão e pressão no cilindro foram realizadas para cada combustível nas diferentes condições testadas. A partir das medições realizadas, foram calculados os parâmetros de desempenho do motor como potência de eixo, consumo específico de combustível e eficiência térmica. Para todas as grandezas medidas foram calculadas as incertezas expandidas das medições.

As medições de pressão no cilindro foram processadas para obter a curva de pressão em função do ângulo de manivela, representativa da condição testada. A partir da análise da curva da segunda derivada da pressão em função do ângulo de manivela foi determinado o atraso de ignição. Uma modelagem zero-dimensional foi utilizada para determinar a taxa de liberação de calor a partir da curva de pressão. A modelagem foi desenvolvida no software MATLAB, envolvendo as propriedades do combustível, um modelo de transferência de calor, as relações geométricas do motor, as propriedades termodinâmicas do gás através da solução de equilíbrio químico, as equações de conservação e as medições da pressão, derivada da pressão, massa de combustível injetado e massa de ar no cilindro.

Modelagem do motor diesel

A modelagem do motor seguiu três etapas: obtenção da taxa de liberação de calor, modelo de combustão e simulação do ciclo completo do motor.

A primeira etapa consistiu em determinar a taxa de liberação de calor dos combustíveis testados nas três rotações, utilizando os dados experimentais de pressão no cilindro.

Na segunda etapa, as taxas de liberação de calor foram ajustadas usando o submodelo de combustão baseado na função Wiebe. Para representar a taxa de liberação de calor foi requerido especificar três fases de combustão: pré-misturada, difusiva (não pré-misturada) e residual. A fase de combustão pré-misturada foi ajustada a uma função Wiebe simples e as fases difusiva e residual foram ajustadas a uma função Wiebe dupla. Correlações em função do diâmetro médio Sauter (*SMD*), o número de Weber do gás e a fração volumétrica de óleo de soja na mistura foram propostas para determinar os parâmetros X_p , X_d , X_r , $\Delta\theta_p$, $\Delta\theta_d$, $\Delta\theta_r$ e a_p da função de Wiebe.

Na terceira etapa, a simulação do motor foi desenvolvida no software MATLAB. Os escoamentos de admissão e escape foram considerados como unidimensionais e isentrópicos. As correlações propostas para massa específica, viscosidade dinâmica e tensão superficial foram utilizadas para calcular as propriedades do combustível nas condições de injeção. O atraso de ignição foi calculado através de uma correlação proposta, relacionando cinco expressões adimensionais (SMD/d_o , Re_D , ϕ_{gl} , $\exp(E_a/RT)$, χ). Na modelagem também foram consideradas as relações geométricas do motor, um modelo de transferência de calor, as propriedades termodinâmicas do gás através da solução de equilíbrio químico, as equações de conservação e o modelo de combustão proposto. Os resultados obtidos foram comparados com os dados experimentais de pressão no cilindro, taxa de liberação de calor e massa de combustível injetado. Adicionalmente, a aplicabilidade da modelagem foi mostrada através de um planejamento experimental fatorial, analisando a operação do motor com as misturas de óleo de soja.

Resultados e discussões

Com relação aos testes na bancada dinamométrica, maior potência e torque foram apresentados pelo combustível 100D(25) e a mistura 50S/50D(25). Provavelmente, o aumento da massa de combustível injetado compensou a diferença no valor LHV desta mistura em relação ao óleo diesel. A mistura 80S/20D(85), nas três rotações testadas, apresentou os menores valores de torque e potência de freio devido ao menor LHV em relação ao óleo diesel (-10,5%). Com relação à eficiência térmica, não foi observada diferença significativa na eficiência térmica dos combustíveis nas diferentes rotações testadas.

A fase de combustão pré-misturada foi comparável para todos os combustíveis a 1800 e 2100 rpm. A fase de combustão pré-misturada foi maior para o combustível 100D(25) e a mistura 50S/50D(25) a 2200 rpm. A combustão foi atrasada para a mistura 80S/20D(85), incrementando a taxa global da reação de combustão nas fases de combustão difusiva e residual, provavelmente influenciado pelo maior teor de oxigênio da mistura 80S/20D(85).

Valores preditos do atraso de ignição, estimados com a correlação proposta, encontram-se dentro de um intervalo de confiança de 95 %. Adicionalmente, foi possível simular o ciclo completo do motor diesel, utilizando as propriedades físico-químicas calculadas, a correlação proposta para o atraso da ignição e o modelo de combustão proposto.

Os resultados da simulação foram validados comparando com os resultados experimentais. Com relação à pressão no cilindro, as diferenças entre os dados experimentais e simulados foram de -10 % a 3 %, aproximadamente, nos cursos de compressão e expansão. Maiores diferenças foram encontradas nos cursos de admissão e exaustão como consequência das informações consideradas para a área de passagem e coeficientes de descarga nas válvulas, assim como possíveis fenômenos de escoamento presentes nos coletores que não podem ser reproduzidos na modelagem desenvolvida.

A taxa de liberação de calor simulada apresentou diferenças de -5 % a 15 % em relação aos dados experimentais. A maior diferença foi observada no início da combustão e no ponto da transição entre as fases de combustão pré-misturada e difusiva devido à mudança da função de Wiebe que descreve cada fase da combustão.

Conclusões

Este trabalho contribuiu para o uso de misturas de óleo de soja em motores de ignição por compressão, envolvendo dados experimentais e o desenvolvimento de um modelo termodinâmico zero-dimensional da operação do motor. Um modelo de combustão considerando duas funções de Wiebe e uma correlação de atraso de ignição foram propostas e expressas em função das propriedades do combustível e do gás no cilindro. Adicionalmente, as medições das propriedades físico-químicas permitiram o desenvolvimento de correlações para massa específica, viscosidade dinâmica e tensão superficial em função da temperatura e da fração volumétrica do óleo de soja na mistura.

Finalmente, este trabalho permitiu observar a influência no processo de combustão, das propriedades do combustível e do gás do cilindro. Portanto, a combustão de misturas de óleo de soja é favorecida com: alta temperatura do combustível, alta rotação do motor, injeção adiantada, baixo *SMD* e alta temperatura e pressão no cilindro no instante da injeção. Consequentemente, o desempenho de um motor diesel alimentado com misturas de óleo vegetal é favorecido quando o combustível é aquecido, o tempo de injeção é adiantado, a pressão de injeção é incrementada ou o motor diesel possui alta relação de compressão.

Palavras-chave: Óleo vegetal *in natura*. Motor de ignição por compressão. Biocombustíveis. Geração distribuída. Taxa de liberação de calor. Modelagem motor diesel.

ABSTRACT

Climate changes and strong worldwide economics dependency of the use of fossil fuels have encouraged the study of alternative energy sources. Biofuels, such as straight vegetable oils, offer opportunities for the distributed electricity generation using compression ignition engines. The present work focuses on the modeling and measurement of performance of a single-cylinder engine operating with blends of straight soybean oil and diesel oil. Initially, one presents the measurement and correlations of physico-chemical properties of blends with volume fractions of soybean oil in the range of 0 to 100 %. Density, dynamic viscosity and surface tension of the blends were correlated with the temperature and volume fraction of soybean oil. The performance of a single-cylinder compression ignition engine, displaced volume of 1200 cm³, compression rate of 17.3, nominal power of 14.7 kW/2200 rpm was measured on static dynamometer for the blends 50 % and 80 % v/v of straight soybean oil in commercial diesel oil S10. The heat release rate was determined from transient in-cylinder pressure measurement, using a standard thermodynamic model programmed in MATLAB software. A simple Wiebe function was used to model the premixed combustion phase and a double Wiebe function, for the diffusive and residual combustion phases. Parameters of the Wiebe functions were curve-fitted to the heat release rate measured, and they were correlated with the Sauter mean diameter, gas Weber number and volume fraction of soybean oil in the blend. The ignition delay was correlated with the Sauter mean diameter, droplet Reynold number, global equivalence ratio, gas temperature using the exponential factor of Arrhenius, and volume fraction of soybean oil. The functions obtained allowed the development of a zero-dimensional modeling for the complete cycle of the engine, programmed in MATLAB software. The modeling was validated comparing the in-cylinder pressure simulated, fuel mass injected and performance parameters with the respective measurements. Finally, the diesel engine modeling was used in a factorial experimental design aiming to estimate the behavior of the engine with different operation conditions.

Keywords: Straight vegetable oil. Compression ignition engines. Biofuels. Distributed generation. Heat release rate. Modeling of diesel engine.

LIST OF FIGURES

Figure 1. Combustion phases of a diesel engine.	58
Figure 2. Heat release rate of diesel fuel, cotton oil and mixture of 40 % of diesel oil.....	62
Figure 3. Maximum in-cylinder pressure as a function of the power for tests with diesel oil and blends with cotton oil.	63
Figure 4. (a) Maximum in-cylinder pressure. (b) Angle of maximum pressure as a function of the load for tests with diesel oil and blends with Karanja oil.	63
Figure 5. Ohnesorge diagram with the break-up mechanisms of diesel, jatropha and pongamia oils.	67
Figure 6. Characteristics of current models used in diesel engines.....	71
Figure 7. A schematic of the diesel spray combustion model proposed by Dec (1997).	74
Figure 8. A schematic of the phenomenological explanation about the combustion of a diesel oil droplet and a binary liquid blend droplet.....	75
Figure 9. Geometrical characteristics of diesel engine.....	87
Figure 10. Control volume considered in the combustion chamber.....	90
Figure 11. Density of soybean oil, diesel oil and two blends as a function of temperature.	97
Figure 12. Dynamic viscosity of soybean oil, diesel oil and two blends as a function of temperature.	99
Figure 13. Surface tension of soybean oil, diesel oil and a blend as a function of temperature.	102
Figure 14. Surface tension of soybean oil blends at 25 and 50 °C.	103
Figure 15. Specific heat of soybean oil, diesel oil and two blends as a function of temperature.	106
Figure 16. Thermal conductivity of soybean oil, diesel oil and two blends as a function of temperature.....	107
Figure 17. Schematic diagram of the experimental set-up.	108
Figure 18. Picture of the diesel engine coupled to electromagnetic dynamometer.....	109

Figure 19. Screen of control and data acquisition system on LabVIEW software.	110
Figure 20. Tomogram of injector nozzle used in the diesel engine (LMPT/UFSC).	112
Figure 21. (a) Piezoelectric pressure sensor. (b) Metallic sleeve for mounting of the pressure sensor. (c) Engine head.	113
Figure 22. Control volume defined for the combustion chamber.	115
Figure 23. Modeling procedure of diesel engine.	119
Figure 24. Simplified schematic of the flow through the valves.	122
Figure 25. Geometric parameters and curtain area of the valves.	125
Figure 26. Brake torque as a function of the speed for all fuels tested at full load condition.	136
Figure 27. Brake power as a function of the speed for all fuels tested at full load condition.	136
Figure 28. Fuel mass injected as a function of the speed for all fuels tested at full load condition.	137
Figure 29. Thermal efficiency as a function of the speed for all fuels tested at full load condition.	137
Figure 30. Mass air flow rate as a function of the speed for all fuels tested at full load condition.	138
Figure 31. Experimental in-cylinder pressure data as a function of crank angle for the fuels tested at 1800 rpm and full load condition.	143
Figure 32. Experimental in-cylinder pressure data as a function of crank angle for the fuels tested at 2100 rpm and full load condition.	143
Figure 33. Experimental in-cylinder pressure data as a function of crank angle for the fuels tested at 2200 rpm and full load condition.	144
Figure 34. Comparison of ignition delays predicted with ignition delays measured for all fuels tested.	147
Figure 35. Heat release rate as a function of crank angle for the fuels tested at 1800 rpm and full load condition.	149
Figure 36. Cumulative energy release as a function of crank angle for the fuels tested at 1800 rpm and full load condition. ...	149

Figure 37. Heat release rate as a function of crank angle for the fuels tested at 2100 rpm and full load condition.	150
Figure 38. Cumulative energy release as a function of crank angle for the fuels tested at 2100 rpm and full load condition.....	150
Figure 39. Heat release rate as a function of crank angle for the fuels tested at 2200 rpm and full load condition.	151
Figure 40. Cumulative energy release as a function of crank angle for the fuels tested at 2200 rpm and full load condition.....	151
Figure 41. Heat release rate as a function of crank angle for 100D(25) at three speeds tested and full load condition.	155
Figure 42. Heat release rate as a function of crank angle for 50S/50D(25) at three speeds tested and full load condition.	155
Figure 43. Heat release rate as a function of crank angle for 50S/50D(85) at three speeds tested and full load condition.	156
Figure 44. Heat release rate as a function of crank angle for 80S/20D(85) at three speeds tested and full load condition.	156
Figure 45. Ohnesorge diagram for all fuels tested at 1800 rpm and full load condition.	157
Figure 46. Experimental heat release rate and Wiebe functions fitted as a function of crank angle for 100D(25) at 1800 rpm.	160
Figure 47. Experimental heat release rate and Wiebe functions fitted as a function of crank angle for the blend 80S/20D(85) at 1800 rpm.	160
Figure 48. Parameter X_p as a function of crank angle for all fuels tested.	161
Figure 49. Parameter X_d as a function of crank angle for all fuels tested.	161
Figure 50. Parameter X_r as a function of crank angle for all fuels tested.	162
Figure 51. Parameter $\Delta\theta_p$ as a function of crank angle for all fuels tested.	162

Figure 52. Parameter $\Delta\theta_d$ as a function of crank angle for all fuels tested.	163
Figure 53. Parameter $\Delta\theta_r$ as a function of crank angle for all fuels tested.	163
Figure 54. Parameter a_p as a function of crank angle for all fuels tested.	164
Figure 55. Parameter a_d as a function of crank angle.	165
Figure 56. Parameter m_p as a function of crank angle.	165
Figure 57. Parameter m_d as a function of crank angle.	166
Figure 58. Parameter m_r as a function of crank angle.	166
Figure 59. Experimental and simulated in-cylinder pressure for 100D(25) at 1800 rpm.	170
Figure 60. Percentage difference between the experimental and simulated in-cylinder pressure for 100D(25) at 1800 rpm.	170
Figure 61. Experimental and simulated heat release rate of the diesel engine operating with 100D(25) at 1800 rpm.	171
Figure 62. Percentage difference between the experimental and simulated heat release rate for 100D(25) at 1800 rpm.	171
Figure 63. In-cylinder gas temperature simulated for 100D(25) at 1800 rpm.	172
Figure 64. Total in-cylinder mass simulated for 100D(25) at 1800 rpm.	172
Figure 65. Intake and exhaust mass flows simulated for 100D(25) at 1800 rpm.	173
Figure 66. Experimental and simulated in-cylinder pressure for 50S/50D(25) at 1800 rpm.	174
Figure 67. Percentage difference between the experimental and simulated in-cylinder pressure for 50S/50D(25) at 1800 rpm.	174
Figure 68. Experimental and simulated heat release rate of the diesel engine operating with 50S/50D(25) at 1800 rpm. ...	175
Figure 69. Percentage difference between the experimental and simulated heat release rate for 50S/50D(25) at 1800 rpm.	175

Figure 70. Experimental and simulated in-cylinder pressure for 80S/20D(85) at 1800 rpm.	176
Figure 71. Percentage difference between the experimental and simulated in-cylinder pressure for 80S/20D(85) at 1800 rpm.	176
Figure 72. Experimental and simulated heat release rate of the diesel engine operating with 80S/20D(85) at 1800 rpm.	177
Figure 73. Percentage difference between the experimental and simulated heat release rate for 80S/20D(85) at 1800 rpm.	177
Figure 74. Simulated heat release rate of the diesel engine operating with the four fuels tested at 1800 rpm.	178
Figure 75. Simulated heat release rate of the diesel engine operating with the four fuels tested at 2100 rpm.	179
Figure 76. Simulated heat release rate of the diesel engine operating with the four fuels tested at 2200 rpm.	179
Figure 77. Simulated in-cylinder pressure of the diesel engine operating with the four fuels tested at 1800 rpm.	180
Figure 78. Simulated in-cylinder pressure of the diesel engine operating with the four fuels tested at 2100 rpm.	180
Figure 79. Simulated in-cylinder pressure of the diesel engine operating with the four fuels tested at 2200 rpm.	181
Figure 80. Function of desirability for maximum thermal efficiency as response.	186
Figure 81. Function of desirability for thermal efficiency above 30 % as response.	187
Figure A1. Ohnesorge diagram: break-up regimes of liquid jets.	212
Figure D1. Geometric parameters of the inlet and exhaust valves.	227
Figure D2. Measurement of the valve lift made on the valve camshaft.	228
Figure D3. Intake valve lift as a function of crank angle.	228
Figure D4. Exhaust valve lift as a function of crank angle.	229

Figure E1. Injected fuel volume as a function of engine speed tested.....	231
Figure F1. Normalized sensitivity coefficient for parameter SMD/d_o	234
Figure F2. Normalized sensitivity coefficient for parameter Re_D	235
Figure F3. Normalized sensitivity coefficient for parameter ϕ_{gt}	235
Figure F4. Normalized sensitivity coefficient for parameter T	236
Figure F5. Normalized sensitivity coefficient for parameter χ	236

LIST OF TABLES

Table 1. Tests reported in the literature about diesel engines fueled with raw vegetable oils and their blends with diesel oil.	55
Table 2. Problems for using straight vegetable oils in diesel engines.....	57
Table 3. Results of tests with preheated crude sunflower oil and diesel fuel.	60
Table 4. Sauter mean diameter for blends of cotton and diesel oils.....	68
Table 5. Combustion submodels used in internal combustion engines.....	76
Table 6. Works about tests with vegetable oils obtaining the heat release rate.....	83
Table 7. Works about modeling of a diesel engine fueled with vegetable oils.....	85
Table 8. Identification of the fuels tested and temperature condition for testing.	95
Table 9. Composition of fatty acids of soybean oil.....	96
Table 10. Equipment or standard used for physico-chemical properties determination.....	97
Table 11. Coefficients of the fitting correlations of the density.....	98
Table 12. Density of fuels tested at injection temperature and percentage difference respect to diesel oil.	98
Table 13. Coefficients of the fitting correlations of the dynamic viscosity.	100
Table 14. Dynamic viscosity of fuels tested at injection temperature and percentage difference respect to diesel oil.	101
Table 15. Coefficients of the fitting correlations of the surface tension.	102
Table 16. Surface tension of fuels tested at injection temperature and percentage difference respect to diesel oil.....	103
Table 17. Results of <i>HHV</i> , <i>LHV</i> , C, H, N and S of soybean and diesel oils.....	104

Table 18. Coefficients of the fitting correlations of the specific heat of soybean and diesel oils.....	105
Table 19. Coefficients of the fitting correlations of the thermal conductivity of soybean and diesel oils.	107
Table 20. Technical specifications of the diesel engine tested.....	111
Table 21. Equations and variables considered for obtaining the heat release rate.....	117
Table 22. Expanded measurement uncertainties as a percentage of the mean value.	118
Table 23. Fitting coefficients, coefficient of determination (R^2) and standard deviation of the fittings for the ignition delay.....	130
Table 24. Equations used in the zero-dimensional modeling of the diesel engine.	132
Table 25. Stoichiometric air/fuel ratio and global equivalence ratio for all fuels at three speeds tested.	139
Table 26. Performance parameters and respective percentage difference in comparison with diesel oil for the fuels tested at three speeds and full load condition.	140
Table 27. Maximum pressure and percentage difference relative to diesel oil at 1800 rpm.	144
Table 28. Maximum pressure and percentage difference relative to diesel oil at 2100 rpm.	145
Table 29. Maximum pressure and percentage difference relative to diesel oil at 2200 rpm.	145
Table 30. Ignition delay of the fuel tested at 1800 rpm.	145
Table 31. Ignition delay of the fuel tested at 2100 rpm.	146
Table 32. Ignition delay of the fuel tested at 2200 rpm.	146
Table 33. Coefficients of the fitting correlation for the ignition delay.....	147
Table 34. Mass fraction burned at 444° CA for all fuels at three speeds tested.	153
Table 35. Crank angle degree of the 10 % and 50 % mass fraction burned for all fuels at three speeds tested.	153
Table 36. <i>SMD</i> , droplet Reynold number and oxygen content for all fuels tested at 1800 rpm and full load condition.	158

Table 37. Fitting coefficients, coefficient of determination (R^2) and standard deviation of the fitting procedure of each combustion parameter.	168
Table 38. Simulated and experimental performance parameters of the diesel engine operating with 100D(25) at three speeds tested.....	182
Table 39. Simulated and experimental performance parameters of the diesel engine operating with 50S/50D(25) at three speeds tested.....	182
Table 40. Simulated and experimental performance parameters of the diesel engine operating with 50S/50D(85) at three speeds tested.....	183
Table 41. Simulated and experimental performance parameters of the diesel engine operating with 80S/20D(85) at three speeds tested.....	183
Table 42. Factors and levels of the 2^4 factorial experimental design.	185
Table 43. Combination of factors and responses for the 2^4 factorial experimental design.	185
Table 44. Analysis of variance for the 2^4 factorial experimental design.	186
Table C1. Expanded measurement uncertainties of the engine operating with 100D(25).	223
Table C2. Expanded measurement uncertainties of the engine operating with 50S/50D(25).	224
Table C3. Expanded measurement uncertainties of the engine operating with 50S/50D(85).	224
Table C4. Expanded measurement uncertainties of the engine operating with 80S/20D(85).	225
Table C5. Expanded measurement uncertainties of the dynamic viscosity.	225
Table C6. Expanded measurement uncertainties of the surface tension.	226
Table D1. Geometric parameters of the inlet and exhaust valves of the engine tested.	227

Table D2. Coefficients of the polynomial function of degree 10 used to calculate the discharge coefficients of the valves.	229
Table G1. Routine for obtaining the heat release rate from experimental pressure data.....	237
Table G2. Routine of complete cycle simulation of diesel engine.....	238

LIST OF ABBREVIATIONS

ANEEL	Agência Nacional de Energia Elétrica
ANOVA	Analysis of variance
ANP	Agência Nacional do Petróleo, Gás Natural e Biocombustíveis
ASTM	American Society for Testing and Materials
BC	Bottom-center crank position
BTC	Before top-center crank position
CA	Crank Angle
CERMAT	Ceramic Materials Research Center
CRFD	Computational Reactive Fluid Dynamics
EOI	End of injection
EVC	Exhaust valve closing
EVO	Exhaust valve opening
HHV	Higher Heating Value
HRR	Heat Release Rate
IVC	Inlet valve closing
IVO	Inlet valve opening
LabCET	Laboratory of Combustion and Thermal Systems Engineering
LHV	Lower Heating Value
LMPT	Porous Media and Thermophysical Properties Laboratory
PBDF	Petroleum Based Diesel Fuel
PCSO	Preheated Crude Sunflower Oil
SMD	Sauter Mean Diameter
SOI	Start of injection
SVO	Straight Vegetable Oil
TC	Top-center crank position

LIST OF SYMBOLS

a	Crank radius	[m]
a_d	Constant, diffusive combustion phase, Wiebe function	[-]
a_p	Constant, premixed combustion phase, Wiebe function	[-]
A	Heat transfer surface area	[m ²]
A_{cc}	Combustion chamber surface area	[m ²]
A_{ch}	Cylinder head surface	[m ²]
A_{cyl}	Cylinder area	[m ²]
A_e	Passage area at exhaust valve	[m ²]
A_i	Passage area at inlet valve	[m ²]
A_{ig}	Parameter of ignition delay model	[ms]
A_{inj}	Empirical parameter of injector nozzle	[-]
A_p	Piston crown surface area	[m ²]
$(AF)_s$	Stoichiometric air/fuel ratio	[kg/kg]
B	Cylinder bore or piston diameter	[m]
c_p	Specific heat at constant pressure	[kJ/(kg·K)]
$c_{p,g}$	Specific heat at constant pressure of in-cylinder gases	[kJ/(kg·K)]
c_s	Specific heat	[kJ/(kg·K)]
\bar{c}_s	Mean specific heat	[kJ/(kg·K)]
$c_{s,b}$	Specific heat of blend	[kJ/(kg·K)]
$c_{s,d}$	Specific heat of diesel oil	[kJ/(kg·K)]
$c_{s,v}$	Specific heat of vegetable oil	[kJ/(kg·K)]
c_v	Specific heat at constant volume	[kJ/(kg·K)]
C_D	Discharge coefficient	[-]
$C_{D,e}$	Discharge coefficient at exhaust valve	[-]
$C_{D,i}$	Discharge coefficient at inlet valve	[-]
$C_{D,max}$	Maximum discharge coefficient of injector nozzle orifice	[-]
C_n	Carbon moles in the fuel molecule	[-]
CA10	Localization of 10 % mass fraction burned	[° CA]
CA50	Localization of 50 % mass fraction burned	[° CA]
CN	Cetane number	[-]

C_1, C_2	Constants, Woschni correlation	[-]
d_o	Injector nozzle hole diameter	[m]
D	Inner seat diameter of the valves	[m]
\bar{D}	Characteristic dimension, Honenberg correlation	[m]
D_m	Mean seat diameter of the valves	[m]
D_s	Steam diameter of the valves	[m]
D_v	Head diameter of the valves	[m]
$D_{v,e}$	Head diameter of the exhaust valve	[m]
$D_{v,i}$	Head diameter of the inlet valve	[m]
E_a	Apparent activation energy of the fuel	[J/mol]
E_{red}	Reduced activation energy, Whitehouse and Way model	[K]
F	Fisher Probability Distribution Function	[-]
$(FA)_s$	Stoichiometric fuel/air ratio	[kg/kg]
G_{ij}	Interaction parameter	[-]
h_a	Enthalpy of air flow	[kJ/kg]
h_c	Convective heat transfer coefficient	[W/(m ² ·K)]
h_e	Enthalpy of exhaust flow	[kJ/kg]
h_f	Enthalpy of fuel flow	[kJ/kg]
h_f^o	Enthalpy of formation of the fuel	[kJ/kg]
h_i	Enthalpy of a flux i	[kJ/kg]
H_m	Hydrogen moles in the fuel molecule	[-]
HHV	Higher Heating Value	[kJ/kg]
$imep$	Indicated mean effective pressure	[kPa]
J	Number of replications	[-]
k	Thermal conductivity	[W/(m·K)]
k_b	Thermal conductivity of blend	[W/(m·K)]
k_d	Thermal conductivity of diesel oil	[W/(m·K)]
k_g	Gas thermal conductivity	[W/(m·K)]
k_{inj}	Empirical parameter of injector nozzle	[-]
k_p	Coverage factor of an uncertainty	[-]
k_v	Thermal conductivity of vegetable oil	[W/(m·K)]
k_w	Thermal conductivity of the wall	[W/(m·K)]
l	Connecting rod	[m]

l_{ef}	Degrees of freedom, combined uncertainty	[-]
$l_{ef,A}$	Degrees of freedom, uncertainties type A	[-]
$l_{ef,B}$	Degrees of freedom, uncertainties type B	[-]
l_v	Instantaneous lift of the valves	[m]
$l_{v,e}$	Instantaneous lift of the exhaust valve	[m]
$l_{v,i}$	Instantaneous lift of the inlet valve	[m]
l_w	Thickness of the wall	[m]
L	Stroke	[m]
L_{inj}	Injector nozzle hole length	[m]
L_{max}	Maximum stroke	[m]
L_v	Maximum lift of the valves	[m]
LHV	Lower Heating Value	[kJ/kg]
m	In-cylinder total mass	[kg]
\dot{m}	Total mass flow	[kg/s]
m_a	Mass of air inducted into the cylinder	[kg]
\dot{m}_a	Mass air flow	[kg/s]
m_d	Parameter of diffusive combustion phase, Wiebe function	[-]
\dot{m}_e	Mass exhaust flow	[kg/s]
m_f	Fuel mass injected per cycle	[mg/cycle]
\dot{m}_f	Mass fuel flow or fuel burning rate	[kg/s]
$m_{f,b}$	Fuel mass burned	[kg]
$m_{f,o}$	Instantaneous fuel mass	[kg]
\dot{m}_i	Mass flow rate of a flux i	[kg/s]
m_{inj}	Fuel mass injected per cycle, Whitehouse-Way model	[mg/cycle]
\dot{m}_{iso}	Isentropic mass flow through the valves	[kg/s]
m_p	Parameter of premixed combustion phase, Wiebe function	[-]
m_r	Parameter of residual combustion phase, Wiebe function	[-]
\dot{m}_{real}	Actual mass flow through the valves	[kg/s]
m_u	Fuel mass unprepared to burn, Whitehouse-Way model	[kg]
n_R	Number of crankshaft revolutions per power stroke	[-]

N	Engine speed	[rpm]
N_k	Nitrogen moles in the fuel molecule	[-]
N_{max}	Maximum speed engine	[rpm]
Nu	Nusselt number	[-]
Oh	Ohnesorge number	[-]
O_l	Oxygen moles in the fuel molecule	[-]
p	Pressure	[kPa]
p	Probability	[-]
p_e	Pressure at exhaust manifold	[kPa]
p_i	Pressure at inlet manifold	[kPa]
p_{inj}	Injection pressure	[kPa]
p_m	Motored cylinder pressure	[Pa]
p_{O_2}	Oxygen partial pressure	[Pa]
p_r	Working-fluid pressure at state reference, Woschni correlation	[Pa]
P_b	Break power	[kW]
P_i	Indicated power per cycle	[kW]
\dot{q}''	Mean heat transfer	[W/m ²]
Q	Heat transfer through of system boundaries	[kJ]
Q_f	Heat release for the fuel	[kJ]
r_c	Compression ratio	[-]
$(r_o - r_i)$	Annular distance between the needle and the wall of the injector nozzle	[m]
R	Universal gas constant	[J/(mol·K)]
R_a	Air constant	[J/(kg·K)]
R_{cc}	Ratio connecting rod/crank radius	[-]
Re	Reynolds number	[-]
Re_D	Droplet Reynold number	[-]
Re_l	Liquid phase Reynold number	[-]
Re_{sp}	Spray Reynold number	[-]
R_g	Gas constant	[J/(kg·K)]
R_k''	Thermal resistance per unit area associated with conduction	[m ² ·K/W]
R^2	Coefficient of determination	[-]

s	Distance between the crank axis and the piston pin axis.	[m]
sfc	Specific fuel consumption	[g/(kW·h)]
$s^2(\bar{x})$	Variance of the global mean of a variable x	
S	Spray penetration	[m]
S_p	Instantaneous piston velocity	[m/s]
$\overline{S_p}$	Mean piston velocity	[m/s]
SC	Sensitivity coefficient	
SMD	Sauter Mean Diameter	[m]
t	Time	[s]
t_{break}	Spray break-up time	[s]
t_c	Residence time of the fuel in the injector nozzle body	[s]
T	Temperature	[K]
T_b	Break torque	[N·m]
$T_{coolant}$	Mean temperature of the outside wall in contact with the coolant fluid	[K]
T_e	Temperature of exhaust gases	[°C]
T_f	Fuel temperature at injection pump inlet	[°C]
T_i	Air temperature at inlet manifold	[°C]
T_{inj}	Fuel temperature at injection conditions	[°C]
T_r	Working-fluid temperature at state reference, Woschni correlation	[K]
T_w	Mean wall temperature	[K]
$T_{w,ch}$	Cylinder head wall temperature	[K]
$T_{w,cyl}$	Cylinder wall temperature	[K]
$T_{w,p}$	Piston wall temperature	[K]
TPC	Fuel preparation rate, Whitehouse and Way model	[kg/s]
TRC	Reaction rate of the prepared fuel, Whitehouse and Way model	[kg/s]
u	Specific internal energy	[kJ/kg]
$u_A(x)$	Uncertainty type A of the variable x	
$u_B(x)$	Uncertainty type B of the variable x	
$u_C(x)$	Combined standard uncertainty, variable x	
$u_i(x)$	Source of uncertainty of the variable x	

u_{sp}	Spray velocity	[m/s]
U	Internal energy	[kJ]
$U(x)$	Expanded uncertainty of the variable x	
v	Fluid velocity	[m/s]
\bar{v}	Mean specific volume	[m ³ /kg]
V	Volume	[m ³]
V_c	Clearance volume	[m ³]
V_d	Displaced or swept volume by the cylinder	[m ³]
V_{inj}	Fuel volume injected	[m ³]
V_r	Working-fluid volume at state reference, Woschni correlation	[m ³]
w	Working fluid velocity, Woschni correlation	[m/s]
w_v	Seat width of the valves	[m]
We	Weber number	[-]
We_g	Gas phase Weber number	[-]
We_l	Liquid phase Weber number	[-]
We_{sp}	Spray Weber number	[-]
W_i	Indicated work per cycle	[kJ]
\bar{x}	Overall mean of all data	
x_d	Mass fraction of diesel oil	[-]
x_i	Concentrations in mass, mol or volume fraction of the i^{th} components	
x_j	Concentrations in mass, mol or volume fraction of the j^{th} components	
\bar{x}_j	Mean value of the observations of each test	
x_v	Mass fraction of vegetable oil	[-]
X_b	Mass fraction burned	[-]
X_d	Mass fraction burned in the diffusive combustion phase, Wiebe function	[-]
X_p	Mass fraction burned in the premixed combustion phase, Wiebe function	[-]
X_r	Mass fraction burned in the residual combustion phase, Wiebe function	[-]
y_1, y_2, \dots, y_{12}	Mole fractions of the combustion products	[-]

Greek letters

α	Significance level of a statistic test	[-]
α_{sp}	Spray angle	[°]
α_t	Thermal diffusivity of the fuel	[m ² /s]
β	Fuel fraction burned, Watson model	[-]
$\bar{\beta}$	Mean thermal expansion coefficient	[1/K]
β_v	Seat angle of the valves	[°]
γ	Ratio of specific heats	[-]
γ_a	Ratio of specific heats of air	[-]
γ_g	Ratio of specific heats of in-cylinder gases	[-]
Δh_s	Sensible enthalpy	[kJ/kg]
Δp	Difference between the injection pressure and chamber pressure	[kPa]
Δt_{CA}	Time of a crank angle degree	[s]
ΔT_f	Rise in the fuel temperature	[K]
ΔT_s	Difference in temperature between the initial fuel temperature and the wall temperature of the injector nozzle	[K]
$\Delta \theta_{comb}$	Combustion duration	[° CA]
$\Delta \theta_d$	Duration period of the diffusive combustion phase	[° CA]
$\Delta \theta_{inj}$	Duration period of injection process	[° CA]
$\Delta \theta_p$	Duration period of the premixed combustion phase	[° CA]
$\Delta \theta_r$	Duration period of the residual combustion phase	[° CA]
ε	Global emissivity	[-]
η	Thermal efficiency	[-]
η_m	Mechanical efficiency	[-]
η_v	Volumetric efficiency	[-]
θ	Crank angle	[° CA]
θ_d	Start of diffusive combustion phase	[° CA]
θ_{evc}	Exhaust valve closing	[° CA]
θ_{evo}	Exhaust valve opening	[° CA]
θ_{ig}	Start of ignition	[° CA]

θ_{inj}	Injection timing	[° CA]
θ_{ivc}	Inlet valve closing	[° CA]
θ_{ivo}	Inlet valve opening	[° CA]
θ_{soi}	Start of injection	[° CA]
μ	Dynamic viscosity	[Pa·s]
μ_b	Blend dynamic viscosity	[Pa·s]
μ_f	Fuel dynamic viscosity	[Pa·s]
μ_g	Gas dynamic viscosity	[Pa·s]
μ_i	Dynamic viscosity i^{th} component of a blend	[Pa·s]
μ_l	Liquid dynamic viscosity	[Pa·s]
ρ	Density	[kg/m ³]
ρ_a	Density of air inducted into the cylinder	[kg/m ³]
ρ_b	Blend density	[kg/m ³]
ρ_d	Diesel oil density	[kg/m ³]
ρ_f	Fuel density	[kg/m ³]
ρ_g	Gas density	[kg/m ³]
ρ_l	Liquid density	[kg/m ³]
ρ_v	Vegetable oil density	[kg/m ³]
σ	Surface tension	[N/m]
σ_b	Blend surface tension	[N/m]
σ_f	Fuel surface tension	[N/m]
σ_l	Liquid surface tension	[N/m]
σ_{SB}	Stefan-Boltzmann constant	[W/(m ² ·K ⁴)]
τ	Ignition delay	[ms]
τ_c	Characteristic time, ignition delay correlation	[ms]
ϕ	Equivalence ratio at any instant	[-]
ϕ_{gl}	Global equivalence ratio	[-]
χ	Volume fraction of vegetable oil in the blend	[-]
χ_1, χ_2	Volume fraction of the components in a binary blend	[-]
ψ	Normalized sensitivity coefficient	[-]
ω	Angular velocity	[rad/s]

TABLE OF CONTENTS

1	INTRODUCTION	47
1.1	MOTIVATION.....	47
1.2	OBJECTIVES.....	49
1.2.1	General objective	49
1.2.2	Specific objectives.....	49
1.3	MAIN CONTRIBUTIONS	50
1.4	THESIS OVERVIEW	50
2	BACKGROUND AND LITERATURE REVIEW	53
2.1	FUEL PROPERTIES FOR DIESEL ENGINE APPLICATION	53
2.1.1	Vegetable oils	54
2.2	COMBUSTION PARAMETERS.....	58
2.3	INJECTION PARAMETERS	65
2.4	PERFORMANCE PARAMETERS	68
2.5	MODELING OF DIESEL ENGINES.....	70
2.5.1	Thermodynamic models.....	71
2.5.2	Multidimensional model	73
2.5.3	Submodels used in internal combustion engines.....	73
2.6	LITERATURE REVIEW	82
2.6.1	Contextualization.....	86
3	GEOMETRICAL AND THERMODYNAMIC ANALYSIS OF DIESEL ENGINE	87
3.1	GEOMETRICAL CHARACTERISTICS	87
3.2	THERMODYNAMIC MODELING	89
4	EXPERIMENTAL METHOD	95
4.1	PHYSICO-CHEMICAL PROPERTIES OF THE FUELS	95
4.1.1	Fuels tested	95
4.1.2	Determination of properties	96
4.2	EXPERIMENTAL SET-UP	108
4.2.1	Engine tested	110
4.2.2	Pressure acquisition.....	112
4.2.3	Experimental testing procedure	113

4.3	POST-PROCESSING OF PRESSURE MEASUREMENTS...	114
4.4	MEASUREMENT UNCERTAINTIES	118
5	MODELING OF THE DIESEL ENGINE.....	119
5.1	COMBUSTION SUBMODEL.....	120
5.2	COMPLETE CYCLE SIMULATION	121
5.2.1	Intake and exhaust	121
5.2.2	Fuel properties at injection conditions	126
5.2.3	Ignition delay	127
5.2.4	In-cylinder pressure and temperature	130
6	RESULTS AND DISCUSSIONS	135
6.1	PERFORMANCE PARAMETERS	135
6.2	IN-CYLINDER PRESSURE.....	142
6.3	IGNITION DELAY	145
6.3.1	Ignition delay correlation	146
6.4	HEAT RELEASE RATE.....	148
6.5	COMBUSTION MODEL	159
6.6	ENGINE CYCLE SIMULATION	169
6.6.1	Pressure, temperature and heat release rate	169
6.6.2	Performance parameters	181
6.7	FACTORIAL EXPERIMENTAL DESIGN.....	184
7	CONCLUSIONS	189
	REFERENCES.....	193
	APPENDIX A. Break-up regimes of liquid jets	211
	APPENDIX B. Combustion models	217
	APPENDIX C. Uncertainties of the measurements	221
	APPENDIX D. Dimensions of the valves and discharge	
	coefficients.....	227
	APPENDIX E. Injected fuel volume.....	231
	APPENDIX F. Sensibility analysis of the ignition delay	
	correlation.....	233
	APPENDIX G. Routines performed in MATLAB software	237

1 INTRODUCTION

Human development is strongly related to the availability of energy sources. Since the 18th century, mineral fuels such as coal and oil have been the main energy sources. These fuels are non-renewable, their exploration and transportation pose threats to the environment, and their burning produces emissions of CO₂ and nitrous oxides, considered as greenhouse gases, among other pollutant emissions. These emissions have contributed to global climate changes and environmental pollution.

As a consequence of the global effort to reduce the use of fossil fuels, renewable and sustainable sources, such as wind, solar, biomass, and biofuels have increased in importance and economic share. Vegetable oils are a possible alternative feedstock for biofuels for the energy, agriculture, industrial and transportation sectors. They can be transformed in biodiesel and bio-jet fuels using transesterification processes, at an increase of cost and complexity. On the other hand, it is also possible to use the vegetable oils as fuels for compression ignition engines in their raw state, thus reducing cost and increasing availability in oil producing remote areas. This work focuses on the use of straight vegetal oils and their blends with diesel oil as fuels for compression ignited internal combustion engines for transportation and decentralized electrical energy generation.

1.1 MOTIVATION

Biomass is an interesting feedstock for energy production in countries such as Brazil, which presents availability of land for energy crops and favorable climatic conditions. Depending on climate, soil conditions and tradition, different studies on the performance of diesel engines fueled with different vegetable oils or biodiesel produced from vegetable oils or animal fat were developed. For example, soybean oil in the USA, rapeseed and sunflower oils in Europe, palm, jatropha and coconut oils in Asia (AGARWAL, 2007). In Brazil, soybean, palm and castor oils have been studied as fuels for internal combustion engines. Soybean and palm are the vegetable oils with the largest productions, while castor oil is a non-edible oil with a relatively large productivity.

The studies related to the use of biofuels are based on tests on dynamometric bench and thermodynamic analysis of the engine performance fueled with the alternative fuel. Differences in the physico-chemical properties of the vegetable oils in comparison with diesel fuel are the main technological challenge. Large molecular structure, high

viscosity and low volatility of the vegetable oils influence significantly the atomization and combustion processes (AGARWAL; KUMAR; AGARWAL, 2008). In order to approximate the physical properties to that of diesel oil at room temperature, technical literature shows the heating and blending with diesel oil as alternatives for using vegetable oils, finding promising results and comparable performance with diesel oil. In spite of the favorable performance results, it is necessary to know how combustion in fact occurs and how it could be improved. Consequently, one finds researches focusing on the spray development of vegetable oils, the combustion process and the emissions formation (RAKOPOULOS; ANTONOPOULOS; RAKOPOULOS, 2006; DAHO *et al.*, 2013; VALLINAYAGAM *et al.*, 2013; QI *et al.*, 2014).

In this context, in the P&D ANEEL project developed in the Laboratory of Combustion and Thermal Systems Engineering (LabCET/UFSC) (HARTMANN *et al.*, 2012), three vegetable oils were tested on dynamometric bench: soybean, sunflower and tung oils. Additionally, blends of 50/50 % v/v vegetable and diesel oils were also tested and the results compared to diesel fuel. The results are reported on the master thesis Garzón (2012). In that work were shown the experimental results and the thermodynamic analysis of the engine performance fueled with three fuels: soybean oil, diesel oil and the blend 50/50 % v/v soybean and diesel oils. Thermodynamic analysis was based on the control volume defined by the engine. The analysis was carried out for an engine speed of 1800 rpm, aiming the use of the engine in an electric generator of 4 poles, 60 Hz. A similar behavior among the three fuels was found in relation to exergetic efficiency and the destroyed exergy. Soybean oil and the corresponding blend were heated, making feasible their use in the diesel engine.

Aiming to continue the study related to the applicability of the soybean oil as an energetic alternative for diesel engines and to understand the combustion process, new tests were carried out, now also measuring the pressure in the combustion chamber. The experimental pressure reading was used to calculate the heat release rate according to an approach zero-dimensional found in the technical literature. The heat release rate shows a better understanding of the phenomenon concerning the burning of soybean oil blends, supporting the development of a combustion model to be considered in the modeling of the engine performance. The modeling is a useful tool for studying different variables on the combustion of vegetable oils, and important in the performance analysis and optimization for using in diesel engines. Here,

the soybean oil was chosen for this study because its availability in the Brazilian market.

Despite a large number of works concerning the estimation of heat release rates using vegetable oils, there are just few results related to burning models of vegetable oils and, the combustion parameters for blends of diesel and soybean oils are not available in the literature. Therefore, this work will apply a zero-dimensional model with a Wiebe function as a combustion model for the operation of a direct injection diesel engine fueled with diesel and soybean oils heated blends.

1.2 OBJECTIVES

1.2.1 General objective

The main objective of this thesis is to perform a theoretical and experimental analysis of the combustion of soybean oil blends used as fuel in a direct injection diesel engine, evaluating the influence of the physico-chemical properties of the blends on the combustion process and the engine performance, using a zero-dimensional thermodynamic model.

1.2.2 Specific objectives

In order to achieve the general objective, the following specific objectives were proposed:

1. To determine the physico-chemical properties of the soybean and diesel oils.
2. To instrument the dynamometric bench available at the laboratory, in order to obtain the experimental pressure data of the combustion chamber.
3. To determine the heat release rate from experimental pressure data of the engine operation with diesel oil and soybean oil blends.
4. To fit the experimental results of heat release rates to a combustion model based on the Wiebe function.
5. To obtain correlations of the combustion parameters of the Wiebe function involving the properties of the fuels tested.
6. To develop a zero-dimensional thermodynamic model of the complete cycle of the diesel engine using the correlations obtained for the combustion process.

7. To evaluate of the engine performance with different soybean oil blends.

1.3 MAIN CONTRIBUTIONS

The main contributions of this work are:

1. The measurement and correlation of physico-chemical properties of the fuel blends as a function of temperature and volumetric fraction of soybean oil.
2. The development of Wiebe function models for the energy release correlating the parameters with physical properties of the fuel and in-cylinder gas, such as the Sauter mean diameter, gas Weber number and the volume fraction of vegetable oil. This strategy favors the understanding of the physical and chemical phenomena during combustion of the soybean oil blends in diesel engines.
3. The development of an ignition delay correlation that involves the geometric characteristics of the injector nozzle, fuel properties and in-cylinder gas properties.

Finally, the approach proposed may also support the combustion analysis of other engines and vegetable oils used in diesel engines for transport or industrial applications.

1.4 THESIS OVERVIEW

The Chapter 1 presents the main scope and the objectives of this work, focusing on the application of vegetable oils in diesel engine.

The Chapter 2 addresses the literature review about the topics covered in this research.

The geometrical characteristics of the diesel engine and the zero-dimensional thermodynamic analysis of the combustion chamber are presented in Chapter 3.

The experimental method is described in Chapter 4. The physico-chemical properties of the fuels tested as well as correlations of these properties as a function of the temperature and volume fraction of vegetable oil in the binary blend are presented. Additionally, the experimentation on the dynamometric bench, the pressure acquisition of the combustion chamber, an approach of post-processing of pressure measurements for obtaining the heat release rate and the uncertainties of the measurements are also presented.

The Chapter 5 presents a combustion model based on the Wiebe function, and the modeling of the complete engine cycle, operating with soybean oil blends.

The analysis and discussion of the results are presented in Chapter 6, emphasizing the experimental pressure data, the heat release rate and the thermodynamic modeling of the engine.

Finally, the Chapter 7 presents the conclusions and the suggestions of future work.

2 BACKGROUND AND LITERATURE REVIEW

Several studies on the applicability of vegetable oils or biodiesel have been conducted in recent decades in order to become feasible their use for diesel engines. Technical literature has demonstrated that differences in the molecular structure influence on the physico-chemical properties which significantly affect the spray pattern of the fuel, and as consequence, the combustion development and engine performance (AGARWAL, 2007; D'ALESSANDRO *et al.*, 2016). First studies have focused on engine performance tests, thermodynamic evaluation and emissions. Furthermore, recent studies focus on the evaluation of combustion process as a mechanism to understand the influence of the different physico-chemical properties.

2.1 FUEL PROPERTIES FOR DIESEL ENGINE APPLICATION

The conventional fuel used in compression ignition engines is the diesel oil, which is obtained through petroleum distillation. Thus, it is a fuel of fossil or mineral origin. Fossil fuels are non-renewable sources of energy and result from decomposition of organic matter over millions of years, during which the material is subjected to high pressures, high temperatures, lack of air and presence of certain bacteria (NARBEL; JANSEN; LIEN, 2014).

In Brazil, a recent resolution for regulation of diesel oil establishes a diesel fuel type A without addition of biodiesel and a diesel fuel type B with addition of biodiesel (Resolution ANP N°50, December 23, 2013). Also, according to national regulations, the diesel fuel type B has a volumetric addition of 8 % of biodiesel (Law 13.263, March 23, 2016).

Biofuels are energy sources obtained from cellulosic biomass, vegetable oils or animal fat. For compression ignition engines, liquid biofuels, usually vegetable oils and esters (biodiesel), may be used. Biodiesel is an ester produced by transesterification, i.e. chemical transformation of vegetable oils or animal fats using alcohols and an acidic or basic compound as catalyst. In this context, many countries, including Brazil, develop researches and applications of biofuels.

A fuel for a diesel engine must present appropriate physico-chemical properties to ensure complete combustion and adequate engine performance. Viscosity, density, surface tension, heating value and cetane number are the most important physico-chemical properties in the fuel atomization and the combustion processes.

High viscosity disturbs the injection process (defective atomization), impairing the combustion. On the other side, a low viscosity helps the injection process (proper atomization) and ensures better combustion.

The cetane number is an indicative of the ignition quality of the fuel. For fuels with low cetane numbers, the ignition may occur late, resulting in incomplete combustion, reduced power out, and poor fuel conversion efficiency. For higher cetane number fuels, with shorter ignition delay, ignition occurs before most the fuel is injected, resulting in smoother engine operation because the rates of heat release and pressure rise are controlled by the injection rate and fuel-air mixing. (HEYWOOD, 1988). Diesel oil has a cetane number in the range of 40 to 55, and for biodiesel, the cetane number is in the range of 45 to 65 (LAPUERTA; ARMAS; RODRÍGUEZ-FERNÁNDEZ, 2008). For most vegetable oils, the cetane number is low, between 29 and 43 (BLIN *et al.*, 2013).

2.1.1 Vegetable oils

Vegetables oils are mainly polyunsaturated triglycerides. Thus, the carbonate chain presents double bonds, decreasing the number of hydrogen atoms and therefore their heating value. Vegetables oils present the higher molecular size and structure more complex (branched) when compared to the diesel fuel.

The long carbonate chains in the molecules of the vegetable oils and the unsaturation bonds produce high viscosity and lower volatility (RAKOPOULOS *et al.*, 2006; AGARWAL; KUMAR; AGARWAL, 2008). The high viscosity of the vegetable oils causes poor atomization, large droplet size and high spray jet penetration. The jet tends to be a dense stream instead of a suitable spray with small drops. As a result, the fuel is not well distributed or mixed for an adequate burning in the combustion chamber. Additionally, the large molecular size, low heating value and high propensity for carbon depositions can produce poor combustion, loss of power and failure of the mechanical components of the engine (AGARWAL; KUMAR; AGARWAL, 2008; FRANCO; NGUYEN, 2011). Studies to evaluate the applicability of vegetable oils search to approximate their physico-chemical properties to that of diesel oil with the objective of obtaining the atomization pattern and the combustion development appropriated for the operation of a diesel engine.

In recent years, different raw vegetable oils and their blends with diesel oil have been tested as fuel in diesel engines. Hartmann *et al.* (2013) presents a complete list of tests with vegetable oils reported in the technical literature, and it is shown in Table 1. Tests of straight vegetable oils (SVO) by short time periods presented promising results, but problems were found when the diesel engines operated on long periods of time (greater than 100 hours). These problems included injector coking, piston ring sticking, as well as, thickening and gelling of engine lubricating oil (ALMEIDA *et al.*, 2002; RAKOPOULOS *et al.*, 2006). These problems are also attributed to high viscosity, low volatility and combustion chemistry, due to different chemical structure of the vegetable oils can produce polymerization, pyrolysis and other reactions that affect the durability of the engine (RYAN; DODGE; CALLAHAN, 1984).

Table 1. Tests reported in the literature about diesel engines fueled with raw vegetable oils and their blends with diesel oil.

Common name (Botanical name)	References
Edible Oils	
Soybean (<i>Glycine max</i>)	Altin <i>et al.</i> (2001); Engelman <i>et al.</i> (1978); Pryor <i>et al.</i> (1983).
Rapeseed (<i>Brassica napus</i>)	Bialkowski <i>et al.</i> (2005); Hazar and Aydin (2010); Kleinova <i>et al.</i> (2009); Nwafor (2003); Peterson <i>et al.</i> (1983); Yilmaz and Morton (2011).
Palm (<i>Elaeis guineensis</i>)	Almeida <i>et al.</i> (2002); Antwi (2008); Bari and Roy (1995); Belchior and Pimentel (2005); Sapaun <i>et al.</i> (1996).
Coconut (<i>Cocos nucifera</i>)	Antwi (2008); Kalam <i>et al.</i> (2003); Machacon <i>et al.</i> (2001).
Cottonseed (<i>Gossypium hirsutum</i> and <i>Gossypium herbaceum</i>)	Altin <i>et al.</i> (2001); Rao and Mohan (2003); He and Bao (2005); Fontaras <i>et al.</i> (2007); Sarada <i>et al.</i> (2010); Balafoutis <i>et al.</i> (2011); Martin and Prithviraj (2011).
Corn (<i>Zea mays</i>)	Altin <i>et al.</i> (2001).
Olive (<i>Olea europaea</i>)	Rakopoulos <i>et al.</i> (2011).
Sunflower (<i>Helianthus annuus</i>)	Altin <i>et al.</i> (2001); Karaosmanoglu <i>et al.</i> (2000); Maziero <i>et al.</i> (2007); Yilmaz and Morton (2011).
Peanut (<i>Arachis hypogaea</i>)	Barsic and Humke (1981); Yilmaz and Morton (2011).

Common name (Botanical name)	References
Safflower (<i>Carthamus tinctorius</i>)	Bettis <i>et al.</i> (1982); Isigigur <i>et al.</i> (1993).
Sesame (<i>Sesamum indicum</i>)	Öner and Altun (2009).
Rice bran (<i>Oryza sativa</i>)	Agarwal (2007); Bari and Roy (1995); Raghu <i>et al.</i> (2011).
Linseed (<i>Linum usitatissimum</i>)	Agarwal (2007).
Poppy seed (<i>Papaver somniferum</i>)	Aksoy (2011).
Mahua (<i>Madhuca longifolia</i>)	Pugazhvidivu and Sankaranarayanan (2010).
Neem (<i>Azadirachta indica</i>)	Sivalakshmi and Balusamy (2011).
Nonedible Oils	
Castor seed (<i>Ricinus communis</i>)	Prasad <i>et al.</i> (2009).
Pongam (or indian beech, karanja, honge) (<i>Pongamia pinnata</i>)	Agarwal and Rajamanoharan (2009); Belagur <i>et al.</i> (2009).
Tobacco seed (<i>Nicotiana tabacum</i>)	Giannelos <i>et al.</i> (2002).
Tung (<i>Aleurites fordii</i>)	Chang and Wan (1947).
Jatropha (<i>Jatropha curcas</i>)	Agarwal and Agarwal (2007); Antwi (2008); Chalatlou <i>et al.</i> (2011); Chauhan <i>et al.</i> (2010); Forson <i>et al.</i> (2004); Kumar <i>et al.</i> (2003); Pramanik (2003); Wang <i>et al.</i> (2010).

Source: Adapted from Hartmann *et al.* (2013).

Altin, Çetinkaya and Yücesu (2001) observed that the high viscosity, the oxidation and the thickening of the vegetable oils in cool conditions, caused problems in the flow and atomization, as well as the emission of weigh particles. Table 2 shows the main problems in the operation of diesel engines with vegetable oils as presented by Harwood (1984). According to the technical literature, in order to get similar physico-chemical properties of straight vegetable oils to that of diesel oil, the following procedures are commonly used: heating, mixtures in small proportions with diesel oil, microemulsions with methanol or ethanol and chemical transformations in biodiesel (HARWOOD, 1984; AGARWAL; KUMAR; AGARWAL, 2008). Although easier in case of the physical properties (viscosity, density and surface tension), differences in the chemical properties can persist with significant influence in the combustion process. In this context, further studies regarding the effect of the chemical properties on the combustion process are still required.

Table 2. Problems for using straight vegetable oils in diesel engines.

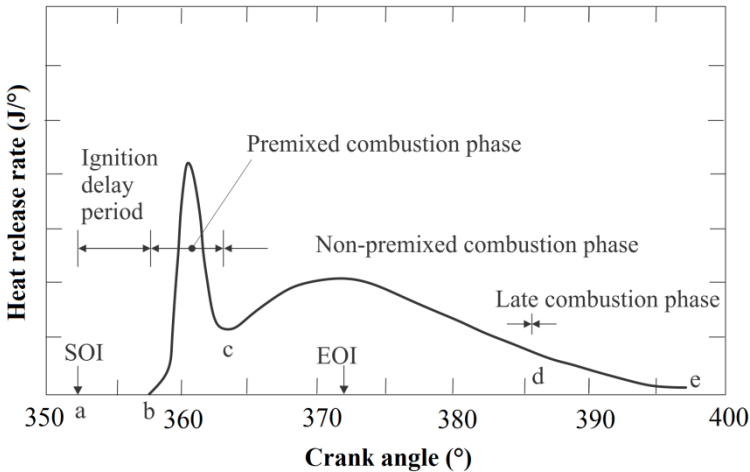
Problem	Probable cause	Potential solution
Low - term		
Cold weather starting.	High viscosity, low cetane, and low flash point of vegetable oils.	Preheat fuel prior to injection. Chemically alter fuel of an ester.
Plugging and gumming of filters, lines and injectors.	Natural gums (phosphatides) in vegetables oil. Other ash.	Partially refine the oil to remove gums. Filter oil to 4 μm .
Engine knocking.	Very low cetane of some oils. Improper injection timing.	Adjust injection timing. Use higher compression engines. Preheat fuel prior to injection. Chemically alter fuel of an ester.
Long - term		
Coking of injector nozzles.	High viscosity of vegetable oil. Incomplete combustion of fuel. Poor combustion at part load with vegetable oils.	Heat fuel prior injection. Switch engine to diesel fuel when operating at part load. Chemically alter the vegetable oil to an ester.
Excessive engine wear.	High viscosity of vegetable oil. Incomplete combustion of fuel. Poor combustion at part load with vegetable oils. Possibly free fatty acids in vegetables oil. Dilution of engine lubricating oil due to blow-by of vegetable oil.	Heat fuel prior injection. Switch engine to diesel fuel when operating at part load. Chemically alter the vegetable oil to an ester. Increase motor oil changes, Motor oil additives to inhibit oxidation.
Failure of engine lubricating oil due to polymerization.	Collection of polyunsaturated vegetables oil blow-by in crankcase to the point where polymerization occurs.	Heat fuel prior injection. Switch engine to diesel fuel when operating at part load. Chemically alter the vegetable oil to an ester. Increase motor oil changes, Motor oil additives to inhibit oxidation. Use vegetables oils low in polyunsaturated.

Source: Harwood (1984).

2.2 COMBUSTION PARAMETERS

The combustion process of an engine consists of four phases: ignition delay, premixed combustion, non-premixed combustion (diffusive or mixing-controlled combustion) and last combustion. These phases are shown in the curve of heat release rate (HRR) as a function of the crank angle θ , as presented in Figure 1.

Figure 1. Combustion phases of a diesel engine.



Source: Adapted from Heywood (1988).

Ignition delay period corresponds to the time between the start of injection (SOI) and the start of ignition. In the period of the premixed combustion, the fuel-air mixture that reached its limits of flammability during the ignition delay period, burns rapidly, resulting in a high heat release rate (maximum point of the curve presented in the Figure 1). In the non-premixed combustion, the burning is governed by the rate of formation of flammable mixture, and is influenced by the fuel atomization, vaporization, fuel vapor-air mixture and ignition reactions. From this point, in the last combustion phase, the burning rate decreases progressively. That corresponds to the burning of a small fraction of fuel that did not yet burn. Temperature reduces during the expansion stroke and the chemical kinetics of reactions is decelerated.

The premixed combustion phase is very important in the combustion process. This is strongly influenced by the engine speed,

load and injection, mainly by the quantity of fuel injected during the ignition delay. The non-premixed combustion phase is governed for the turbulence in the cylinder as a result of the movement of air and the fuel injected (KUMAR; CHAUHAN; VARUN, 2013).

The engine performance is directly associated to the combustion process, taking into account different parameters such as ignition delay, heat release rate, maximum pressure, combustion duration and maximum temperature.

The ignition delay is related to previously physical and chemical effects, very significant for an effective combustion efficiency and the formation of pollutants (AWAD *et al.*, 2013). The physical ignition delay is the time between the start of injection and the attainment of chemical reaction conditions. During this period, the fuel is atomized, vaporized, mixed with air and heated until the ignition temperature. The viscosity dominates this period, which is lower for fuels of low viscosity. Chemical ignition delay is the time of formation of OH radicals that corresponds to the chemical pre-reactions until the ignition (MOLLENHAUER; TSCHOEKE, 2010; SHAHABUDDIN *et al.*, 2013). The ignition delay involves factors, such as fuel type, fuel quality (cetane number), air/fuel ratio, compression ratio, thermodynamic state of air in the cylinder (pressure and temperature), injection pressure, injection angle, swirl of air in the cylinder and piston velocity (MOLLENHAUER; TSCHOEKE, 2010; SAYIN; GUMUS; CANAKCI, 2012). This parameter can be determined from the experimental measurement of the in-cylinder pressure and fuel injection rate in respect to crank angle.

The start of combustion can be determined using methods found in the literature. A method uses the curve of the second derivative of the pressure as a function of the crank angle. At the start of combustion, the in-cylinder pressure increases rapidly, representing a minimum point in the curve of the first derivative of the pressure after the injection angle, and therefore, a zero point in the curve of the second derivative of the pressure (REDDY *et al.*, 1993; LATA; MISRA, 2011). The start of combustion can also be determined in the curve of heat release rate, which corresponds to the point where the heat release rate becomes zero and then tends to be positive, after the injection timing (LATA; MISRA, 2011). A method based on the $\log p - \log v$ curve, identifies the start of combustion as the point where the straight line proportion of compression process will start deviating from its path (YOUNG; LIENESCH, 1978). Another method determines the start of combustion as the location of 1 %, 5 % or 10 % of the mass fraction burned (CARR

et al., 2011; TUNKA; POLCAR, 2017). The value estimated as the start of combustion can be different with each method. In this work, the method based on the curve of the second derivative of the pressure as a function of the crank angle was used because it employs the experimental pressure data directly, eliminating the influence of assumptions made for obtaining the heat release rate. Additionally, this method represents a mathematical answer to a physical effect produced in the combustion chamber and it was also used to determine the start of injection (see section 5.2.3).

Injection can be advanced for the vegetable oils or biodiesel when compared to diesel fuel. This can be explained because to differences in the physical properties between these biofuels and diesel oil. The pressure in the pump outlet increases more rapidly when the biofuel is injected as a result of the low compressibility. Additionally, their higher viscosity reduces pump leakages leading to an increase in the injection line pressure (BIALKOWSKI *et al.*, 2005; BENJUMEA; AGUDELO; AGUDELO, 2009; PUHAN *et al.*, 2010). A poor atomization and an inadequate mixture between air and fuel produce the physical ignition delay in the vegetable oils. According to Nwafor and Rice (1996), the advance of the injection timing helps to compensate the effect of the ignition delay. This phenomenon is shown in the work of Canakci, Ozsezen and Turkcan (2009) with preheated crude sunflower oil at 75 °C. The results of the injection and ignition for preheated crude sunflower oil and diesel fuel are presented in Table 3. Due to high viscosity and low volatility of sunflower oil, the maximum in-cylinder pressure decreased slightly in all speed tested. The start of injection for sunflower oil was 1° crank angle (CA), 1.5° CA and 0.75° CA, advanced when compared to diesel fuel at 1000 rpm, 2000 rpm and 3000 rpm, respectively.

Table 3. Results of tests with preheated crude sunflower oil and diesel fuel.

Engine speed (rpm)	Fuel	Maximum pressure (MPa)	Start of injection (°BTC)	Start of ignition (°BTC)	Ignition delay (°)
1000	PBDF	8.68	18.75	13.50	5.25
	PCSO	8.61	19.75	13.25	6.50
2000	PBDF	9.21	20.00	12.75	7.25
	PCSO	9.03	21.50	11.75	9.75
3000	PBDF	10.04	22.00	12.00	10.00
	PCSO	9.94	22.75	10.25	12.50

Source: Adapted from Canakci, Ozsezen and Turkcan (2009).

In the case of vegetable oils, results reported by Canakci, Ozsezen and Turkcan (2009) shows an ignition delay in the range of 1.25° CA to 2.5° CA, higher than for diesel fuel. In the case of mixtures of vegetable oils, Rakopoulos *et al.* (2006) found an ignition delay equal to 1° CA, also higher in comparison to diesel fuel.

The heat release rate represents the rate of heat generation during the fuel combustion, which follows the development of the combustion processes, particularly the premixed and non-premixed phases. In other words, the heat release rate is obtained from the energy conservation equation for the close system phase of the engine cycle (compression and expansion strokes), using the readings of in-cylinder pressure. Then, the heat release rate can be expressed by

$$\frac{dQ_f}{dt} = \frac{\gamma}{\gamma-1} p \frac{dV}{dt} + \frac{1}{\gamma-1} V \frac{dp}{dt} + \frac{dQ}{dt} \quad (2.1)$$

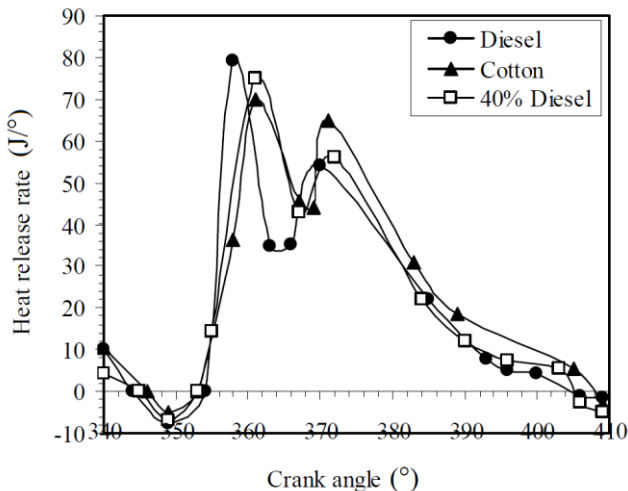
where dQ_f/dt is the heat release rate for the fuel, p is the in-cylinder pressure, V is the cylinder volume, γ is the ratio of specific heats of the gas and dQ/dt is the heat transferred to the wall.

A large number of works related to heat release rate for vegetable oils have been reported in the technical literature. In case of vegetable oils, Leenus, Varuvel and Prithviraj (2011) determined the heat release rate for a diesel engine of direct injection with cotton oil, diesel fuel and different blends, as shown in Figure 2. It is clear that heat release rate is higher for diesel oil due to the premixed combustion phase, what is higher for this fuel. The smaller premixed combustion phase of the cotton oil was influenced for its high viscosity and low volatility that produce poor atomization and reduction of the rate of mixture air–fuel. The combustion of the diffusive phase is higher with cotton oil due to its late combustion. High premixed combustion phase is observed with the addition of diesel oil, because the highest amount of fuel prepared during the period of ignition delay, that lead a high burning of fuel in the initial phase of the combustion.

The maximum in-cylinder pressure has a direct relation with the produced work in the engine cycle. The point corresponding to the maximum pressure refers to a crank angle position in relation to the Top Center (TC). The maximum in-cylinder pressure depends on the combustion rate at the initial combustion phases. Several works related to in-cylinder pressure have been also reported in the technical literature. Leenus, Varuvel and Prithviraj (2011) worked with mixtures

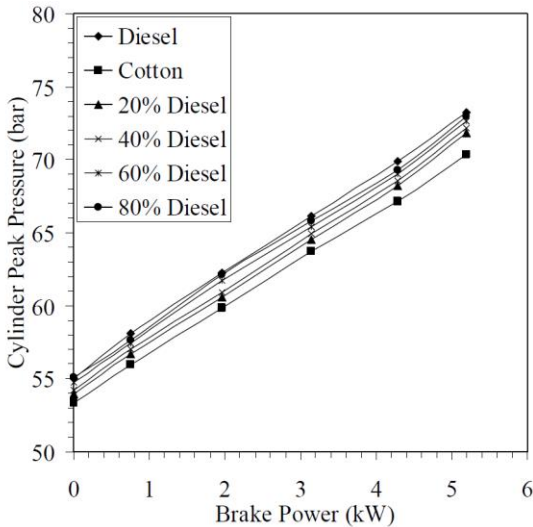
of cotton oil with diesel oil, showing that the more cotton oil amount is, the low the maximum in-cylinder pressure, when compared to diesel fuel (see Figure 3). That is because of a small premixed combustion phase. Similar results were found by Agarwal and Dhar (2013) from tests with mixtures of Karanja oil, observing the influence of the engine load. In case of low loads (low mean effective pressures), no significant differences were observed in the maximum pressure measured. Otherwise, for high loads (high mean effective pressures), lower values were measured in case of vegetable oil blends. The difference in the maximum pressure increases with the increase of the load. The rate of increase of the maximum pressure varied of $3 \text{ bar}/^\circ \text{ CA}$ at low engine loads to more than $6 \text{ bar}/^\circ \text{ CA}$ at high loads. For all loads, the increase rate of the maximum pressure was higher for diesel fuel. A high release of energy in the final phase of the combustion caused a high difference in the maximum pressure at high load of the engine. The angle of the maximum in-cylinder pressure was displaced far from TC position with the increase of the engine load because more amount of fuel must be injected for high load, which takes more time for combustion. This displacement in relation to TC increases with the amount of vegetable oil in the blend, as shown in Figure 4.

Figure 2. Heat release rate of diesel fuel, cotton oil and mixture of 40 % of diesel oil.



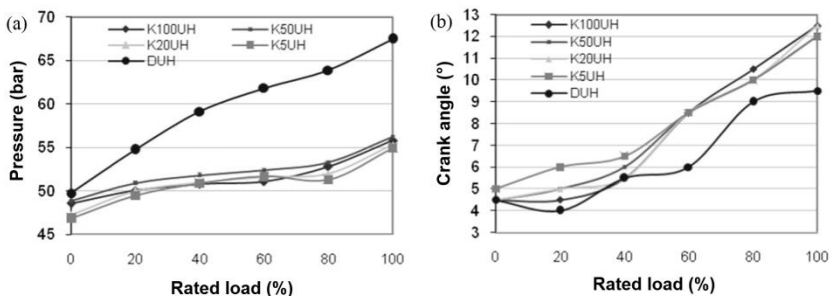
Source: Adapted from Leenus, Varuvel and Prithviraj (2011).

Figure 3. Maximum in-cylinder pressure as a function of the power for tests with diesel oil and blends with cotton oil.



Source: Leenus, Varuvel and Prithviraj (2011).

Figure 4. (a) Maximum in-cylinder pressure. (b) Angle of maximum pressure as a function of the load for tests with diesel oil and blends with Karanja oil.



Source: Adapted from Agarwal and Dhar (2013).

Nwafor and Rice (1996) tested rapeseed oil and blends of 25 %, 50 % and 75 % v/v with diesel oil in an engine diesel. The maximum pressure was measured for diesel oil. In case of blends, the maximum pressure decreases as a consequence of the rapeseed oil chemical and physical characteristics. Engine knocking problem was observed in case

of partial loads using rapeseed oil and blends, because of the high ignition delay and the low in-cylinder temperature. For rapeseed oil, a low premixed combustion phase was observed in consequence of the low heat release rate.

The combustion duration is defined as the angular interval between the start of combustion and end of combustion. Maximum in the cumulative heat release can be defined as the end of combustion (LATA; MISRA; MEDHEKAR, 2011). Another approach specifies as end of combustion, the time of 90 % of mass fraction burned (ALAGUMALAI, 2015; MA *et al.*, 2015). In the case of tests with vegetable oils and biodiesel, the combustion duration increases with the addition of the biofuel due to the presence of components with high viscosity and low volatility in comparison to diesel oil, which increases the droplet size. Big droplets with low volatility take more time for mixing and for burning (SAYIN; GUMUS; CANAKCI, 2012; AGARWAL; DHAR, 2013).

Also for rapeseed oil, in the study about the oxygen enrichment in the intake air, the combustion parameters as ignition delay, heat release rate, maximum pressure and temperature in the combustion chamber were determined by Li *et al.* (2013). The emissions and particulates were measured at oxygen concentrations (by volume) from 21 % (no enrichment) to 24 % and compared to diesel results. The oxygen enrichment in the intake air decreased the ignition delay and premixed combustion phase. The in-cylinder peak pressure and temperature increased from 6 % to 9 % in the case that the oxygen concentration increased from 21 % to 24 %, improving the engine efficiency. Particulates reduced significantly (60 % with an increase of 1 % of O₂). Emissions of CO and unburned hydrocarbons were also reduced while the NO_x emissions increased as the oxygen enrichment rate increased (50 % with an increase of 1 % of O₂). The reduction of particulates was attributed to an increase in the soot oxidation, and the reduction of the ignition delay was attributed to the accelerated pre-ignition reactions. Results showed that the oxygen enrichment method can be adequate for the combustion of vegetable oils in diesel engine, reducing CO, hydrocarbon emission and particulates.

Daho *et al.* (2013) studied the combustion of cotton oil and diesel fuel at 2500 rpm and at three condition loads: 25 %, 50 % and 100 %. The premixed combustion phase was more significant for the loads of 25 % and 50 %. At full load, the combustion was more diffusive. The premixed combustion was lower for cotton oil at the mentioned three loads tested. The ignition delay reduced with the increase of the load. At

low load (25 %), the in-cylinder temperature was less favorable for the decomposition and evaporation of the cotton oil, resulting in a higher ignition delay. At loads of 50 % and 100 %, the in-cylinder temperature was adequate for evaporation and decomposition, breaking the components of low molecular weight, and reducing the ignition delay.

2.3 INJECTION PARAMETERS

The fuel injection system is a fundamental system for the operation of diesel engines. The parameters that define the fuel injection system are:

- Injection timing. It is the instant of starting of the main fuel injection, specified in crank angle and taken as reference the piston position in relation to TC.
- Injection pressure. It is the fuel pressure during its injection related to the opening pressure of nozzle needle. The injection pressure has an important effect on the combustion parameters and the performance of the compression ignition engine (SAYIN; GUMUS; CANAKCI, 2012). The fuel injection system is characterized by the injection pressure. Mechanical systems of fuel injection work with injection pressures about of 20 MPa (200 bar). In the case of electronic systems of fuel injection, the injection pressure reaches values among 100 MPa (1000 bar) or 200 MPa (2000 bar).
- Fuel injection rate. It corresponds to the fuel amount injected into the combustion chamber, expressed in mg/injection.

In the evaluation of the diesel engine operation with alternative fuels, the injection pressure and the injection timing changing provide different responses in the performance, showing opportunities of using vegetable oils or biodiesel in diesel engines.

The effect of the injection pressure was reported by Sayin, Gumus and Canakci (2012), who tested blends of rapeseed biodiesel with diesel oil at 18, 20, 22 and 24 MPa. For all fuels tested, the increase of the injection pressure decreased the ignition delay and increased the maximum rate of pressure rise. High pressure rise rates mean high proportion of fuel injected that burns on the premixed combustion phase, therefore, high maximum pressure in the cylinder.

In the work of Agarwal and Dhar (2013), the authors concluded that blends with low concentration of karanja oil (up to 20 %) can be used directly in unmodified diesel engines. They observed that a small amount of karanja oil in the blend alters significantly the in-cylinder

combustion process, due to changes in the fuel atomization and the fuel-air mixing process. For proportions greater than 20 % of karanja oil, the authors suggest modifications in the engine, optimizing the injection timing and preheating the mixtures.

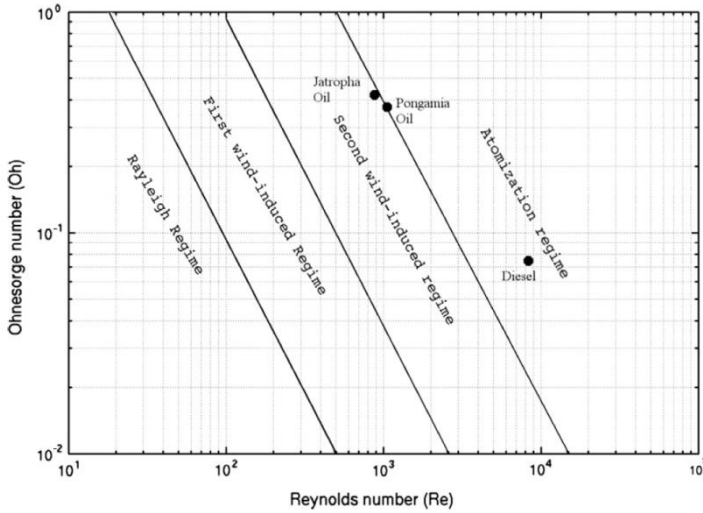
Wander *et al.* (2011) tested soybean oil blends changing $\pm 2^\circ$ CA the original injection timing of the engine. The authors noted that a moderate advance of the injection timing is adequate for low-speed operations such as agricultural applications.

In case of alternative fuels, parametric studies are commonly used to analyze the influence of the injection parameters and to optimize the operation of the engine. Reddy and Ramesh (2006) tested a direct injection diesel engine operated with *Jatropha* oil. The injection timing, injector opening pressure, injection rate and air swirl level were changed to study their influence on performance, emissions and combustion. In the case of *jatropha* oil, the thermal efficiency increased with a reduction in the emissions of hydrocarbons and particulate matter when the injection timing is advanced 3° CA. The increase of the injection pressure from 205 bar to 220 bar improved significantly the performance, emissions and heat release characteristics. A reduction in the ignition delay was also observed, probably, as a consequence of better spray formation.

The jet pattern is a significant factor in the combustion process. It is influenced by the injection parameters and the physical properties of the fuel. The primary disintegration or break-up regime of the fuel jet in diesel engines must be the atomization regime. Further information on the break-up regimes (Ohnesorge diagram), the atomization process and the spray structure are shown in APPENDIX A.

The physical properties influence significantly on the break-up regime as defined in the Ohnesorge diagram through the dimensionless numbers of Reynolds, Weber and Ohnesorge. With injection parameters defined, each fuel will present characteristics of spray and, therefore different parameters of combustion and engine performance. In this context, Deshmukh *et al.* (2012) studied the spray characteristics of two vegetable oils injected at 60°C , *jatropha* oil and *pongamia* oil, comparing the spray regime with the diesel oil injected at 30°C . It can be observed in Figure 5 that the *jatropha* oil and the *pongamia* oil did not present an atomization regime suitable for operation in diesel engines.

Figure 5. Ohnesorge diagram with the break-up mechanisms of diesel, jatropha and pongamia oils.



Source: Adapted from Deshmukh *et al.* (2012).

Daho *et al.* (2013) studied the drop size distribution of cottonseed oil, diesel oil and blends of 20 %, 40 %, 60 % and 80 % v/v at temperature between 25 and 30 °C. Table 4 shows the results of the Sauter Mean Diameter (SMD) obtained for the cottonseed oil blends. For high percentages of cottonseed oil in the blend (> 80 %), the behavior of the blend was similar to pure vegetable oil, presenting a droplet size distribution greater than that suitable for diesel engines. The proportion of large droplets increased with the cotton oil due to the kinematic viscosity and surface tension increase, which is unfavorable for complete evaporation in the combustion chamber, especially at low engine load. Results observed in the evaporation showed that mixtures with moderate proportion of cotton oil (≤ 40 %) produce good evaporation.

Table 4. Sauter mean diameter for blends of cotton and diesel oils.

Fuel*	SMD (μm)
Diesel	20.68
CSO20	24.09
CSO40	28.45
CSO60	35.66
CSO80	57.84
CSO100	75.63

*CSOXX represents a blend with XX percentage of cottonseed oil.

Source: Adapted from Daho *et al.* (2013).

2.4 PERFORMANCE PARAMETERS

Performance of a diesel engine is evaluated using some parameters as torque, power, mean effective pressure, specific fuel consumption, thermal efficiency, volumetric efficiency and mechanical efficiency. Basic concepts about these performance parameters are presented in technical literature related to internal combustion engines such as Obert (1971), Taylor (1985) and Heywood (1988).

Engine torque is measured by tests on dynamometric bench. In this bench, the engine is coupled to the dynamometer rotor and a load cell measures the force resulting on the dynamometer stator. The torque exerted on the stator is calculated from this force and the distance to the rotation center. The power delivered by the engine is the product of torque and angular speed. The torque and power measured by tests on dynamometric bench are called as brake torque T_b and brake power P_b , respectively.

Gas pressure exerted on the piston head produces the indicated work. Integrating around the pressure-volume curve, the net indicated work per cycle W_i is obtained as

$$W_i = \oint p(V) dV \quad (2.2)$$

The indicated power per cycle P_i is calculated from W_i by

$$P_i = \frac{W_i N}{n_R} \quad (2.3)$$

where n_R is the number of crankshaft revolutions for each power stroke and N is the engine speed expressed in rps.

In the engine operation, part of indicated power is used to overcome the friction of the mechanical components of the engine, and to drive the engine accessories. The ratio of brake power and indicated power is called as mechanical efficiency η_m .

A useful engine performance measure is the mean effective pressure $imep$, used for design calculations and to compare engines. This measure represents a theoretical pressure that if applied on the piston during the expansion stroke, it will produce the indicated work per cycle. Therefore, $imep$ is obtained by dividing the work per cycle by the cylinder volume displaced V_d per cycle. Then,

$$imep = \frac{P_i n_R}{V_d N} \quad (2.4)$$

The fuel consumption is measured as the fuel mass per unit time \dot{m}_f . A more useful parameter is the specific fuel consumption sfc , being the fuel flow rate per unit power output. It measures how efficiently an engine is using the fuel supplied to produce work

$$sfc = \frac{\dot{m}_f}{P_b} \quad (2.5)$$

Characteristic curves of torque, power and specific fuel consumption are plotted as a function of speed or load when engines are tested on dynamometric bench. Other important parameters are the thermal efficiency and volumetric efficiency of the engine.

Thermal efficiency or fuel conversion efficiency represents the ratio of the work produced per cycle to the amount of fuel energy supplied by the fuel. The thermal efficiency η is calculated as

$$\eta = \frac{P_b}{\dot{m}_f LHV} \quad (2.6)$$

where LHV corresponds to the lower heating value of the fuel.

Volumetric efficiency measures the effectiveness of the induction process of an engine because some elements of the intake system can

restrict the amount of air intake. Volumetric efficiency is defined as the ratio of the mass of air inducted into the cylinder per cycle and the mass of air of the volume displaced by the piston. Then,

$$\eta_v = \frac{m_a}{\rho_a V_d} \quad (2.7)$$

where η_v is the volumetric efficiency and m_a and ρ_a represent the mass and density of the air inducted into the cylinder, respectively.

Concerning tests with vegetable oils and diesel oil, several works of the technical literature report reduction of torque and power using vegetable oils due to their lower *LHV* which is partly compensated by the density increase. Furthermore, it is found an increase in brake specific fuel consumption with efficiency reduction or comparable efficiency to the performance with diesel oil. However, some results that contrast these trends are also found when performance parameters are compared. These results may be motivated by different engine technologies, operating conditions and fuel quality among different studies (CAPUANO *et al.*, 2017).

2.5 MODELING OF DIESEL ENGINES

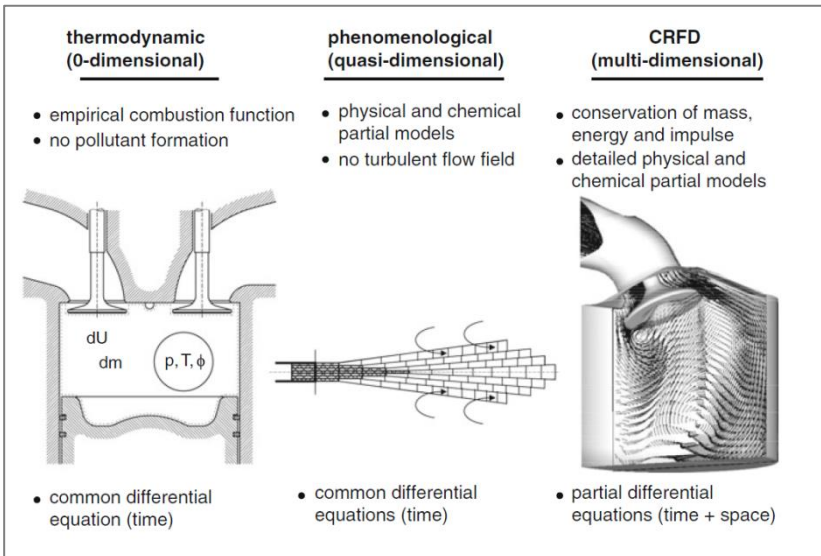
The mathematical modeling of the combustion process helps the understanding of the physical and chemical phenomena, reducing test time and costs. By using simulation tools, the influence of different parameters or design characteristics on engine performance can be observed, in order to guide the experimental work (SILVA, 1993).

Thermodynamic models have been effective tools to analyze the engine performance and its sensitivity to several operation parameters (RAKOPOULOS; GIAKOUKIS, 2006). The theoretical models used in internal combustion engines can be classified into two main groups: thermodynamic models and fluid dynamics models (HEYWOOD, 1988; RAMADHAS; JAYARAJ; MURALEEDHARAN, 2006; AWAD *et al.*, 2013; KUMAR; CHAUHAN; VARUN, 2013). The thermodynamic models are based on the energy conservation equation and are used to analyze the performance characteristics of the engine, evaluating the properties as a function of the crank angle or time. Fluid dynamics models are based on the numerical solution of the conservation equations of mass, energy, momentum and chemical species, providing

detailed information about the flow. These models are also known as multidimensional models.

In general, the modeling of internal combustion engines can be classified as zero-dimensional, quasi-dimensional and multidimensional (LAKSHMINARAYANAN; YOGESH, 2010). Figure 6 shows a short summary of each modeling.

Figure 6. Characteristics of current models used in diesel engines.



Source: Adapted from Stiesch; Eckert and Rakowski (2012).

2.5.1 Thermodynamic models

The thermodynamic models can be classified in two subgroups: single zone model and multizone model. Additionally, a thermodynamic model can also be qualified as a zero-dimensional model and a quasi-dimensional model. Some basic characteristics of this classification according to Heywood (1988) are:

- Zero-dimensional: absence of any flow modeling and the geometric features of the flow cannot be predicted.
- Quasi-dimensional: additional information is specified as the diesel fuel spray shapes and some relations that describe physical or chemical phenomena.

2.5.1.1 Zero-dimensional modeling

In the zero-dimensional modeling, the gas mixture in the combustion chamber is considered homogeneous, without gradients of temperature, pressure and concentration of chemical species (AWAD *et al.*, 2013). The time is the only independent variable. It is assumed that the injected fuel vaporizes, mixes and reacts instantaneously in the combustion chamber. So there are not considered phenomena such as evaporation of droplets, penetration of air inside the fuel spray and pre-flame reactions (KUMAR; CHAUHAN; VARUN, 2013). The thermodynamic properties of the fluid are determined as a function of time.

The zero-dimensional modeling can be validated through a direct method or an indirect method (REDDY *et al.*, 1993). The direct method is based on the measurement of flame position versus time. This method requires the modification of the combustion chamber with the installation of quartz windows and the use of high speed camera. The indirect method is based on measurements of in-cylinder pressure. The in-cylinder pressure readings corresponding to a working cycle are used to calculate the apparent heat-release rate. In the opposite way, the in-cylinder pressure can be estimated from a combustion submodel that estimates the heat release rate. The parameters of the combustion submodel are adjusted based on previous experimental data.

2.5.1.2 Quasi-dimensional modeling

The quasi-dimensional modeling is an intermediate-complexity modeling, offers more complete results than zero-dimensional models and requires less computational capability than multidimensional models. In this modeling, physical or chemical submodels are included to describe phenomena such as spray formation, air-fuel mixture, fuel injection rate and the formation of chemical species in the emissions of exhaust gases (PARIOTIS; KOSMADAKIS; RAKOPOULOS, 2012). This modeling can be used to study emissions of pollutants, mainly the formation of nitrogen oxides (NO_x), unburned hydrocarbons and particulate matter. It offers fast and efficient calculations based on important parameters such as injection pressure, injection timing, swirl ratio and intake pressure (LAKSHMINARAYANAN; YOGESH, 2010).

In quasi-dimensional modeling, the cylinder gases can be subdivided into two basic zones: zone of burned gases (combustion products) and zone of unburned gases. The two zones are considered as

two thermodynamic systems with interactions of heat and mass among the zones and their surroundings. Requirements or controls in the formation of pollutants have motivated the development of more complex models such as four zones or multi-zones, which provide more precision and flexibility to study complex phenomena such as the formation of nitric oxide and particulate matter in the cylinders of engine (RAKOPOULOS; GIAKOUMIS, 2006).

2.5.2 Multidimensional model

The multidimensional models are also known as fluid dynamics models or CRFD (Computational Reactive Fluid Dynamics) models. Multidimensional modeling is based on the local solution of the conservation equations that govern the fluid (mass, energy and momentum), describing the physical phenomena as a function of the space and the time. This modeling includes submodels for the spray formation and combustion phenomenon. It uses a numerical solution, providing geometric information of the flow up to three dimensions. CRFD models are also used to study the internal mechanism of the diesel jet and flame propagation in the combustion chamber (RAMADHAS; JAYARAJ; MURALEEDHARAN, 2006).

2.5.3 Submodels used in internal combustion engines

The main submodels used for modeling a diesel engine are here presented, including processes such as combustion, ignition delay and heat transfer.

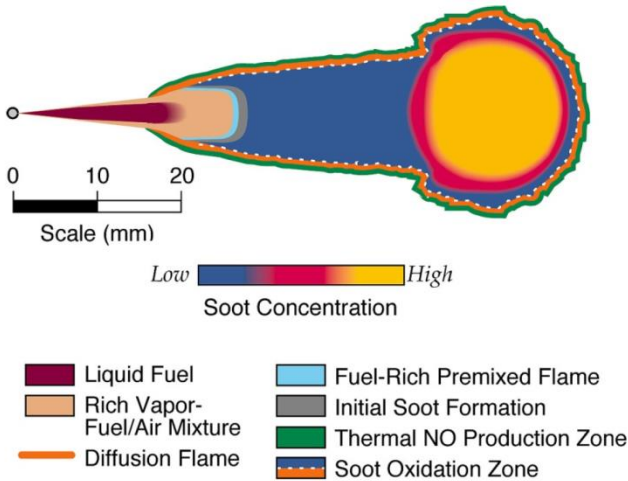
2.5.3.1 Combustion

The combustion submodels are basically required for determining the fuel burning rate. Different combustion submodels for internal combustion engines have been developed to study engine performance and the formation of pollutants.

In relation to diesel spray combustion, Dec (1997) proposed a conceptual model based on laser-sheet imaging, evidencing the actual development of the combustion phases. Figure 7 shows a schematic of this diesel spray combustion model. The combustion during the premixed burn occurs under fuel-rich conditions (equivalence ratios of 2 - 4), and that this premixed combustion leads to the initial soot formation. Soot occurs throughout the jet cross-section. The soot

appears just downstream of the liquid-fuel region and grows in size and volume fraction as it flows downstream, eventually being oxidized at the diffusion flame, which appears only around the jet periphery. The fuel undergoes rich premixed combustion prior to reaching the diffusion flame (DEC, 1997).

Figure 7. A schematic of the diesel spray combustion model proposed by Dec (1997).

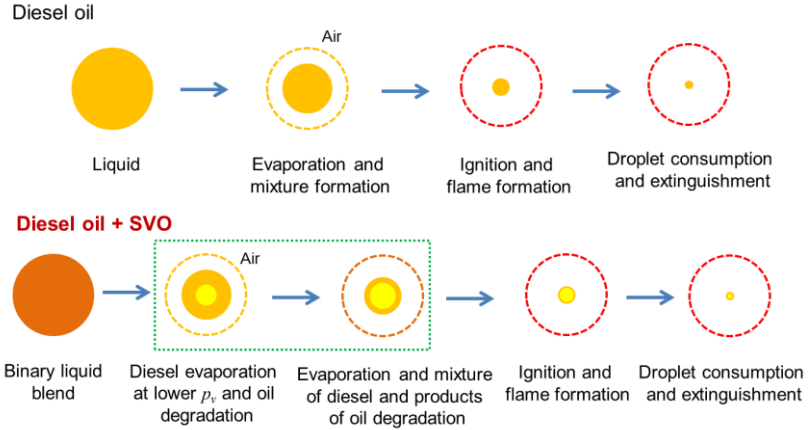


Source: Adapted from Flynn *et al.* (1999).

Regarding droplet combustion, Figure 8 shows a schematic of a conceptual model proposed for the combustion of a diesel oil droplet and a binary liquid blend droplet (diesel oil + straight vegetable oil). This conceptual model is based on the different volatility of diesel oil and vegetable oils. Considering a diesel oil droplet, it heats, evaporates and mixes with surrounding air. The vapor mixture reaches the inflammability limits, ignites and forms the flame. Finally, the droplet is consumed and extinguishes. In the case of a binary liquid blend droplet, the droplet heats, the diesel oil present in the blend, evaporates first, but at lower vapor pressure because the concentration is smaller than one, reducing the evaporation rate. The vegetable oil degrades due to the heating and the products of oil degradation also evaporate. The vapor diesel and products of oil degradation mix with surrounding air. These products of oil degradation can help the ignition or can inhibit the ignition. The gas mixture reaches the inflammability limits, ignites and forms the flame to consume the droplet completely. This

phenomenological explanation considers that the binary liquid blend (diesel oil + straight vegetable oil) presents less volatility than diesel oil and, the heating and evaporation process of vegetable oil is not still known.

Figure 8. A schematic of the phenomenological explanation about the combustion of a diesel oil droplet and a binary liquid blend droplet.



Some combustion submodels for internal combustion engines are presented in Table 5. The Wiebe function is the most common combustion submodel. The Wiebe function is a simplified model of the combustion phenomenon based on the kinetic theory of chemical reactions and chain reactions. Wiebe postulated that the variation in the number of molecules of the main reactants that participate in the effective events of reaction in the time interval is directly proportional to the variation of the number of active centers. The active centers that initiate the effective reactions were denominated by Wiebe as effective centers (GHOJEL, 2010). The Wiebe function is widely used in internal combustion engine to describe the mass fraction burned in the combustion process as an alternative to predict the combustion rate instead of the complicated turbulent reacting flame front calculation (YELIANA *et al.*, 2011). Basically, the Wiebe function is presented as follows

$$X_b = 1 - \exp \left[-a \left(\frac{\theta - \theta_{ig}}{\Delta\theta_{comb}} \right)^{m+1} \right] \quad (2.8)$$

where X_b represents the mass fraction burned of fuel at the instant θ , θ_{ig} corresponds to the angle of ignition starting, $\Delta\theta_{comb}$ corresponds to the combustion duration and the constants a and m are parameters of the Wiebe function. The constant a represents the percentage of fuel burned at the end of the combustion and the constant m represents the order of the overall combustion reaction. The value of the constant a is calculated as a function of the mass fraction burned at the end of combustion (GHOJEL, 2010), according to the following equation,

$$a = -\ln(1 - X_b) \quad (2.9)$$

Table 5. Combustion submodels used in internal combustion engines.

Author	Specialty of model	Remark
Austen and Lyn (1960)	Direct relation between fuel injection pump and heat release rate	Absence of universal constants.
Whitehouse and Way (1969)	Estimation of the preparation rate and reaction rate of fuel.	Diffusion of oxygen in the fuel and reaction based on the Arrhenius equation.
Wiebe (1970)	Exponential decay function with empirical constants	No effect of injection rate and combustion chamber
Shahed <i>et al.</i> (1973) Dent and Mehta (1981) Hiroyasu <i>et al.</i> (1983)	Detailed computation of two-dimensional axisymmetric spray	Engine dependent constant No effect of load and speed
Watson and Pilley (1980)	Exponential function with empirical constants. Rapid premixed combustion phase, slow non-premixed combustion phase that controls the process.	Ignition delay empirically related to each phase of combustion.
Cartillieri and Johns (1983) Gosman <i>et al.</i> (1985)	Three-dimensional finite volume technique	Large volume of calculation
Chmela and Orthaber (1999)	Mixing controlled combustion	No effect of wall impingement

Source: Adapted from Lakshminarayanan and Yogesh (2010).

The heat release rate dQ_f/dt is calculated as

$$\frac{dQ_f}{dt} = LHV \frac{dm_f}{dt} \quad (2.10)$$

where LHV is the lower calorific value of the fuel and dm_f/dt the fuel burning rate, being calculated from the fuel fraction burned,

$$\frac{dm_f}{dt} = m_f \frac{dX_b}{dt} \quad (2.11)$$

m_f is the fuel mass injected per cycle and dX_b/dt is the fuel fraction burned rate. The fuel fraction burned rate is obtained from the derivation as a function of the angle θ of the expression of the mass fraction burned, equation (2.8). Thus,

$$\frac{dX_b}{d\theta} = \frac{a(m+1)}{(\Delta\theta_{comb})} \left(\frac{\theta - \theta_{ig}}{\Delta\theta_{comb}} \right)^m \left\{ \exp \left[-a \left(\frac{\theta - \theta_{ig}}{\Delta\theta_{comb}} \right)^{m+1} \right] \right\} \quad (2.12)$$

and, as a function of time,

$$\frac{dX_b}{dt} = \frac{dX_b}{d\theta} \frac{d\theta}{dt} \quad (2.13)$$

As the original Wiebe function does not adequately reproduce the two peaks of the heat release rate, specifically in the case of direct injection diesel engines, researchers in the late 1960s and early 1970s concluded that the combination of two Wiebe functions would be more suitable for the simulation of heat release in diesel engines. The double Wiebe function consists of two main portions, one portion corresponds to the premixed combustion phase and another corresponds to the non-premixed or diffusive combustion phase. Thus, the fuel fraction burned is expressed as

$$X_b = 1 - X_p \left\{ \exp \left[-a \left(\frac{\theta - \theta_{ig}}{\Delta\theta_p} \right)^{m_p+1} \right] \right\} - X_d \left\{ \exp \left[-a \left(\frac{\theta - \theta_{ig}}{\Delta\theta_d} \right)^{m_d+1} \right] \right\} \quad (2.14)$$

where X_p and X_d represent the mass fraction burned in the premixed and diffusive combustion phases, respectively. Similarly, each portion has a factor m and a duration period of the phase, $\Delta\theta_p$ and $\Delta\theta_d$. The fuel burning rate is expressed as

$$\begin{aligned} \frac{dX_b}{d\theta} = & \frac{a(m_p+1)(\theta - \theta_{ig})^{m_p}}{\Delta\theta_p} \left(\frac{\theta - \theta_{ig}}{\Delta\theta_p} \right)^{m_p} \left\{ \exp \left[-a \left(\frac{\theta - \theta_{ig}}{\Delta\theta_p} \right)^{m_p+1} \right] \right\} + \\ & \frac{a(m_d+1)(\theta - \theta_{ig})^{m_d}}{\Delta\theta_d} \left(\frac{\theta - \theta_{ig}}{\Delta\theta_d} \right)^{m_d} \left\{ \exp \left[-a \left(\frac{\theta - \theta_{ig}}{\Delta\theta_d} \right)^{m_d+1} \right] \right\} \end{aligned} \quad (2.15)$$

Additional information regarding combustion submodels, not considered in this work, is presented in APPENDIX B.

2.5.3.2 Ignition delay

As mentioned in section 2.2, ignition delay is the time between the start of injection and the start of ignition. Current studies regarding fuel injection into environment at constant temperature and pressure have shown that the equivalence ratio, the air temperature and the pressure are important parameters on the ignition delay (HEYWOOD, 1988). Often, the ignition delay is correlated from experimental data using the modified Arrhenius equation,

$$\tau = A_{ig} P^{-n} \phi_{gl}^{-m} \exp \left(\frac{E_a}{RT} \right) \quad (2.16)$$

where τ is the ignition delay, ϕ_{gl} is the global equivalence ratio of the mixture, E_a is the apparent activation energy of the fuel and R is the universal gas constant. The constants A_{ig} , n , m and also E_a are fitted according to the experimental data. A_{ig} is the pre-exponential factor of the equation, and the exponents n and m represent the effect on the

ignition delay of the gas pressure and global equivalence ratio, respectively.

There are different correlations to predict the ignition delay depending on the engine characteristics and the working fluid. The empirical formula proposed by Hardenberg and Hase (1979) to predict the ignition delay in a direct injection diesel engine is widely used in the technical literature and has presented a good agreement with experimental data over different engine operation conditions. The equation of Hardenberg and Hase is expressed as

$$\tau = \left(0.36 + 0.22\bar{S}_p\right) \exp \left[E_a \left(\frac{1}{RT} - \frac{1}{17190} \right) \left(\frac{21.2}{p - 12.4} \right)^{0.63} \right] \quad (2.17)$$

where \bar{S}_p is the mean piston velocity (m/s), p is the charge pressure (bar) and T is the charge temperature (K), taken at TC conditions. The ignition delay is obtained in crank angle degrees, and the apparent activation energy E_a (J/mol) is expressed as a function of the cetane number CN of the fuel,

$$E_a = \frac{618840}{CN + 25} \quad (2.18)$$

2.5.3.3 Heat transfer

In general, the convective and radiative heat transfer are considered in-cylinder gas to the cylinder head, valves, cylinder walls and piston, expressed as

$$\frac{dQ}{dt} = h_c A (T - T_w) + \varepsilon \sigma_{SB} A (T^4 - T_w^4) \quad (2.19)$$

where A is the heat exchange area, h_c is the convective heat transfer coefficient, σ_{SB} is the constant of Stefan-Boltzmann ($\sigma_{SB} = 5.67 \times 10^{-8}$ W/(m²·K⁴)), T is the mean gas temperature, T_w is the mean wall temperature and ε can be considered as an overall emissivity.

The convective heat transfer coefficient h_c is determined using available correlations in the technical literature, obtained from experimental data and fitted according to each case. The found correlations in the literature take into account geometric characteristics

of the engine, fluid properties and fitting constants, representing phenomena that can influence on the convective heat transfer as the turbulence effect and the combustion process.

Annand (1963) proposed a correlation that considers the gas velocity as the average velocity of the piston \bar{S}_p and uses the piston diameter as the characteristic dimension, so that

$$Nu = aRe^b \quad (2.20)$$

$$h_c = a \frac{k_g}{B} Re^b \quad (2.21)$$

$$h_c = a \frac{k_g}{B} \left(\frac{\rho_g \bar{S}_p B}{\mu_g} \right)^b \quad (2.22)$$

where a and b are constants of the model, estimated as $0.35 \leq a \leq 0.8$ and $b = 0.7$ for a normal combustion, B is the cylinder bore, k_g , ρ_g and μ_g are the thermal conductivity, density and dynamic viscosity of gas, respectively. It was observed that the constant a increases with the charge motion and the design characteristics of the engine.

A correlation widely used to calculate the heat-transfer coefficient was reported by Woschni (1979), assuming the Nusselt number defined as

$$Nu = 0.035 Re^m \quad (2.23)$$

In this case, conversely to the previous correlation, Nu and Re numbers are calculated considering the working fluid at velocity w ,

$$\frac{h_c B}{k_g} = 0.035 \left(\frac{\rho_g w B}{\mu_g} \right)^m \quad (2.24)$$

where $\rho_g = p/R_g T$, $k_g \propto T^{0.75}$, $\mu_g \propto T^{0.62}$ and R_g is the gas constant, resulting in the heat-transfer coefficient defined as

$$h_c = C_0 B^{m-1} p^m w^m T^{0.75-1.62m} \quad (2.25)$$

The velocity w changes with the engine stroke. Therefore, the fluid velocity considers the effects of intake, compression, combustion and exhaust, as shown in the following correlation,

$$w = \left[C_1 \bar{S}_p + C_2 \frac{VT_r}{p_r V_r} (p - p_m) \right] \quad (2.26)$$

where V is the displaced volume, p is the instantaneous cylinder pressure, p_m is the motored cylinder pressure at the same crank angle as p , and finally, T_r , p_r and V_r are working-fluid temperature, pressure and volume, respectively, at some reference state (e.g. inlet valve closing). The constants of the equation (2.26) are expressed as

$C_1 = 6.18$	$C_2 = 0$	Admission and exhaust
$C_1 = 2.28$	$C_2 = 0$	Compression
$C_1 = 6.18$	$C_2 = 3.24 \times 10^{-3}$	Combustion and expansion

According to the technical literature, $m = 0.8$, resulting in

$$h_c = 3.26 B^{-0.2} p^{0.8} w^{0.8} T^{-0.55} \quad (2.27)$$

Hohenberg (1979) modified the Woschni correlation to give better predictions of heat fluxes. The modifications include a characteristic dimension \bar{D} based on the instantaneous volume of the cylinder instead of bore B , as well as changes in the effective gas velocity, and in the exponent of the temperature term (HEYWOOD, 1988). The characteristic dimension \bar{D} was defined considering an equivalent sphere with volume equal to the instantaneous volume of the cylinder V ,

$$V = \frac{\pi}{6} \bar{D}^3 \quad (2.28)$$

$$\bar{D} = CV^{0.33} \quad (2.29)$$

where C is a constant. The term $B^{-0.2}$ of equation (2.27) can be expressed as a function of the instantaneous volume as

$$B^{-0.2} = \bar{D}^{-0.2} = CV^{-0.066} \quad (2.30)$$

The effective gas velocity was expressed involving the effects of turbulence, swirl and combustion,

$$w^{0.8} = p^{0.2} T^{0.1} (\bar{S}_p + C_2)^{0.8} \quad (2.31)$$

The product $p^{0.8} T^{-0.55}$ of equation (2.27) was modified based on systematic tests with variations of temperature and pressure, resulting in the Hohenberg equation. The pressure is expressed in bar. Thus

$$h_c = 130V^{-0.06} p^{0.8} T^{-0.4} (\bar{S}_p + 1.4)^{0.8} \quad (2.32)$$

2.6 LITERATURE REVIEW

Innumerable articles are found in the technical literature about the modeling of diesel engine fueled with diesel oil or biofuels obtained from different oleaginous sources. In the case of vegetable oils, the studies based on pressure readings to calculate the heat release rate have increased in the last decade. Nevertheless, there are few works related to specific models for the combustion of blends of vegetable oils in diesel engine.

In Table 6 are shown selected works regarding in-cylinder pressure readings and heat release rates for several pure vegetable oils and blends. Results regarding the performance, emissions and combustion parameters are compared in relation to diesel oil.

In Table 7 are shown a few works found in the literature about modeling of a diesel engine fueled with vegetable oils.

Table 6. Works about tests with vegetable oils obtaining the heat release rate.

Author	Vegetable oil	Country	Remarks
Kumar, Ramesh and Nagalingam (2003)	Jatropha oil	India	Pure jatropha oil test, its biodiesel and a blend of 3:7 volumetric ratio with methanol. Test at different loads and 1500 rpm.
Reddy and Ramesh (2006)	Jatropha oil	India	Parametric study considering: injection timing, injection rate, injection pressure and swirl.
Geo, Nagarajan and Nagalingam (2008)	Rubber seed oil	India	Tests of vegetable oil and its biodiesel in a dual fuel operation with hydrogen at different loads.
Agarwal and Dhar (2010)	Karanja oil	India	Tests with karanja oil heated and unheated at different loads and 1500 rpm.
Geo, Nagarajan and Nagalingam (2010)	Rubber seed oil / Diethyl ether	India	Study on the combustion of an engine fueled with rubber seed oil and injection of diethyl ether at different flow rates (100, 150 and 200 g/h).
Rakopoulos <i>et al.</i> (2010)	Cottonseed oil	Greece	Comparison of the combustion parameters of the engine operation with cottonseed oil and its biodiesel.
Leenus, Varuvel and Prithviraj (2011)	Cotton seed oil	India	Test of blends with 20 %, 40 %, 60 %, 80 % and 100 % of cottonseed oil.
Kasiraman, Nagalingam and Balakrishnan (2012)	Cashew nut shell oil / Camphor oil	India	Tests of the engine fueled with pure cashew nut shell oil blended with 10 %, 20 % and 30 % of camphor oil.
Leenus <i>et al.</i> (2012)	Cotton seed oil	India and France	Comparison of three alternatives: heating, blending with diesel oil and transesterification.

Author	Vegetable oil	Country	Remarks
Rakopoulos (2012)	Cotton seed and Sunflower oils	Greece	Tests of blends with 10 % and 20 % of the cotton oil and sunflower oil as well as their respective biodiesel at different loads.
Agarwal and Dhar (2013)	Karanja oil	India	Testing of karanja oil blends (10 %, 20 %, 50 % and 100 %).
Daho <i>et al.</i> (2013)	Cottonseed oil	France	Drop size distribution analysis. Test of blends with 20 %, 40 %, 60 %, 80 % and 100% of cottonseed oil.
Li <i>et al.</i> (2013)	Rapeseed oil	United Kingdom and Poland	Tests with rapeseed oil for different proportions of O_2 in the intake air (21 % - 24 %).
Rakopoulos (2013)	Cottonseed oil, Biodiesel from cottonseed oil/ Butanol, Diethyl ether	Greece	Test of cottonseed oil and its biodiesel blended with 20 % n-butanol or 20% diethyl ether.
Sharon <i>et al.</i> (2013)	Used palm oil/Diesel oil/ Butanol	India	Blends of 50 % used palm oil with diesel oil and butanol at different proportions.
Vallinayagam <i>et al.</i> (2013)	Pine oil	Singapore	Test of blends with 25 %, 50 % and 75 % of pine oil.
Qi <i>et al.</i> (2014)	Rapeseed oil	Republic of China and United States	Test of blends with 20 % and 50 % of rapeseed oil and diesel oil at different loads
Rakopoulos <i>et al.</i> (2014)	Cottonseed and Sunflower oils	Greece	Test in heavy duty diesel engine of blends with 10 % and 20 % of cottonseed and sunflower oils and their respective biodiesel. Test at three load conditions and two rotations.

Table 7. Works about modeling of a diesel engine fueled with vegetable oils.

Author	Vegetable oil	Country	Modeling/ Combustion submodel	Remarks
Rakopoulos, Antonopoulos and Rakopoulos (2006)	Typical (mean) vegetable oil	Greece	Two-dimensional/ Whitehouse-Way	Multi-zone model. Typical (mean) vegetable oil (estimation of composition and properties). Comparison of vegetable oil, its biodiesel and diesel oil. Study of droplet size and spray development. Analysis of the distribution of the equivalence ratio in the spray.
Rakopoulos, Antonopoulos and Rakopoulos (2007)	Cottonseed oil	Greece	Two-dimensional/ Arrhenius type equation	Multi-zone model. Cottonseed oil, its biodiesel and diesel oil. Experimental evaluation of pressure, heat release rate and emissions. Study of the spray development and the equivalence ratio distribution in the spray.
Ruan, Cheng and Lee (2008)	Cottonseed, linseed and peanut oils	Republic of China and United States	Multi-dimensional	Use of GT-POWER software with experimental data. Study of the fuel influence and the injection pressure on performance, emissions and

Author	Vegetable oil	Country	Modeling/ Combustion submodel	Remarks
				combustion parameters.
Singh and Sahoo (2012)	Jatropha oil	India	Zero-dimensional/ Wiebe function	Experimental evaluation with jatropha oil heated and unheated.

2.6.1 Contextualization

As shown in this chapter, vegetable oils have been studied as an alternative fuel for diesel engines, being demonstrated their technical reliability through experimental results. Recent studies have focused on the combustion performance of vegetable oils, considering that the understanding combustion process could favor the operation of diesel engines with vegetable oils. Analyses of heat release rate have been widely developed, especially with the cottonseed, jatropha and karanja oils. These studies presented interesting results about combustion parameters such as ignition delay, maximum pressure and fuel burning rate, enhancing the development of combustion models and, therefore, the development of simulations about the diesel engine operation.

The modeling of diesel engines is an analysis tool that reduces time and experimental costs in the analysis of different operating conditions. As it was presented, there are few models developed for diesel engines fueled with vegetable oils and, the combustion parameters for blends of diesel and soybean oils are not available in the literature. In this context, this doctoral thesis shows a Wiebe function application as a combustion model for the operation of a direct injection diesel engine fueled with soybean oil blends. This work extends the analysis and results of previous works, i.e., the experimental and thermodynamic analysis of a diesel engine operating with soybean oil (GARZÓN *et al.*, 2013, 2015), the determination of the physico-chemical properties of the soybean and diesel oils (GARZÓN; BAZZO; OLIVEIRA, 2015), the in-cylinder pressure data processing (ZARZA, 2015; GARZÓN *et al.*, 2016; SCHROEDER, 2016) and the estimation of the heat release rate from measurements (PARGA, 2015; GARZÓN; OLIVEIRA; BAZZO, 2016).

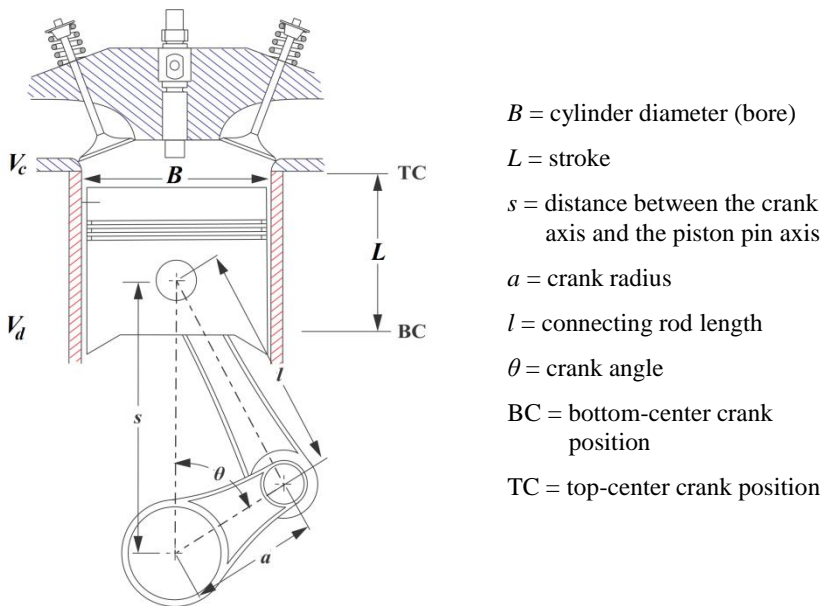
3 GEOMETRICAL AND THERMODYNAMIC ANALYSIS OF DIESEL ENGINE

This chapter presents important factors for the diesel engine modeling. These factors are the geometrical characteristics of the diesel engine and the zero-dimensional thermodynamic analysis of the combustion chamber.

3.1 GEOMETRICAL CHARACTERISTICS

The geometrical characteristics presented in Figure 9 are considered to calculate the area and the volume of the cylinder as a function of the crank angle θ .

Figure 9. Geometrical characteristics of diesel engine.



Source: Adapted from Heywood (1988).

The total volume V is expressed as

$$V = V_c + V_d \quad (3.1)$$

where V_c is the clearance volume and V_d is the displaced or swept volume by the cylinder. Considering the geometrical parameters L and s , the volume V is

$$V = V_c + \frac{\pi B^2}{4} L \quad (3.2)$$

where

$$L = l + a - s \quad (3.3)$$

$$s = a \cos(\theta) + [l^2 - a^2 \sin^2(\theta)]^{0.5} \quad (3.4)$$

Considering the equations (3.3) and (3.4) in equation (3.2) comes

$$V = V_c + \frac{\pi B^2}{4} \left\{ l + a - a \cos(\theta) - [l^2 - a^2 \sin^2(\theta)]^{0.5} \right\} \quad (3.5)$$

Now, defining $R_{cc} = l/a$ and the cylinder area as $A_p = \pi B^2/4$, the equation (3.5) becomes

$$\frac{V}{V_c} = 1 + \frac{V_d}{2V_c} \left\{ R_{cc} + 1 - \cos(\theta) - [R_{cc}^2 - \sin^2(\theta)]^{0.5} \right\} \quad (3.6)$$

Rearranging equation (3.6), the total volume of cylinder is

$$V = V_c \left[1 + \frac{(r_c - 1)}{2} \left\{ R_{cc} + 1 - \cos(\theta) - [R_{cc}^2 - \sin^2(\theta)]^{0.5} \right\} \right] \quad (3.7)$$

where the compression ratio r_c is expressed as

$$r_c = \frac{V_d + V_c}{V_c} \quad (3.8)$$

Similarly, the combustion chamber surface area is given by

$$A_{cc} = A_{ch} + A_p + \pi BL \quad (3.9)$$

where A_{ch} is the cylinder head surface and A_p is the piston crown surface area. Taking the stroke (L) and the distance between the crank axis and the piston pin axis (s), equations (3.3) and (3.4), respectively,

$$A_{cc} = A_{ch} + A_p + \pi B \left\{ l + a - a \cos(\theta) - \left[l^2 - a^2 \sin^2(\theta) \right]^{0.5} \right\} \quad (3.10)$$

Finally, considering again $R_{cc} = l/a$ and the maximum stroke $L_{max} = 2a$, the cylinder area is

$$A_{cc} = A_{ch} + A_p + \pi B \frac{L_{max}}{2} \left\{ R_{cc} + 1 - \cos(\theta) - \left[R_{cc}^2 - \sin^2(\theta) \right]^{0.5} \right\} \quad (3.11)$$

The piston displacement velocity is also an important parameter to be considered in the analysis. The mean piston velocity and the instantaneous piston velocity, \bar{S}_p and S_p , respectively are

$$\bar{S}_p = 2L_{max}N \quad (3.12)$$

$$S_p = \frac{\pi \bar{S}_p}{2} \sin(\theta) \left[1 + \frac{\cos(\theta)}{\left[R_{cc}^2 - \sin^2(\theta) \right]^{0.5}} \right] \quad (3.13)$$

3.2 THERMODYNAMIC MODELING

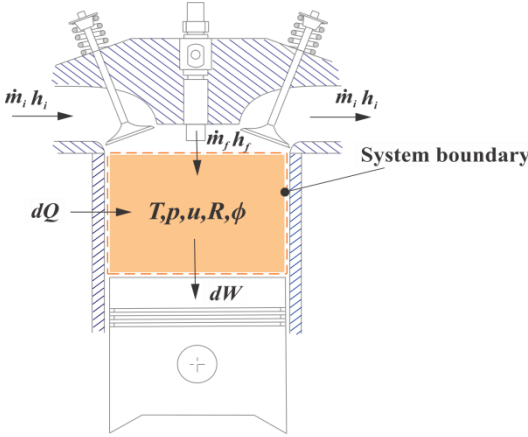
A moving boundary inside the combustion chamber of the engine cylinder, as represented in Figure 10, takes into account the mass balance, the heat release rate, the heat transfer to the environment as well as the corresponding power output. The chemical species balancing and the equation of state are also considered in the thermodynamic analysis.

As assumed before, the thermodynamic problem is solved using the zero-dimensional modeling and so considering no temperature, pressure and chemical species concentration gradients in the cylinder volume, subjected to the following hypotheses:

1. Mass transfer only through the valves and the injector nozzle, i.e., the blow-by through piston rings is not considered.
2. Homogeneous mixture of air and combustion products.

3. The gas as a mixture of ideal gases.
4. The burning as a homogeneous combustion, acting as a uniform heat source.
5. Kinetic and potential energies not considered.
6. Thermodynamic equilibrium at each instant.

Figure 10. Control volume considered in the combustion chamber.



The energy conservation is accomplished considering the combustion chamber as an open system, so that

$$\frac{dU}{dt} = \frac{dQ}{dt} - p \frac{dV}{dt} + \sum_i \dot{m}_i h_i \quad (3.14)$$

where dQ/dt represents the heat transfer rate through of system boundaries, $p dV/dt$ is the work rate done by the system due to system boundary displacement, \dot{m}_i is the mass flow rate across the system boundary, h_i is the enthalpy of flux i , dU/dt is the rate of internal energy of the gas inside the system boundary. Expressing the internal energy in specific form u and rearranging \dot{m}_i for the corresponding mass air flow \dot{m}_a , mass exhaust flow \dot{m}_e and mass fuel flow \dot{m}_f , the equation (3.14) becomes

$$\frac{d(mu)}{dt} = \frac{dQ}{dt} - p \frac{dV}{dt} + h_a \frac{dm_a}{dt} + h_e \frac{dm_e}{dt} + h_f \frac{dm_f}{dt} \quad (3.15)$$

Applying the chain rule on the left side, one obtains

$$m \frac{du}{dt} + u \frac{dm}{dt} = \frac{dQ}{dt} - p \frac{dV}{dt} + h_a \frac{dm_a}{dt} + h_e \frac{dm_e}{dt} + h_f \frac{dm_f}{dt} \quad (3.16)$$

The mass conservation is expressed as

$$\frac{dm}{dt} = \frac{dm_a}{dt} + \frac{dm_e}{dt} + \frac{dm_f}{dt} \quad (3.17)$$

where dm/dt is the total mass flow, dm_a/dt is the mass air flow, dm_e/dt is the mass flow of exhaustion gases and dm_f/dt is the mass fuel flow.

The global equivalence ratio ϕ_{gl} is defined as the ratio of the actual fuel/air ratio to the stoichiometric ratio. Thus,

$$\phi_{gl} = \frac{1}{(FA)_s} \frac{m_f}{m_a} \quad (3.18)$$

where $(FA)_s$ corresponds to the stoichiometric fuel/air ratio. The equivalence ratio changes with the air variation and the fuel variation, so that the differential form of the equivalence ratio is

$$\frac{d\phi}{dt} = \phi_{gl} \left(\frac{1}{m_f} \frac{dm_f}{dt} - \frac{1}{m_a} \frac{dm_a}{dt} \right) \quad (3.19)$$

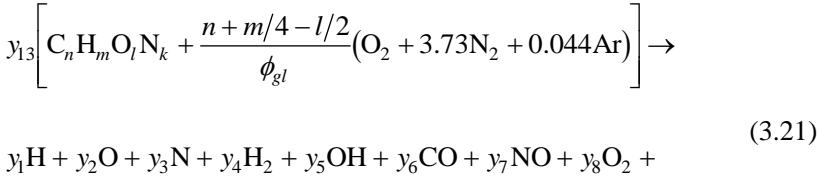
As mentioned before, the equation of state is also considered in the analysis as an ideal gas mixture. So, in a differential form,

$$\frac{1}{V} \frac{dV}{dt} + \frac{1}{p} \frac{dp}{dt} = \frac{1}{T} \frac{dT}{dt} + \frac{1}{R_g} \frac{dR_g}{dt} + \frac{1}{m} \frac{dm}{dt} \quad (3.20)$$

where R_g is the gas constant.

The thermodynamic properties are determined taking into account the molar fractions of the combustion products. Here the reaction rate is sufficiently high so that the reagents and products are in chemical equilibrium at each condition of T and p . According to Olikara and

Borman (1975), the combustion reaction of a hydrocarbon in an internal combustion engine can be represented as



where y_1, y_2, \dots, y_{12} are the molar fractions of the combustion products, y_{13} represents the number of moles of fuel resulting in one mole of products. The following 12 species are observed as products of combustion: H, O, N, H₂, OH, CO, NO, O₂, H₂O, CO₂, N₂, Ar. As a consequence, considering also the number of moles of fuel, 13 equations are then required. For the first equation, one has the sum of the molar fractions equal to one,

$$\sum_{i=1}^{12} y_i = 1 \quad (3.22)$$

For chemical elements C, H, N, O and Ar five equations relate to the chemical species are considered,

$$C: y_6 + y_{10} = n y_{13} \quad (3.23)$$

$$H: y_1 + 2y_4 + y_5 + 2y_9 = m y_{13} \quad (3.24)$$

$$O: y_2 + y_5 + y_6 + y_7 + 2y_8 + y_9 + 2y_{10} = 2y_{13} \left(\frac{l}{2} + \frac{n + m/4 - l/2}{\phi_{gl}} \right) \quad (3.25)$$

$$N: y_3 + y_7 + 2y_{11} = 2y_{13} \left[\frac{k}{2} + 3.73 \left(\frac{n + m/4 - l/2}{\phi_{gl}} \right) \right] \quad (3.26)$$

$$\text{Ar: } y_{12} = y_{13} (0.0444) \left(\frac{n + m/4 - l/2}{\phi_{gl}} \right) \quad (3.27)$$

Seven additional equations are now considered from chemical equilibrium criterion among the products,



The solution for the chemical equilibrium was obtained using the specific subroutines developed by Olikara and Borman (1975).

The heat transfer from in-cylinder gas by convection and radiation to the cylinder head, cylinder walls and piston is estimated, as mentioned in Chapter 2, considering the equation

$$\frac{dQ}{dt} = h_c A (T - T_w) + \varepsilon \sigma_{SB} A (T^4 - T_w^4) \quad (2.19)$$

where the global emissivity ε includes the contribution of emitted radiation for drops and particulate material eventually formed during the combustion. Here a mean value of $\varepsilon = 0.576$ in the combustion process and $\varepsilon = 0$ in other processes of the cycle are considered, as reported by Watson and Janota (1982). As already mentioned in Chapter 2, the mean convective heat transfer coefficient is obtained from a correlation. For this work was used the Hohenberg correlation, as follows,

$$h_c = 130V^{-0.06} p^{0.8} T^{-0.4} (\bar{S}_p + 1.4)^{0.8} \quad (2.32)$$

The wall temperature T_w is estimated considering an electrical circuit analogy, assuming a mean temperature of the outside wall directly in contact with the coolant fluid. Thus, the mean heat transfer \dot{q}'' is calculated as,

$$\dot{q}'' = \frac{T_w - T_{coolant}}{R_k''} \quad (3.35)$$

where $T_{coolant}$ is the mean temperature of the outside wall in contact with the coolant fluid and R_k'' is the thermal resistance per unit area associated with conduction given by

$$R_k'' = \frac{l_w}{k_w} \quad (3.36)$$

where l_w and k_w are the thickness and thermal conductivity of the wall, respectively.

$T_{coolant}$ values are considered according to data reported in technical literature. Wall temperatures T_w are assumed (cylinder head, cylinder wall and piston), a complete cycle simulation of the diesel engine is performed and the mean heat transferred to each wall is calculated. Replacing \dot{q}'' and $T_{coolant}$ in equation (3.35), wall temperatures T_w are calculated and compared with the values assumed. The new values obtained for each wall temperature are again introduced in the complete cycle simulation and the procedure is performed successively to reach convergence in the wall temperatures. Final wall temperature values are considered in later simulations.

4 EXPERIMENTAL METHOD

The experimental method consisted in the determination of the physico-chemical properties of the fuels and tests on a dynamometer bench with in-cylinder pressure measurements and respective post-processing of the pressure measurements for obtaining the heat release rate.

4.1 PHYSICO-CHEMICAL PROPERTIES OF THE FUELS

The fuels tested, their physico-chemical properties and the correlations developed to describe the properties as a function of temperature and volume fraction of vegetable oil in the blends are presented in this section.

4.1.1 Fuels tested

Fuels tested in this study were diesel oil and two blends of soybean oil with diesel oil. The blends tested were: 50/50 % v/v, soybean and diesel oils, and 80/20 % v/v, soybean and diesel oils. Table 8 shows the fuels tested with their respective label and temperature for testing. The blend of 50/50 % v/v was tested in two temperature levels. The high level (85 °C) was determined in order to obtain a similar break-up regime to diesel oil at 25 °C. This condition was evaluated following the criterion for the onset of jet atomization reported by Reitz and Bracco (1979). This criterion is shown in APPENDIX A.

Table 8. Identification of the fuels tested and temperature condition for testing.

Fuel	Temperature (°C)	Label
Diesel oil	25	100D(25)
50/50 % v/v, soybean/diesel	25	50S/50D(25)
	85	50S/50D(85)
80/20 % v/v, soybean/diesel	85	80S/20D(85)

Soybean oil tested suffered no refining or transesterification, only filtering. It was bought from a supplier of São Paulo state in Brazil. Vegetable oils are composed of fatty acid triglycerides, which determine the different physical and chemical properties of each vegetable oil. Table 9 shows the composition of fatty acids of soybean oil, indicating

the structure of the fatty acids as the number of carbon atoms and the number of double bonds. Diesel oil tested was commercial Brazilian diesel oil (known as diesel S10). Commercial Brazilian diesel oil has a volumetric addition of 8 % of biodiesel in accordance with national regulations (Law 13.263, March 23, 2016).

Table 9. Composition of fatty acids of soybean oil.

Fatty acids	Structure	(%)
Palmitic acid	C16:0	9.9 – 12.2
Stearic acid	C18:0	3 – 5.4
Oleic acid	C18:1	17.7 – 26
Linoleic acid	C18:2	49.7 – 56.9
Linolenic acid	C18:3	5.5 – 9.5

Source: Adapted from Fonseca and Gutierrez (1974) and Costa *et al.* (2000).

4.1.2 Determination of properties

Density, dynamic viscosity, and surface tension are the fuel properties that more significantly affect the spray behavior. These properties were measured and analyzed to study the effect of the tested fuels on performance of the diesel engine. In addition, the heat value and the chemical composition of the soybean and diesel oils were also measured. The specific heat and thermal conductivity were calculated from data and correlations found in the technical literature. The current standards or equipment used for determination of the physico-chemical properties are shown in Table 10.

In relation to density, dynamic viscosity and surface tension, experimental results were used to find correlations of these properties as a function of the temperature and of the volume fraction of vegetable oil in a binary blend. These correlations can be used in the estimation of these properties of binary blends between soybean and diesel oils. The correlations are valid in the experimental temperature range (20 °C to 90 °C).

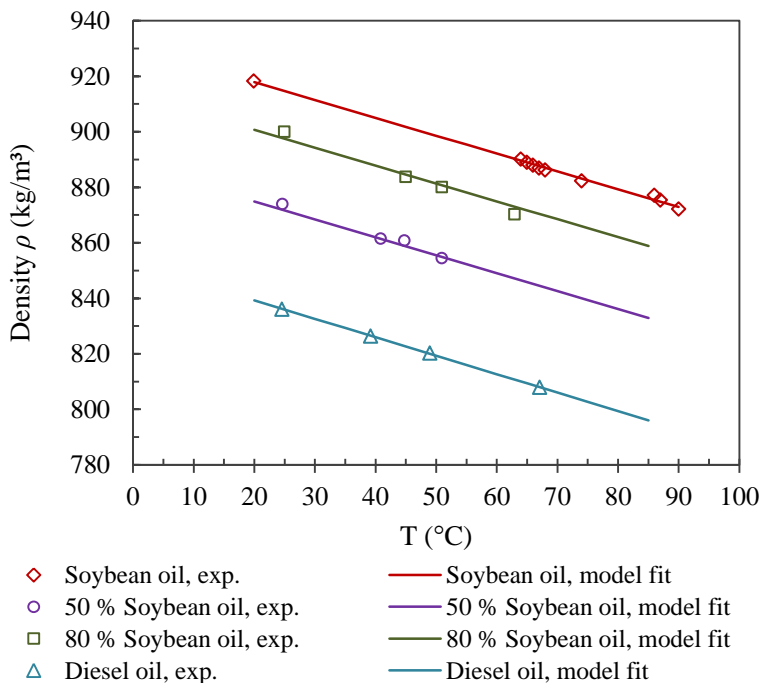
4.1.2.1 Density

Experimental results of density are presented in the Figure 11 for diesel oil, soybean oil, blend 50 % soybean oil and blend 80 % soybean oil. Soybean oil shows the highest density and the diesel oil the lowest density, being a medium value for the density of the blend of 50 %.

Table 10. Equipment or standard used for physico-chemical properties determination.

Property	Equipment or standard	Laboratory
Dynamic viscosity	Rotacional viscosimeter, HAAKE VT550	CERMAT (UFSC)
Density	Electronic balance, Archimedes' principle	LabCET (UFSC)
Surface tension	Tensiometer, Du Nouy	Central de Análise (UFSC)
High and Lower Heat value	ASTM D240	CIENTEC - Fundação de Ciência e Tecnologia
Carbon, Hydrogen and Nitrogen	ASTM D5291	CIENTEC - Fundação de Ciência e Tecnologia
Sulfur	ASTM D1552	CIENTEC - Fundação de Ciência e Tecnologia

Figure 11. Density of soybean oil, diesel oil and two blends as a function of temperature.



One can observe the density decreases linearly with temperature. Therefore the experimental data were described by the expression,

$$\rho = a + bT \quad (4.1)$$

where a and b are the fitting coefficients concerning the correlations of density of soybean and diesel oils. The corresponding values are shown in Table 11. For expressing the density of binary blends as a function of temperature and volume fraction of components, it was used the mixing rule,

$$\rho_b = \chi\rho_v + (1 - \chi)\rho_d \quad (4.2)$$

where χ is the volume fraction of vegetable oil in the blend and the subscripts v , d and b correspond to the data of vegetable oil, diesel oil and blend, respectively. ρ_v and ρ_d follow equation (4.1).

Table 12 shows the density of fuels tested at injection temperature and its percentage difference respect to diesel oil. One can observe the density increase with the addition of vegetable oil in the blend and the effect of the heating in the density decrease.

Table 11. Coefficients of the fitting correlations of the density.

Fuel	a	b	R^2
Soybean oil	930.7	-0.6421	0.9979
Diesel oil	845.0	-0.6494	0.9976

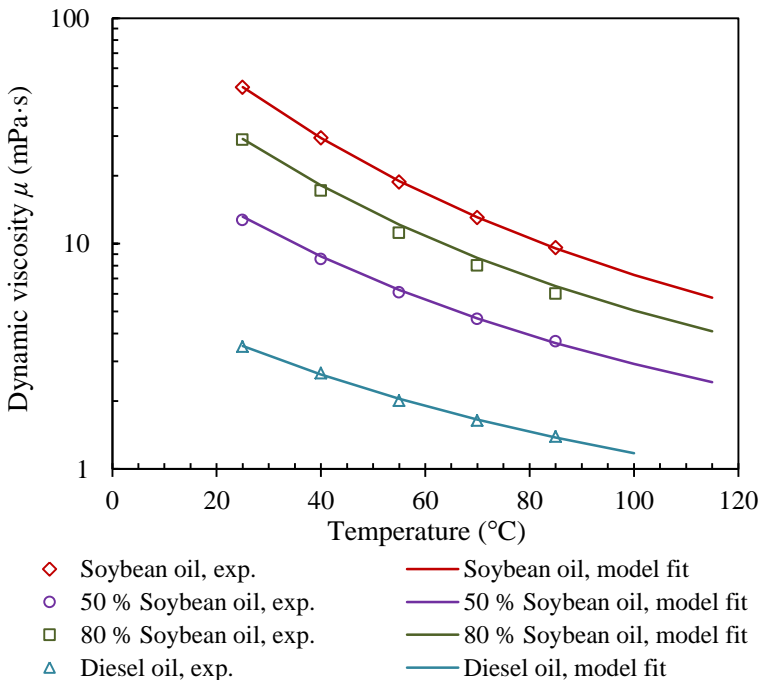
Table 12. Density of fuels tested at injection temperature and percentage difference respect to diesel oil.

Fuel	Injection temperature (°C)	Density (kg/m ³)	% Difference
100D(25)	25	828.7 ± 3.0	
50S/50D(25)	25	871.7 ± 2.2	5.18
50S/50D(85)	85	832.9 ± 2.2	0.51
80S/20D(85)	85	858.8 ± 2.7	3.63

4.1.2.2 Dynamic viscosity

Experimental results of the dynamic viscosity of soybean oil, diesel oil and two blends as a function of temperature are presented in Figure 12. The measurements were carried out since 25 °C until 85 °C with increments of 15 °C. The model fit for each fuel is also presented. One can observe the significant difference between the dynamic viscosity of soybean oil and diesel oil, the decrease of dynamic viscosity with the temperature and the fit of the model proposed with the experimental results.

Figure 12. Dynamic viscosity of soybean oil, diesel oil and two blends as a function of temperature.



A modified Andrade-type equation was used in this work to express the effect of temperature on the dynamic viscosity according to Azian *et al.* (2001), therefore

$$\mu = \exp\left(a + \frac{b}{T} + \frac{c}{T^2}\right) \quad (4.3)$$

where μ is dynamic viscosity, T is temperature, a , b and c are the coefficients of model fit. The coefficients were determined by least square regression from experimental data, and these constants as presented in Table 13 together with the coefficient of determination, R^2 , indicating a proper fit of the data to the statistical model. The Grunberg-Nissan mixing rule is widely used for predicting the dynamic viscosity of liquid mixtures (REID; PRAUSNITZ; POLING, 1987) as

$$\ln \mu_b = \sum_i^n x_i \ln \mu_i + \sum_i^n \sum_j^n x_i x_j G_{ij} \quad (4.4)$$

where μ_b is the absolute viscosity of the blend, μ_i the absolute viscosity i^{th} component, x_i and x_j the concentrations (in mass, mol or volume fraction) of the i^{th} and j^{th} components, G_{ij} the interaction parameter, and n the number of components. When the components of a mixture have similar chemical structure, it is expected that they do not interact with each other and consequently the interaction parameter can be neglected (BENJUMEA; AGUDELO; AGUDELO, 2008). For vegetable oils blends can be assumed the condition of similar chemical structure because the blends form miscible solutions at all proportions within the temperature range tested. Therefore, neglecting the interaction parameter, the dynamic viscosity of the blend is expressed as

$$\ln \mu_b = x_1 \ln \mu_1 + x_2 \ln \mu_2 \quad (4.5)$$

Table 13. Coefficients of the fitting correlations of the dynamic viscosity.

Fuel	a	b	c	R^2
Soybean oil	1.3999	-1.8827×10^3	7.8383×10^5	0.9999
Diesel oil	-0.8988	-5.8537×10^2	3.6610×10^5	0.9993

Table 14 shows the dynamic viscosity of fuels tested at injection temperature and its percentage difference in relation to the diesel oil. Results present a similar behavior to the density results. The dynamic

viscosity increases with the addition of vegetable oil in the blend and it decreases with the increase of the temperature.

Table 14. Dynamic viscosity of fuels tested at injection temperature and percentage difference respect to diesel oil.

Fuel	Injection temperature (°C)	Dynamic viscosity (mPa·s)	Difference (%)
100D(25)	25	3.51 ± 0.22	
50S/50D(25)	25	13.19 ± 0.43	275.6
50S/50D(85)	85	3.62 ± 0.18	3.2
80S/20D(85)	85	6.47 ± 0.23	84.2

4.1.2.3 Surface tension

The surface tension was measured for soybean oil, diesel oil and the blend of 50 % soybean oil at different temperatures. The measurements were carried out at 25, 40 and 50 °C for diesel oil and at 25, 40, 50, 70 and 80 °C for soybean oil and the blend of 50 % soybean oil. Surface tension measurements of soybean and diesel oils showed surface tension decreases linearly with temperature, thus dependence of surface tension with temperature was expressed by equation (4.6). Similar result was presented for Esteban *et al.* (2012).

$$\sigma = aT + b \quad (4.6)$$

where σ is surface tension, a and b are constants determined from experimental data which are shown in Table 15. As it is observed in the experimental results, and in the a coefficient of the correlations, the surface tension decreases lightly with the increase of temperature. Blend surface tensions were estimated from Modified Macleod-Sugden correlation presented in Reid *et al.* (1987), which is shown in equation (4.7) simplified for a binary blend.

$$\sigma_b = \left[\chi_1 \sigma_1^{1/4} + \chi_2 \sigma_2^{1/4} \right]^4 \quad (4.7)$$

Results experimental and model fit are presented in Figure 13. For the blend, the maximum difference between experimental and calculated data was 3.2 % at 25 °C. This difference is reduced with the increase of the temperature. One can be observed the model fit reproduces the extreme values that correspond to the pure fuels of the binary blend. This behavior is shown in Figure 14, where also is observed that the surface tension increases with the increase the volume fraction of vegetable oil in the blend.

Table 15. Coefficients of the fitting correlations of the surface tension.

Fuel	a	b	R^2
Soybean oil	-0.0818	34.6706	0.9977
Diesel oil	-0.0710	29.5350	0.9994

Figure 13. Surface tension of soybean oil, diesel oil and a blend as a function of temperature.

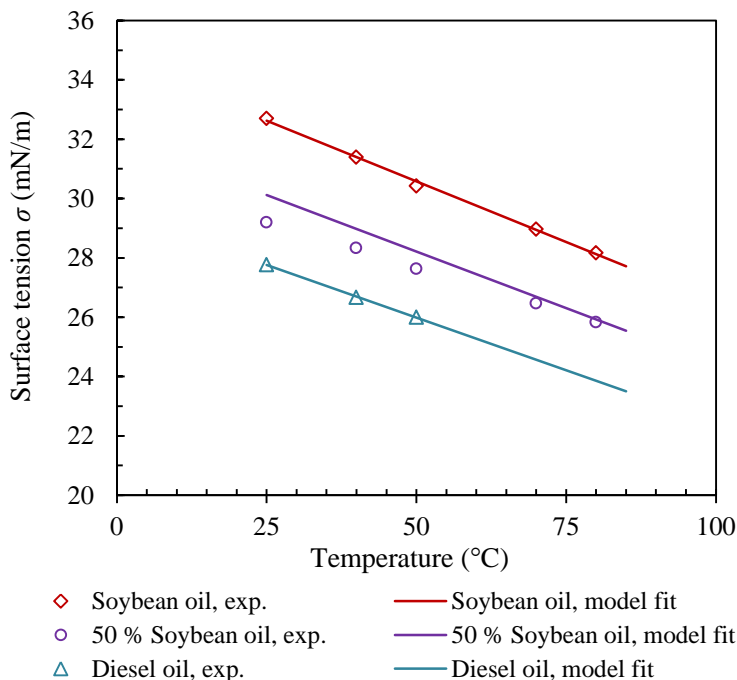


Figure 14. Surface tension of soybean oil blends at 25 and 50 °C.

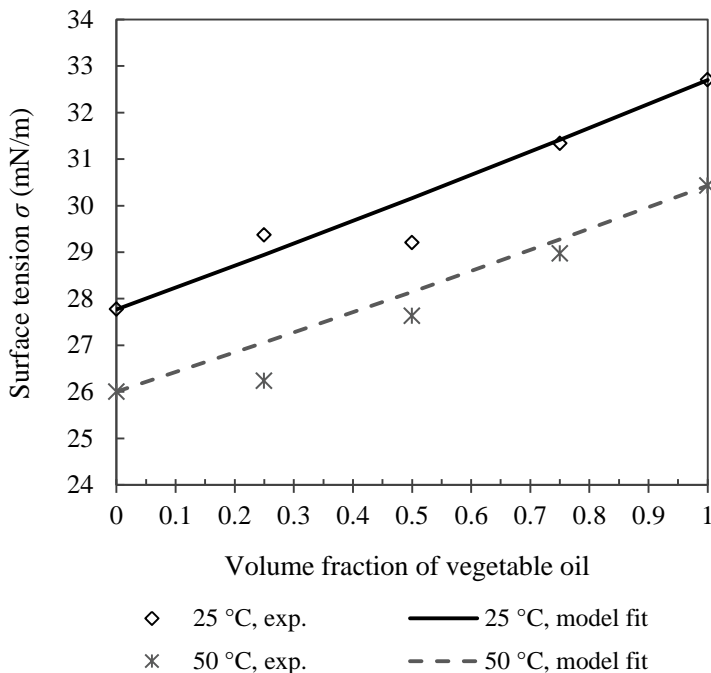


Table 16 shows the surface tension of fuels tested at injection temperature and its percentage difference respect to diesel oil.

Table 16. Surface tension of fuels tested at injection temperature and percentage difference respect to diesel oil.

Fuel	Injection temperature (°C)	Surface tension (mN/m)	% Difference
100D(25)	25	27.76 ± 0.40	
50S/50D(25)	25	30.12 ± 0.28	8.5
50S/50D(85)	85	25.54 ± 0.28	-8.0
80S/20D(85)	85	26.83 ± 0.32	-3.3

4.1.2.4 Heat value and chemical composition

Results of High Heat Value (*HHV*), Low Heat Value (*LHV*), content of carbon, hydrogen, nitrogen and sulfur of soybean and diesel oils are presented in Table 17. In relation to *LHV*, the highest content of carbon and hydrogen of diesel oil influences on its *LHV*, which is about 13 % higher than *LHV* of soybean oil. An empirical formula of soybean oil was calculated from content of carbon, hydrogen and oxygen. Molecular formula of soybean oil was estimated from its empirical formula and the assumption of soybean oil as a triglyceride (molecule with six atoms of oxygen). Diesel oil was modeled as dodecane.

Table 17. Results of *HHV*, *LHV*, C, H, N and S of soybean and diesel oils.

Property	Soybean oil	Diesel oil
<i>HHV</i> (kJ/kg)	39440	45345
<i>LHV</i> (kJ/kg)	36950	42435
Carbon, C (%)	77.67	85.79
Hydrogen, H (%)	11.52	13.52
Sulfur, S (%)	< 0.04	< 0.04
Nitrogen, N (%)	0.02	0.05
Oxygen, O (%)	10.76	0.61
Molecular formula	$C_{57.4}H_{101.5}O_6$	$C_{12}H_{26}$

4.1.2.5 Specific heat

The specific heat of the pure fuels was calculated from experimental data found in the technical literature. Specific heat data of diesel oil were taken from the library of CONVERGE CFD software (2016), and specific heat data of soybean oil were taken from Clark, Waldeland and Cross (1946). The specific heat values of each fuel were fitted as a function of temperature using a quadratic function with the expression

$$c_s = aT^2 + bT + c \quad (4.8)$$

where c_s is the specific heat (kJ/(kg·K)), a , b and c are the fitting coefficients and T is the fuel temperature (K). Table 18 shows the coefficients of the fitting correlations of specific heat of soybean and

diesel oils, including the respective coefficient of determination. For the binary blends, the specific heat was modelled with the expression

$$c_{s,b} = x_v c_{s,v} + x_d c_{s,d} \quad (4.9)$$

where x_v and x_d are the mass fractions and $c_{s,b}$, $c_{s,v}$ and $c_{s,d}$ are the specific heat of the blend, soybean oil and diesel oil, respectively.

Table 18. Coefficients of the fitting correlations of the specific heat of soybean and diesel oils.

Fuel	a	b	c	R^2
Soybean oil	3.956×10^{-6}	-1.598×10^{-4}	1.630	0.9767
Diesel oil	4.368×10^{-6}	1.168×10^{-4}	1.795	0.9999

Figure 15 shows the specific heat as a function of temperature of the diesel oil, soybean oil, blend 50 % soybean oil and blend 80 % soybean oil. One observes that the specific heat increases with the temperature, and the soybean oil presents the highest specific heat, which decreases with the reduction of the volume fraction of vegetable oil in the blend. At 300 K, the specific heat of soybean oil is about 13 % lower than that diesel oil.

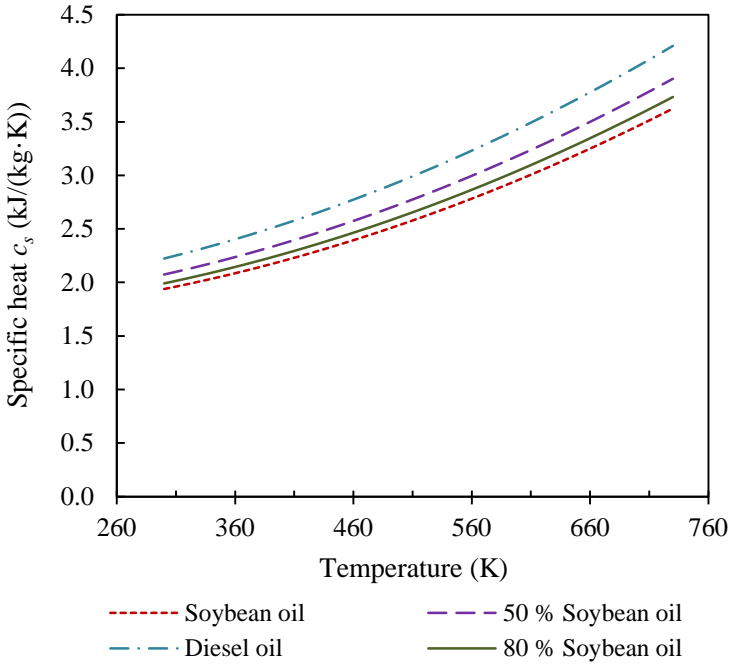
4.1.2.6 Thermal conductivity

The thermal conductivity of the pure fuels was calculated from experimental data and correlations found in the technical literature. Thermal conductivity data of diesel oil were taken from the library of CONVERGE CFD software (2016), and were fitted as a function of the temperature using a linear function. Thus,

$$k_d = aT + b \quad (4.10)$$

where k_d is the thermal conductivity of diesel oil (W/(m·K)), a and b are the fitting coefficients and T is the temperature (K). For calculating the thermal conductivity of soybean oil was used the following correlation developed by Hoffmann *et al.* (2016).

Figure 15. Specific heat of soybean oil, diesel oil and two blends as a function of temperature.



$$k_v = aT^2 + bT + c \quad (4.11)$$

where k_v is the thermal conductivity of soybean oil (W/(m·K)), a , b and c are the fitting coefficients and T is the fuel temperature ($^{\circ}\text{C}$). The coefficients of these fitting correlations and the coefficient of determination are presented in Table 19. For the binary blends, the thermal conductivity was calculated according to the correlation of Jamieson *et al.* (1975) *apud* Reid *et al.* (1987), so that

$$k_b = x_1 k_1 + x_2 k_2 + (k_2 - k_1) (1 - x_2^{0.5}) x_2 \quad (4.12)$$

where x_i and k_i are the mass fraction and thermal conductivity, respectively of the component i , so that $k_2 \geq k_1$.

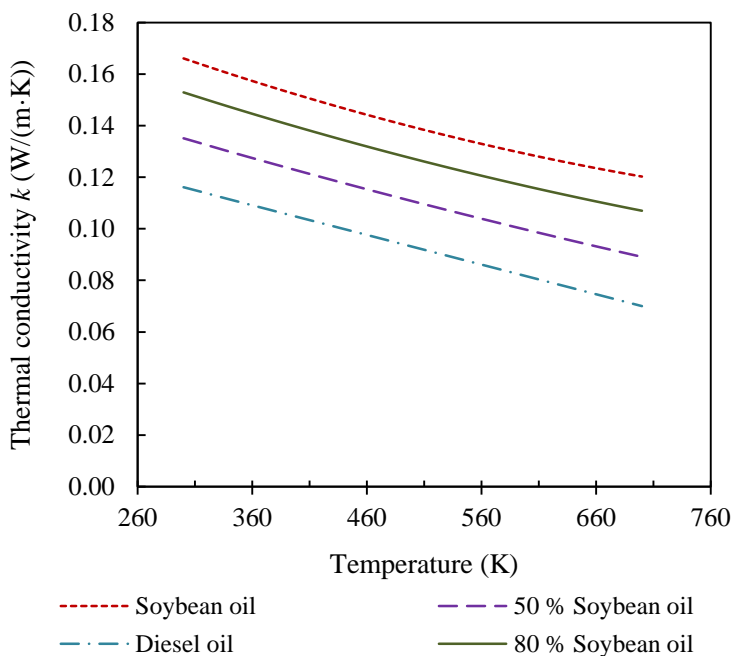
Table 19. Coefficients of the fitting correlations of the thermal conductivity of soybean and diesel oils.

Fuel	a	b	c	R^2
Soybean oil*	9.200×10^{-8}	-1.563×10^{-4}	0.1702	0.9949
Diesel oil	-1.151×10^{-4}	0.151	-	0.9999

*Taken from Hoffmann *et al.* (2016).

Figure 16 shows the thermal conductivity as a function of temperature of the diesel oil, soybean oil, blend 50 % soybean oil and blend 80 % soybean oil. The highest thermal conductivity is presented for the soybean oil, decreasing with the reduction of the volume fraction of vegetable oil in the blend. At 300 K, the thermal conductivity of soybean oil is 43 % higher than that diesel oil. Moreover, it is also observed that the thermal conductivity decreases with the temperature increase.

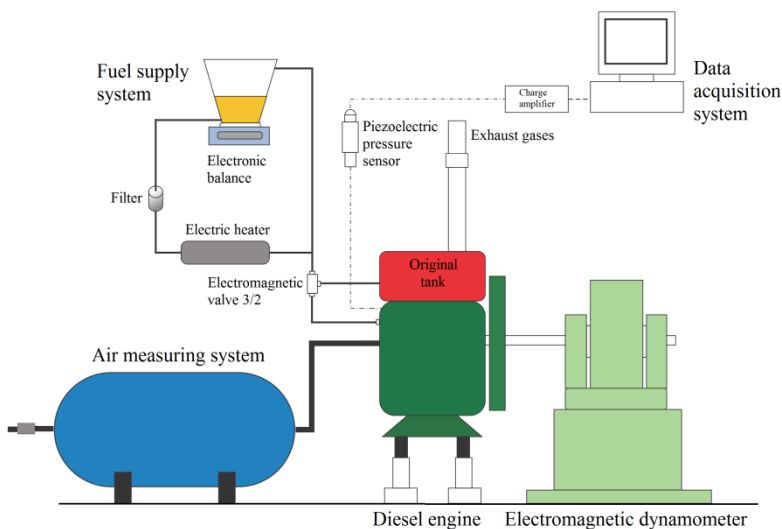
Figure 16. Thermal conductivity of soybean oil, diesel oil and two blends as a function of temperature.



4.2 EXPERIMENTAL SET-UP

The tests with a diesel engine were carried out on a dynamometric bench available at LabCET. The experimental setup is composed for a single cylinder, 4-stroke, direct injection diesel engine (Yanmar, model YT22E) and 14.7 kW of power coupled to an electromagnetic dynamometer (Schenk, model W70). The dynamometric bench is equipped with a fuel supply system, a measurement system of the in-cylinder pressure, an air measuring system and a control and data acquisition system. In Figure 17, it is shown a schematic diagram of the experimental set-up. A picture of the bench can be seen in the Figure 18.

Figure 17. Schematic diagram of the experimental set-up.

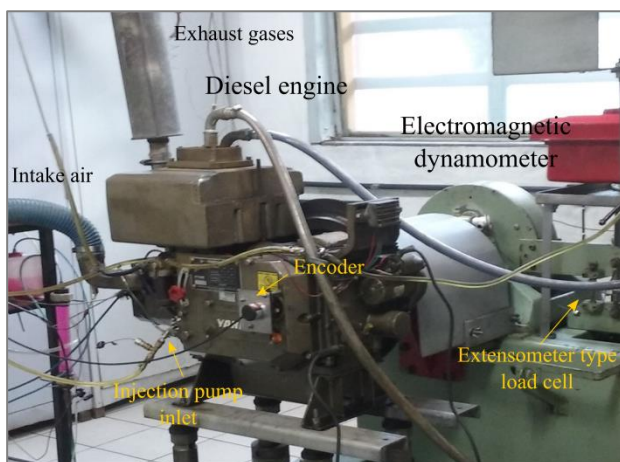


An electric heater comprised of an aluminum tube (12.7 mm diameter), electrical resistance of 119 Ω and ceramic insulation was manufactured to heat the vegetable oil blend before its entry to the engine. An electromagnetic 3/2 valve was installed to switch to the fuel employed. This enables the passage of the diesel oil from the original tank or of the fuel under test. The fuel consumption was measured using an electronic balance (Marte, model AD5000) with serial

communication. The instant reading of the data allowed the calculation of the fuel flow.

The engine torque was measured with an extensometer type load cell installed on the dynamometer arm. The speed was measured with an incremental encoder 360 pulses/revolution (Autonics, model E40S) coupled to the starter shaft, which is coupled to crankshaft through a gear system with 1:2 speed ratio. The break power was then calculated from the readings of torque and speed.

Figure 18. Picture of the diesel engine coupled to electromagnetic dynamometer.



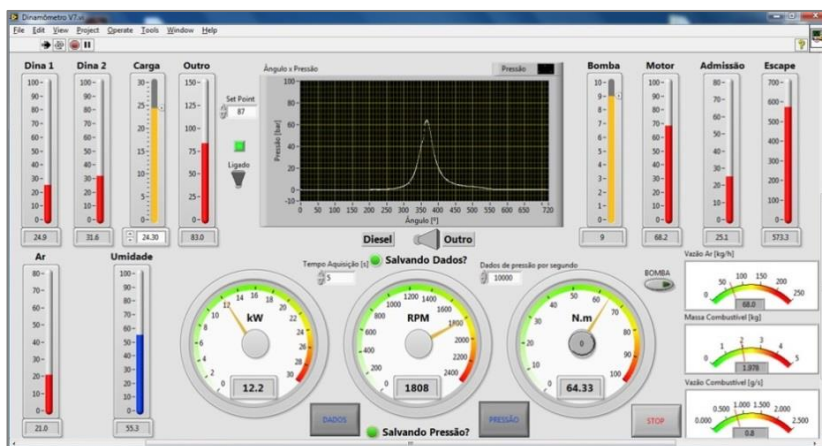
The inducted air mass was measured with a hot-film mass air-flow meter (Bosch, model HFM 2). An air reservoir was coupled between the intake manifold and the air-mass meter to prevent that fluctuations and vibrations in the flow affect the air measurement. In order to assure uniformity of the flow and the measurement of the air-mass rate, the tank used as air reservoir has a volume 185 times larger than the cylinder volume. According to Taylor (1985), the air reservoir must have as minimal volume, 50 times the cylinder volume. Temperature and relative humidity of the air inducted was measured through a humidity sensor and a temperature sensor installed before the mass air-flow meter. A thermocouple was installed in the intake manifold, close to intake valve to register the air temperature inducted. The measurements of temperature and relative humidity were considered to calculate the corresponding air density.

For cooling of the engine and of the dynamometer, the bench has a water pumping system that circulates the engine cooling water through a plate heat exchanger.

A set of thermocouples were installed at the engine cooling water outlet, the exhaust manifold, the intake manifold, the heater outlet and the injection pump inlet.

A data acquisition system was developed with LabVIEW 2011 software, using two acquisition boards to register the different variables. The electronic control during the tests was also made with LabVIEW 2011 software (LabVIEW Software, 2016). Figure 19 shows the screen of this control and data acquisition system, indicating the instantaneous readings and the different control.

Figure 19. Screen of control and data acquisition system on LabVIEW software.



4.2.1 Engine tested

The direct injection diesel engine used in the dynamometric bench has the technical specifications shown in Table 20.

The engine has a mechanical injection system set at 200 bar of injection pressure. The rotation control system is a mechanical governor that regulates the maximum rotation. In this case, it operates from 2100 rpm as a limiting mechanism of maximum rotation. The mechanical governor is constituted by a system of counterweights, springs and joints that acts whenever the rotation moves away from the maximum value. In its function of rotation control, the governor directly

drives the injection pump (mechanical drive pump) to regulate the fuel flow rate.

Table 20. Technical specifications of the diesel engine tested.

Item	Specifications
Type	Diesel, 1 horizontal cylinder, 4-stroke
Injection system	Direct
Injection pressure	200 bar
Injection timing	15° BTC
Cylinder diameter	115 mm
Stroke	115 mm
Cylinder capacity	1194 cm ³
Compression ratio	17.3
IVO – IVC	654° CA – 278° CA
EVO – EVC	444° CA – 64° CA
Power	14.7 kW (20 CV) / 2200 rpm
Specific fuel consumption	238 g/kWh (175 g/CVh)
Cooling	Water
Starting system	Manual or electric
Net weight	195 kg – 180 kg
Dimensions	965 x 450 x 699 mm
Lubrication system	Forced, trochoid pump

In relation to diesel engine injector, it has five holes of diameter equal to 0.3 mm. A tomography of the injector nozzle was taken in order to determine this diameter. The tomography was performed at Porous Media and Thermophysical Properties Laboratory (LMPT) at UFSC. Figure 20 shows a tomogram of injector nozzle. The diameter was measured from this picture using ImageJ, an image processing program (ImageJ, 2016).

Figure 20. Tomogram of injector nozzle used in the diesel engine (LMPT/UFSC).



4.2.2 Pressure acquisition

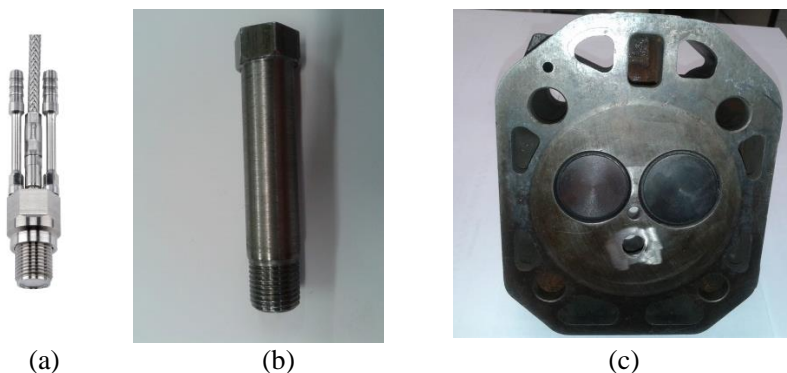
A piezoelectric pressure sensor (Kistler, model 6041B) was used to measure the in-cylinder pressure. The sensor was installed in the cylinder head, according to technical specifications and its signal was synchronized with the incremental encoder to determinate the in-cylinder pressure for each crank angle. The measuring range of the sensor is 0 – 250 bar, which is adequate for internal combustion engines. Pressure sensor was connected to a charge amplifier (Kistler, model 5018A) and its signal was registered through data acquisition system (National Instrument, model SCB-68).

The experimental pressure data requires a processing in order to eliminate spurious data and to obtain the representative pressure curve at condition tested. The in-cylinder pressure data processing consists of four steps: spurious data elimination, averaging many cycles, filtering and fitting of average pressure data. This data processing was implemented with 50 cycles according to procedure performed by Zarza (2015), using MATLAB software (MATLAB, 2013). The sample representativeness (50 cycles) was tested calculating the maximum pressure and the crank angle at maximum pressure for 20, 30, 40, 50, 80 and 100 cycles. A maximum difference of 0.15 % was observed among the results, therefore, smaller than the estimated measurement uncertainty. Thus, it was verified that a sample of 50 cycles is a

representative sample to calculate the pressure curve with no disturbing the accuracy of the results.

The readings of piezoelectric pressure sensor were synchronized with the incremental encoder to register the pressure values each 0.5° CA of crank angle. The piezoelectric pressure sensor was installed according to technical specifications to guarantee the performance and reliability measurements. A cooling system was required for the sensor because high temperatures can damage it or affect its sensitivity. For mounting the sensor, it was used a metallic sleeve due to the cooling water channels in the engine head. The pressure sensor, mounting sleeve and engine head drilled are presented in Figure 21.

Figure 21. (a) Piezoelectric pressure sensor. (b) Metallic sleeve for mounting of the pressure sensor. (c) Engine head.



4.2.3 Experimental testing procedure

Before starting each test, the valves of the diesel engine are opened and the charge amplifier is reset in reference to the atmospheric pressure. The tests were performed at the maximum flow rate of the injection pump. In each test the engine operation was started with diesel fuel until the heating period was completed, i.e., when the cooling water temperature reached 60°C . The diesel oil was then replaced by the fuel under test. After reaching stable operation with the new fuel (steady readings), the brake process was started with the dynamometer. The load was applied in order to accomplish 1800, 2100 and 2200 rpm.

For each load the engine operated until steady state, which was verified by the stabilization of the data. Measurements of torque, speed, power output, fuel consumption and air flow mass were recorded in the

steady state. The measurements were registered at intervals of five seconds, making fifteen readings under each load condition. Additionally, in-cylinder pressure readings were recorded in the steady state during 20 seconds with a frequency of 10000 S/s.

4.3 POST-PROCESSING OF PRESSURE MEASUREMENTS

As mentioned before, the heat release rate is an important parameter to be considered along of the combustion process. The post-processing of pressure measurements is known as the heat release rate analysis, and it is performed during the compression and expansion strokes, while the valves remain closed. The combustion chamber is modeled according to zero-dimensional modeling proposed by Krieger and Borman (1966). The model assumes a homogenous mixture of air and combustion products, at every instant, i.e. there are no gradients of temperature, pressure and chemical concentration species in the domain analysis. The gas mixture is considered as perfect gases. The combustion is assumed as a uniform heat source. Non-equilibrium compositions, fuel vaporization and mixing of air and fuel are neglected.

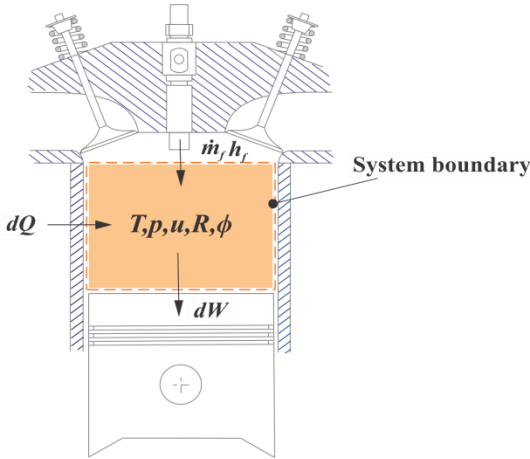
According to the control volume shown in Figure 22, the intake and exhaust valves are both closed. The only mass flow across the boundary is the fuel injected, assuming no leaks through possible gaps in the cylinder. The energy and the mass conservation equations, equations (3.15) and (3.17), simplified for this control volume are

$$\frac{d(mu)}{dt} = \frac{dQ}{dt} - p \frac{dV}{dt} + h_f \frac{dm_f}{dt} \quad (4.13)$$

$$\frac{dm}{dt} = \frac{dm_f}{dt} \quad (4.14)$$

Following the hypothesis that fuel injection is the only mass changing in the cylinder and that the single combustion model assumes a complete burning instantaneously as it enters the combustion chamber, and also that the thermodynamics states of the working fluid are affected by the chemical energy release, the term dm_f/dt can be considered as the mass burning rate of the fuel.

Figure 22. Control volume defined for the combustion chamber.



The equivalence ratio ϕ at each instant is

$$\frac{d\phi}{dt} = \frac{1}{m_a(FA)_s} \frac{dm_f}{dt} \quad (4.15)$$

Since the properties of the gases in the cylinder are function of T , p and ϕ , the internal energy u and the gas constant R_g can be expressed as,

$$\frac{du}{dt} = \frac{\partial u}{\partial T} \frac{dT}{dt} + \frac{\partial u}{\partial p} \frac{dp}{dt} + \frac{\partial u}{\partial \phi} \frac{d\phi}{dt} \quad (4.16)$$

$$\frac{dR_g}{dt} = \frac{\partial R_g}{\partial T} \frac{dT}{dt} + \frac{\partial R_g}{\partial p} \frac{dp}{dt} + \frac{\partial R_g}{\partial \phi} \frac{d\phi}{dt} \quad (4.17)$$

The temperature variation as a function of time and the fuel burning rate is obtained from equations (4.13) to (4.17) and also equation (3.20), the equation of state in differential form. So,

$$\frac{dT}{dt} = \frac{\left[\frac{1}{V} \frac{dV}{dt} + \left(\frac{1}{p} - \frac{1}{R_g} \frac{\partial R_g}{\partial p} \right) \frac{dp}{dt} - \left(\frac{1}{R_g m_a (FA)_s} \frac{\partial R_g}{\partial \phi} + \frac{1}{m} \right) \frac{dm_f}{dt} \right]}{\frac{1}{T} + \frac{1}{R_g} \frac{\partial R_g}{\partial T}} \quad (4.18)$$

$$\frac{dm_f}{dt} = \frac{\frac{dQ}{dt} - \left(\frac{m}{V} B + p \right) \frac{dV}{dt} - \left[mB \left(\frac{1}{p} - \frac{1}{R_g} \frac{\partial R_g}{\partial p} \right) + m \frac{\partial u}{\partial p} \right] \frac{dp}{dt}}{u - h_f + \frac{m}{m_a (FA)_s} \frac{\partial u}{\partial \phi} - B - \frac{mB}{R_g m_a (FA)_s} \frac{\partial R_g}{\partial \phi}} \quad (4.19)$$

where $B = \frac{\partial u}{\partial T} \left(\frac{1}{T} + \frac{1}{R_g} \frac{\partial R_g}{\partial T} \right)^{-1}$.

The volume variation is calculated from geometrical relations of the engine as presented in Chapter 3. The values of pressure and the corresponding first derivative were obtained from experimental data collected from the pressure sensor. The thermodynamic properties and the corresponding partial derivatives related to the temperature, pressure and equivalence ratio are determined by using the routines proposed by Olikara and Borman (1975) as shown in Chapter 3. The fuel enthalpy at injection conditions is calculated according to procedure described in section 5.2.2. The equations (4.18) and (4.19) are solved numerically to obtain the mean gas temperature and the fuel mass burned. It is a nonlinear ordinary differential equations (ODE) system, as presented in Table 21, in this work solved by Runge Kutta method using MATLAB software (MATLAB, 2013). A general algorithm of the routine written for obtaining the heat release rate is presented in APPENDIX G.

As shown in Chapter 2, the heat release rate is calculated from the fuel burning rate and its *LHV*, so that

$$\frac{dQ_f}{dt} = LHV \frac{dm_f}{dt} \quad (2.10)$$

Table 21. Equations and variables considered for obtaining the heat release rate.

Equations	
$\frac{dm_f}{dt} = \frac{\frac{dQ}{dt} - \left(\frac{m}{V}A + p\right)\frac{dV}{dt} - \left[mA \left(\frac{1}{p} - \frac{1}{R_g} \frac{\partial R_g}{\partial p} \right) + m \frac{\partial u}{\partial p} \right] \frac{dp}{dt}}{u - h_f + \frac{m}{m_a(FA)_s} \frac{\partial u}{\partial \phi} - A - \frac{mA}{R_g m_a(FA)_s} \frac{\partial R_g}{\partial \phi}}$	(4.19)
$\frac{dT}{dt} = \frac{\left[\frac{1}{V} \frac{dV}{dt} + \left(\frac{1}{p} - \frac{1}{R_g} \frac{\partial R_g}{\partial p} \right) \frac{dp}{dt} - \left(\frac{1}{R_g m_a(FA)_s} \frac{\partial R_g}{\partial \phi} + \frac{1}{m} \right) \frac{dm_f}{dt} \right]}{\frac{1}{T} + \frac{1}{R_g} \frac{\partial R_g}{\partial T}}$	(4.18)
$\frac{d\phi}{dt} = \frac{1}{m_a(FA)_s} \frac{dm_f}{dt}$	(4.15)
$\frac{dQ_f}{dt} = LHV \frac{dm_f}{dt}$	(2.10)
$\frac{dQ}{dt} = h_c A (T - T_w) + \varepsilon \sigma_{SB} A (T^4 - T_w^4)$	(2.19)
$h_c = 130V^{-0.06} p^{0.8} T^{-0.4} (\bar{S}_p + 1.4)^{0.8}$	(2.32)
$p = f(\text{experimental data})$	
$V = V_c \left[1 + \frac{(r_c - 1)}{2} \left\{ R_{cc} + 1 - \cos(\theta) - \left[R_{cc}^2 - \sin^2(\theta) \right]^{0.5} \right\} \right]$	(3.7)
$u = f(T, p, \phi)$	Thermodynamic properties and chemical equilibrium
$R_g = f(T, p, \phi)$	
Number of equations = 10	
Variables	
$V, p, T, \phi, u, R_g, m_f, Q_f, Q, h_c$	
Number of variables = 10	

4.4 MEASUREMENT UNCERTAINTIES

The procedure followed to calculate the expanded uncertainties of the measurements is described in APPENDIX C. Moreover, the corresponding uncertainties of the measurements on the dynamometric bench and of the density, dynamic viscosity and surface tension measurements are also presented in APPENDIX C.

Table 22 presents the expanded measurement uncertainties as a percentage of the mean value for a probability of 95 %. These values were determined after analyzing the values obtained for the different tests carried out on the dynamometric bench.

Table 22. Expanded measurement uncertainties as a percentage of the mean value.

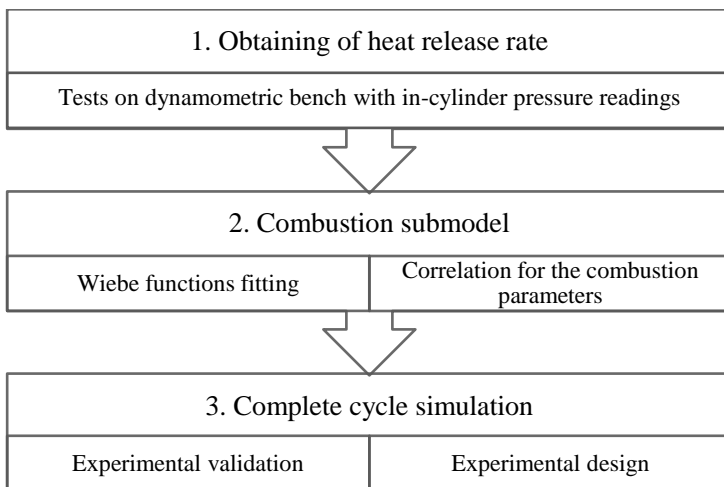
Measurements	Expanded uncertainty (%)*
Engine speed	± 0.4
Break torque	± 1.7
Break power	± 1.7
Fuel mass flow rate	± 3.2
Specific fuel consumption	± 3.6
Thermal efficiency	± 3.6
Air mass flow rate	± 4.2
Exhaust gas temperature	± 1.0

*The expanded measurement uncertainties are for a probability of 95 %.

5 MODELING OF THE DIESEL ENGINE

This chapter focuses on the diesel engine modeling following the procedure delineated in Figure 23.

Figure 23. Modeling procedure of diesel engine.



The first step consists in determining the heat release rate of the fuels tested at three speeds using the in-cylinder pressure experimental data as described in Chapter 4.

In the second step, the heat release rates are fitted using the combustion submodel with the Wiebe function discussed in Chapter 2.

In the third step, the combustion model is used in the simulation of the diesel engine operating with different soybean oil blends and operation conditions. The results obtained are compared with the experimental data. Finally, an experimental design is carried out in order to investigate the best engine operating conditions for the soybean oil blends. A general algorithm about the simulation procedure is presented in APPENDIX G.

5.1 COMBUSTION SUBMODEL

The fuel burning rate obtained from the measurements was curve-fitted to a Wiebe function. The experimental results indicated the need to represent the heat release rate through three phases: premixed, diffusive and residual. In order to evaluate each combustion phase, the premixed combustion phase was fitted to a simple Wiebe function and the diffusive and residual phases were fitted to a double Wiebe function. The total heat release rate corresponds to the two functions, respectively valid for each period of the burning. Thus, one has, for the premixed combustion phase

$$\frac{dX_b}{d\theta} = \frac{a_p X_p (m_p + 1)}{\Delta\theta_p} \left(\frac{\theta - \theta_{ig}}{\Delta\theta_p} \right)^{m_p} \left\{ \exp \left[-a_p \left(\frac{\theta - \theta_{ig}}{\Delta\theta_p} \right)^{m_p + 1} \right] \right\} \quad (5.1)$$

and for the non-premixed and residual combustion phases

$$\frac{dX_b}{d\theta} = \frac{a_d X_d (m_d + 1)}{\Delta\theta_d} \left(\frac{\theta - \theta_d}{\Delta\theta_d} \right)^{m_d} \left\{ \exp \left[-a_d \left(\frac{\theta - \theta_d}{\Delta\theta_d} \right)^{m_d + 1} \right] \right\} + \quad (5.2)$$

$$\frac{a_r X_r (m_r + 1)}{\Delta\theta_r} \left(\frac{\theta - \theta_d}{\Delta\theta_r} \right)^{m_r} \left\{ \exp \left[-a_r \left(\frac{\theta - \theta_d}{\Delta\theta_r} \right)^{m_r + 1} \right] \right\}$$

where the crank angles θ_{ig} and θ_d correspond to the start of ignition and start of diffusive combustion phase, respectively, being $\theta_d = \theta_{ig} + \Delta\theta_p$.

The curve fit of the combustion parameters were obtained as follows. Initially, the heat release rate of the engine operating with diesel oil at 1800, 2100 and 2200 rpm were curve-fitted with the Wiebe functions. The same parameters a_d , m_p , m_d and m_r obtained for diesel oil at each speed were applied to all fuels. The parameters X_p and $\Delta\theta_p$ were obtained from respective heat release rate. Finally, the fitted parameters were a_p , X_d , X_r , $\Delta\theta_d$ and $\Delta\theta_r$.

5.2 COMPLETE CYCLE SIMULATION

The simulation of the diesel engine followed the geometrical characteristics and hypotheses presented in Chapter 3. The inlet and exhaust flows were considered as compressible, unidimensional and isentropic flows. As commented before, for the combustion chamber, a zero-dimensional modeling applied to the control volume presented in Figure 10 was used. The heat release rate was calculated from the combustion submodel fitted to the experimental data. The heat transfer to the walls was modeled considering heat exchange by convection and radiation, using the Hohenberg correlation for calculating the heat-transfer coefficient. The simulation provided the values of pressure and temperature as a function of time for the engine operating cycle, which allowed calculating the performance parameters of the engine such as work, power, mean effective pressure, specific fuel consumption and efficiency.

In this modeling, the input data are the transient flows of air and fuel and the volume variation of the combustion chamber. The output data are the variation of the mean pressure, mean temperature and composition of the gas mixture within the cylinder. In addition, the fuel properties are considered at the injection conditions. Finally, a model for the ignition delay is developed and included.

The MATLAB software was used for solving the equations of the model (MATLAB, 2013).

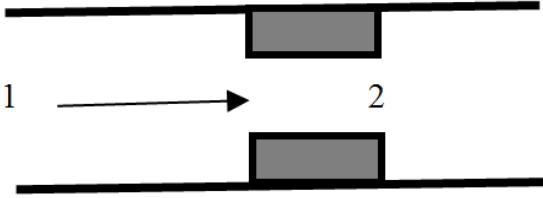
5.2.1 Intake and exhaust

The flows through the inlet and exhaust valves are considered as one-dimensional and isentropic. Considering a steady-state flow in a restriction, as shown in Figure 24, the energy conservation equation becomes

$$h_1 + \frac{v_1^2}{2} = h_2 + \frac{v_2^2}{2} \quad (5.3)$$

where h and v correspond to the enthalpy and velocity of the fluid in sections 1 and 2, before and after the valve, respectively.

Figure 24. Simplified schematic of the flow through the valves.



Rearranging equation (5.3) and considering the fluid as an ideal gas, the velocity in section 2 is

$$v_2 = \sqrt{2c_p(T_1 - T_2) + v_1^2} \quad (5.4)$$

Now considering the isentropic mass flow through the valve,

$$\dot{m}_{iso} = \rho_1 v_1 A_1 = \rho_2 v_2 A_2 \quad (5.5)$$

the fluid density in section 2 can be expressed as a function of the density in section 1,

$$\frac{\rho_2 T_2}{P_2} = \frac{\rho_1 T_1}{P_1} \quad (5.6)$$

$$\rho_2 = \frac{\rho_1 T_1 P_2}{P_1 T_2} \quad (5.7)$$

$$\rho_2 = \frac{P_1 T_1 P_2}{R_g T_1 P_1 T_2} \quad (5.8)$$

Furthermore, recalling that for an isentropic process,

$$\frac{T_2}{T_1} = \left(\frac{P_2}{P_1} \right)^{(\gamma-1)/\gamma} \quad (5.9)$$

and that, for ideal gases $R_g = c_p - c_v$ and $\gamma = c_p/c_v$, the equation for expressing the isentropic mass flow \dot{m}_{iso} is obtained by substituting equations (5.4) and (5.8) into equation (5.5)

$$\dot{m}_{iso} = \frac{A_2 p_1}{\sqrt{R_g T_1}} \left(\frac{p_2}{p_1} \right)^{1/\gamma} \sqrt{1 - \left(\frac{p_2}{p_1} \right)^{(\gamma-1)/\gamma}} \sqrt{\frac{2\gamma}{(\gamma-1)}} \quad (5.10)$$

The relationship between the actual mass flow \dot{m}_{real} and the isentropic mass flow is given by a discharge coefficient C_D defined as

$$C_D = \frac{\dot{m}_{real}}{\dot{m}_{iso}} \quad (5.11)$$

Thus, the actual mass flow through the inlet valve \dot{m}_a is defined as

$$\dot{m}_a = \frac{C_{D,i} A_i p_i}{\sqrt{R_g T_i}} \left(\frac{p}{p_i} \right)^{1/\gamma} \sqrt{1 - \left(\frac{p}{p_i} \right)^{(\gamma-1)/\gamma}} \sqrt{\frac{2\gamma}{(\gamma-1)}} \quad (5.12)$$

where A_i is the passage area at the inlet valve, $C_{D,i}$ is the discharge coefficient at the inlet valve, p_i is the pressure at the intake manifold, T_i is the inlet temperature, R_g is the gas constant, and p is the gas pressure in the cylinder. This equation is valid for subsonic flow. When

$$\frac{p}{p_i} \leq \left[\frac{2}{1 + \gamma} \right]^{\gamma/(\gamma-1)} \quad (5.13)$$

the flow reaches a critical condition of Mach number $M = 1$ (sonic flow), where only the upstream properties affect the mean flow rate. At this condition, the mass flow rate becomes

$$\dot{m}_a = \frac{C_{D,i} A_i P_i}{\sqrt{R_g T_i}} \gamma^{1/2} \left(\frac{2}{\gamma + 1} \right)^{(\gamma+1)/2(\gamma-1)} \quad (5.14)$$

Similarly, the actual mass flow through the exhaust valve \dot{m}_e is defined for a one-dimensional isentropic subsonic flow as

$$\dot{m}_e = \frac{C_{D,e} A_e P}{\sqrt{R_g T}} \left(\frac{P_e}{P} \right)^{1/\gamma} \sqrt{1 - \left(\frac{P_e}{P} \right)^{(\gamma-1)/\gamma}} \sqrt{\frac{2\gamma}{(\gamma-1)}} \quad (5.15)$$

where A_e is the passage area at the exhaust valve, $C_{D,e}$ is the discharge coefficient at the exhaust valve, T is the mean gas temperature in the cylinder and P_e the pressure in the exhaust manifold. When

$$\frac{P_e}{P} \leq \left[\frac{2}{1 + \gamma} \right]^{\gamma/(\gamma-1)} \quad (5.16)$$

the flow becomes choked and mass flow rate becomes

$$\dot{m}_e = \frac{C_{D,e} A_e P}{\sqrt{R_g T}} \gamma^{1/2} \left(\frac{2}{\gamma + 1} \right)^{(\gamma+1)/2(\gamma-1)} \quad (5.17)$$

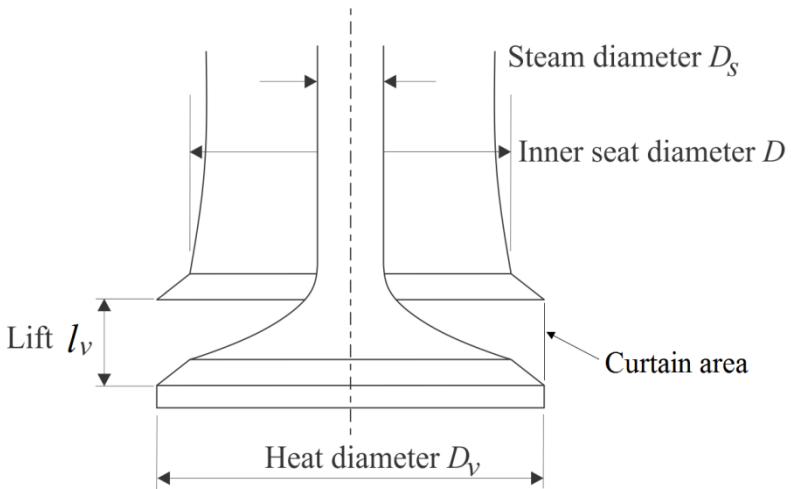
In order to calculate the area of passage A_i and A_e at the inlet and exhaust valves, the dimensions of the engine valves and the corresponding valve lift as a function of the crank angle were used. The valve lift was measured on the valve camshaft, which also allowed determining the opening and closing angle of the valves, as well as the final injection angle. The curtain area of each valve, defined as a function of the head diameter of the valve D_v and of the instantaneous lift l_v , was used to calculate the passage area. Thus, the passage areas for the inlet and exhaust valves, respectively, are

$$A_i = \pi D_{v,i} l_{v,i} \quad (5.18)$$

$$A_e = \pi D_{v,e} l_{v,e} \quad (5.19)$$

Figure 25 shows the geometric parameters of the valves and the localization of the curtain area. The respective dimensions of the valves and the measurement procedure of the valve lift are presented in APPENDIX D.

Figure 25. Geometric parameters and curtain area of the valves.



The discharge coefficients $C_{D,i}$ and $C_{D,e}$ are estimated as a function of the dimensionless instantaneous valve lift according to the experimental curve described by Kastner, Williams and White (1963). The experimental data were fitted to a polynomial function of degree 10. Consequently, the corresponding discharge coefficient is

$$C_D = \sum_{i=1}^{11} c_i \left(\frac{l_v}{D_v} \right)^{i-1} \quad (5.20)$$

where c_i corresponds to every fitting coefficient of the polynomial function of degree 10. These coefficients are shown in APPENDIX D.

5.2.2 Fuel properties at injection conditions

The physical properties of the fuel at the injection conditions as well as the mass fuel injected are estimated using the correlations for density, dynamic viscosity, surface tension and specific heat as presented in Chapter 4.

The fuel temperature increases because of the heat transfer from the engine to the injector nozzle body. Consequently, the fuel temperature at injection conditions is considered as the sum of the temperature measured at inlet injection pump plus the rise in the fuel temperature calculated by (BYATT-SMITH *et al.*, 1996),

$$\Delta T_f = \sqrt{\frac{t_c}{\pi}} \frac{\sqrt{\alpha_t}}{2(r_o - r_i)} \Delta T_s \quad (5.21)$$

where ΔT_f corresponds to the temperature increase, t_c is the time interval of the quiescent part of the cycle (residence time of the fuel in the injector nozzle body), α_t is the fuel thermal diffusivity, $(r_o - r_i)$ is the annular distance between the needle and the wall of the injector, ΔT_s is the temperature difference between the initial fuel temperature and the wall temperature of the injector nozzle. Fuel thermal diffusivity is calculated considering the temperature measured at inlet injection pump.

The fuel enthalpy h_f at injection conditions is calculated considering the enthalpy of formation of the fuel h_f^o and the sensible enthalpy Δh_s , as,

$$h_f = h_f^o + \Delta h_s \quad (5.22)$$

$$\Delta h_s = \bar{c}_s (T_2 - T_1) + \bar{v} (1 - \bar{\beta} T_2) (p_2 - p_1) \quad (5.23)$$

where \bar{c}_s , \bar{v} and $\bar{\beta}$ refer to the mean specific heat, the mean specific volume and the mean thermal expansion coefficient, respectively. Here, in this work, \bar{c}_s is estimated considering the states (T_2, p_1) and (T_1, p_1) , according to correlations presented in section 4.1.2.5. Additionally, \bar{v} and $\bar{\beta}$ are estimated considering the states (T_2, p_1) and (T_2, p_2) , taking data from EES Engineering Equation Software (2016) for dodecane (diesel oil) and experimental data reported by Freitas *et al.* (2013) for

soybean oil. Finally, T_1 and p_1 are the temperature and pressure at the reference state, T_2 and p_2 are the temperature and pressure at the injection state.

The enthalpy of formation of the fuel h_f^o is determined from LHV measured, assuming complete combustion with air to saturated combustion products.

Fuel mass injected

The engine tested has a mechanical injection system that operates at constant injected fuel volume for each engine speed. In this context, the measurement of the mass of diesel oil injected per cycle and the corresponding specific mass of the diesel oil, allowed for curve fitting of the injected fuel volume as a function of the engine speed. This curve is used for the simulation of the engine operating with other blends and also at any speed. The corresponding curve for the injected fuel volume is shown in APPENDIX E.

5.2.3 Ignition delay

As discussed before, the ignition delay is an important parameter in the combustion process, and is defined as the time interval between the start of the injection and the start of the combustion. For determining both angles, the method proposed by Reddy *et al.* (1993) was used.

The method is based on the analysis of the pressure curve as a function of the crank angle, considering that the behavior of the pressure is influenced by the injection and the burning of the fuel. At the time the injection starts, the rate of pressure rise inside the combustion chamber decreases due to evaporation of the fuel, which reduces the in-cylinder temperature and slows down the rate of pressure rise. This phenomenon represents an inflection point in the pressure curve and a maximum point on the corresponding first derivative curve. At the beginning of the combustion, an inverse phenomenon occurs. The release of energy by combustion produces a sudden rise in temperature and pressure, representing a new inflection point on the pressure curve and a minimum point on the first derivative curve. The inflection points represent maximum or minimum points on the first derivative curve and, therefore, zero values on the corresponding second derivative curve. Following this analysis, the injection and ignition angles were

determined as the crank angles where $d^2p/d\theta^2 = 0$ in the time interval analyzed.

A dimensional analysis was performed in order to fit experimental data concerning the ignition delay to a model based on the fuel properties, in-cylinder gas properties and diameter of the injector nozzle, aiming to represent some physical effects (e.g., evaporation) and chemical effects involved in the ignition delay. Consequently, a dimensionless expression f was obtained from a set proposed of dimensionless numbers, such that

$$\frac{\tau}{\tau_c} = f \left(\frac{SMD}{d_o}, Re_D, \phi_{gl}, \exp \left(\frac{E_a}{RT} \right), \chi \right) \quad (5.24)$$

where τ_c corresponds to a characteristic time, SMD is the Sauter Mean Diameter, d_o is the diameter of the injector nozzle, Re_D is the droplet Reynolds number, ϕ_{gl} is the global equivalence ratio and χ is the volume fraction of the vegetable oil. Additionally, $\exp(E_a/RT)$ corresponds to an expression related to Arrhenius equation that involves the mean gas temperature T , activation energy E_a and universal constant of gases R . The characteristic time τ_c was related to the time of injection duration. The SMD was calculated using the correlation proposed by Hiroyasu and Arai (1990) that relates the Reynolds number and the Weber number of the spray. Thus,

$$\frac{SMD}{d_o} = 0.38 Re_{sp}^{0.25} We_{sp}^{-0.32} \left(\frac{\mu_f}{\mu_g} \right)^{0.37} \left(\frac{\rho_f}{\rho_g} \right)^{-0.47} \quad (5.25)$$

where Re_{sp} is the spray Reynolds number, We_{sp} is the spray Weber number, μ_f and μ_g are the dynamic viscosity of the fuel and gas, respectively, ρ_f and ρ_g are the density of the fuel and gas, respectively. Re_D , Re_{sp} and We_{sp} are expressed as

$$Re_D = \frac{\rho_g (u_{sp} - S_p) SMD}{\mu_g} \quad (5.26)$$

$$\text{Re}_{sp} = \frac{\rho_f u_{sp} d_o}{\mu_f} \quad (5.27)$$

$$\text{We}_{sp} = \frac{\rho_f u_{sp}^2 d_o}{\sigma_f} \quad (5.28)$$

where u_{sp} is the spray velocity, S_p is the piston velocity (gas velocity) and σ_f is the surface tension of the fuel. The gas dynamic viscosity is calculated as $\mu_g = 4.57 \times 10^{-7} T^{0.645}$, according to Annand (1963).

The physical and chemical analyses of the problem suggest some possible forms for the function f of the ignition delay. Some forms tested were,

Correlation 1

$$\tau = \tau_c \left[62.5 \left(\frac{SMD}{d_o} \right)^2 \text{Re}_D^{-0.5} + 0.173 \phi_{gl}^b \exp\left(\frac{E_a}{RT}\right) \exp(\chi^c) \right] \quad (5.29)$$

Correlation 2

$$\tau = \tau_c \left(\frac{SMD}{d_o} \right)^b \text{Re}_D^c \phi_{gl}^d \exp\left(\frac{E_a}{RT}\right) \exp(\chi^e) \quad (5.30)$$

Correlation 3

$$\tau = \tau_c \left(\frac{SMD}{d_o} \right)^{2b} \text{Re}_D^{-b} \phi_{gl}^c \exp\left(\frac{E_a}{RT}\right) \exp(\chi^d) \quad (5.31)$$

In equations (5.29), (5.30) and (5.31), the coefficient τ_c was assumed equal to the mean value of the time (ms) concerning the fuel injection duration (30° crank angle), calculated at different engine speeds. The coefficients b , c , d , e and E_a were determined using LAB Fit software, an available tool for fitting procedure (LAB Fit Curve Fitting Software, 2011) as shown in Table 23, with the corresponding coefficient of determination (R^2) and the standard deviation. The ignition delay is expressed in milliseconds. The positive or negative

signal of each fitting coefficient is consistent with the physical effect of each variable on the ignition delay. One emphasizes that the correlations obtained are applicable for a maximum volume fraction of 80 % of vegetable oil in the blend.

Table 23. Fitting coefficients, coefficient of determination (R^2) and standard deviation of the fittings for the ignition delay.

Correlation tested	Fitting coefficients		R^2	Standard deviation
Correlation 1	τ_c	2.400	0.861	0.0295
	b	- 0.282		
	E_a	3106.761		
	c	12.536		
Correlation 2	τ_c	2.400	0.886	0.0273
	b	0.010		
	c	- 0.209		
	d	- 0.211		
	E_a	897.704		
	e	11.466		
Correlation 3	τ_c	2.400	0.842	0.0315
	b	0.130		
	c	- 0.166		
	E_a	2073.506		
	d	12.555		

According to the found results, the correlation 2 presents the best coefficient of determination and, consequently, it was selected for using in the diesel engine simulation.

5.2.4 In-cylinder pressure and temperature

The in-cylinder pressure and the corresponding temperature are calculated using the energy conservation equation and the mass conservation equation for the open system defined by the combustion chamber. As discussed before, the following equations are considered:

$$m \frac{du}{dt} + u \frac{dm}{dt} = \frac{dQ}{dt} - p \frac{dV}{dt} + h_a \frac{dm_a}{dt} + h_e \frac{dm_e}{dt} + h_f \frac{dm_f}{dt} \quad (3.16)$$

$$\frac{dm}{dt} = \frac{dm_a}{dt} + \frac{dm_e}{dt} + \frac{dm_f}{dt} \quad (3.17)$$

Rearranging both equations, one has

$$m \frac{du}{dt} = \frac{dQ}{dt} - p \frac{dV}{dt} + \sum_i (h_i - u) \frac{dm_i}{dt} \quad (5.32)$$

where the subscript i is used for representing the air inlet, exhaust gases and the fuel flow.

Replacing equations (4.16) and (4.17) in equations (3.20) and (5.32), respectively, and rearranging terms, the following expressions for the pressure and temperature variations are obtained.

$$\frac{dp}{dt} = p \left(\left(\frac{1}{T} + \frac{1}{R_g} \frac{\partial R_g}{\partial T} \right) \frac{dT}{dt} + \frac{1}{R_g} \frac{\partial R_g}{\partial \phi} \frac{d\phi}{dt} + \frac{1}{m} \frac{dm}{dt} - \frac{1}{V} \frac{dV}{dt} \right) \left(1 - \frac{p}{R_g} \frac{\partial R_g}{\partial p} \right)^{-1} \quad (5.33)$$

$$\frac{dT}{dt} = \frac{\left[\frac{B-p}{V} \frac{dV}{dt} + \frac{1}{m} \left[\frac{dQ}{dt} + \sum_i (h_i - u - B) \frac{dm_i}{dt} \right] - \left[\frac{\partial u}{\partial \phi} + \frac{B}{R_g} \frac{\partial R_g}{\partial \phi} \right] \frac{d\phi}{dt} \right)}{\frac{\partial u}{\partial T} + B \left(\frac{1}{T} + \frac{1}{R_g} \frac{\partial R_g}{\partial T} \right)} \quad (5.34)$$

where

$$B = p \frac{\partial u}{\partial p} \left(1 - \frac{p}{R_g} \frac{\partial R_g}{\partial p} \right)^{-1} \quad (5.35)$$

The variation of the equivalence ratio as already discussed, it is considered as presented in equation (3.19).

$$\frac{d\phi}{dt} = \phi_{g,i} \left(\frac{1}{m_f} \frac{dm_f}{dt} - \frac{1}{m_a} \frac{dm_a}{dt} \right) \quad (3.19)$$

The solution of the system of ordinary differential equations, consisting of equations (5.33), (5.34), and (3.19) provides the values of temperature, pressure and equivalence ratio, respectively, for each cycle of engine operation. The variables involved were calculated according to relations presented previously and the nonlinear ordinary differential equations (ODE) system was solved by Runge Kutta method using MATLAB software (MATLAB, 2013). Table 24 summarizes the equations used in the zero-dimensional modeling of the diesel engine.

Table 24. Equations used in the zero-dimensional modeling of the diesel engine.

Equations	
$\frac{dm}{dt} = \frac{dm_a}{dt} + \frac{dm_e}{dt} + \frac{dm_f}{dt}$	(3.17)
$\frac{dp}{dt} = p \left(\left(\frac{1}{T} + \frac{1}{R_g} \frac{\partial R_g}{\partial T} \right) \frac{dT}{dt} + \frac{1}{R_g} \frac{\partial R_g}{\partial \phi} \frac{d\phi}{dt} + \frac{1}{m} \frac{dm}{dt} - \frac{1}{V} \frac{dV}{dt} \right) \left(1 - \frac{p}{R_g} \frac{\partial R_g}{\partial p} \right)^{-1}$	(5.33)
$\frac{dT}{dt} = \frac{\left[\frac{B-p}{V-m} \frac{dV}{dt} + \frac{1}{m} \left[\frac{dQ}{dt} + \sum_i (h_i - u - B) \frac{dm_i}{dt} \right] - \left[\frac{\partial u}{\partial \phi} + \frac{B}{R_g} \frac{\partial R_g}{\partial \phi} \right] \frac{d\phi}{dt} \right]}{\frac{\partial u}{\partial T} + B \left(\frac{1}{T} + \frac{1}{R_g} \frac{\partial R_g}{\partial T} \right)}$	(5.34)
$\frac{d\phi}{dt} = \phi_{gl} \left(\frac{1}{m_f} \frac{dm_f}{dt} - \frac{1}{m_a} \frac{dm_a}{dt} \right)$	(3.19)
$V = V_c \left[1 + \frac{(r_c - 1)}{2} \left\{ R_{cc} + 1 - \cos(\theta) - \left[R_{cc}^2 - \sin^2(\theta) \right]^{0.5} \right\} \right]$	(3.7)
$\dot{m}_a = \frac{C_{D,i} A_i P_i}{\sqrt{R_g T_i}} \left(\frac{p}{p_i} \right)^{1/\gamma} \sqrt{1 - \left(\frac{p}{p_i} \right)^{(\gamma-1)/\gamma}} \sqrt{\frac{2\gamma}{(\gamma-1)}}$	(5.12)
$\dot{m}_e = \frac{C_D A_e p}{\sqrt{R_g T}} \left(\frac{p_e}{p} \right)^{1/\gamma} \sqrt{1 - \left(\frac{p_e}{p} \right)^{(\gamma-1)/\gamma}} \sqrt{\frac{2\gamma}{(\gamma-1)}}$	(5.15)
$\frac{dQ}{dt} = h_c A (T - T_w) + \varepsilon \sigma_{SB} A (T^4 - T_w^4)$	(2.19)
$h_c = 130V^{-0.06} p^{0.8} T^{-0.4} (\bar{S}_p + 1.4)^{0.8}$	(2.32)

Equations	
$\frac{dm_f}{dt} = f(\text{combustion model})$	
$\tau = a \left(\frac{SMD}{d_o} \right)^b \text{Re}_D^c \phi_{gl}^d \exp\left(\frac{E_a}{RT}\right) \exp(\chi^e)$	Parameter fitted from experimental data
$h_a = f(T, p)$	Intake air properties
$h_e = f(T, p, \phi)$	Thermodynamic properties and chemical equilibrium
$u = f(T, p, \phi)$	
$R_g = f(T, p, \phi)$	
$\gamma = f(T, p, \phi)$	
<i>Number of equations = 16</i>	
Variables	
$V, p, T, \phi, u, R_g, m_f, m_a, m_e, m, \tau, h_a, \gamma, h_e, Q, h_c$	
<i>Number of variables = 16</i>	

6 RESULTS AND DISCUSSIONS

This chapter presents the experimental results related to the performance parameters, in-cylinder pressure, ignition delay and heat release rate. The combustion model fitted from experimental data and the results of the diesel engine simulation are also presented. Finally, it is shown the applicability of the diesel engine modeling through a factorial experimental design with the fuel temperature, the volume fraction of vegetable oil, the injection timing and the speed as the factors tested.

6.1 PERFORMANCE PARAMETERS

The performance parameters of the diesel engine operating with each fuel tested were determined through tests on the dynamometric bench described in Chapter 4. Tests were carried out at maximum flow rate of the injection pump (full load). The brake torque, brake power, fuel mass injected and thermal efficiency as a function of speed are shown with the respective expanded uncertainty of Figure 26 to Figure 29. A line dashed was drawn in these figures to indicate the effect beginning of the mechanical governor that regulates the maximum engine speed. As a consequence of the mechanical governor action, it is observed a significant change in the curves, mainly, in the fuel mass injected and thermal efficiency.

One observes that the blend 80S/20D(85), at the three speeds tested, presents the lowest values of brake torque and brake power because to its lower *LHV* in comparison to diesel oil (-10.5 %). The increase in the fuel mass injected was not sufficient to compensate the difference in the *LHV* value due to the injection of constant volumes at each speed (injection system operation).

In relation to blend 50S/50D(25), the brake torque and brake power are comparable to the results presented with the diesel oil at three speeds tested. In this case, the increase of the fuel mass rate balanced the difference in the *LHV* value in relation to diesel oil. This behavior is also observed for the blend 50S/50D(85) at 1800 rpm.

As shown in Table 12, the blends 50S/50D(25) and 80S/20D(85) present higher density than diesel oil, consequently, the mass fuel injected per cycle increases for these blends (see Figure 28).

Figure 26. Brake torque as a function of the speed for all fuels tested at full load condition.

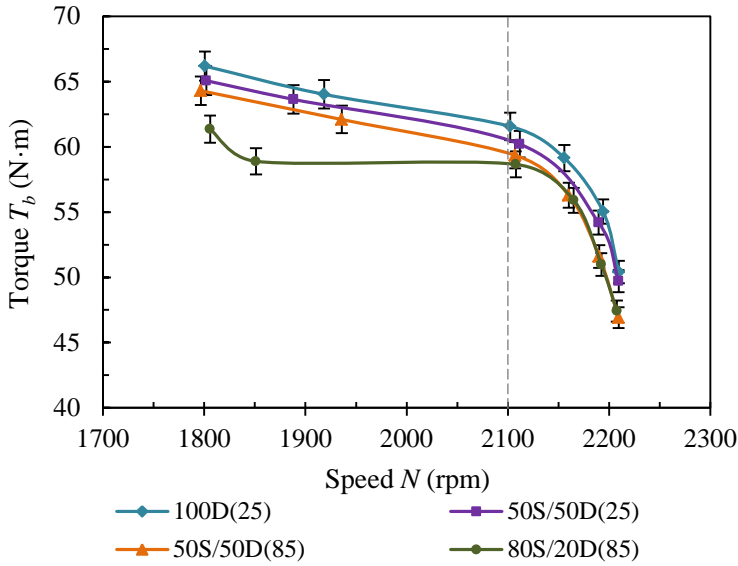


Figure 27. Brake power as a function of the speed for all fuels tested at full load condition.

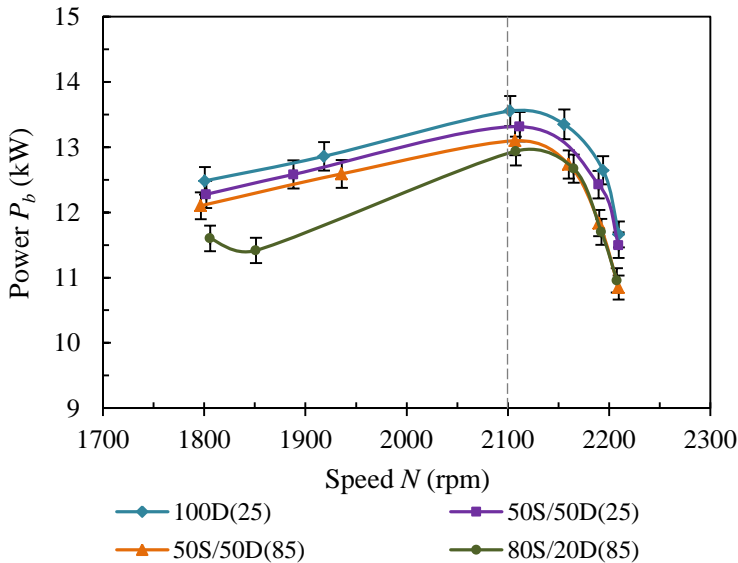


Figure 28. Fuel mass injected as a function of the speed for all fuels tested at full load condition.

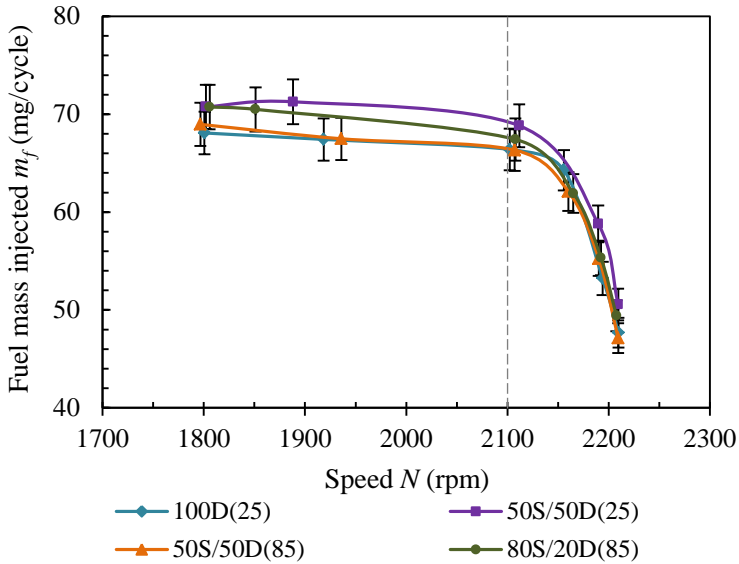
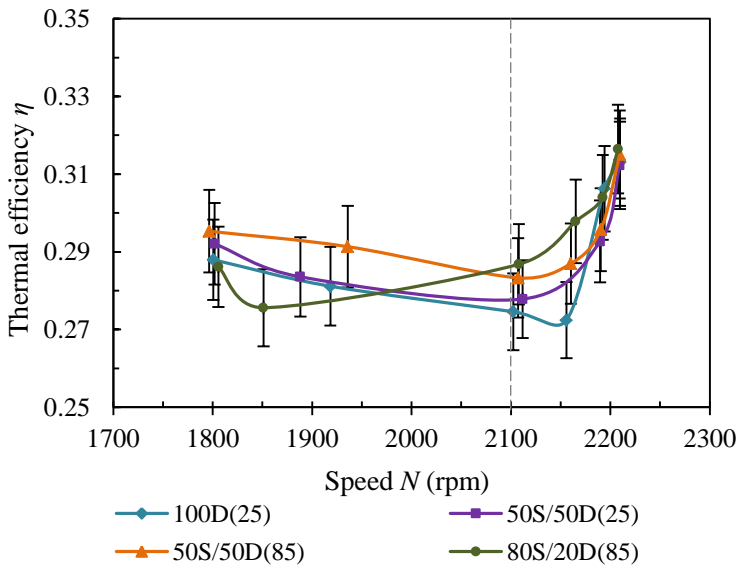


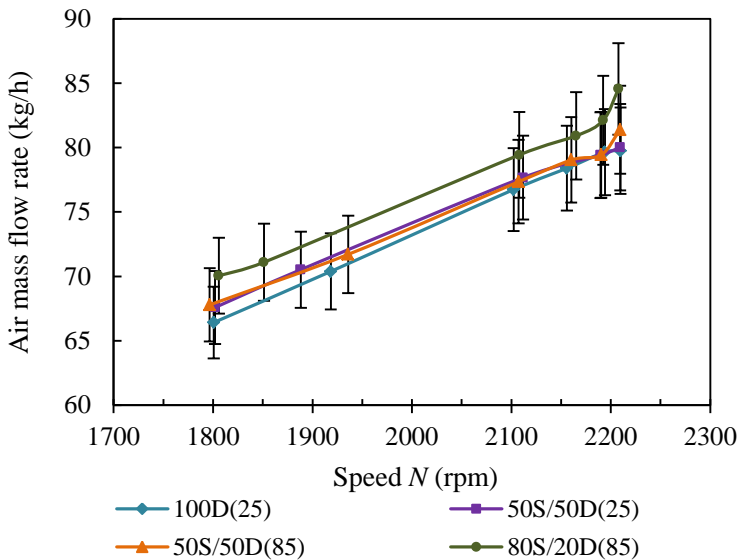
Figure 29. Thermal efficiency as a function of the speed for all fuels tested at full load condition.



In regards to thermal efficiency, Figure 29 shows a tendency to increase for the blends 50S/50D(85) and 80S/20D(85) at 2100 rpm. However, considering the expanded uncertainties, there is no significant difference in the thermal efficiency presented for all fuels in the range of speed tested. In addition, thermal efficiency increases at 2200 rpm for all fuels tested, as a result of the reduction of the fuel mass injected produced by the mechanical governor action.

Mass air flow rate for all fuels tested as a function of speed is shown in Figure 30. Measurements are presented with the respective expanded uncertainties. For all fuels, one observes the increase of the air mass flow rate with the engine speed and comparable results among fuels, considering the expanded uncertainties.

Figure 30. Mass air flow rate as a function of the speed for all fuels tested at full load condition.



Additional information related to the stoichiometric air/fuel ratio and global equivalence ratio at each speed tested is presented in Table 25. 100D oil presents the highest stoichiometric air/fuel ratio and global equivalence ratio, representing combustion of a richer mixture. The stoichiometric air/fuel ratio decreases with the volume fraction of

vegetable oil in the blend. Correspondingly, the lowest global equivalence ratio was obtained with the blend 80S/20D.

Table 25. Stoichiometric air/fuel ratio and global equivalence ratio for all fuels at three speeds tested.

Fuel	$(AF)_s$	1800 rpm	2100 rpm	2200 rpm
		ϕ_{gl}	ϕ_{gl}	ϕ_{gl}
100D(25)	14.92	0.83	0.81	0.59
50S/50D(25)	14.23	0.77	0.76	0.57
50S/50D(85)	14.23	0.74	0.74	0.52
80S/20D(85)	12.82	0.70	0.69	0.50

Results of volumetric efficiency and mean effective pressure are presented in Table 26. Furthermore, a comparison of the performance parameters, indicating the percentage difference in relation to diesel oil is also presented in Table 26.

Table 26. Performance parameters and respective percentage difference in comparison with diesel oil for the fuels tested at three speeds and full load condition.

	100D(25)	50S/50D(25)	50S/50D(85)	80S/20D(85)
<i>LHV</i> (kJ/kg)	42435	39566 -6.8	39566 -6.8	37968 -10.5
1800 rpm				
Brake torque (N·m)	66.19	65.07 -1.7	64.30 -2.8	61.35 -7.3
Brake power (kW)	12.48	12.28 -1.7	12.10 -3.1	11.60 -7.1
Mean effective pressure (kPa)	696.50	684.49 -1.7	676.77 -2.8	645.46 -7.3
Fuel mass rate (g/s)	1.022	1.06 4.0	1.03 1.1	1.06 4.2
Specific fuel consumption (g/(kW·h))	294.62	311.54 5.7	307.12 4.2	330.28 12.1
Volumetric efficiency	0.868	0.885 2.0	0.892 2.8	0.921 6.1
Thermal efficiency	0.288	0.292 1.4	0.295 2.6	0.286 -0.6
Mass fuel injected (mg/cycle)	68.09	70.76 3.9	68.97 1.3	70.74 3.9
2100 rpm				
Brake torque (N·m)	61.57	60.21 -2.2	59.35 -3.6	58.65 -4.7
Brake power (kW)	13.55	13.31 -1.8	13.10 -3.4	12.94 -4.5
Mean effective pressure (kPa)	647.70	633.40 -2.2	624.47 -3.6	616.70 -4.8
Fuel mass rate (g/s)	1.163	1.211 4.1	1.165 0.1	1.18 1.8
Specific fuel consumption (g/(kW·h))	308.95	327.47 6.0	320.14 3.6	329.52 6.7
Volumetric efficiency	0.859	0.868 1.1	0.868 1.1	0.894 4.1
Thermal efficiency	0.275	0.278 1.2	0.283 3.2	0.287 4.4
Mass fuel injected (mg/cycle)	66.40	68.82 3.7	66.33 -0.1	67.43 1.6

	100D(25)	50S/50D(25)	50S/50D(85)	80S/20D(85)
<i>LHV</i> (kJ/kg)	42435	39566 -6.8	39566 -6.8	37968 -10.5
2200 rpm				
Brake torque (N·m)	50.40	49.70 -1.4	46.91 -6.9	47.42 -5.9
Brake power (kW)	11.66	11.50 -1.4	10.85 -7.0	10.96 -6.1
Mean effective pressure (kPa)	530.27	522.77 -1.4	493.34 -7.0	498.63 -6.0
Fuel mass rate (g/s)	0.878	0.93 6.0	0.87 -1.2	0.91 3.5
Specific fuel consumption (g/(kW·h))	270.97	291.42 7.5	287.86 6.2	298.67 10.2
Volumetric efficiency	0.849	0.855 0.7	0.871 2.6	0.909 7.0
Thermal efficiency	0.313	0.312 -0.3	0.315 0.6	0.316 1.1
Mass fuel injected (mg/cycle)	47.68	50.55 6.0	47.12 -1.2	49.41 3.6

6.2 IN-CYLINDER PRESSURE

In-cylinder pressure data as a function of crank angle for the fuels tested at 1800, 2100 e 2200 rpm are shown in the Figure 31, Figure 32 and Figure 33. In these figures, the crank angle equal to 360° CA corresponds to the top-center in the compression stroke. The highest pressures are observed at low speeds as a consequence of the high load and, therefore, the highest fuel amount injected per cycle.

In general, high pressure values are related to the fuel *LHV*, the ignition delay and the development of the heat release rate in the premixed phase during the combustion of each sample.

The start of the ignition produces a slope change of the pressure curves, close to 360° CA. In this context, one observes an ignition more delayed for the blend 80S/20D(85) at 1800 and 2100 rpm. In the case of 2200 rpm (Figure 33), the pressure curve does not show difference in the start of ignition for the four fuels tested.

The maximum pressure value presented for each fuel at each speed and the corresponding crank angle is shown in the Table 27 to Table 29, including the percentage difference relative to diesel oil. At 1800 rpm, the highest maximum pressure was presented for diesel oil and the blend 50S/50D(25). For the blend 50S/50D(85), the maximum pressure decreased about 1.5 % in comparison to diesel oil. The lowest maximum pressure was presented by the blend 80S/20D(85), being about 6 % lower than the maximum pressure of the diesel oil. Similar behavior was observed at 2100 rpm, decreasing to 4 % the difference between the maximum pressure of the diesel oil and the blend 80S/20D(85). At 2200 rpm, for the three blends, the maximum pressure decreased about 1 % in comparison to diesel oil.

Figure 31. Experimental in-cylinder pressure data as a function of crank angle for the fuels tested at 1800 rpm and full load condition.

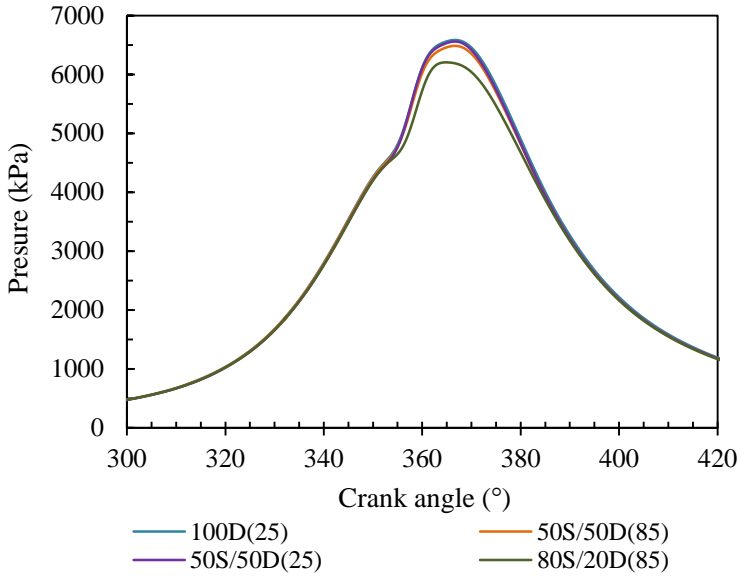


Figure 32. Experimental in-cylinder pressure data as a function of crank angle for the fuels tested at 2100 rpm and full load condition.

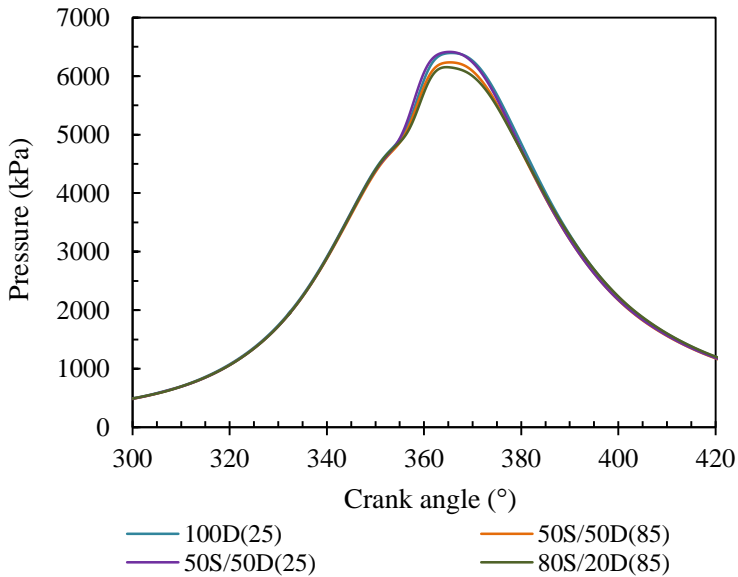


Figure 33. Experimental in-cylinder pressure data as a function of crank angle for the fuels tested at 2200 rpm and full load condition.

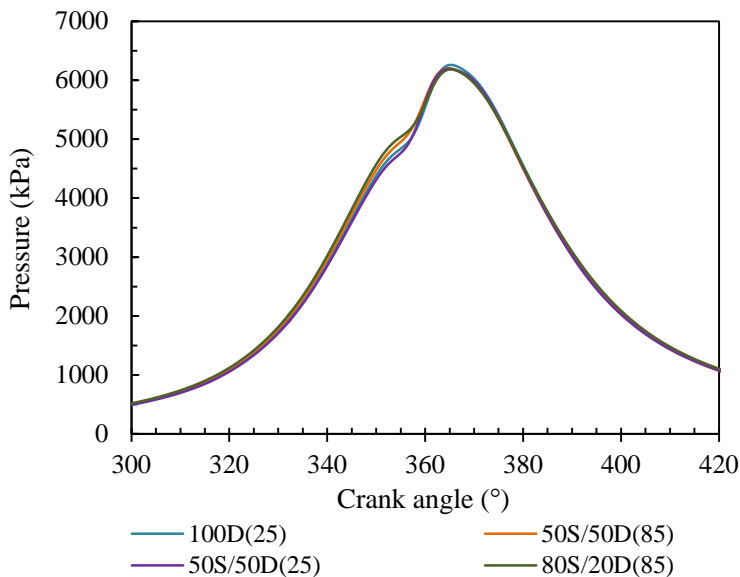


Table 27. Maximum pressure and percentage difference relative to diesel oil at 1800 rpm.

1800 rpm			
Fuel	Maximum pressure (kPa)	Difference (%)	Angle at maximum pressure (° CA)
100D(25)	6584.7 ± 22.4		366.5
50S/50D(25)	6557.7 ± 19.3	-0.41	366.5
50S/50D(85)	6484.8 ± 23.1	-1.52	366.5
80S/20D(85)	6204.8 ± 36.0	-5.77	365.0

Table 28. Maximum pressure and percentage difference relative to diesel oil at 2100 rpm.

2100 rpm			
Fuel	Maximum pressure (kPa)	Difference (%)	Angle at maximum pressure ($^{\circ}$ CA)
100D(25)	6395.1 \pm 25.6		365.5
50S/50D(25)	6413.3 \pm 19.1	0.28	365.5
50S/50D(85)	6234.6 \pm 26.1	-2.51	365.5
80S/20D(85)	6152.3 \pm 16.2	-3.80	364.5

Table 29. Maximum pressure and percentage difference relative to diesel oil at 2200 rpm.

2200 rpm			
Fuel	Maximum pressure (kPa)	Difference (%)	Angle at maximum pressure ($^{\circ}$ CA)
100D(25)	6259.9 \pm 18.8		365.0
50S/50D(25)	6195.8 \pm 19.8	-1.02	365.0
50S/50D(85)	6202.2 \pm 14.4	-0.92	364.5
80S/20D(85)	6183.2 \pm 14.3	-1.22	365.0

6.3 IGNITION DELAY

Experimental results about ignition delay are presented for all fuels tested at 1800, 2100 and 2200 rpm in the Table 30, Table 31, and Table 32, respectively. The expanded uncertainty for ignition delay was calculated as ± 0.71 .

Table 30. Ignition delay of the fuel tested at 1800 rpm.

1800 rpm			
Fuel	Start of injection ($^{\circ}$ CA)	Start of ignition ($^{\circ}$ CA)	Ignition delay ($^{\circ}$ CA)
100D(25)	345.0	352.5	7.5
50S/50D(25)	345.0	352.5	7.5
50S/50D(85)	345.5	353.0	7.5
80S/20D(85)	345.5	354.0	8.5

Table 31. Ignition delay of the fuel tested at 2100 rpm.

2100 rpm			
Fuel	Start of injection (° CA)	Start of ignition (° CA)	Ignition delay (° CA)
100D(25)	345.0	353.5	8.5
50S/50D(25)	344.5	353.0	8.5
50S/50D(85)	345.0	353.5	8.5
80S/20D(85)	345.0	354.5	9.5

Table 32. Ignition delay of the fuel tested at 2200 rpm.

2200 rpm			
Fuel	Start of injection (° CA)	Start of ignition (° CA)	Ignition delay (° CA)
100D(25)	344.5	355.0	10.5
50S/50D(25)	345.0	354.5	9.5
50S/50D(85)	345.0	354.5	9.5
80S/20D(85)	345.0	355.5	10.5

6.3.1 Ignition delay correlation

As exposed in the Chapter 5, the ignition delay results were fitted to the equation

$$\tau = \tau_c \left(\frac{SMD}{d_o} \right)^b \text{Re}_D^c \phi_{gl}^d \exp\left(\frac{E_a}{RT}\right) \exp(\chi^e) \quad (5.30)$$

expressing the ignition delay as a function of the Sauter Mean Diameter, droplet Reynolds number, equivalence ratio, expression $\exp(E_a/RT)$ and volume fraction of the vegetable oil in the blend.

In Figure 34 is presented the comparison of ignition delays predicted with equation (5.30) with corresponding values measured. Moreover, the confidence intervals for a probability of 95 % are also shown in Figure 34, indicating that the predicted values for this correlation are estimated within this interval. The corresponding values of the coefficients of this fitting correlation are again presented in Table 33.

Figure 34. Comparison of ignition delays predicted with ignition delays measured for all fuels tested.

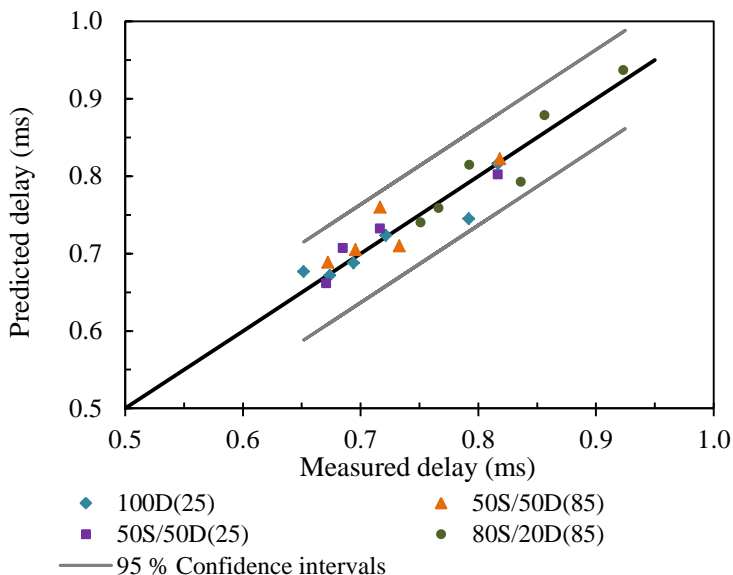


Table 33. Coefficients of the fitting correlation for the ignition delay.

Fitting coefficients	
τ_c	2.400
b	0.010
c	- 0.209
d	- 0.211
E_a	897.704
e	11.466

Coefficient of determination R^2 : 0.886
Standard deviation of the fitting: 0.0273

A sensitivity analysis was performed in order to determine the influence of each parameter of the correlation on the ignition delay. The respective curves of the sensitivity analysis are shown in APPENDIX F.

6.4 HEAT RELEASE RATE

The heat release rate obtained for the fuels at 1800, 2100 and 2200 rpm are presented in the Figure 35, Figure 37 and Figure 39, respectively. The corresponding cumulative energy release of these tests is also presented in the Figure 36, Figure 38 and Figure 40.

The heat release rate, especially in the non-premixed combustion phase, increases with the load, i.e., with the speed reduction, where the mass fuel injected per cycle increases. Observing the curves of cumulative energy release, the combustion performance presents a similar behavior in the premixed combustion phase for all fuels tested, changing in the non-premixed combustion phase, where is observed a significant difference among the fuels tested.

In relation to the speed of 1800 rpm, one observes in Figure 35 that all fuels present similar premixed combustion phase, corresponding to the similar ignition delay presented for the fuels at 1800 rpm as shown in Table 30. In the case of the blend 80S/20D(85), the ignition delay is slightly higher respect to the other fuels. The diesel oil and the blends 50S/50D(25) and 50S/50D(85) presented the highest peak of the heat release rate in the diffusive phase. From 380° CA, approximately, the heat release rate increases for the blend 80S/20D(85) in comparison with the other fuels (residual combustion phase), which shows the combustion delay of this blend and the effect of the highest oxygen content in the fuel that favors the burning, such that the cumulative energy release is high for the blends 80S/20D(85) and 50S/50D(85). The 100D(25) oil presented the lowest cumulative energy release. Similar results are reported by Kannan *et al.* (2012) in their work with oxygenated fuels.

At 2100 rpm, it was presented similar premixed combustion phase for all fuels tested (similar ignition delay). For the blends 50S/50D(85) and 80S/20D(85), the ignition delay is slightly higher respect to the other fuels. The diesel oil and the blend 80S/20D(85) presented the highest peak of the heat release rate in the diffusive phase. In the residual combustion phase, the blend 80S/20D(85) presented the highest heat release rate. Once more, the blend 80S/20D(85) presented the highest cumulative energy release, increasing the overall reactive rate in the diffusive and residual combustion phases. The burning of the blends 50S/50D(25) and 50S/50D(85) presented similar cumulative energy release, being slightly higher for the blend 50S/50D(85). The diesel oil presented the lowest cumulative energy release.

Figure 35. Heat release rate as a function of crank angle for the fuels tested at 1800 rpm and full load condition.

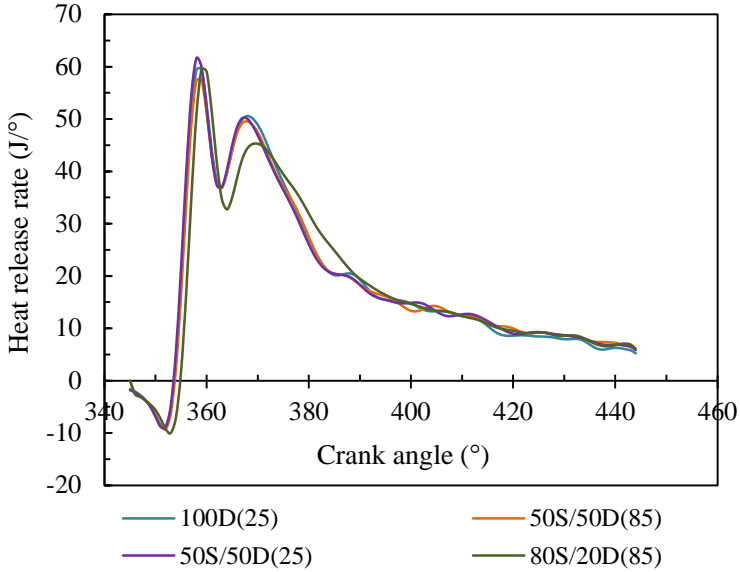


Figure 36. Cumulative energy release as a function of crank angle for the fuels tested at 1800 rpm and full load condition.

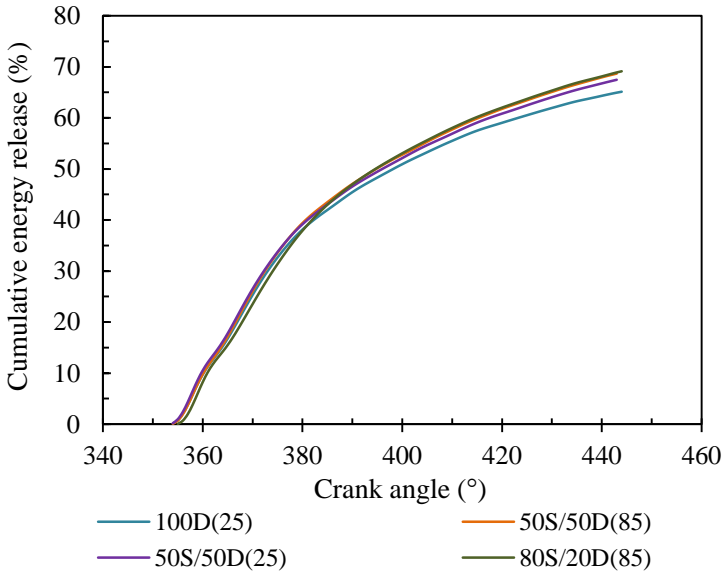


Figure 37. Heat release rate as a function of crank angle for the fuels tested at 2100 rpm and full load condition.

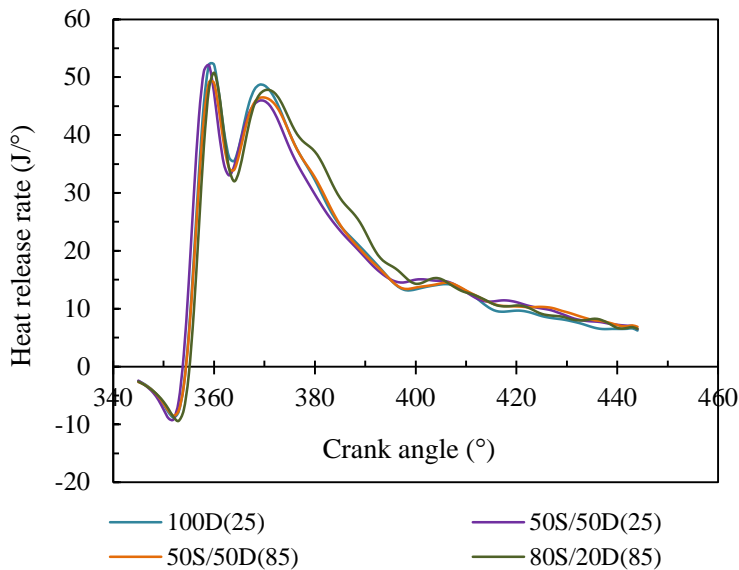


Figure 38. Cumulative energy release as a function of crank angle for the fuels tested at 2100 rpm and full load condition.

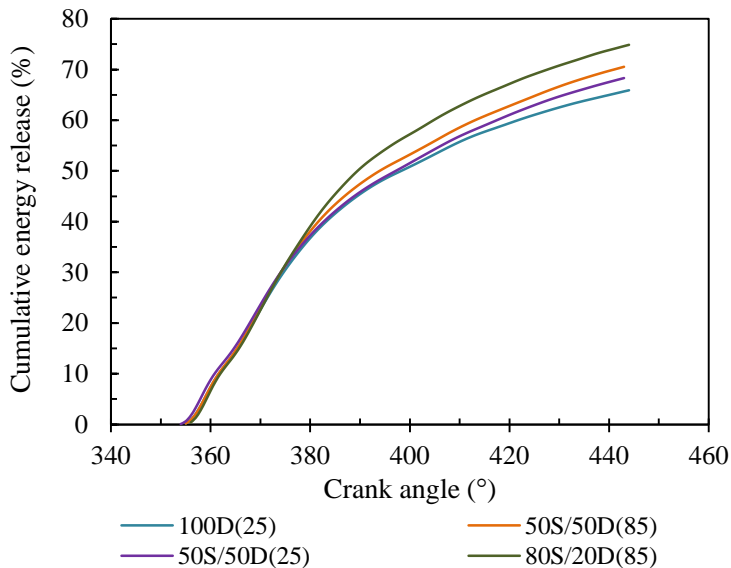


Figure 39. Heat release rate as a function of crank angle for the fuels tested at 2200 rpm and full load condition.

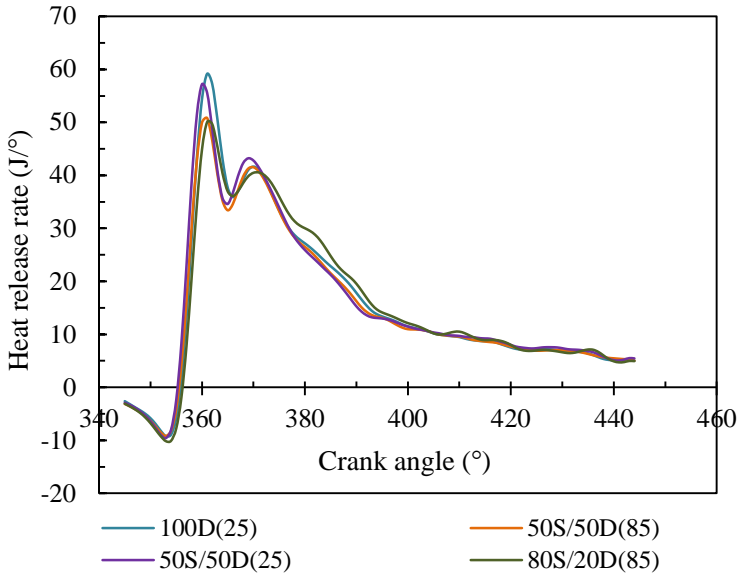
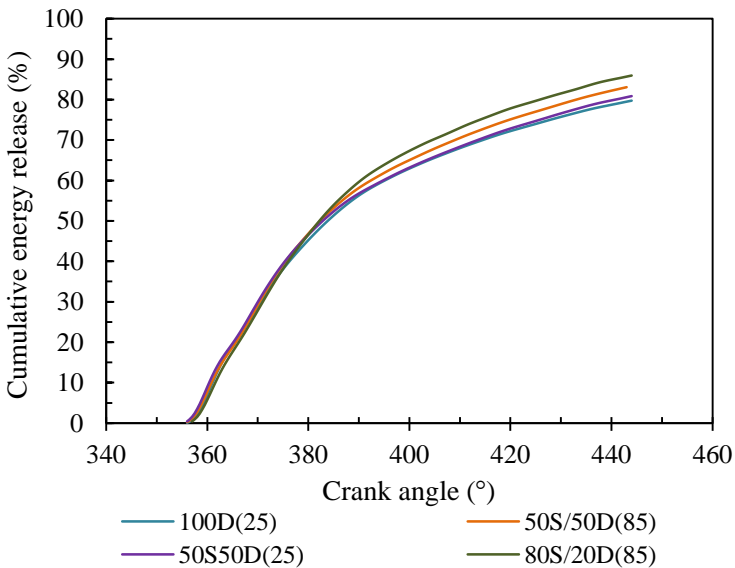


Figure 40. Cumulative energy release as a function of crank angle for the fuels tested at 2200 rpm and full load condition.



Considering the speed of 2200 rpm, the highest heat release rate in the premixed combustion phase was observed for the fuel 100D(25) and the blend 50S/50D(25), being moderately low for the other two fuels. The peak of the heat release rate in the diffusive phase was similar for all fuels. In the residual combustion phase, the heat release rate was higher for the blend 80S/20D(85). The cumulative energy release was similar for diesel oil and the blend 50S/50D(25), increasing for the blend 50S/50D(85), and finally, for the blend 80S/20D(85).

The curves of the heat release rate were developed over compression and expansion strokes of the engine operating cycle, when valves are closed. Consequently, the final point of the curves is 444° CA, where the exhaust valve starts to open. Based on the curves of cumulative energy release, one observes that the total mass fuel injected did not burn completely, continuing the burning during the exhaust stroke. Table 34 presents the mass fraction burned at 444° CA for all fuels at three speeds tested. The values of the mass fraction burned are lower than 100 %. One can consider that the low values calculated for the total mass fraction burned are a consequence of the model employed for the heat-transfer coefficient which probably underestimates the heat transfer for the walls, and therefore, the heat release rate is also underestimated, signifying low mass fraction burned.

Further analysis was developed, changing the Hohenberg correlation for the Annand correlation to calculate the heat-transfer coefficient in the system of equations solved to obtain the heat release rate. When the Annand correlation was used with constants $a = 0.8$ and $b = 0.7$, the fraction mass burned increased about 10 %. This analysis shows the Hohenberg correlation is not adequate to represent the heat transfer for the engine studied.

As shown in Table 34, the mass fraction burned increases with the speed increase or load reduction where the mass fuel injected per cycle is less. Additionally, the highest mass fraction burned was presented for the blend 80S/20D(85) at all speeds, being more significant this difference at 2100 rpm in comparison to 100D(25).

Combustion process can be compared through the localization in crank angle degrees of 10 % and 50 % mass fraction burned, identified as CA10 and CA50. Table 35 shows the CA10 and CA50 for all fuels at three speeds tested.

Table 34. Mass fraction burned at 444° CA for all fuels at three speeds tested.

Fuel	Mass fraction burned		
	1800 rpm	2100 rpm	2200 rpm
100D(25)	0.650	0.657	0.795
50S/50D(25)	0.675	0.683	0.806
50S/50D(85)	0.687	0.705	0.831
80S/20D(85)	0.689	0.746	0.857

Table 35. Crank angle degree of the 10 % and 50 % mass fraction burned for all fuels at three speeds tested.

Fuel	1800 rpm		2100 rpm		2200 rpm	
	CA10	CA50	CA10	CA50	CA10	CA50
100D(25)	360.0	398.0	361.5	398.0	361.0	384.0
50S/50D(25)	359.5	396.0	361.0	397.0	360.5	383.0
50S/50D(85)	360.0	395.0	361.5	394.0	361.0	382.5
80S/20D(85)	361.0	394.5	362.0	389.5	361.5	382.0

Concerning CA10, one observes a combustion delay for blend 80S/20D(85) at 1800 rpm and comparable results among the fuels at 2100 and 2200 rpm. The turbulence and swirl effect, present near to the TC, especially at high speeds, can favor the similar CA10 found for all fuels at 2100 and 2200 rpm. In the case of CA50, combustion was advanced for blend 80S/20D(85) at 2100 rpm as a consequence of the low global equivalence ratio and high diffusive and residual combustion rates. Furthermore, CA50 was advanced for blends 50S/50D(85) and 80S/20D(85) at 1800 and 2200 rpm due to lower global equivalence ratio in comparison with the other fuels. For all fuels, significant differences are observed in the CA50 values comparing the speed 2100 and 2200 rpm due to a high difference in the global equivalence ratio (see Table 25).

Figure 41 shows the heat release rate for 100D(25) at three speeds tested. The heat release rate in the premixed phase was higher at 1800 and 2200 rpm. At 2200 rpm, the high heat release rate in the premixed combustion phase is associated with the highest ignition delay. At 1800 rpm, the high premixed combustion rate is related to the load increase and the time increase per each crank angle degree corresponding to the speed reduction, what favors the air-fuel mixing

and the burning. The combustion efficiency, here represented by the mass fraction burned, was similar at 1800 and 2100 rpm (see Table 34). Similarly, one can see that the highest combustion efficiency is presented at 2200 rpm, being coherent with the lowest global equivalence ratio ($\phi_{gl} = 0.59$, see Table 25) and the turbulence produced by high speed that favors the air-fuel mixing.

Figure 42 shows the heat release rate for 50S/50D(25) at three speeds tested. One observes a similar behavior to the curves of heat release rate obtained for diesel oil.

Figure 43 shows the heat release rate for 50S/50D(85) at three speeds tested. The highest heat release rate in the premixed and diffusive combustion phases are presented at 1800 rpm, showing the effect of the load increase. The heat release rate in the premixed combustion phase is similar at 2100 and 2200 rpm, increasing the heat release rate in the residual combustion phase for the speed of 2100 rpm.

Figure 44 shows the heat release rate for 80S/20D(85) at three speeds tested. The highest peak of the heat release rate in the premixed combustion phase was presented at 1800 rpm. At 2100 and 2200 rpm, the diffusive and residual combustion phases increased, such that the cumulative release energy is higher at these speeds than at 1800 rpm.

For all fuels, the lowest diffusive combustion rate was obtained at 2200 rpm because the lowest mass fuel injected. For fuels 100D(25), 50S/50D(25) and 50S/50D(85), the highest diffusive combustion rate was obtained at 1800 rpm (higher mass fuel injected), decreasing in the residual combustion phase as a consequence of high heat transfer (higher time per crank angle and higher gas temperature). At 2100 rpm, it was observed the highest residual combustion rate, favored by the tumble and swirl effects, possibly present in the combustion chamber at that engine speed. In the case of the blend 80S/20D(85), the highest diffusive and residual combustion rates were observed at 2100 rpm as a consequence of the combustion delay and the effect of the turbulence and blend oxygen content that favor the burning at this speed.

Figure 41. Heat release rate as a function of crank angle for 100D(25) at three speeds tested and full load condition.

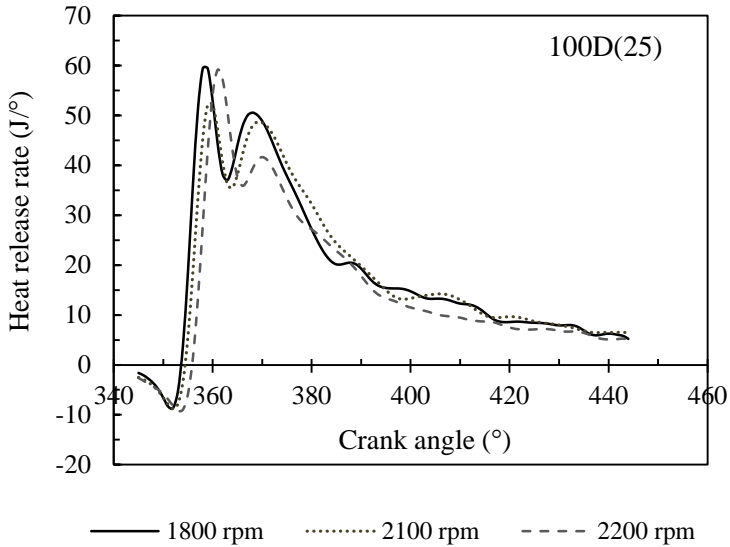


Figure 42. Heat release rate as a function of crank angle for 50S/50D(25) at three speeds tested and full load condition.

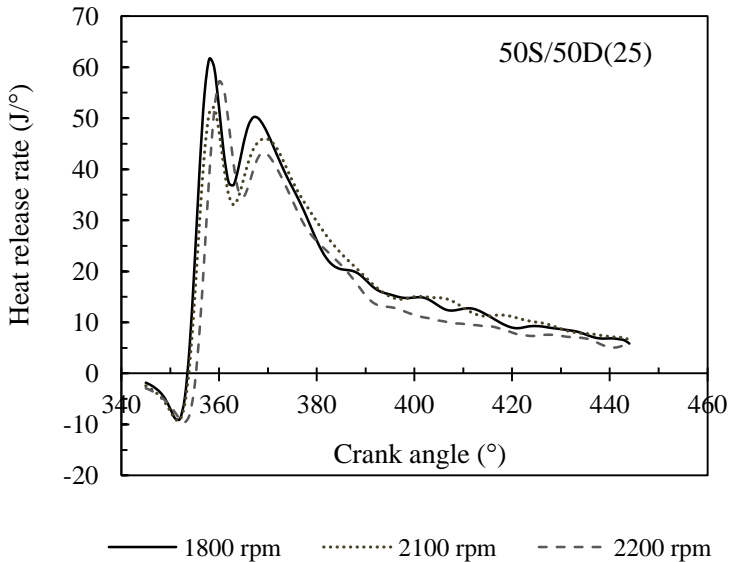


Figure 43. Heat release rate as a function of crank angle for 50S/50D(85) at three speeds tested and full load condition.

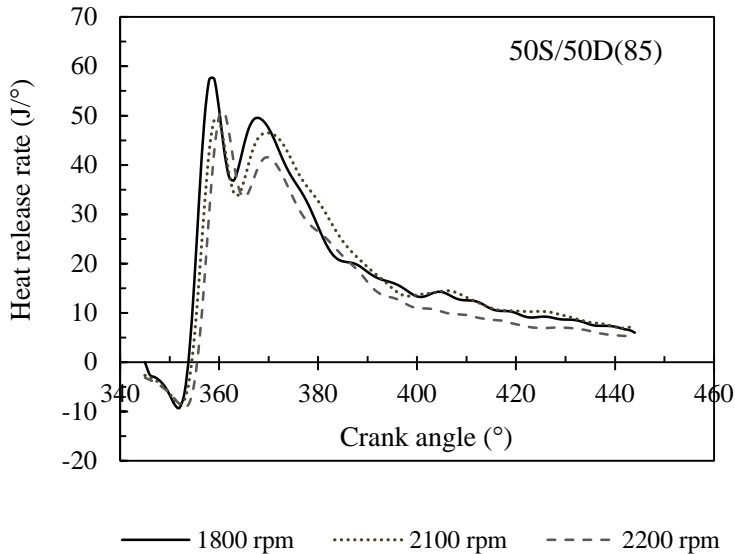
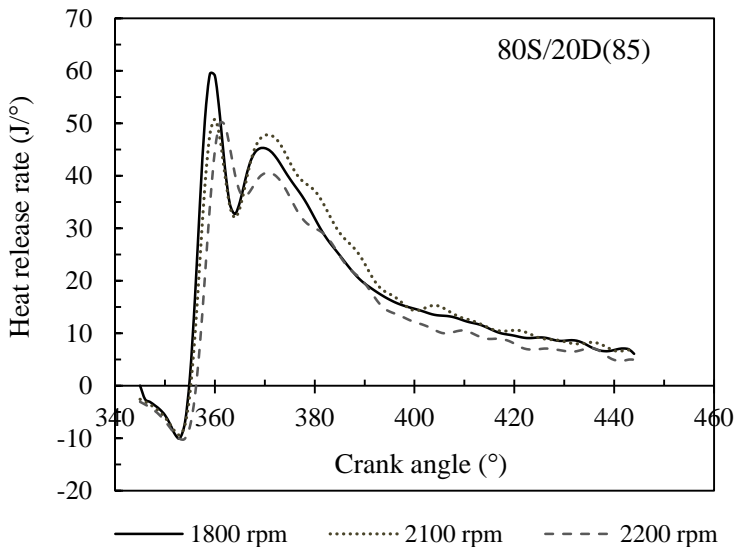


Figure 44. Heat release rate as a function of crank angle for 80S/20D(85) at three speeds tested and full load condition.



In order to help understanding the combustion process, the break-up regime (Ohnesorge diagram), SMD , droplet Reynolds number and oxygen content were estimated for all fuels tested at 1800 rpm and results are shown in Figure 45 and Table 36.

According to Ohnesorge diagram, blend 50S/50D(25) do not present the atomization regime required for diesel engine combustion and the break-up regime of the blend 80S/20D(85) is between second wind-induced and atomization regimes. In the case of the blend 50S/50D(85), the heating favored the break-up, reaching the atomization regime.

Concerning the results shown in Table 36, blend 50S/50D(25) presents the highest SMD , being 15.5 % higher than SMD of 100D(25). The highest droplet Reynolds number is also presented by blend 50S/50D(25) and the blend 80S/20D(85) has the maximum oxygen content.

Figure 45. Ohnesorge diagram for all fuels tested at 1800 rpm and full load condition.

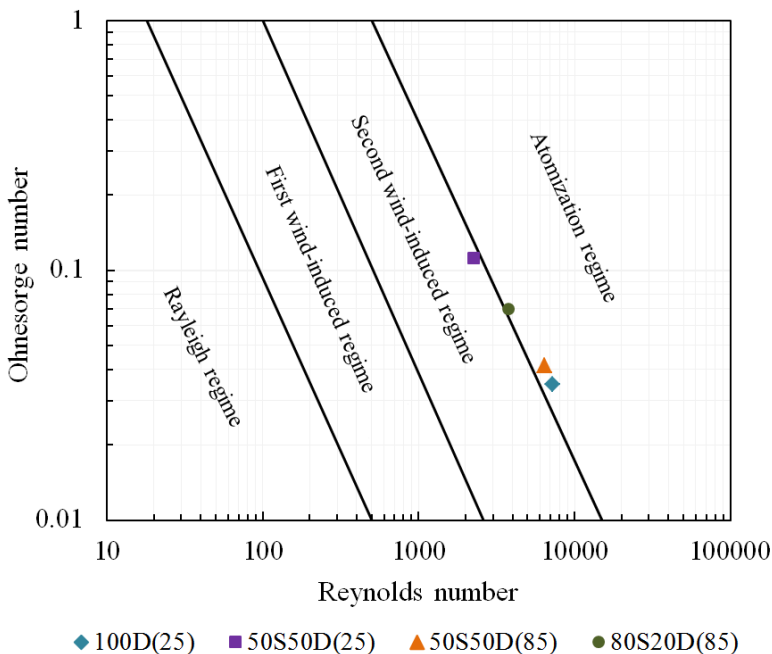


Table 36. *SMD*, droplet Reynold number and oxygen content for all fuels tested at 1800 rpm and full load condition.

Fuel	<i>SMD</i> (μm)	Re_D	O ₂ (%)
100D(25)	22.20	737.24	-
50S50D(25)	25.65	851.84	5.66
50S50D(85)	21.91	727.58	5.66
80S20D(85)	23.40	776.87	8.81

Although blends 80S/20D and 50S/50D(25) are not in atomization regime and present the highest *SMD*, the diesel engine operated satisfactorily with these blends and the combustion results were comparable with the other two fuels. In the case of the blend 50S/50D(25), one can suggest that the highest *SMD* favored the droplet Reynold number and, therefore, the constant evaporation. For the blend 80S/20D(85), the high *SMD* and the highest fraction of vegetable oil, lead to a combustion delay, characterized by high diffusive and residual combustion phases, however, the oxygen content favored its combustion.

Additionally, as explained in Chapter 2 in relation to the combustion of a binary liquid blend droplet (diesel + straight vegetable oil), products of oil degradation can help or can inhibit the ignition, therefore, it is not clear what occurs in the premixed combustion phase when compared the blends 50S/50D(25) and 50S/50D(85).

6.5 COMBUSTION MODEL

As exposed in Chapter 5, the combustion model proposed consists of a simple Wiebe function (premixed phase) and a double Wiebe function (diffusive and residual phases). Then,

$$\frac{dX_b}{d\theta} = \frac{a_p X_p (m_p + 1) \left(\frac{\theta - \theta_{ig}}{\Delta\theta_p} \right)^{m_p}}{\Delta\theta_p} \left\{ \exp \left[-a_p \left(\frac{\theta - \theta_{ig}}{\Delta\theta_p} \right)^{m_p + 1} \right] \right\} \quad (5.1)$$

$$\frac{dX_b}{d\theta} = \frac{a_d X_d (m_d + 1) \left(\frac{\theta - \theta_d}{\Delta\theta_d} \right)^{m_d}}{\Delta\theta_d} \left\{ \exp \left[-a_d \left(\frac{\theta - \theta_d}{\Delta\theta_d} \right)^{m_d + 1} \right] \right\} + \quad (5.2)$$

$$\frac{a_r X_r (m_r + 1) \left(\frac{\theta - \theta_d}{\Delta\theta_r} \right)^{m_r}}{\Delta\theta_r} \left\{ \exp \left[-a_r \left(\frac{\theta - \theta_d}{\Delta\theta_r} \right)^{m_r + 1} \right] \right\}$$

The experimental heat release rate and the Wiebe functions fitted for 100D(25) and the blend 80S/20D(85) at 1800 rpm are presented in Figure 46 and Figure 47, respectively, showing good accuracy between the experimental and fitted data. This fitting procedure was developed using LAB Fit Software (LAB Fit Curve Fitting Software, 2011), and a value of about $R^2 = 0.9$ was obtained for all fuels and engine speeds tested.

The Wiebe function parameters fitted for each fuel were analyzed to determine the influence of the fuel or engine in each parameter. The parameters X_p , X_d , X_r , $\Delta\theta_p$, $\Delta\theta_d$, $\Delta\theta_r$ and a_p are shown of the Figure 48 to the Figure 54, as a function of each fuel and the engine speed.

Figure 46. Experimental heat release rate and Wiebe functions fitted as a function of crank angle for 100D(25) at 1800 rpm.

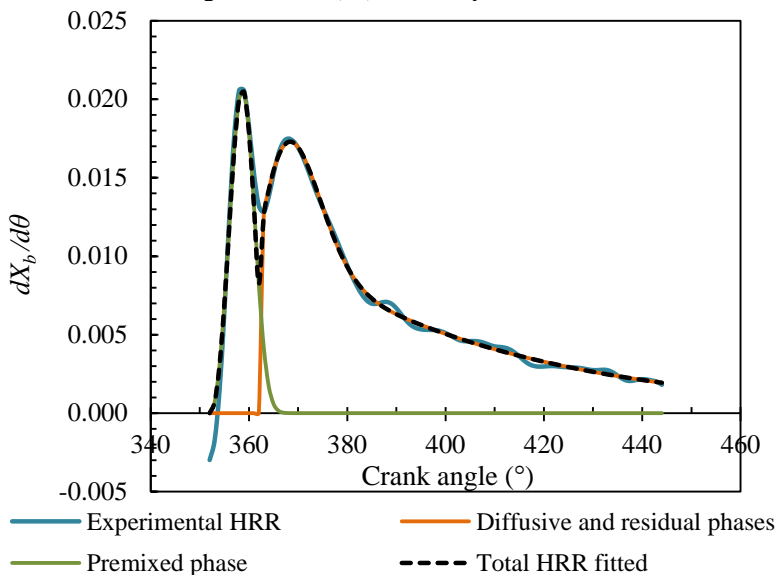


Figure 47. Experimental heat release rate and Wiebe functions fitted as a function of crank angle for the blend 80S/20D(85) at 1800 rpm.

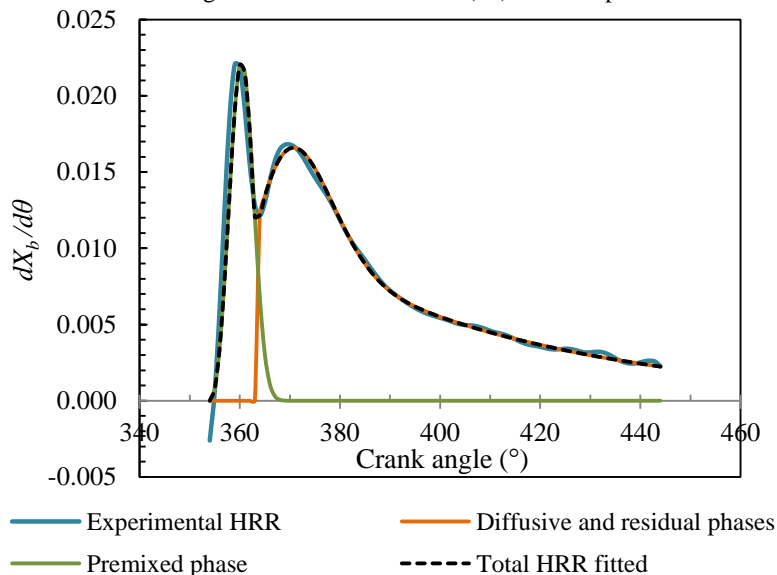


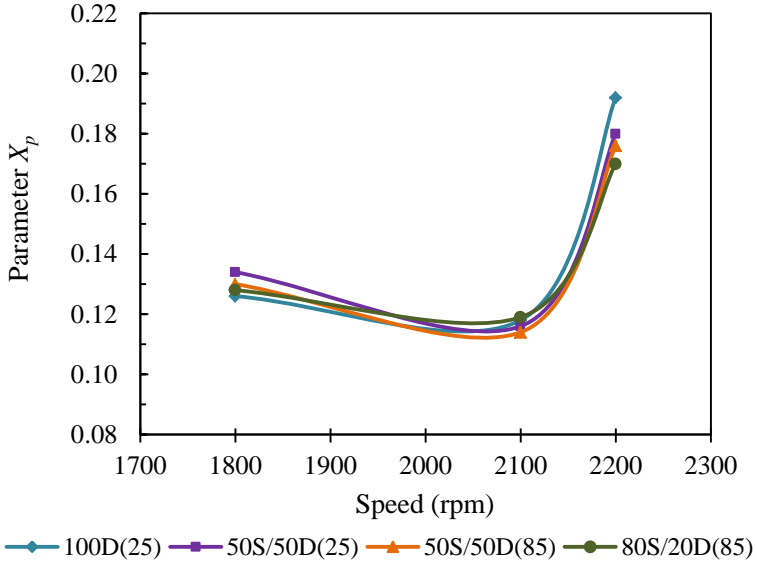
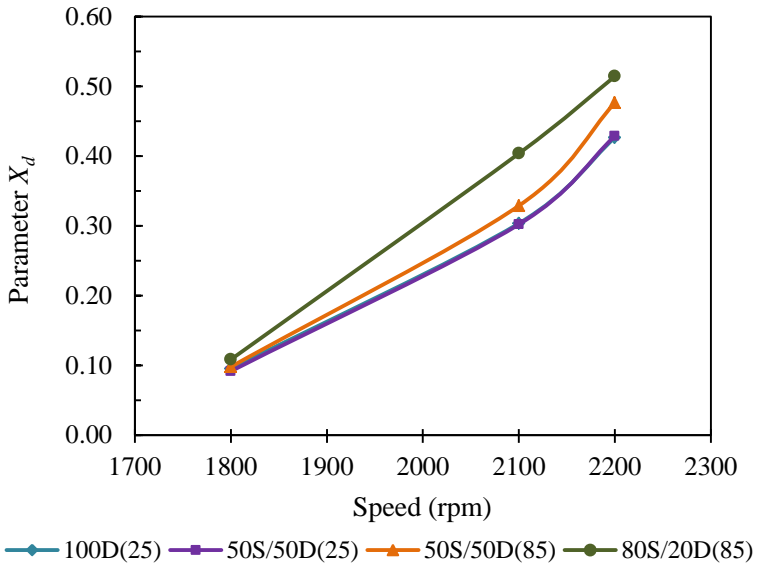
Figure 48. Parameter X_p as a function of crank angle for all fuels tested.Figure 49. Parameter X_d as a function of crank angle for all fuels tested.

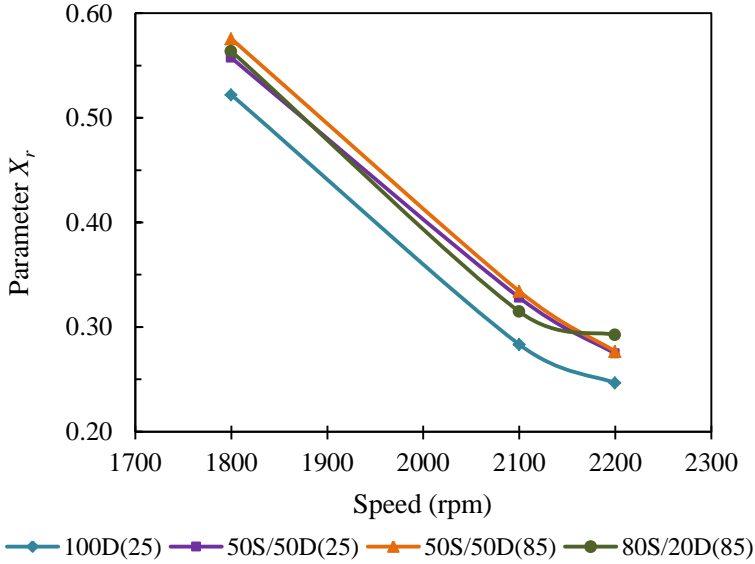
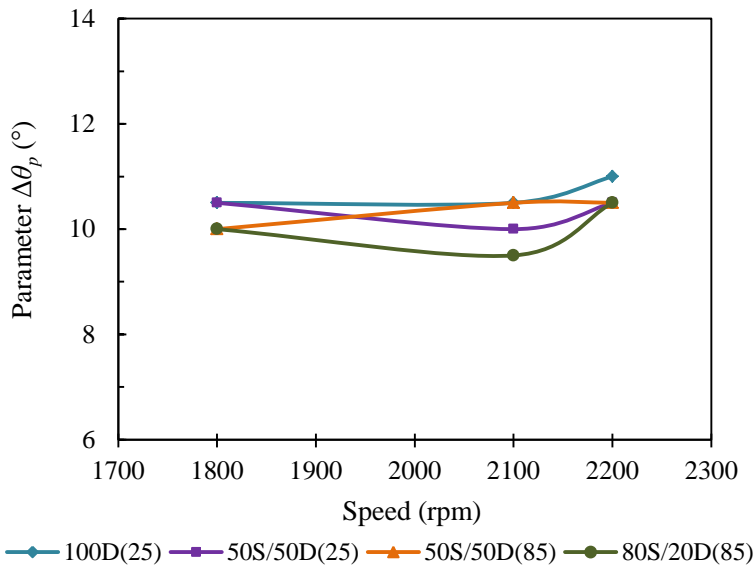
Figure 50. Parameter X_r as a function of crank angle for all fuels tested.Figure 51. Parameter $\Delta\theta_p$ as a function of crank angle for all fuels tested.

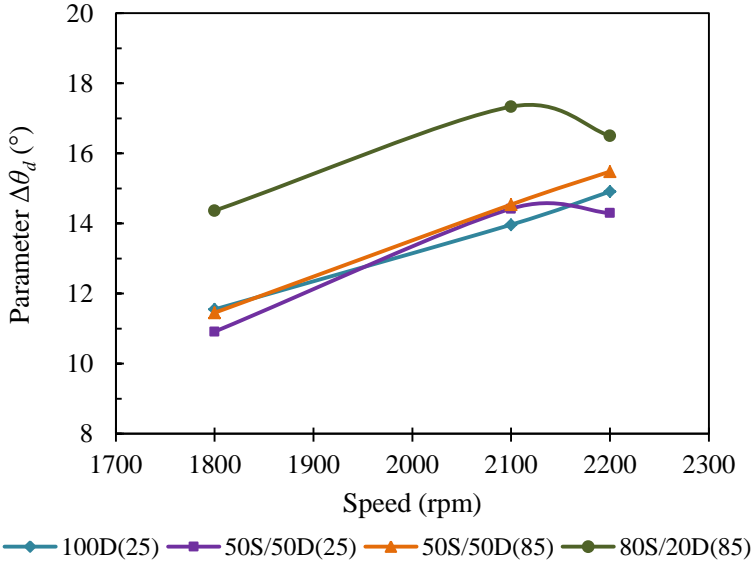
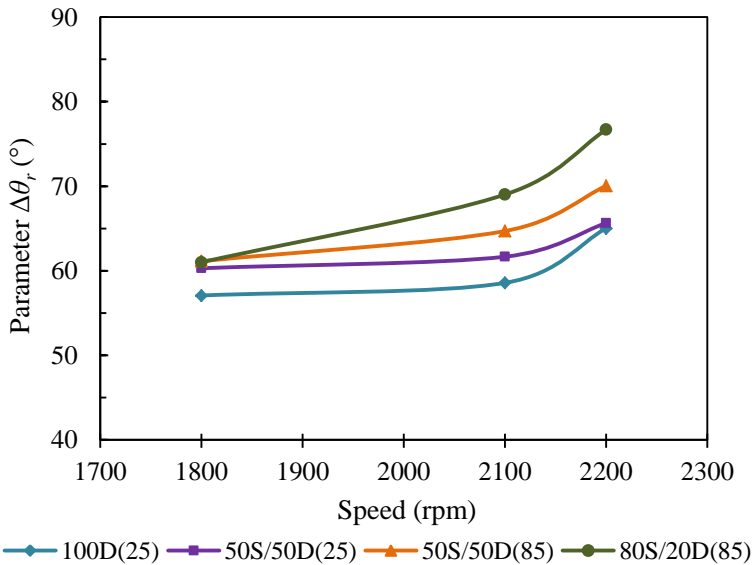
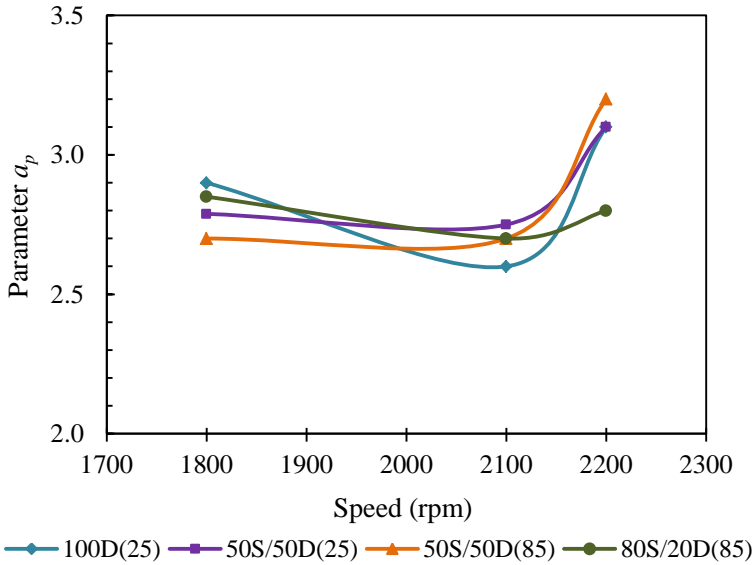
Figure 52. Parameter $\Delta\theta_d$ as a function of crank angle for all fuels tested.Figure 53. Parameter $\Delta\theta_r$ as a function of crank angle for all fuels tested.

Figure 54. Parameter a_p as a function of crank angle for all fuels tested.

The same parameters a_d , m_p , m_d and m_r found for diesel oil were used for all fuels, thus, it was considered that these parameters only change due to engine speed, and its behavior is shown of the Figure 55 to the Figure 58.

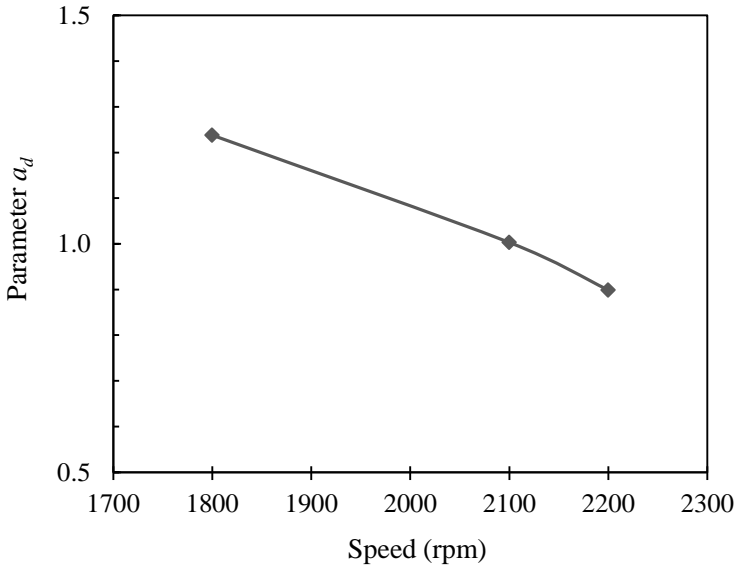
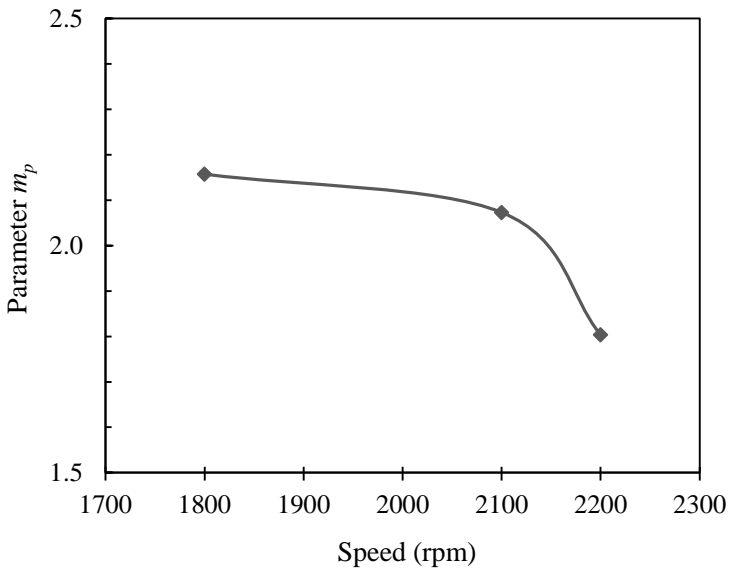
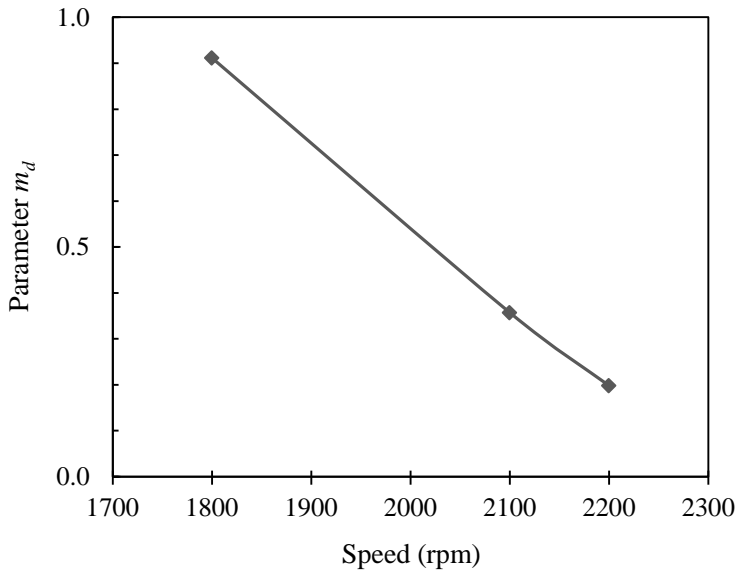
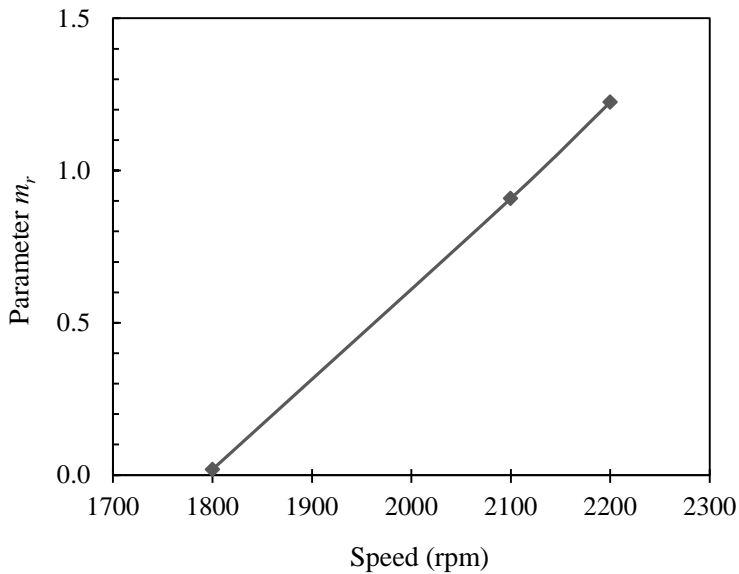
Figure 55. Parameter a_d as a function of crank angle.Figure 56. Parameter m_p as a function of crank angle.

Figure 57. Parameter m_d as a function of crank angle.Figure 58. Parameter m_r as a function of crank angle.

Analyzing the behavior obtained for these parameters, and considering physical variables that can influence on them, the following correlations were obtained to reproduce the responses of the mass fraction burned and the combustion duration for each combustion phase. The correlations were performed for the range of speed of 1800 to 2200 rpm and for the fuel properties depicted in Figure 45. Dimensionless variables were used in the correlations in order to generalize the applicability to other engines and speed conditions. However, this applicability was not still tested.

$$X_p = a \left(\frac{N}{N_{max}} \right)^b We_g^c \quad (6.1)$$

$$X_d = a \left(\frac{N}{N_{max}} \right)^b \left(\frac{SMD}{d_o} \right)^c \exp(\chi^d) \quad (6.2)$$

$$X_r = a \left(\frac{N}{N_{max}} \right)^b \quad (6.3)$$

$$\Delta\theta_d = a \left(\frac{N}{N_{max}} \right)^b \left(\frac{SMD}{d_o} \right)^c \exp(\chi^d) \quad (6.4)$$

$$\Delta\theta_r = a \left(\frac{N}{N_{max}} \right)^b We_g^c \exp(\chi^d) \quad (6.5)$$

where a , b , c and d are the fitting coefficients, N is the speed engine, N_{max} is the maximum speed engine, SMD is the Sauter mean diameter of the droplet, d_o is the nozzle diameter, We_g is the gas phase Weber number and χ is the volume fraction of the vegetable oil in the blend. For this case, $N_{max} = 2300$ rpm and $d_o = 0.0003$ m. In addition, We_g is calculated as

$$We_g = \frac{\rho_g (u_{sp} - S_p)^2 SMD}{\sigma_f} \quad (6.6)$$

As the parameter $\Delta\theta_p$ does not present significant variation among the fuels and for the speed range tested, it was considered

$\Delta\theta_p = 10$ for $N \leq 2100$ rpm and $\Delta\theta_p = 11$ for $N > 2100$ rpm. In relation to parameter a_p , it was fitted as a function of the speed (N) because there is not significant difference among fuels.

$$a_p = \frac{a + bN}{1 + cN + dN^2} \quad (6.7)$$

The variables used in these correlations were chosen with the objective to include physical information about fuel, gas phase and engine operating conditions. Table 37 shows the respective fitting coefficients, the coefficient of determination (R^2) and the standard deviation of each fitting procedure. In general, the positive or negative signal of each fitting coefficient is consistent with the physical effect of each variable on the respective parameter.

Table 37. Fitting coefficients, coefficient of determination (R^2) and standard deviation of the fitting procedure of each combustion parameter.

Combustion parameter	Fitting coefficients	R^2	Standard deviation
X_p	a	17.1975	0.9677
	b	1.1430	
	c	-1.0317	
X_d	a	0.3321	0.9900
	b	7.4948	
	c	- 0.2370	
	d	7.0311	
X_r	a	0.2318	0.9804
	b	-3.5543	
$\Delta\theta_d$	a	5.1344	0.9263
	b	1.2626	
	c	- 0.4428	
	d	7.9782	
$\Delta\theta_r$	a	124.9010	0.7655
	b	0.5958	
	c	- 0.1357	
	d	10.2830	
a_p	a	99.0439	0.5849
	b	- 4.1461x10 ⁻²	
	c	2.0583x10 ⁻²	
	d	- 9.0406x10 ⁻⁶	

6.6 ENGINE CYCLE SIMULATION

This section presents the results of in-cylinder pressure, heat release rate, in-cylinder temperature, intake mass flow, exhaust mass flow, total in-cylinder mass and performance parameters of the engine cycle simulation, operating with the all fuels tested. In order to validate the simulation process, the results obtained through the simulation are compared with the respective experimental data.

6.6.1 Pressure, temperature and heat release rate

Figure 59 shows the experimental and simulated in-cylinder pressure for the engine fueled with 100D(25), operating at 1800 rpm. The percentage differences between the experimental data and simulated data are presented in Figure 60, showing the highest differences in the corresponding periods of the intake and exhaust strokes. This result is possibly influenced by the calculation of the passage areas of the inlet and exhaust valves and the respective discharge coefficients, considering that this information was not measured and was assumed based on technical information found in the literature. Additionally, the intake and exhaust mass flow can be influenced by the tuning and ram phenomena, which were not considered in this model. On the other hand, the lowest differences are presented when the valves are closed (compression and expansion strokes), being about $\pm 10\%$, which is an acceptable value for the comparison between experimental and simulated data. In general, the simulated in-cylinder pressure follows the behavior of the in-cylinder pressure of the diesel engine tested.

The experimental and simulated heat release rate for the performance of the diesel engine with 100D(25) at 1800 rpm is shown in Figure 61, and the respective percentage differences are presented in Figure 62. One observes that the simulation reproduces the experimental results with differences in the range of -5% to 15% . The highest differences are presented in the combustion beginning and the transition between premixed and non-premixed combustion phases, which can be explained due to changing in the Wiebe function that describes the heat release rate. Additionally, it was defined, the heat release rate showed the behavior with the three combustion phases.

In relation to other variables, the in-cylinder gas temperature, total in-cylinder mass and the intake and exhaust mass flows are shown of the Figure 63 to Figure 65. The behavior obtained for each variable is corresponding with the characteristic behavior of a diesel engine.

Figure 59. Experimental and simulated in-cylinder pressure for 100D(25) at 1800 rpm.

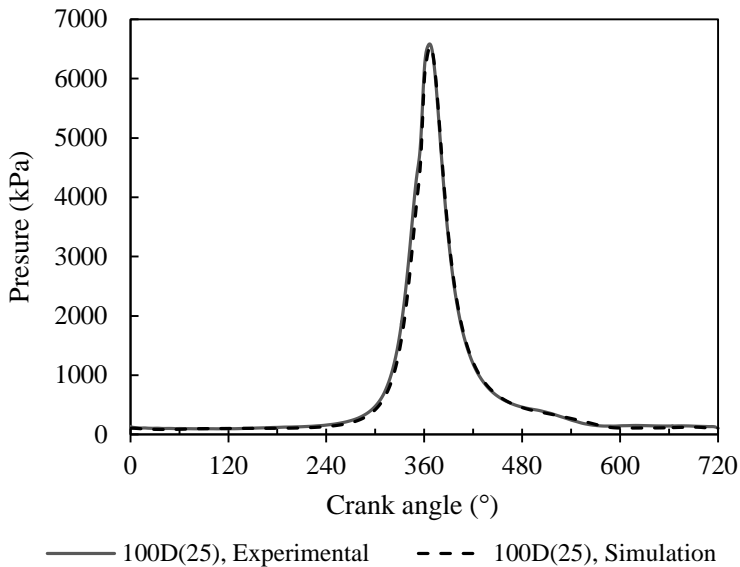


Figure 60. Percentage difference between the experimental and simulated in-cylinder pressure for 100D(25) at 1800 rpm.

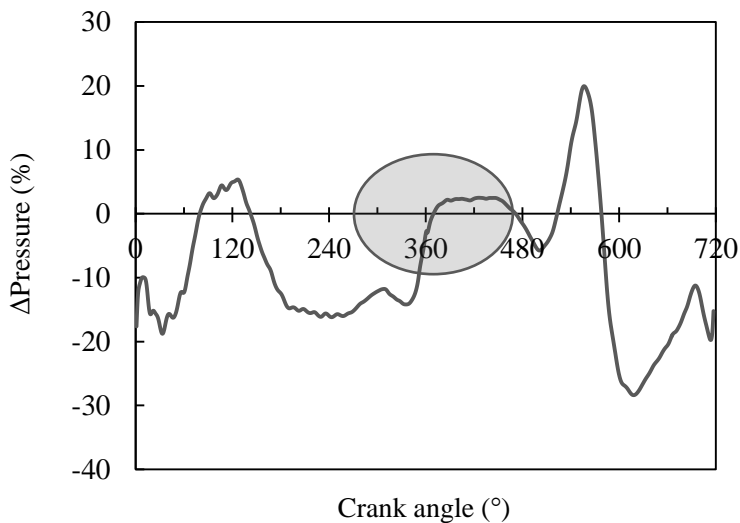


Figure 61. Experimental and simulated heat release rate of the diesel engine operating with 100D(25) at 1800 rpm.

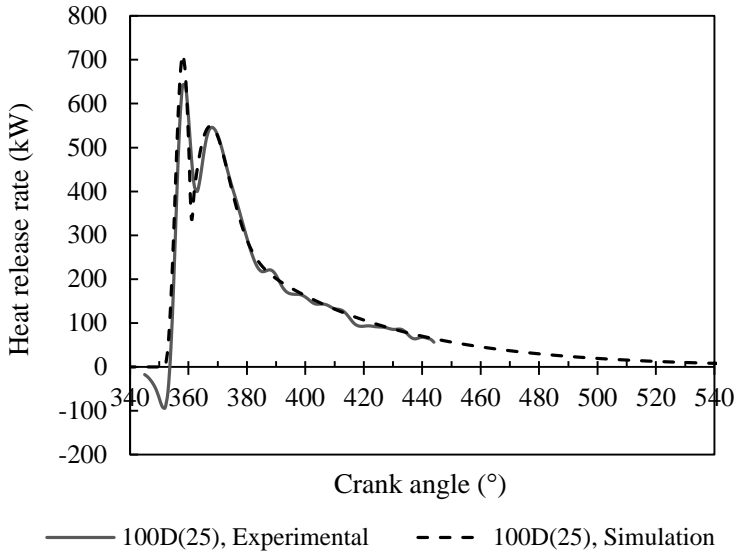


Figure 62. Percentage difference between the experimental and simulated heat release rate for 100D(25) at 1800 rpm.

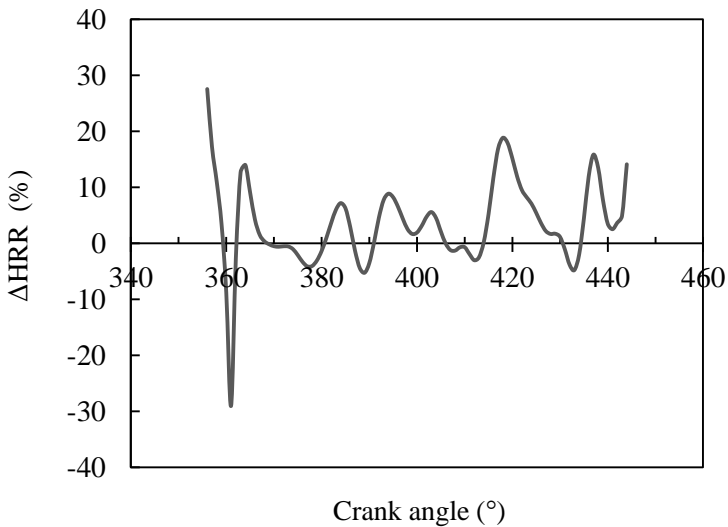


Figure 63. In-cylinder gas temperature simulated for 100D(25) at 1800 rpm.

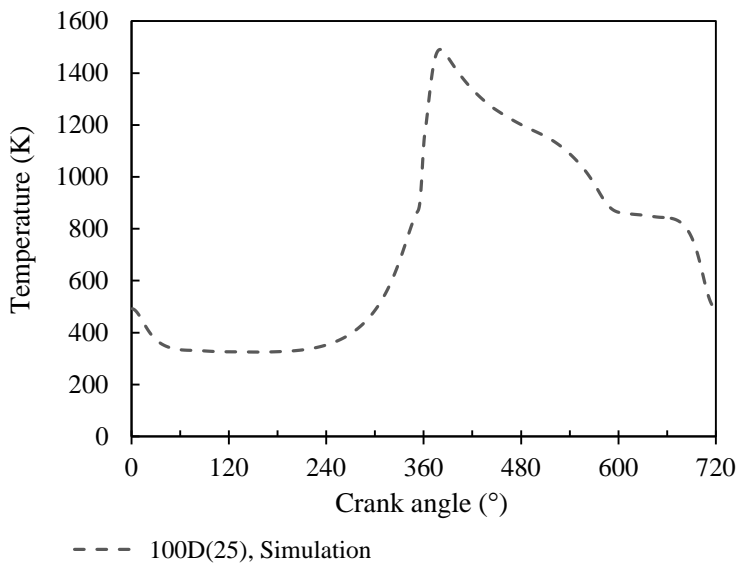


Figure 64. Total in-cylinder mass simulated for 100D(25) at 1800 rpm.

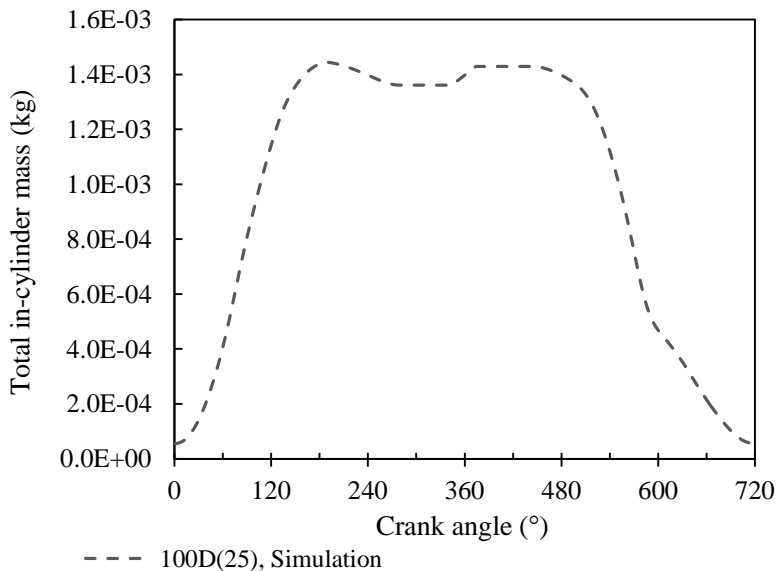
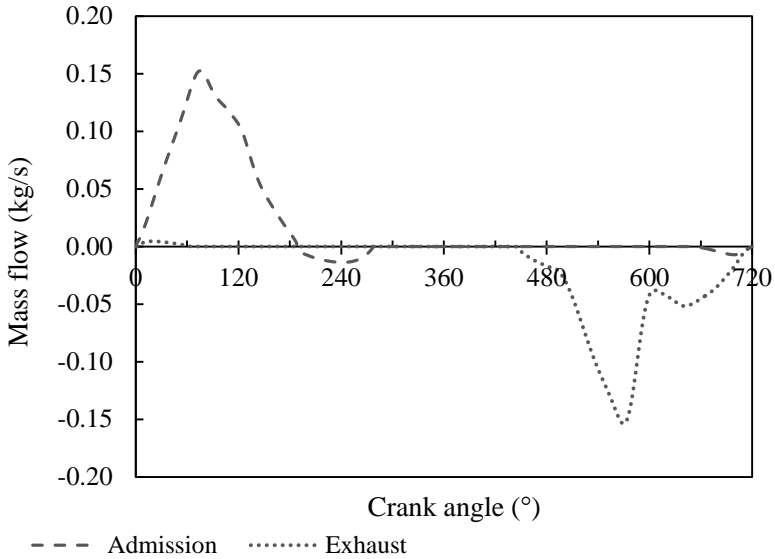


Figure 65. Intake and exhaust mass flows simulated for 100D(25) at 1800 rpm.



In order to show that the simulation replicated reasonably the experimental data of other blends, some results are also presented. The In-cylinder pressure and heat release rate for the operation of diesel engine with 50S/50D(25) at 1800 rpm as well as the respective figure about the percentage differences between experimental and simulated data are shown of the Figure 66 to Figure 69. Likewise, the results for the operation of diesel engine with 80S/20D(85) at 1800 rpm are shown of the Figure 70 to Figure 73. In general, a similar behavior was observed in the comparison between experimental and simulated data of the all fuels at speeds tested.

Figure 66. Experimental and simulated in-cylinder pressure for 50S/50D(25) at 1800 rpm.

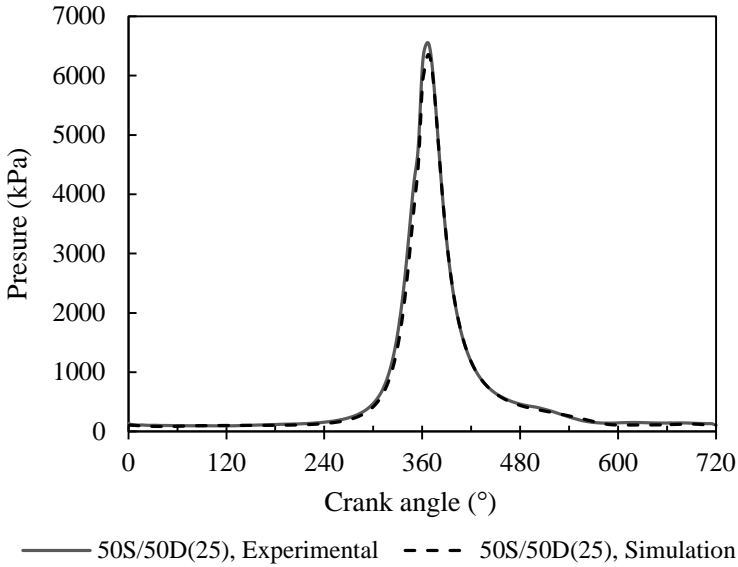


Figure 67. Percentage difference between the experimental and simulated in-cylinder pressure for 50S/50D(25) at 1800 rpm.

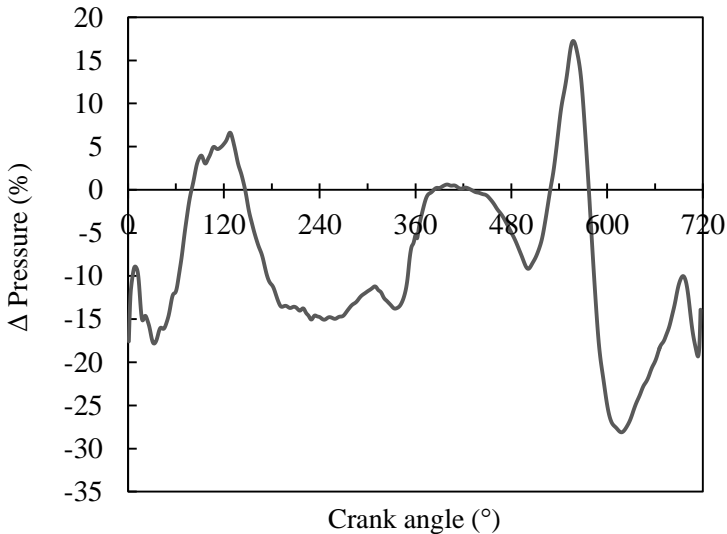


Figure 68. Experimental and simulated heat release rate of the diesel engine operating with 50S/50D(25) at 1800 rpm.

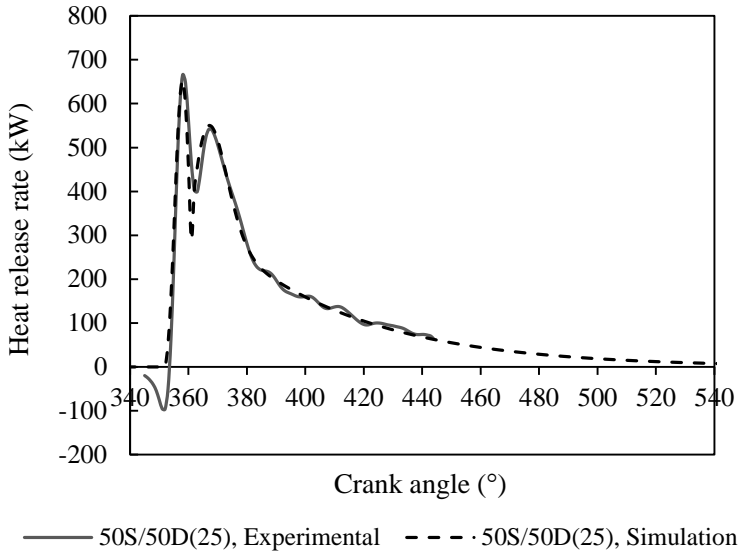


Figure 69. Percentage difference between the experimental and simulated heat release rate for 50S/50D(25) at 1800 rpm.

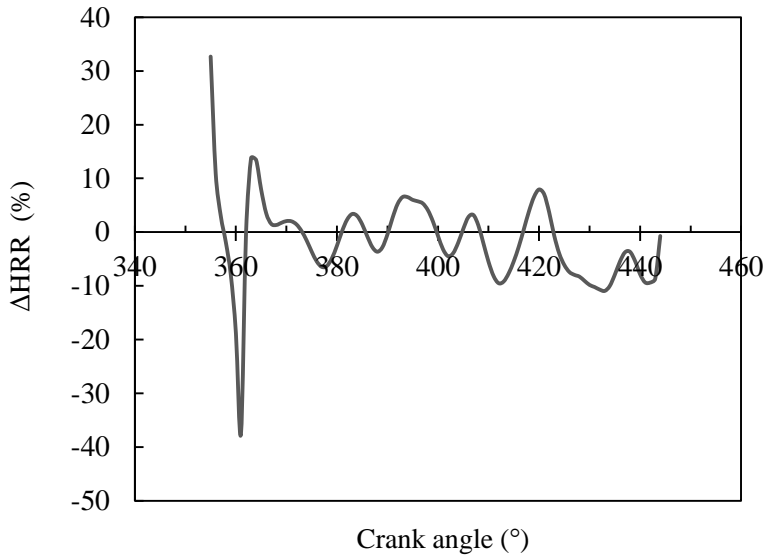


Figure 70. Experimental and simulated in-cylinder pressure for 80S/20D(85) at 1800 rpm.

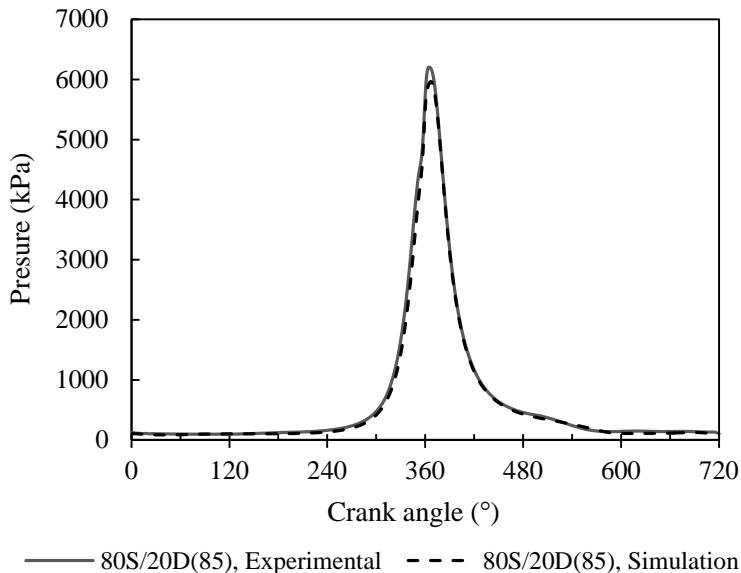


Figure 71. Percentage difference between the experimental and simulated in-cylinder pressure for 80S/20D(85) at 1800 rpm.

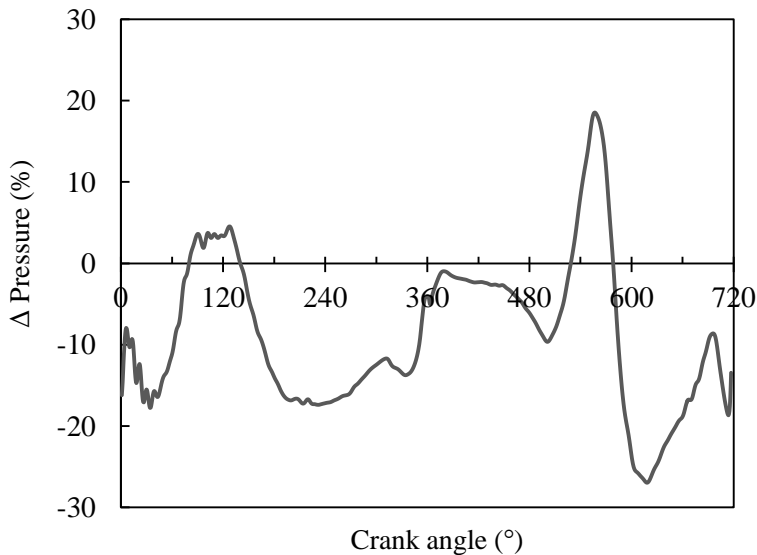


Figure 72. Experimental and simulated heat release rate of the diesel engine operating with 80S/20D(85) at 1800 rpm.

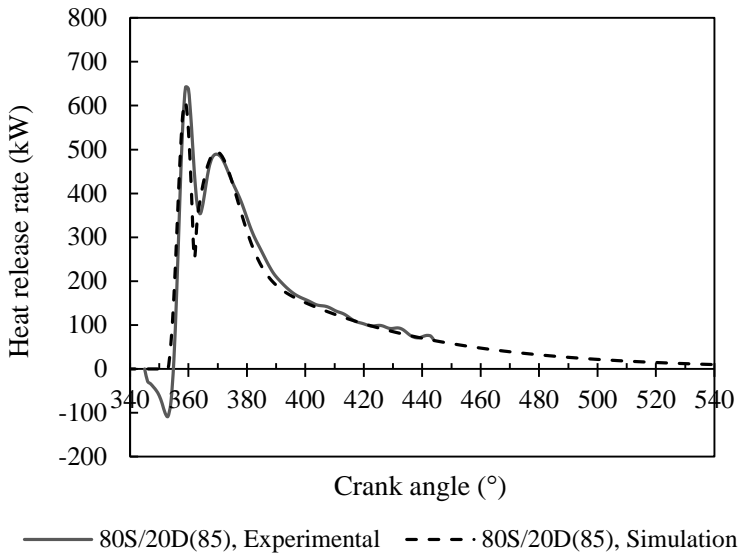
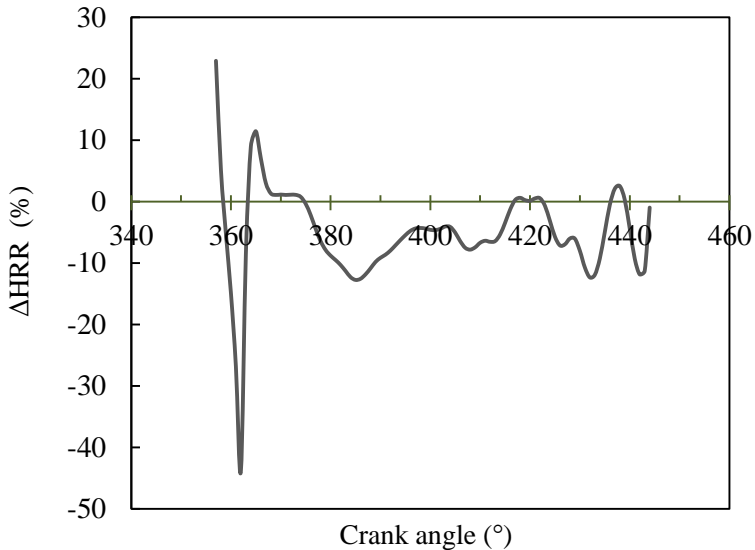


Figure 73. Percentage difference between the experimental and simulated heat release rate for 80S/20D(85) at 1800 rpm.



Additionally, the curves of the heat release rate for the four fuels at each speed tested are presented of the Figure 74 to the Figure 76. Comparing these figures with the respective experimental results shown of the Figure 35 to Figure 39, it is observed the analogous behavior with the experimental results, and the sensibility of the modeling in relation to the engine operation with different soybean oil blends. In the curves of the simulated heat release rate, it is also observed the point where ends the Wiebe function that describes the premixed combustion phase and starts the Wiebe function that describes the non-premixed and residual combustion phases. This point is shown as a little modification in the curves of the heat release rate. Nevertheless, this modification is not significant in the global simulation of the diesel engine cycle.

The simulated in-cylinder pressures for the four fuels at each speed tested are presented of the Figure 77 to the Figure 79. In a general form, the pressure results show a comparable behavior with the experimental data presented of the Figure 31 to the Figure 33, however it is also observed an unusual changing in the curve, close to TC, which is produced by the changing among the Wiebe functions, coinciding with that point. This effect is more significant at 2200 rpm.

Figure 74. Simulated heat release rate of the diesel engine operating with the four fuels tested at 1800 rpm.

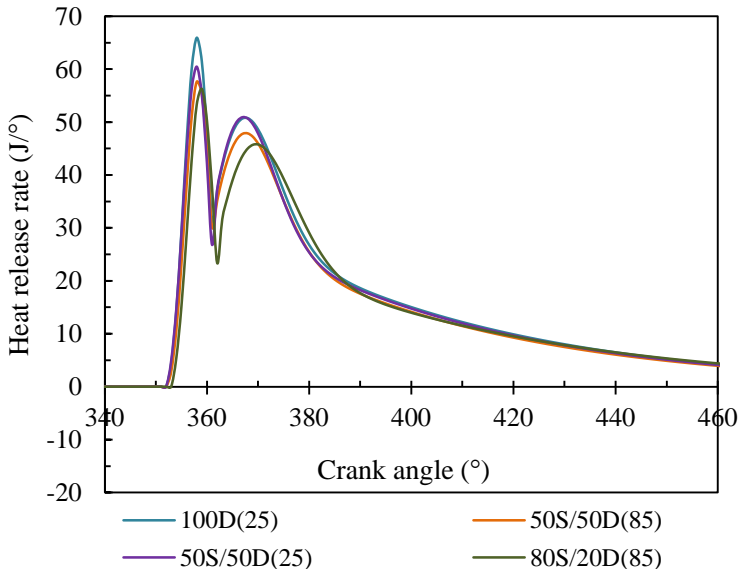


Figure 75. Simulated heat release rate of the diesel engine operating with the four fuels tested at 2100 rpm.

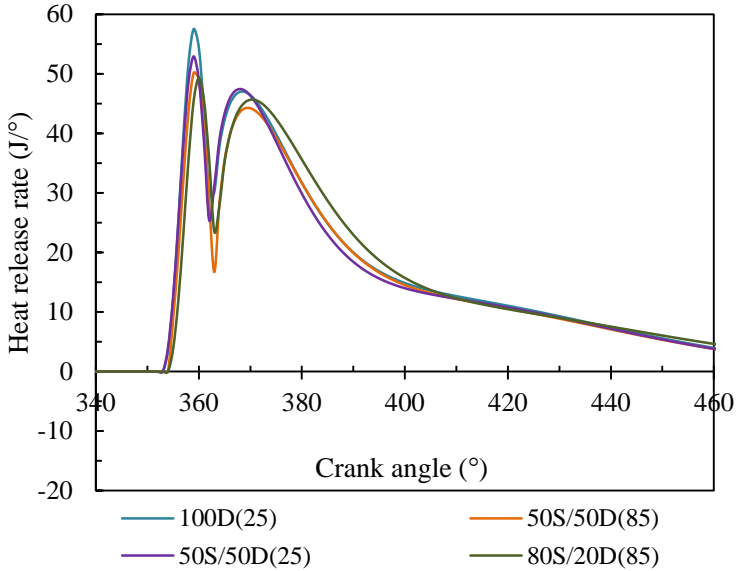


Figure 76. Simulated heat release rate of the diesel engine operating with the four fuels tested at 2200 rpm.

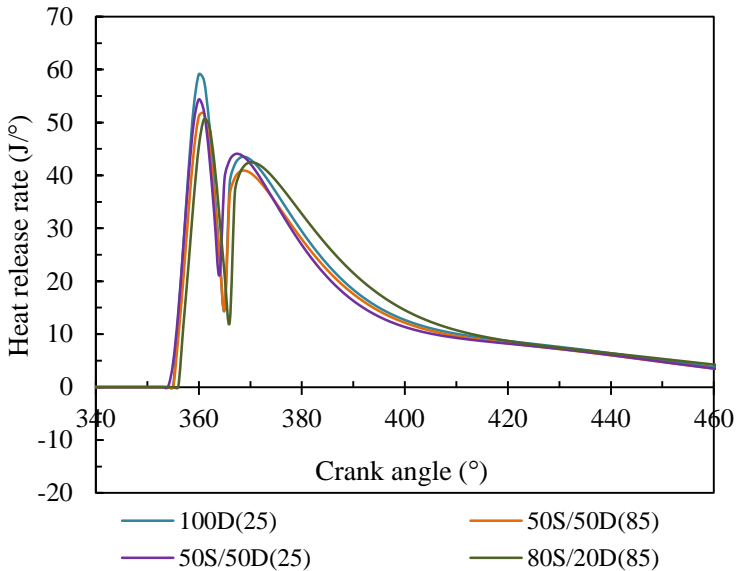


Figure 77. Simulated in-cylinder pressure of the diesel engine operating with the four fuels tested at 1800 rpm.

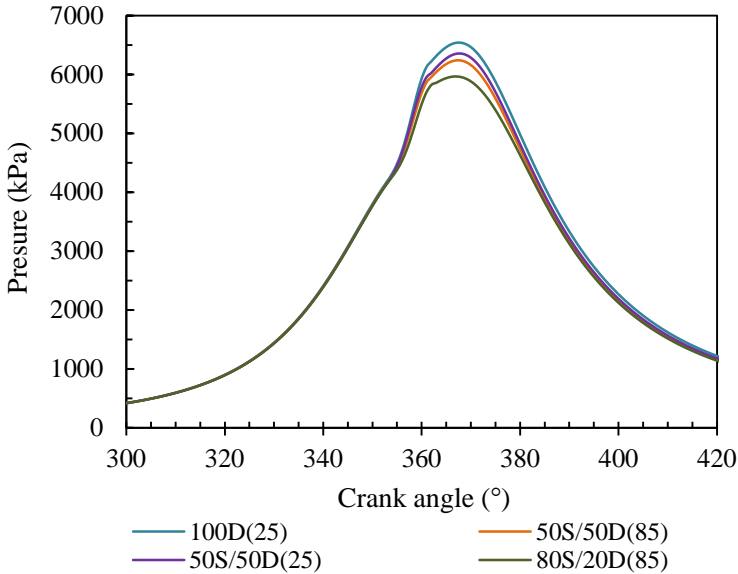


Figure 78. Simulated in-cylinder pressure of the diesel engine operating with the four fuels tested at 2100 rpm.

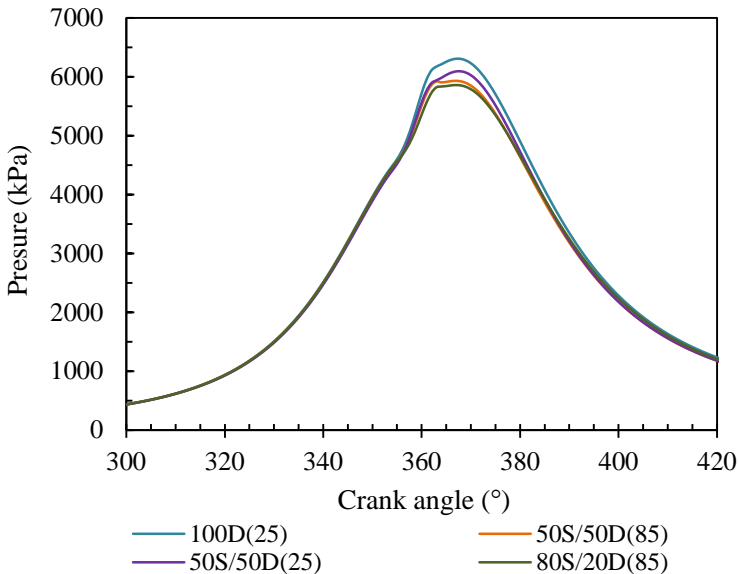
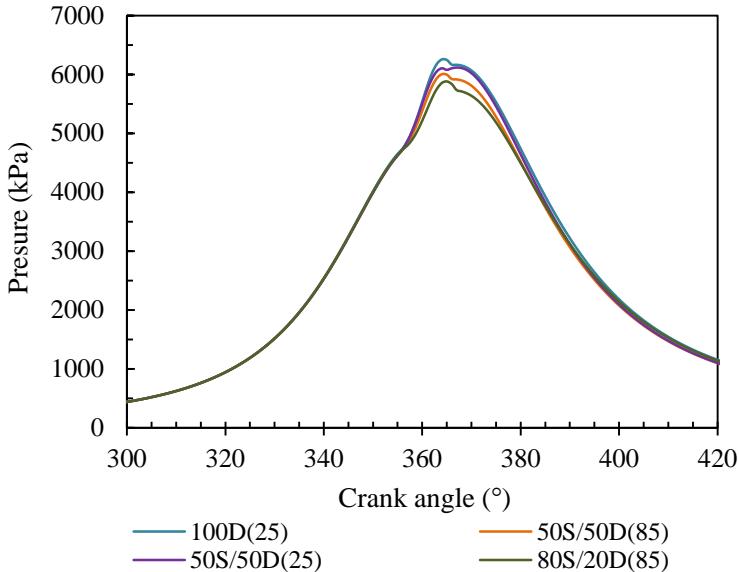


Figure 79. Simulated in-cylinder pressure of the diesel engine operating with the four fuels tested at 2200 rpm.



6.6.2 Performance parameters

In order to validate the simulation process, the performance parameters were also compared with the experimental results, as shown of Table 38 to Table 41.

One observes coherence between the simulated results and the experimental data, considering that the simulated parameters correspond to indicated parameters and the experimental data to brake parameters. With the indicated and brake power was possible to calculate the mechanical efficiency of the engine, which presented a coherent value (see Table 38 to Table 41), and decreased with the speed increase, as expected for the diesel engine tested.

The simulated mass fuel injected is very close to the experimental datum, being 5 % the maximum difference.

In the case of the volumetric efficiency, the high differences between simulated and experimental data can be a consequence of the information considered for the passage area and discharge coefficients of the valves, as well as, the occurrence in the manifolds of phenomena as the tuning and ram effects.

Table 38. Simulated and experimental performance parameters of the diesel engine operating with 100D(25) at three speeds tested.

Parameters	1800 rpm		2100 rpm		2200 rpm	
	Simulation	Experiment	Simulation	Experiment	Simulation	Experiment
Work (kJ)	0.897	0.832	0.869	0.775	0.780	0.636
Power (kW)	13.45	12.48	15.20	13.55	14.30	11.66
Mean effective pressure (kPa)	750.79	696.50	727.35	647.70	653.15	530.27
Specific fuel consumption (g/(kW·h))	273.31	294.62	275.12	308.95	230.68	270.97
Volumetric efficiency	0.932	0.868	0.966	0.859	0.954	0.849
Thermal efficiency	0.310	0.288	0.308	0.275	0.368	0.313
Mass fuel injected (mg/cycle)	68.09	68.09	66.40	66.40	49.99	47.68
Mechanical efficiency	0.928		0.891		0.815	

Table 39. Simulated and experimental performance parameters of the diesel engine operating with 50S/50D(25) at three speeds tested.

Parameters	1800 rpm		2100 rpm		2200 rpm	
	Simulation	Experiment	Simulation	Experiment	Simulation	Experiment
Work (kJ)	0.848	0.819	0.811	0.761	0.730	0.627
Power (kW)	12.72	12.28	14.19	13.31	13.39	11.50
Mean effective pressure (kPa)	709.98	684.49	678.79	633.40	611.40	522.77
Specific fuel consumption (g/(kW·h))	303.92	311.54	310.00	327.47	259.15	291.42
Volumetric efficiency	0.938	0.885	0.981	0.868	0.960	0.855
Thermal efficiency	0.299	0.292	0.294	0.278	0.351	0.312
Mass fuel injected (mg/cycle)	71.60	70.76	69.82	68.82	52.57	50.55
Mechanical efficiency	0.965		0.938		0.859	

Table 40. Simulated and experimental performance parameters of the diesel engine operating with 50S/50D(85) at three speeds tested.

Parameters	1800 rpm		2100 rpm		2200 rpm	
	Simulation	Experiment	Simulation	Experiment	Simulation	Experiment
Work (kJ)	0.819	0.807	0.795	0.748	0.711	0.592
Power (kW)	12.28	12.10	13.91	13.10	13.04	10.85
Mean effective pressure (kPa)	685.65	676.77	665.67	624.47	595.37	493.34
Specific fuel consumption (g/(kW·h))	301.59	307.12	302.87	320.14	254.97	287.86
Volumetric efficiency	0.937	0.892	0.971	0.868	0.959	0.871
Thermal efficiency	0.301	0.295	0.300	0.283	0.356	0.315
Mass fuel injected (mg/cycle)	68.61	68.97	66.90	66.33	50.37	47.12
Mechanical efficiency	0.985		0.941		0.832	

Table 41. Simulated and experimental performance parameters of the diesel engine operating with 80S/20D(85) at three speeds tested.

Parameters	1800 rpm		2100 rpm		2200 rpm	
	Simulation	Experiment	Simulation	Experiment	Simulation	Experiment
Work (kJ)	0.798	0.773	0.822	0.739	0.743	0.598
Power (kW)	11.97	11.60	14.39	12.94	13.62	10.96
Mean effective pressure (kPa)	668.24	645.46	688.30	616.70	621.78	498.63
Specific fuel consumption (g/(kW·h))	319.00	330.28	301.97	329.52	251.68	298.67
Volumetric efficiency	0.939	0.921	0.970	0.894	0.957	0.909
Thermal efficiency	0.296	0.286	0.313	0.287	0.376	0.316
Mass fuel injected (mg/cycle)	70.73	70.74	68.96	67.43	51.92	49.41
Mechanical efficiency	0.969		0.899		0.805	

6.7 FACTORIAL EXPERIMENTAL DESIGN

The diesel engine modeling can be used as a tool to evaluate the engine performance under different operating conditions. Analysis on the influence of the main variables and determination of optimal conditions can be obtained when results are analyzed, for instance, with statistical tests. This section presents an example of the applicability of the diesel engine modeling, using a statistical method to analyze the engine operating with soybean oil blends.

In this context, a factorial experimental design was performed in order to analyze some variables that influence on the thermal efficiency of the diesel engine operating with soybean oil blends. Additionally, this procedure allowed determining the favorable conditions to operate soybean oil blends in diesel engine.

The main factors considered for this analysis are: volume fraction of soybean oil in the blend (χ), fuel temperature (T_f), injection timing (θ_{inj}) and speed (N). Two levels (higher (+) and lower (-)) were selected for each factor, and the combination of these variable levels results in $2^4 = 16$ experiments of a factorial experimental design. The response analyzed was the thermal efficiency, which was obtained for each experiment using the simulation of the diesel engine. Table 42 shows the factors and levels considered in the 2^4 factorial experimental design. The combination of the factors and the respective response of thermal efficiency are presented in Table 43.

The statistical method denominated Analysis of Variance (ANOVA) was used to evaluate the influence of each one of the factors on the thermal efficiency. The ANOVA was performed in the Statistica software (Statistica, 2017), considering a confidence interval of 95 % ($\alpha = 0.05$ of significance level).

The analysis of variance for the factorial experimental design is presented in Table 44. The ANOVA test identified a significant effect ($p < 0.05$) for all factors tested, where p is the probability calculated using the F -distribution (Fisher Probability Distribution Function). The interactions among the factors were also evaluated, presenting a significant effect with exception of the interactions of the volume fraction and the fuel temperature with the injection timing.

The function Desirability of the Statistica software allows determining the combination of factors that satisfies an objective. For this analysis, two objectives were considered. First, obtaining the maximum thermal efficiency, and second, obtaining thermal efficiency

values above 30 %. For the first objective, Figure 80 shows that the desirability (objective) is satisfied with 95.8 % of probability when the factors are: volume fraction = 0.25, fuel temperature = 85 °C, injection timing = 343° CA and speed = 2100 rpm. For this combination of factors, the thermal efficiency is 31.5 %. For the second objective, Figure 81 shows that the objective is satisfied with 100 % of probability for the following condition: volume fraction ≤ 0.375 , fuel temperature ≥ 70 °C, injection timing ≤ 346 ° CA and speed ≥ 1950 rpm.

Table 42. Factors and levels of the 2^4 factorial experimental design.

Levels	Factors			
	Volume fraction (χ)	Fuel temperature (T_f)	Injection timing (θ_{inj})	Speed (N)
Lower (-)	0.25	25	343	1800
Higher (+)	0.75	85	347	2100

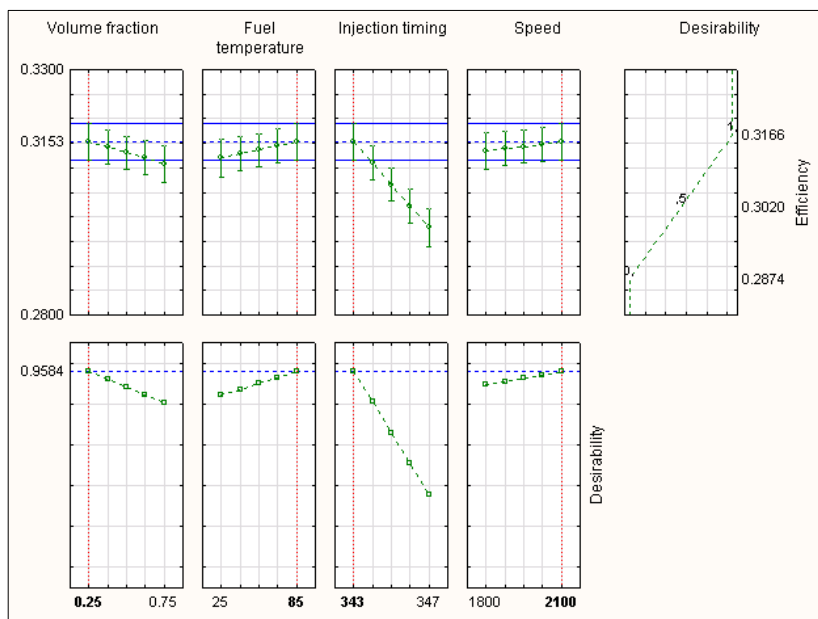
Table 43. Combination of factors and responses for the 2^4 factorial experimental design.

Experiment number	Factors				Response
	χ	T_f	θ_{inj}	N	η
1	0.25	85	343	2100	0.314
2	0.25	25	343	1800	0.313
3	0.75	25	347	2100	0.290
4	0.25	25	347	2100	0.292
5	0.25	25	347	1800	0.297
6	0.75	85	347	2100	0.295
7	0.75	25	343	2100	0.308
8	0.75	85	343	1800	0.306
9	0.75	85	343	2100	0.317
10	0.25	85	347	2100	0.295
11	0.75	85	347	1800	0.290
12	0.75	25	343	1800	0.302
13	0.25	85	347	1800	0.297
14	0.25	25	343	2100	0.310
15	0.75	25	347	1800	0.287
16	0.25	85	343	1800	0.314

Table 44. Analysis of variance for the 2^4 factorial experimental design.

Factors	Sum of square	Degree of freedom	Mean square	<i>F</i>	<i>p</i>
(1) Volume fraction	0.000080	1	0.000080	158.52	0.000056
(2) Temperature	0.000045	1	0.000045	88.61	0.000228
(3) Injection timing	0.001229	1	0.001229	2427.10	0.000000
(4) Speed	0.000015	1	0.000015	29.77	0.002812
1 by 2	0.000008	1	0.000008	15.81	0.010573
1 by 3	0.000000	1	0.000000	0.47	0.521649
1 by 4	0.000072	1	0.000072	142.42	0.000073
2 by 3	0.000002	1	0.000002	4.54	0.086268
2 by 4	0.000009	1	0.000009	17.78	0.008357
3 by 4	0.000009	1	0.000009	18.01	0.008138
Error	0.000003	5	0.000001		
Total sum of square	0.001472	15			

Figure 80. Function of desirability for maximum thermal efficiency as response.



7 CONCLUSIONS

This work addressed the use of soybean oil blends in compression ignition engines, involving measurements and the development of a zero-dimensional thermodynamic model to estimate the engine performance.

The physical properties of the fuel mixtures were either measured or obtained from the literature and curve-fitted to correlations as a function of the temperature and the volume fraction of vegetable oil. The chemical composition, higher and lower heat values of the diesel and soybean oils were also measured. The transient pressure trace was used to determine the heat release curve and to obtain the parameters of the Wiebe function. Knowledge of the properties allowed determining the amount of preheating needed in order that the properties of the mixture approach those of diesel oil, as well as, allowed for the development of correlations for the parameters of the Wiebe function and ignition delay time. The pressure curve was also used to compare the results obtained from the model.

Tests on the dynamometric bench were carried out for diesel oil and two blends, 50/50 % v/v and 80/20 % v/v of soybean and diesel oils. The fuels were labeled as 100D(25), 50S/50D(25), 50S/50D(85) and 80S/20D(85), indicating the respective volume proportion of soybean and diesel oils, and the fuel temperature at injection pump inlet. Different loads were applied in order to test the engine at 1800, 2100 and 2200 rpm. Measurements of torque, speed, power output, fuel consumption and air flow mass were recorded at steady state, supplying information to calculate the corresponding performance parameters of the diesel engine. Additionally, the in-cylinder pressure readings were recorded and processed to calculate the heat release rate for each fuel at the three speeds tested. The experimental results related to the performance parameters and in-cylinder pressure showed an adequate behavior and reliable with the fuel heat values and the load condition tested. The highest values of power and torque were presented for the fuel 100D(25) and blend 50S/50D(25). The increase of the fuel mass injected compensated the difference in the *LHV* value of this blend in relation to diesel oil. The blend 80S/20D(85), at the three speeds tested, presented the lowest values of brake torque and brake power because to its lower *LHV* in comparison to diesel oil (-10.5 %). In relation to the thermal efficiency, there was no significant difference for all fuels in the range of speed tested.

A zero-dimensional approach was used to obtain the heat release rate from the measured in-cylinder pressure data. The heat release rates evidence the premixed and non-premixed (diffusive) combustion phases. Additionally, a significant residual combustion phase was also observed.

The premixed combustion phase was similar for all fuels tested at 1800 and 2100 rpm. The highest premixed combustion phase for the fuel 100D(25) and the blend 50S/50D(25) was observed at 2200 rpm. For the blend 80S/20D(85), the high *SMD* (Sauter Mean Diameter) and the highest fraction of vegetable oil lead to a combustion delay, characterized by high diffusive and residual combustion phases. However, the oxygen content favored its combustion. Products of vegetable oil degradation may increase or inhibit the ignition, depending on their chemical nature. Therefore, it is not clear what occurs in the premixed combustion phase when comparing the blends 50S/50D(25) and 50S/50D(85). In the case of the blend 50S/50D(25), it is suggested that the highest *SMD* increased the droplet Reynold number and, therefore, the evaporation constant.

The fuel burning rate was curve-fitted to a Wiebe function. The measurement indicated the need to consider three combustion phases: premixed, non-premixed and residual. In order to evaluate each combustion phase, the premixed combustion phase was fitted to a simple Wiebe function and the non-premixed and residual phases were fitted to a double Wiebe function. The fitted heat release rates showed good accuracy when compared to the measurements, corresponding to a coefficient of determination of about $R^2 = 0.9$ for all fuels and engine speeds tested.

A combustion submodel was proposed considering two Wiebe functions and the parameters X_p , X_d , X_r , $\Delta\theta_p$, $\Delta\theta_d$, $\Delta\theta_r$ and a_p expressed as a function of the Sauter mean diameter, speed, gas Weber number and volume fraction of vegetable oil.

Additionally, an ignition delay correlation was proposed including five dimensionless expressions (SMD/d_0 , Re_D , ϕ_{gl} , $\exp(E_a/RT)$ and χ), correlating injection parameters, fuel properties and in-cylinder gas properties. The predicted values by the correlation were estimated within the 95 % confidence interval.

The complete cycle simulation was performed using a zero-dimensional approach. The inlet and exhaust flows were considered as compressible, unidimensional and isentropic. The fuel properties were calculated at the injection conditions using the found physico-chemical correlations. The ignition delay and the heat release rate were calculated

using the proposed correlations. The pressure and temperature found from simulation were considered for calculating the operating parameters of the engine such as the work, power, mean effective pressure, specific fuel consumption and thermal efficiency.

The predictions of in-cylinder pressure, heat release rate and performance parameters were compared with the measurements to test the simulation. For the in-cylinder pressure, the differences between experimental and simulated data were within $\pm 10\%$ in both compression and expansion strokes. Higher differences were found for the intake and exhaust strokes, probably influenced by uncertainties in the estimated passage areas of the intake and exhaust valves and the respective discharge coefficients. Additionally, the intake and exhaust mass flow can be influenced by the tuning and ram phenomena, which were not considered in the simulation process. Concerning the heat release rate, the simulation reproduces the experimental data with differences in the range of -5% to 15% . The highest difference occurred in the combustion beginning and transition between premixed and non-premixed combustion phases, due to the changing in the Wiebe function that describes the heat release rate. Likewise, in relation to performance parameters, it was observed consistence between the simulated and experimental data.

Finally, this work allowed observing the influence of the fuel properties and in-cylinder gas properties on the combustion process. In this context, the combustion of soybean oil blends is enhanced with high fuel temperature, high engine speed, low injection timing, low *SMD* and high in-cylinder temperature as well as pressure at injection timing. Therefore, the performance of a diesel engine fueled with vegetable oil blends is favored when the fuel is heated, the injection timing advances, the injection pressure increases or the diesel engine has a high compression ratio.

Future work

The following studies are proposed:

- Performing tests with other vegetable oils and other diesel engines, expanding the range of operating conditions and injection parameters tested.
- Development of a quasi-dimensional (multi-zone) modeling for the diesel engine fueled with vegetable oil blends.

- Using an image-based method to identify the phenomena that control the spray behavior during its evolution in the combustion chamber.
- Combustion analysis of droplets of vegetable oil and diesel oil (measurement and simulation) in order to evaluate and identify the effects of the oil degradation products.
- Performing tests with measurement of emissions to provide additional data for the analysis of the combustion of the soybean oil blends.

REFERENCES

- AGARWAL, A. K. Biofuels (alcohols and biodiesel) applications as fuels for internal combustion engines. **Progress in Energy and Combustion Science**, v. 33, n. 3, p. 233–271, 2007.
- AGARWAL, A. K.; DHAR, A. Karanja Oil Utilization in a Direct-Injection Engine by Preheating. Part 1: Experimental Investigations of Engine Performance, Emissions, and Combustion Characteristics. **Proceedings of the Institution of Mechanical Engineers, Part D: Journal of Automobile Engineering**, v. 224, n. 1, p. 73–84, 2010.
- AGARWAL, A. K.; RAJAMANOCHARAN, K. Experimental investigations of performance and emissions of Karanja oil and its blends in a single cylinder agricultural diesel engine. **Applied Energy**, v. 86, n. 1, p. 106–112, 2009.
- AGARWAL, D.; AGARWAL, A. K. Performance and emissions characteristics of Jatropa oil (preheated and blends) in a direct injection compression ignition engine. **Applied Thermal Engineering, Heat Powered Cycles – 04**. v. 27, n. 13, p. 2314–2323, 2007.
- AGARWAL; DHAR, A. Experimental investigations of performance, emission and combustion characteristics of Karanja oil blends fuelled DIC engine. **Renewable Energy**, v. 52, p. 283–291, 2013.
- AGARWAL; KUMAR, L.; AGARWAL, A. K. Performance evaluation of a vegetable oil fuelled compression ignition engine. **Renewable Energy**, v. 33, n. 6, p. 1147–1156, 2008.
- AKSOY, F. The Effect of Opium Poppy Oil Diesel Fuel Mixture on Engine Performance and Emissions. **International Journal of Environmental Science & Technology**, v. 8, n. 1, p. 57–62, 2011.
- ALAGUMALAI, A. Combustion characteristics of lemongrass (*Cymbopogon flexuosus*) oil in a partial premixed charge compression ignition engine. **Alexandria Engineering Journal**, v. 54, n. 3, p. 405–413, 2015.
- ALMEIDA, S. C. A. de; BELCHIOR, C. R.; NASCIMENTO, M. V. G.; VIEIRA, L. dos S. R.; FLEURY, G. Performance of a diesel generator fuelled with palm oil. **Fuel**, v. 81, n. 16, p. 2097–2102, 2002.

ALTIN, R.; ÇETINKAYA, S.; YÜCESU, H. S. The potential of using vegetable oil fuels as fuel for diesel engines. **Energy Conversion and Management**, v. 42, n. 5, p. 529–538, 2001.

ANNAND, W. J. D. Heat transfer in the cylinders of reciprocating internal combustion engines. **Proceedings of the Institution of Mechanical Engineers**, v. 177, n. 36, p. 973–990, 1963.

ANTWI, E. **Experimental analysis of vegetable oil blends in a compression ignition (CI) engine**. 2008. 134 p. Master thesis (Mechanical engineering) – Kwame Nkrumah University of Science and Technology, Ghana, 2008.

AUSTEN, A. E. W.; LYN, W.-T. Relation between Fuel Injection and Heat Release in a Direct-Injection Engine and the Nature of the Combustion Processes. **Proceedings of the Institution of Mechanical Engineers: Automobile Division**, v. 14, n. 1, p. 47–62, 1960.

AWAD, S.; VARUVEL, E. G.; LOUBAR, K.; TAZEROUT, M. Single zone combustion modeling of biodiesel from wastes in diesel engine. **Fuel**, v. 106, p. 558–568, 2013.

AZIAN, M. N.; KAMAL, A. A. M.; PANAU, F.; TEN, W. K. Viscosity Estimation of Triacylglycerols and of Some Vegetable Oils, Based on Their Triacylglycerol Composition. **Journal of the American Oil Chemists' Society**, v. 78, n. 10, p. 1001–1005, 2001.

BALAFOUTIS, A.; FOUNTAS, S.; NATSIS, A.; PAPADAKIS, G. Performance and Emissions of Sunflower, Rapeseed, and Cottonseed Oils as Fuels in an Agricultural Tractor Engine. **ISRN Renewable Energy**, v. 2011, p. 1–12, 2011.

BARI, S.; ROY, M. M. Prospect of rice bran oil as an alternative to diesel fuel. In: FIFTH INTERNATIONAL CONFERENCE ON SMALL ENGINES, THEIR FUELS AND THE ENVIRONMENT, 1995, University of Reading, UK. **Proceedings...** University of Reading, UK, 1995, p. 31–36.

BARSIC, N. J.; HUMKE, A. L. Performance and Emissions Characteristics of a Naturally Aspirated Diesel Engine with Vegetable Oil Fuels. **SAE Technical Paper**, n. 810262, p. 1–18, 1981.

BAUMGARTEN, C. **Mixture formation in internal combustion engine**. Berlin: Springer-Verlag Berlin Heidelberg, 2006.

BELAGUR, V. K.; REDDY, V.; WADAWADAGI, S. B. Effect of Injection Pressure on Performance, Emission and Combustion Characteristics of Direct Injection Diesel Engine Running on Blends of Pongamia Pinnata Linn (Honge oil) Oil and Diesel Fuel. **Agricultural Engineering International: CIGR Journal**, 2009.

BELCHIOR, C. R. P.; PIMENTEL, V. S. de B. The use of palm oil in Diesel engine. In: 18TH INTERNATIONAL CONGRESS OF MECHANICAL ENGINEERING - COBEM 2005, 2005, Ouro Preto - MG. **Proceedings...** . Ouro Preto - MG, 2005.

BENJUMEA, P.; AGUDELO, J.; AGUDELO, A. Basic properties of palm oil biodiesel–diesel blends. **Fuel**, v. 87, n. 10–11, p. 2069–2075, 2008.

BENJUMEA, P.; AGUDELO, J.; AGUDELO, A. Effect of altitude and palm oil biodiesel fuelling on the performance and combustion characteristics of a HSDI diesel engine. **Fuel**, v. 88, n. 4, p. 725–731, 2009.

BETTIS, B. L.; PETERSON, C. L.; AULD, D. L.; DRISCOLL, D. J.; PETERSON, E. D. Fuel Characteristics of Vegetable Oil from Oilseed Crops in the Pacific Northwest. **Agronomy Journal**, v. 74, n. 2, p. 335–339, 4/01 1982.

BIALKOWSKI, M. T.; PEKDEMIR, T.; REUBEN, R.; BRAUTSCH, M.; TOWERS, D. P.; ELSBETT, G. Preliminary approach towards a CDI system modification operating on neat rapeseed oil. **Journal of KONES Internal Combustion Engines**, v. 12, p. 1–12, 2005.

BLIN, J.; BRUNSCHWIG, C.; CHAPUIS, A.; CHANGOTADE, O.; SIDIBE, S. S.; NOUMI, E. S.; GIRARD, P. Characteristics of vegetable oils for use as fuel in stationary diesel engines—Towards specifications for a standard in West Africa. **Renewable and Sustainable Energy Reviews**, v. 22, n. Supplement C, p. 580–597, 2013.

BYATT-SMITH, J.; DAY, R.; HARLEN, O.; LISTER, J.; SMITH, S. L.; PLEASE, C. P.; STONE, R.; HOWISON, S. D.; FOWLER, A.

Temperature of Diesel Fuel Spray at Injector Nozzle Hole Exit. **The MIIS Eprints Archive**, v. ESGI 29, 1996.

CANAKCI, M.; OZSEZEN, A. N.; TURKCAN, A. Combustion analysis of preheated crude sunflower oil in an IDI diesel engine. **Biomass and Bioenergy**, v. 33, n. 5, p. 760–767, 2009.

CAPUANO, D.; COSTA, M.; DI FRAIA, S.; MASSAROTTI, N.; VANOLI, L. Direct use of waste vegetable oil in internal combustion engines. **Renewable and Sustainable Energy Reviews**, v. 69, p. 759–770, 2017.

CARR, M. A.; CATON, P. A.; HAMILTON, L. J.; COWART, J. S.; MEHL, M.; PITZ, W. J. An Experimental and Modeling-Based Study into the Ignition Delay Characteristics of Diesel Surrogate Binary Blend Fuels. In: 2011 INTERNAL COMBUSTION ENGINE DIVISION FALL TECHNICAL CONFERENCE, ICEF2011, 2011, Morgantown, WV, United States. **Proceedings...** . Morgantown, WV, United States, 2011.

CARTILLIERI, W.; JOHNS, R. J. R. Multidimensional Modelling of Engine Processes: Progress and Prospects. In: 15TH CIMAC CONGRESS, 1983, Paris. **Proceedings...** . Paris, 1983.

CHALATLON, V.; ROY, M. M.; DUTTA, A.; KUMAR, S. Jatropha Oil Production and an Experimental Investigation of Its Use as an Alternative Fuel in a DI Diesel Engine. **Journal of Petroleum Technology and Alternative Fuels**, v. 2, n. 5, p. 76–85, 2011.

CHANG, C.-C.; WAN, S.-W. China's Motor Fuels from Tung Oil. **Industrial & Engineering Chemistry**, v. 39, n. 12, p. 1543–1548, 1947.

CHAUHAN, B. S.; KUMAR, N.; DU JUN, Y.; LEE, K. B. Performance and emission study of preheated Jatropha oil on medium capacity diesel engine. **Energy**, v. 35, n. 6, p. 2484–2492, 2010.

CHMELA, F. G.; ORTHABER, G. C. Rate of heat release prediction for direct injection diesel engine basic on purely mixing controlled combustion. **SAE Technical Paper**, v. 1, n. 1999-1–186, 1999.

CLARK, P. E.; WALDELAND, C. R.; CROSS, R. P. Specific Heats of Vegetable Oils from 0° to 280° C. **Industrial & Engineering Chemistry**, v. 38, n. 3, p. 350–353, 1946.

CONVERGE CFD Software. Madison, WI: Convergent science, 2016.

COSTA, P.; ROSSI, L.; ZAGONEL, G.; RAMOS, L. The utilization of used frying oil for the production of biodiesel (in Portuguese). **Química Nova**, v. 23, n. 4, p. 531–537, 2000.

DAHO, T.; VAITILINGOM, G.; OUIHINGA, S. K.; PIRIOU, B.; ZONGO, A. S.; OUOBA, S.; KOULIDIATI, J. Influence of engine load and fuel droplet size on performance of a CI engine fueled with cottonseed oil and its blends with diesel fuel. **Applied Energy**, v. 111, p. 1046–1053, 2013.

D’ALESSANDRO, B.; BIDINI, G.; ZAMPILLI, M.; LARANCI, P.; BARTOCCHI, P.; FANTOZZI, F. Straight and waste vegetable oil in engines: Review and experimental measurement of emissions, fuel consumption and injector fouling on a turbocharged commercial engine. **Fuel**, v. 182, p. 198–209, 2016.

DEC, J. E. A Conceptual Model of DI Diesel Combustion Based on Laser-Sheet Imaging. **SAE Technical Paper**, v. 970873, p. 1–30, 1997.

DENT, J. C.; MEHTA, P. S. Phenomenological combustion model for a quiescent chamber diesel engine. **SAE Technical Paper**, n. 811235, 1981.

DESHMUKH, D.; MADAN MOHAN, A.; ANAND, T. N. C.; RAVIKRISHNA, R. V. Spray characterization of straight vegetable oils at high injection pressures. **Fuel**, v. 97, p. 879–883, 2012.

EES Engineering Equation Software. Madison, WI: F-Chart Software, 2016.

ENGELMAN, H. W.; GUENTHER, D. A.; SILVIS, T. W. Vegetable oil as a diesel fuel. In: ENERGY TECHNOLOGY CONFERENCE AND EXHIBITION, 1978, New York. **Diesel and Gas Engine Power Division of ASME, New York**. New York: ASME, 1978, paper No.78-DGP-19.

ESTEBAN, B.; RIBA, J.-R.; BAQUERO, G.; PUIG, R.; RIUS, A. Characterization of the surface tension of vegetable oils to be used as fuel in diesel engines. **Fuel**, v. 102, p. 231–238, 2012.

FLYNN, P. F.; DURRETT, R. P.; HUNTER, G. L.; LOYE, A. O.; AKINYAMI, O. C.; DEC, J. E.; WESTBROOK, C. Diesel combustion: an integrated view combining laser diagnostics, chemical kinetics, and empirical validation. **SAE Technical Paper**, v. 1999-1-509, p. 1–17, 1999.

FONSECA, H.; GUTIERREZ, L. E. Composition in fatty acids of vegetable oils and animal fats (in Portuguese). **Anais da Escola Superior de Agricultura Luiz de Queiroz**, v. 31, p. 485–490, 1974.

FONTARAS, G.; SAMARAS, Z.; MILTSIOS, G. Experimental Evaluation of Cottonseed Oil-Diesel Blends as Automotive Fuels via Vehicle and Engine Measurements. **SAE Technical Paper**, n. 2007-24-0126, p. 1–10, 2007.

FORSON, F. K.; ODURO, E. K.; HAMMOND-DONKOH, E. Performance of jatropha oil blends in a diesel engine. **Renewable Energy**, v. 29, n. 7, p. 1135–1145, 2004.

FRANCO, Z.; NGUYEN, Q. D. Flow properties of vegetable oil–diesel fuel blends. **Fuel**, v. 90, n. 2, p. 838–843, 2011.

FREITAS, S. V. D.; E SILVA, F. A.; PASTORIZA-GALLEGO, M. J.; PIÑEIRO, M. M.; LIMA, Á. S.; COUTINHO, J. A. P. Measurement and Prediction of Densities of Vegetable Oils at Pressures up to 45 MPa. **Journal of Chemical & Engineering Data**, v. 58, n. 11, p. 3046–3053, 2013.

GARZÓN, N. A. N. **Experimental and exergetic analysis of the operation of a diesel engine with vegetable oil (in Portuguese)**. 2012. 189 p. Master thesis (Mechanical Engineering) – UFSC, Florianópolis, SC, 2012.

GARZÓN, N. A. N.; BAZZO, E.; OLIVEIRA, A. A. M. Theoretical analysis of atomization in a diesel engine fueled with soybean oil. In: 23RD ABCM INTERNATIONAL CONGRESS OF MECHANICAL ENGINEERING - COBEM 2015, 2015, Rio de Janeiro-RJ. **Proceedings...** Rio de Janeiro-RJ: ABCM, 2015.

GARZÓN, N. A. N.; HARTMANN, R. M.; OLIVEIRA, A. A. M.; BAZZO, E. Analysis and measurement of the performance and emissions of a diesel engine operating with straight soybean oil. In: 8TH MEDITERRANEAN COMBUSTION SYMPOSIUM - MCS 8, 2013, Çesme, Izmir, Turkey. **Proceedings...** . Çesme, Izmir, Turkey: ICHMT-The Combustion Institute, 2013, p. 160.

GARZÓN, N. A. N.; OLIVEIRA, A. A. M.; BAZZO, E. Heat release rate of a compression ignition engine fueled with diesel oil and a diesel-straight soybean oil blend. In: 16TH BRAZILIAN CONGRESS OF THERMAL SCIENCES AND ENGINEERING - ENCIT 2016, 2016, Vitória-ES. **Proceedings...** . Vitória-ES: ABCM, 2016.

GARZÓN, N. A. N.; OLIVEIRA, A. A. M.; HARTMANN, R. M.; BAZZO, E. Experimental and Thermodynamic Analysis of a Compression Ignition Engine Operating with Straight Soybean Oil. **Journal of the Brazilian Society of Mechanical Sciences and Engineering**, v. 37, n. 5, p. 1467–1478, 2015.

GARZÓN, N. A. N.; ZARZA, H. M.; SCHROEDER, F.; SANTOS; OLIVEIRA, A. A. M.; BAZZO, E. Application of statistical procedures for the analysis of the combustion chamber pressure curve of compression-ignition engines (in Portuguese). In: JORNADAS IBEROAMERICANAS DE MOTORES TÉRMICOS Y LUBRICACIÓN - MTL 2016, 2016, La Plata, Argentina. **Actas de MTL 2016 Jornadas Iberoamericanas de Motores Térmicos y Lubricación**, La Plata, Argentina: Universidad Nacional de La Plata, 2016, p. 279–294.

GEO, E. V.; NAGARAJAN, G.; NAGALINGAM, B. Studies on dual fuel operation of rubber seed oil and its bio-diesel with hydrogen as the inducted fuel. **International Journal of Hydrogen Energy**, v. 33, n. 21, p. 6357–6367, 2008.

GEO, V. E.; NAGARAJAN, G.; NAGALINGAM, B. Studies on improving the performance of rubber seed oil fuel for diesel engine with DEE port injection. **Fuel**, v. 89, n. 11, p. 3559–3567, 2010.

GHOJEL, J. I. Review of the Development and Applications of the Wiebe Function: A Tribute to the Contribution of Ivan Wiebe to Engine Research. **International Journal of Engine Research**, v. 11, n. 4, p. 297–312, 2010.

GIANNELOS, P. N.; ZANNIKOS, F.; STOURNAS, S.; LOIS, E.; ANASTOPOULOS, G. Tobacco seed oil as an alternative diesel fuel: physical and chemical properties. **Industrial Crops and Products**, v. 16, n. 1, p. 1–9, 2002.

GONÇALVES, A.; SOUSA, A. de. **Fundamentals of scientific and industrial metrology (in Portuguese)**. 1. ed. Barueri: Manole Ltda, 2008.

GOSMAN, A. D.; TSUI, Y. Y.; WATKINS, A. P. Calculation of Unsteady Three-dimensional Flow in a Model Motored reciprocating Engine and Comparison with Experiment. In: 5TH INTERNATIONAL TURBULENT SHEAR FLOW MEETING, 1985, Cornell University, Ithaca, NY. **Proceedings...** . Cornell University, Ithaca, NY, 1985.

HAMBY, D. M. A Review of Techniques for Parameter Sensitivity Analysis of Environmental Models. **Environmental Monitoring and Assessment**, v. 32, n. 2, p. 135–154, 1994.

HARDENBERG, H. O.; HASE, F. W. An empirical formula for computing the pressure rise delay for a fuel from its cetane number and from the relevant parameters of direct-injection diesel engine. **SAE Technical Paper**, v. 88, n. 790493, 1979.

HARTMANN, R. M.; GARZON, N. N.; HARTMANN, E. M.; OLIVEIRA, A. A. M.; BAZZO, E. Vegetable Oils of Soybean, Sunflower and Tung as Alternative Fuels for Compression Ignition Engines. **International Journal of Thermodynamics**, v. 16, n. 2, p. 87–96, 2013.

HARTMANN, R. M.; HARTMANN, E. M.; MARTIN, C. A.; GARZÓN, N. A. N.; MONTEIRO, J. O. D.; VIEIRA, G. C.; OLIVEIRA, A., A. M.; BAZZO, E. **Study of the Use of Bio-oils in Diesel Engines for Distributed Thermoelectric Generation - P&D ANEEL (in Portuguese)**. Florianópolis, SC: Eletrosul/FAPEU, 2012.

HARWOOD, H. J. Oleochemicals as a Fuel: Mechanical and Economic Feasibility. **Journal of the American Oil Chemists' Society**, v. 61, n. 2, p. 315–324, 1984.

HAZAR, H.; AYDIN, H. Performance and emission evaluation of a CI engine fueled with preheated raw rapeseed oil (RRO)–diesel blends. **Applied Energy**, v. 87, n. 3, p. 786–790, 2010.

HE, Y.; BAO, Y. D. Study on cottonseed oil as a partial substitute for diesel oil in fuel for single-cylinder diesel engine. **Renewable Energy**, v. 30, n. 5, p. 805–813, 2005.

HEYWOOD, J. B. **Internal Combustion Engine Fundamentals**. 1. ed. New York: McGraw-Hill, 1988.

HIROYASU, H.; ARAI, M. Structures of fuel sprays in diesel engines. **SAE Technical Paper**, n. 900475, 1990.

HIROYASU, H.; KADOTA, T.; ARAI, M. Development and use of a spray combustion modeling to predict diesel engine efficiency and pollutant emissions, Part 1. Combustion Modeling. **The Japan Society of Mechanical Engineers**, v. 26, p. 569–575, 1983.

HOFFMANN, J. F.; HENRY, J.-F.; VAITILINGOM, G.; OLIVES, R.; CHIRTOC, M.; CARON, D.; PY, X. Temperature dependence of thermal conductivity of vegetable oils for use in concentrated solar power plants, measured by 3omega hot wire method. **International Journal of Thermal Sciences**, v. 107, p. 105–110, 2016.

HOHENBERG, G. F. Advanced approaches for heat transfer calculations. **SAE Technical Paper**, v. 88, n. 790825, 1979.

ImageJ. Bethesda, MD: National Institute of Health, 2016.

INMETRO. **Evaluation of Measurement Data - A Guide to Expression of Measurement Uncertainty - GUM 2008 (in Portuguese)**. Duque de Caxias, RJ: INMETRO/CICMA/SEPIN, 2012.

ISIĞİGÜR, A.; KARAOSMANOĞLU, F.; AKSOY, H. A.; HAMDULLAHPUR, F.; GÜLDER, Ö. L. Safflower Seed Oil of Turkish Origin as a Diesel Fuel Alternative. **Applied Biochemistry and Biotechnology**, v. 39–40, n. 1, p. 89–105, 1993.

KALAM, M. A.; HUSNAWAN, M.; MASJUKI, H. H. Exhaust emission and combustion evaluation of coconut oil-powered indirect injection diesel engine. **Renewable Energy**, v. 28, n. 15, p. 2405–2415, 2003.

KANNAN, D.; PACHAMUTHU, S.; NURUN NABI, M.; HUSTAD, J. E.; LØVÅS, T. Theoretical and experimental investigation of diesel engine performance, combustion and emissions analysis fuelled with the blends of ethanol, diesel and jatropha methyl ester. **Energy Conversion and Management**, v. 53, n. 1, p. 322–331, 2012.

KARAOSMANOĞLU, F.; KURT, G.; ÖZAKTAŞ, T. Long term CI engine test of sunflower oil. **Renewable Energy**, v. 19, n. 1, p. 219–221, 2000.

KASIRAMAN, G.; NAGALINGAM, B.; BALAKRISHNAN, M. Performance, emission and combustion improvements in a direct injection diesel engine using cashew nut shell oil as fuel with camphor oil blending. **Energy**, Asia-Pacific Forum on Renewable Energy 2011. v. 47, n. 1, p. 116–124, 2012.

KASTNER, L. J.; WILLIAMS, T. J.; WHITE, J. B. Poppet Inlet Valve Characteristics and Their Influence on the Induction Process. **Proceedings of the Institution of Mechanical Engineers**, v. 178, n. 1, p. 955–975, 1963.

KLEINOVA, A.; VAILING, I.; FRANTA, R.; MIKULEC, J.; CVENGROŠ, J. Vegetable oils as Diesel Fuels for Rebuilt Vehicles. In: 44TH INTERNATIONAL PETROLEUM CONFERENCE, SEPTEMBER 21-22, 2009, Bratislava, Slovak Republic. **Proceedings...** Bratislava, Slovak Republic, 2009.

KRIEGER, R. B.; BORMAN, G. L. The computation of apparent heat release for internal combustion engines. **The American Society of Mechanical Engineers**, v. 66- WA/DGP-4, p. 1–16, 1966.

KUMAR, M. S.; RAMESH, A.; NAGALINGAM, B. An experimental comparison of methods to use methanol and Jatropha oil in a compression ignition engine. **Biomass and Bioenergy**, v. 25, n. 3, p. 309–318, 2003.

KUMAR, S.; CHAUHAN, M. K.; VARUN. Numerical modeling of compression ignition engine: A review. **Renewable and Sustainable Energy Reviews**, v. 19, p. 517–530, 2013.

LAB Fit Curve Fitting Software. Campina Grande, PB: Universidade Federal de Campina Grande, Centro de Ciências e Tecnologia, Departamento de Física, ATDE, 2011.

LabVIEW Software. Austin, TX: National Instruments, 2016.

LAKSHMINARAYANAN, P. A.; YOGESH, V. A. **Modeling diesel combustion.** Dordrecht: Springer Science + Business Media B. V., 2010.

LAPUERTA, M.; ARMAS, O.; RODRÍGUEZ-FERNÁNDEZ, J. Effect of biodiesel fuels on diesel engine emissions. **Progress in Energy and Combustion Science**, v. 34, n. 2, p. 198–223, 2008.

LATA, D. B.; MISRA, A. Analysis of ignition delay period of a dual fuel diesel engine with hydrogen and LPG as secondary fuels. **International Journal of Hydrogen Energy**, v. 36, n. 5, p. 3746–3756, 2011.

LATA, D. B.; MISRA, A.; MEDHEKAR, S. Investigations on the combustion parameters of a dual fuel diesel engine with hydrogen and LPG as secondary fuels. **International Journal of Hydrogen Energy**, 2010 Asian/APEC BioH2. v. 36, n. 21, p. 13808–13819, 2011.

LEENUS, J. M.; VARUVEL, E. G.; PRITHVIRAJ, D. Effect of diesel addition on the performance of cottonseed oil fuelled DI diesel engine. **International Journal of Energy and Environment**, v. 2, n. 2, p. 321–330, 2011.

LEENUS, M.; EDWIN GEO, V.; KINGSLY JEBARAJ, D.; NAGALINGAM, B. A comparative analysis of different methods to improve the performance of cotton seed oil fuelled diesel engine. **Fuel**, Special Section: ACS Clean Coal. v. 102, p. 372–378, 2012.

LEFEBVRE, A. H. **Atomization and sprays.** 1. ed. Boca Raton, FL: Taylor&Francis Group, 1989.

LI, H.; BILLER, P.; HADAVI, S. A.; ANDREWS, G. E.; PRZYBYLA, G.; LEA-LANGTON, A. Assessing combustion and emission performance of direct use of SVO in a diesel engine by oxygen enrichment of intake air method. **Biomass and Bioenergy**, v. 51, p. 43–52, 2013.

MA, F.; ZHAO, C.; ZHANG, F.; ZHAO, Z.; ZHANG, Z.; XIE, Z.; WANG, H. An Experimental Investigation on the Combustion and Heat Release Characteristics of an Opposed-Piston Folded-Cranktrain Diesel Engine. **Energies**, v. 8, n. 7, p. 6365–6381, 2015.

MACHACON, H. T. C.; SUGIHARA, Y.; SHIGA, S.; MATSUMOTO, Y.; KARASAWA, T.; NAKAMURA, H.; OBOKATA, T. Operation and Combustion Characteristics of a DI Diesel Engine Fueled with Biomass Oil-Diesel Fuel Blends. **SAE Technical Paper**, n. 2001-28-0030, p. 1–8, 2001.

MARTIN, M.; PRITHVIRAJ, D. Performance of pre-heated cottonseed oil and diesel fuel blends in a compression ignition engine. **Jordan journal of mechanical and industrial engineering**, v. 5, n. 3, 2011.

MATLAB. Natick, MA: The MathWorks, Inc., 2013.

MAZIERO, J.; CORREA, I.; UNGARO, M.; BERNARDI, J.; STORINO, M. Diesel Engine Performance With Raw Sunflower Oil Fuel (in Portuguese). **Current Agricultural Science and Technology**, v. 13, n. 2, 2007.

MOLLENHAUER, K.; TSCHOEKE, H. **Handbook of diesel engines**. Berlin: Springer, 2010.

NARBEL, P.; JANSEN, J. P.; LIEN, J. R. **Energy Technologies and Economics**. [s.l.] Springer International Publishing Switzerland, 2014. v. 1

NWAFOR, O. M. I. The effect of elevated fuel inlet temperature on performance of diesel engine running on neat vegetable oil at constant speed conditions. **Renewable Energy**, v. 28, n. 2, p. 171–181, 2003.

NWAFOR, O. M. I.; RICE, G. Performance of rapeseed oil blends in a diesel engine. **Applied Energy**, v. 54, n. 4, p. 345–354, 1996.

OBERT, E. F. **Internal combustion engines (in Portuguese)**. Porto Alegre: Editora Globo, 1971.

OLIKARA, C.; BORMAN, G. L. A computer program for calculating properties of equilibrium combustion products with some applications to I.C. engines. **SAE Technical Paper**, n. 750468, p. 1–21, 1975.

ÖNER, C.; ALTUN, Ş. Biodiesel production from inedible animal tallow and an experimental investigation of its use as alternative fuel in a direct injection diesel engine. **Applied Energy**, v. 86, n. 10, p. 2114–2120, 2009.

PARGA, B. G. **Combustion analysis of a diesel engine operating with diesel oil and soybean oil blends (in Portuguese)**. 2015. 115 p. Undergraduate thesis (Mechanical Engineering) – UFSC, Florianópolis, SC, 2015.

PARIOTIS, E. G.; KOSMADAKIS, G. M.; RAKOPOULOS, C. D. Comparative analysis of three simulation models applied on a motored internal combustion engine. **Energy Conversion and Management**, v. 60, p. 45–55, 2012.

PETERSON, C. L.; AULD, D. L.; KORUS, R. A. Winter Rape Oil Fuel for Diesel Engines: Recovery and Utilization. **Journal of the American Oil Chemists' Society**, v. 60, n. 8, p. 1579–1587, 1983.

PRAMANIK, K. Properties and use of jatropha curcas oil and diesel fuel blends in compression ignition engine. **Renewable Energy**, v. 28, n. 2, p. 239–248, 2003.

PRASAD, C. . S. N.; REDDY, K. V. K.; KUMAR, B. S. .; RAMJEE, E.; HEBBEL, O. D.; NIVENDGI, M. C. Performance and emission characteristics of a diesel engine with castor oil. **Indian Journal of Science and Technology**, v. 2, n. 10, 2009.

PRYOR, R. W.; HANNA, M. A.; SCHINSTOCK, J. L.; BASHFORD, L. L. Soybean Oil Fuel in a Small Diesel Engine. **Transactions of the ASAE**, v. 26, n. 2, p. 333, 1983.

PUGAZHVADIVU, M.; SANKARANARAYANAN, G. Experimental studies on a diesel engine using mahua oil as fuel. **Indian journal of science and technology**, v. 3, n. 7, p. 788–792, 2010.

PUHAN, S.; SARAVANAN, N.; NAGARAJAN, G.; VEDARAMAN, N. Effect of biodiesel unsaturated fatty acid on combustion characteristics of a DI compression ignition engine. **Biomass and Bioenergy**, v. 34, n. 8, p. 1079–1088, 2010.

QI, D. H.; LEE, C. F.; JIA, C. C.; WANG, P. P.; WU, S. T. Experimental investigations of combustion and emission characteristics

of rapeseed oil–diesel blends in a two cylinder agricultural diesel engine. **Energy Conversion and Management**, v. 77, p. 227–232, 2014.

RAGHU, R.; RAMADOSS, G.; SAIRAM, K.; ARULKUMAR, A. Experimental Investigation on the Performance and Emission Characteristics of a DI Diesel Engine Fueled with Preheated Rice Bran Oil. **European Journal of Scientific Research**, v. 64, n. 3, p. 400–414, 2011.

RAKOPOULOS; ANTONOPOULOS, K. A.; RAKOPOULOS, D. C. Multi-zone modeling of Diesel engine fuel spray development with vegetable oil, bio-diesel or Diesel fuels. **Energy Conversion and Management**, v. 47, n. 11–12, p. 1550–1573, 2006.

RAKOPOULOS; ANTONOPOULOS, K. A.; RAKOPOULOS, D. C.; HOUNTALAS, D. T.; GIAKOUMIS, E. G. Comparative performance and emissions study of a direct injection Diesel engine using blends of Diesel fuel with vegetable oils or bio-diesels of various origins. **Energy Conversion and Management**, v. 47, n. 18–19, p. 3272–3287, 2006.

RAKOPOULOS, C. D.; ANTONOPOULOS, K. A.; RAKOPOULOS, D. C. Development and application of multi-zone model for combustion and pollutants formation in direct injection diesel engine running with vegetable oil or its bio-diesel. **Energy Conversion and Management**, v. 48, n. 7, p. 1881–1901, 2007.

RAKOPOULOS, C. D.; RAKOPOULOS, D. C.; GIAKOUMIS, E. G.; DIMARATOS, A. M. Investigation of the combustion of neat cottonseed oil or its neat bio-diesel in a HSDI diesel engine by experimental heat release and statistical analyses. **Fuel**, v. 89, n. 12, p. 3814–3826, 2010.

RAKOPOULOS, D. C. Heat release analysis of combustion in heavy-duty turbocharged diesel engine operating on blends of diesel fuel with cottonseed or sunflower oils and their bio-diesel. **Fuel**, v. 96, p. 524–534, 2012.

RAKOPOULOS, D. C. Combustion and emissions of cottonseed oil and its bio-diesel in blends with either n-butanol or diethyl ether in HSDI diesel engine. **Fuel**, v. 105, p. 603–613, 2013.

RAKOPOULOS, D. C.; RAKOPOULOS, C. D.; GIAKOUKIS, E. G.; DIMARATOS, A. M.; FOUNTI, M. A. Comparative environmental behavior of bus engine operating on blends of diesel fuel with four straight vegetable oils of Greek origin: Sunflower, cottonseed, corn and olive. **Fuel**, v. 90, n. 11, p. 3439–3446, 2011.

RAKOPOULOS, D.; RAKOPOULOS, C.; GIAKOUKIS, E.; DIMARATOS, A.; KAKARAS, E. Comparative Evaluation of Two Straight Vegetable Oils and Their Methyl Ester Biodiesels as Fuel Extenders in HDDI Diesel Engines: Performance and Emissions. **Journal of Energy Engineering**, v. 140, n. 3, p. A4014001/1-11, 2014.

RAKOPOULOS; GIAKOUKIS, E. G. Second-law analyses applied to internal combustion engines operation. **Progress in Energy and Combustion Science**, v. 32, n. 1, p. 2–47, 2006.

RAMADHAS, A. S.; JAYARAJ, S.; MURALEEDHARAN, C. Theoretical modeling and experimental studies on biodiesel-fueled engine. **Renewable Energy**, v. 31, n. 11, p. 1813–1826, 2006.

RAO, G. A. P.; MOHAN, P. R. Effect of supercharging on the performance of a DI Diesel engine with cotton seed oil. **Energy Conversion and Management**, v. 44, n. 6, p. 937–944, 2003.

REDDY, J. N.; RAMESH, A. Parametric studies for improving the performance of a Jatropha oil-fuelled compression ignition engine. **Renewable Energy**, v. 31, n. 12, p. 1994–2016, 2006.

REDDY, P.; KRISHNA, D.; MALLAN, K. R.; GANESAN, V. Evaluation of combustion parameters in direct injection diesel engines – an easy and reliable method. **SAE Technical Paper**, n. 930605, p. 159–165, 1993.

REID, R.; PRAUSNITZ, J.; POLING, B. **The Properties of Gases and Liquids**. 4. ed. New York: McGraw-Hill, 1987.

REITZ, R. D.; BRACCO, F. B. On the dependence of spray angle and other spray parameters on nozzle design and operating conditions. **SAE Technical Paper**, n. 790494, p. 1–19, 1979.

RUAN, D.; CHENG, W.; LEE, C. Comparison of Performance and Combustion Characteristics of Diesel Fuel and Vegetable Oils in DI

Diesel Engine. **SAE Technical Paper**, v. 1, n. 2008-01-1639, p. 1049–1055, 2008.

RYAN, T. W.; DODGE, L. G.; CALLAHAN, T. J. The Effects of Vegetable Oil Properties on Injection and Combustion in Two Different Diesel Engines. **Journal of the American Oil Chemists Society**, v. 61, n. 10, p. 1610–1619, 1984.

SAPUAN, S. M.; MASJUKI, H. H.; AZLAN, A. The Use of Palm Oil as Diesel Fuel Substitute. **Proceedings of the Institution of Mechanical Engineers, Part A: Journal of Power and Energy**, v. 210, n. 1, p. 47–53, 1996.

SARADA, S. N.; SHAILAJA, M.; RAJU, A. S. R.; RADHA, K. K. Optimization of injection pressure for a compression ignition engine with cotton seed oil as an alternate fuel. **International Journal of Engineering, Science and Technology**, v. 2, n. 6, 2010.

SAYIN, C.; GUMUS, M.; CANAKCI, M. Effect of fuel injection pressure on the injection, combustion and performance characteristics of a DI diesel engine fueled with canola oil methyl esters-diesel fuel blends. **Biomass and Bioenergy**, v. 46, p. 435–446, 2012.

SCHROEDER, F. R. **Characterization of ignition delay of diesel oil and two soybean oil blends, using the combustion chamber pressure readings of a compression-ignition engine (in Portuguese)**. 2016. 73 p. Undergraduate thesis (Mechanical Engineering) – UFSC, Florianópolis, SC, 2016.

SHAHABUDDIN, M.; LIAQUAT, A. M.; MASJUKI, H. H.; KALAM, M. A.; MOFIJUR, M. Ignition delay, combustion and emission characteristics of diesel engine fueled with biodiesel. **Renewable and Sustainable Energy Reviews**, v. 21, p. 623–632, 2013.

SHAHED, S. M.; CHIU, W. S.; YUMLU, V. S. A preliminary model for the formation of nitric oxides in DI diesel engine and its application in parametric studies. **SAE Technical Paper**, n. 730083, 1973.

SHARON, H.; JAI SHIVA RAM, P.; JENIS FERNANDO, K.; MURALI, S.; MUTHUSAMY, R. Fueling a stationary direct injection diesel engine with diesel-used palm oil–butanol blends – An

experimental study. **Energy Conversion and Management**, v. 73, p. 95–105, 2013.

SILVA, L. L. C. Simulation of the thermodynamic processes in diesel cycle internal combustion engines. **SAE Technical Paper**, n. 931899, p. 1–11, 1993.

SINGH, B. P.; SAHOO, P. K. Theoretical modeling and experimental studies on vegetable oil fueled conventional engine. **BIOINFO Mechanical Engineering**, v. 2, n. 1, p. 16–23, 2012.

SIVALAKSHMI, S.; BALUSAMY, T. Experimental Investigation on a Diesel Engine Fuelled with Neem Oil and Its Methyl Ester. **Thermal Science**, v. 15, n. 4, p. 1193–1204, 2011.

Statistica. Palo Alto, CA: TIBCO Software, Inc., 2017.

STIESCH, G.; ECKERT, P.; RAKOWSKI, S. Phenomenological Combustion Models. In: MERKER, G.; SCHWARZ, C.; TEICHMANN, R. (Ed.). **Combustion Engine Development. Mixture formation, combustion, emissions and simulation**. Berlin: Springer Berlin Heidelberg, 2012. p. 415–441.

TAYLOR, C. F. **Internal Combustion Engine in Theory and Practice**. 2. ed. Cambridge, Mass: Mit University Press Group Ltd, 1985.

TUNKA, L.; POLCAR, A. Effect of Various Ignition Timings on Combustion Process and Performance of Gasoline Engine. **Acta Universitatis Agriculturae et Silviculturae Mendelianae Brunensis**, v. 65, n. 2, p. 545–554, 2017.

VALLINAYAGAM, R.; VEDHARAJ, S.; YANG, W. M.; LEE, P. S.; CHUA, K. J. E.; CHOU, S. K. Combustion performance and emission characteristics study of pine oil in a diesel engine. **Energy**, v. 57, p. 344–351, 2013.

WANDER, P. R.; ALTAFINI, C. R.; MORESCO, A. L.; COLOMBO, A. L.; LUSA, D. Performance analysis of a mono-cylinder diesel engine using soy straight vegetable oil as fuel with varying temperature and injection angle. **Biomass and Bioenergy**, v. 35, n. 9, p. 3995–4000, 2011.

WANG, Y.; HUANG, Y.; ROSKILLY, A. P.; DING, Y.; HEWITT, N. Trigenation running with raw jatropha oil. **Fuel Processing Technology**, v. 91, n. 3, p. 348–353, 2010.

WATSON, N.; JANOTA, M. S. **Turbocharging the Internal Combustion Engine**. 1. ed. New York: John Wiley & Sons, Inc., 1982.

WATSON, N.; PILLEY, A. D. A combustion correlation for diesel engine simulation. **SAE Technical Paper**, n. 800029, 1980.

WHITEHOUSE, N. D.; WAY, R. Rate of Heat Release in Diesel Engines and Its Correlation with Fuel Injection Data. **Proceedings of the Institution of Mechanical Engineers, Conference Proceedings**, v. 184, n. 10, p. 17–27, 1969.

WIEBE, I. T. **Progress of combustion and cycle process in combustion engines**. 1. ed. Berlin: VEB Verlag Technik, 1970.

YELIANA, Y.; COONEY, C.; WORM, J.; MICHALEK, D. J.; NABER, J. D. Estimation of double-Wiebe function parameters using least square method for burn durations of ethanol-gasoline blends in spark ignition engine over variable compression ratios and EGR levels. **Applied Thermal Engineering**, v. 31, n. 14–15, p. 2213–2220, out. 2011.

YILMAZ, N.; MORTON, B. Effects of preheating vegetable oils on performance and emission characteristics of two diesel engines. **Biomass and Bioenergy**, v. 35, n. 5, p. 2028–2033, 2011.

YOUNG, M. B.; LIENESCH, J. H. An Engine Diagnostic Package (EDPAC) - Software for Analyzing Cylinder Pressure-Time Data. **SAE Technical Paper**, n. 780967, 1978.

ZARZA, H. D. M. **Obtaining and processing of cylinder pressure data of a diesel engine for application in the combustion analysis (in Portuguese)**. 2015. 71 p. Undergraduate thesis (Mechanical Engineering) – UFSC, Florianópolis, SC, 2015.

APPENDIX A. Break-up regimes of liquid jets

On the surface of the jet are produced oscillations and perturbations due to the action of cohesive and disruptive forces. Consequently, the relative jet velocity and the properties of the liquid and surrounding gas determine the different break-up regimes of a liquid jet. The break-up regimes are characterized by the distance between the nozzle and the point of first droplet formation (break-up length) and the size of the droplets that are produced (BAUMGARTEN, 2006).

Wolfgang von Ohnesorge in 1930s proposed some criteria for classifying the break-up regimes. These criteria were based on dimensionless analysis, where were considered the relative importance of gravitational, inertial, surface tension and viscous forces (LEFEBVRE, 1989). Thus, Ohnesorge showed that the break-up regimes could be divided in three regimes, represented on a graph (Ohnesorge diagram) described by the liquid Reynolds number (Re_l), the liquid Weber number (We_l) and the Ohnesorge number (Oh), defined as

$$Re_l = \frac{\rho_l u_{sp} d_o}{\mu_l} \quad (\text{A.1})$$

$$We_l = \frac{\rho_l u_{sp}^2 d_o}{\sigma_l} \quad (\text{A.2})$$

$$Oh = \frac{\sqrt{We}}{Re} \quad (\text{A.3})$$

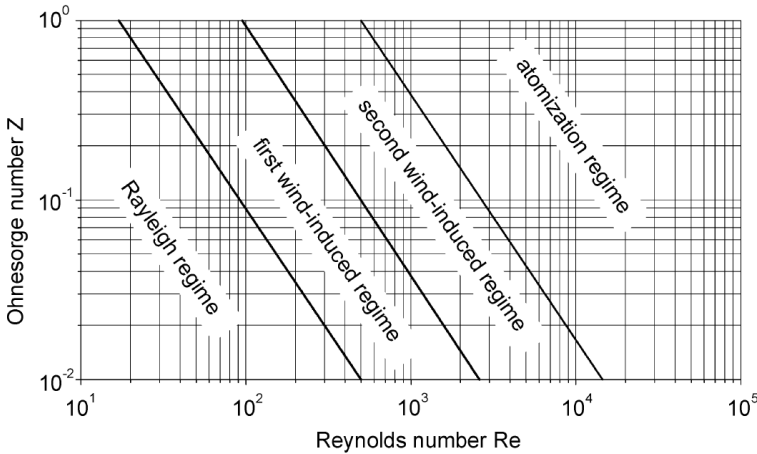
$$Oh = \sqrt{\frac{\rho_l u_{sp}^2 d_o}{\sigma_l}} \frac{\mu_l}{\rho_l u_{sp}^2 d_o} = \frac{\mu_l}{\sqrt{\rho_l d_o \sigma_l}} \quad (\text{A.4})$$

where ρ_l , u_{sp} , μ_l and σ_l are the density, velocity, dynamic viscosity and surface tension of the fluid, respectively, and d_o is the characteristic length (injector nozzle hole diameter). The Reynolds number describes the ratio of inertial forces to viscous forces of the fluid. The Weber number represents the ratio between the inertial force and the surface tension force, therefore, indicates whether the kinetic or the surface

tension energy is dominant. Finally, the Ohnesorge number represents the ratio of internal viscosity dissipation to the surface tension energy.

Further studies have been carried out by other researchers in order to improve the Ohnesorge diagram. Figure A1 shows the current Ohnesorge diagram that classifies the break-up regimes in four modes of disintegration: the Rayleigh regime, the first and second wind-induced regime, and the atomization regime.

Figure A1. Ohnesorge diagram: break-up regimes of liquid jets.



Source: Adapted from Baumgarten (2006).

According to Lefebvre (1989) and Baumgarten (2006), the four break-up regimes present the following behavior.

- Rayleigh regime: the break-up occurs due to the growth of axisymmetric oscillations of the jet surface, initiated by liquid inertia and surface tension forces. The drop diameters are higher than the nozzle hole diameter.
- First wind-induced regime: the increase of the relative velocity increases the surface tension effect between the jet and the surrounding gas, accelerating the break-up process. The break-up length decreases and the drop diameters are about the same as the jet diameter.
- Second wind-induced regime: the break-up occurs due to the unstable growth of short-wavelength surface wave that are initiated by jet turbulence and amplified by aerodynamic

forces due to the relative velocity between gas and jet. The wave growth is opposed by surface tension. The break-up length decreases and the drop diameters are much less than the jet diameter.

- Atomization regime: the jet disintegrates instantaneously after the jet leaves the nozzle (at the nozzle exit). Average drop diameters are much less than the jet diameter. This is the relevant regime for engine sprays. The theoretical description of the atomization regime is much more complex than in any other regime, because the disintegration process strongly depends on the flow conditions inside the nozzle hole.

These break-up regimes are known as primary break-up. The disintegration of the drops formed into drops of smaller sizes is called secondary break-up and is due to aerodynamic forces caused by the relative velocity between droplets and surrounding gas. In consequence, the secondary break-up increases with the We number increase.

Criterion for the onset of jet atomization

The atomization regime is the regime of interest for internal combustion engines. The atomization of fuel favors mixture formation and consequently the performance of the diesel engine. Different jet atomization mechanisms have been proposed. Reitz and Bracco (1979) conducted experiments to study jet atomization. A spray chamber was used for testing different operating conditions, including the conditions commonly found in automotive applications. The spray chamber allowed to change injection pressure, gas density, liquid viscosity, nozzle L/d_o ratios, and it allowed observing the breakup process photographically. The authors found that aerodynamic effects, liquid turbulence, jet velocity profile effects, and liquid supply pressure oscillations, each could not alone explain the experimental results. The aerodynamic effects at the liquid/gas interface, supplemented by cavitation and/or wall boundary layer velocity profile relaxation effects are the major components of the atomization mechanism.

Reitz and Bracco (1979) based on the aerodynamic hypothesis and their experimental results proposed a criterion for the onset of jet atomization. This criterion establishes that the atomization occurs if

$$\sqrt{\frac{\rho_l}{\rho_g}} \leq k_{inj} \quad \text{for} \quad (A.5)$$

$$\frac{\rho_l}{\rho_g} \left(\frac{Re_l}{We_l} \right)^2 > 1$$

or

$$\left(\frac{\rho_l}{\rho_g} \frac{We_l}{Re_l} \right)^{1/3} \leq k_{inj} \quad \text{for} \quad (A.6)$$

$$\frac{\rho_l}{\rho_g} \left(\frac{Re_l}{We_l} \right)^2 < 1$$

where ρ_l , ρ_g are the liquid and gas densities, respectively. Re_l and We_l are the dimensionless number of Reynolds and Weber expressed for the liquid phase as shown in equations (A.1) and (A.2). The constant k_{inj} is a parameter obtained empirically related to the ratio of the length L_{inj} and the diameter d_o of the nozzle orifice. Thus,

$$k_{inj} = \frac{18.3}{\sqrt{A_{inj}}} \quad (A.7)$$

$$A_{inj} = 3 + \frac{L_{inj}/d_o}{3.6} \quad (A.8)$$

This criterion incorporates the effects of gas density, liquid properties, the geometric characteristics of the orifice, and the operating conditions through the liquid velocity u_{sp} . The velocity of the jet at the outlet plane of the orifice is

$$u_{sp} = C_D \left[\frac{2(p_{inj} - p_g)}{\rho_l} \right]^{0.5} \quad (A.9)$$

where C_D is the coefficient of discharge, p_{inj} is the injection pressure, and p_g is the gas pressure. According to Lefebvre (1989), the coefficient of discharge for round orifices can be estimated as

$$C_D = \frac{1}{\left[\frac{1}{C_{D,max}} + \frac{20(1+2.25L)}{Re_l} \right]} \quad (A.10)$$

$$C_{D,max} = 0.827 - 0.0085L \quad (A.11)$$

Spray structure

The spray structure can be basically described by the Sauter mean droplet diameter (SMD), spray cone angle (α_{sp}) and the spray penetration (S). The SMD is the diameter of a model drop whose volume-to-surface-area ratio is equal to the ratio of the sum of all droplet volumes in the spray to the sum of all droplet surface areas (BAUMGARTEN, 2006). Thus,

$$SMD = \frac{\sum_{i=1}^n d_i^3}{\sum_{i=1}^n d_i^2} \quad (A.12)$$

In the technical literature, the SMD is usually estimated from correlations that involve the fuel properties, injection pressure, and the dimensionless numbers of Weber and Reynolds. The most common correlation used to estimate the SMD is the correlation proposed by Hiroyasu and Arai (1990), so that

$$\frac{SMD}{d_o} = 0.38 Re_l^{0.25} We_l^{-0.32} \left(\frac{\mu_l}{\mu_g} \right)^{0.37} \left(\frac{\rho_l}{\rho_g} \right)^{-0.47} \quad (A.13)$$

where μ_l and μ_g are the liquid and gas dynamic viscosities, respectively.

Based on the aerodynamic surface wave theory of jet break-up, Reitz and Bracco (1979) found that the spray cone angle follows the relationship

$$\tan\left(\frac{\alpha_{sp}}{2}\right) = \frac{4\pi}{A} \left(\frac{\rho_g}{\rho_l}\right)^{0.5} \frac{\sqrt{3}}{6} \quad (\text{A.14})$$

In relation to the spray penetration, Hiroyasu and Arai (1990) proposed correlations that consider the spray penetration as a process of two stages, separated by the break-up time, t_{break} . Thus,

$$S = 0.39 \left(\frac{2\Delta p}{\rho_l}\right)^{0.5} t \quad t < t_{break} \quad (\text{A.15})$$

$$S = 2.95 \left(\frac{\Delta p}{\rho_g}\right)^{0.25} (d_o \cdot t)^{0.5} \quad t > t_{break} \quad (\text{A.16})$$

and

$$t_{break} = \frac{28.65 \rho_l d_o}{(\rho_g \Delta p)^{0.5}} \quad (\text{A.17})$$

where Δp is the difference between the injection pressure and chamber pressure and t is the time. The first stage starts at the beginning of injection and ends at the moment the liquid jet begins to disintegrate ($t = t_{break}$). During this time, the injection pressure has a more significant effect on the jet motion and the spray penetration changes linearly with time (the spray tip velocity is constant). For the second stage, the spray penetration increases as $t^{0.5}$ and the main parameter that influences on the jet motion is the gas density.

APPENDIX B. Combustion models

The combustion models of Whitehouse and Way (1969) and Watson and Pilley (1980) are described in this appendix.

Whitehouse and Way (1969) proposed a semi-empirical combustion model, commonly used in single zone modeling. The liquid fuel is injected into the cylinder as a conical jet that forms the firing zone. Before the burning, the fuel must be heated, evaporated and mixed with sufficient amount of air entering by diffusion from the air zone. The fuel is prepared for the chemical process and burns according to the chemical reaction. The model is composed of two parts, the first predicts the fuel preparation rate (TPC) based on the oxygen diffusion in the fuel, and the second part predicts the fuel reaction rate (TRC) based on the Arrhenius equation.

The fuel preparation rate is calculated by

$$TPC = K m_{inj}^{1-x} m_u^x p_{O_2}^m \quad (B.1)$$

where m_{inj} corresponds to the mass fuel injected at a given time and m_u represents the fuel mass unprepared to burn. p_{O_2} is the oxygen partial pressure and the constants K , x and m are empirical constants. The fuel mass injected and the fuel mass unprepared are calculated as

$$m_{inj} = \int_0^t \frac{dm_{inj}}{dt} dt \quad (B.2)$$

$$m_u = m_{inj} - \int_0^t TPC dt \quad (B.3)$$

The reaction rate of the prepared fuel is estimated with an Arrhenius equation given as

$$TRC = \frac{K'}{N\sqrt{T}} \exp(-E_{red}/T) \int_0^t (TPC - TRC) dt \quad (B.4)$$

where E_{red} is the reduced activation energy, N the engine speed and K' a constant. The integral term represents the available fuel amount to react

(prepared and not yet reacted). The term p_{O_2}/\sqrt{T} is obtained from the ratio $(p_{O_2}/T)\sqrt{T}$, where p_{O_2}/T is proportional to the oxygen density and \sqrt{T} is proportional to the velocity of gas molecules. The constants K' and E_{red} should be dependent only on the fuel and not at all on the engine (WHITEHOUSE; WAY, 1969). Finally, the combustion rate is given by the following relations

$$dm_f / dt = TRC \quad \text{whether } TRC < TPC \quad (B.5)$$

$$dm_f / dt = TPC \quad \text{whether } TRC > TPC \quad (B.6)$$

Watson and Pilley (1980) developed a combustion model of a compression ignition engine where they proposed a rapid premixed combustion phase followed by a slower mixing controlled combustion phase. The fuel fraction injected that burns in each phase is empirically linked to the duration of the ignition delay. Each combustion phase is described as an algebraic function. Thus,

$$X_b = \beta f_1 + (1 - \beta) f_2 \quad (B.7)$$

$$f_1 = 1 - \left(1 - \left(\frac{\theta - \theta_{ig}}{\Delta\theta_{comb}} \right)^{K_1} \right)^{K_2} \quad (B.8)$$

$$f_2 = 1 - \exp \left(-K_3 \left(\frac{\theta - \theta_{ig}}{\Delta\theta_{comb}} \right)^{K_4} \right) \quad (B.9)$$

$$\begin{aligned} \frac{dX_b}{d\theta} = & \frac{\beta K_2 K_1}{\Delta\theta_{comb}} \left(1 - \left(\frac{\theta - \theta_{ig}}{\Delta\theta_{comb}} \right)^{K_1} \right)^{K_2-1} \left(\frac{\theta - \theta_{ig}}{\Delta\theta_{comb}} \right)^{K_1-1} + \\ & (1 - \beta) \left[\exp \left(-K_3 \left(\frac{\theta - \theta_{ig}}{\Delta\theta_{comb}} \right)^{K_4} \right) \right] \left(\frac{\theta - \theta_{ig}}{\Delta\theta_{comb}} \right)^{K_4-1} \frac{K_3 K_4}{\Delta\theta_{comb}} \end{aligned} \quad (B.10)$$

where f_1 and f_2 correspond to expressions for each combustion phase similar to the Wiebe function, β is a factor that indicates the fuel fraction burned during the premixed combustion phase. The factor β can be expressed empirically as a function of the amount of fuel injected into the cycle and the ignition delay τ .

$$\beta = 1 - \frac{am_f^b}{\tau^c} \quad (\text{B.11})$$

The constants of the model K_1 , K_2 , K_3 , K_4 , a , b , c are empirical coefficients. Watson e Pilley (1980) in their combustion model of a turbocharged truck engine proposed the following relations and ranges of values for the different constants of the model, where ϕ_{gl} is the global fuel/air equivalence ratio.

$$K_1 = 2 + 1.25 \times 10^{-8} (\tau N)^{2.4} \quad (\text{B.12})$$

$$K_2 = 5000 \quad (\text{B.13})$$

$$K_3 = \frac{14.2}{\phi_{gl}^{0.644}} \quad (\text{B.14})$$

$$K_4 = 0.79 K_3^{0.25} \quad (\text{B.15})$$

$$0.80 < a < 0.95$$

$$0.25 < b < 0.45 \quad (\text{B.16})$$

$$0.25 < c < 0.5$$

APPENDIX C. Uncertainties of the measurements

A measurement is composed of the base result and the measurement uncertainty. The base result is the measured value and it corresponds to the central position of the measurement result, i.e., the closest value to the true value. The measurement uncertainty is the portion of doubt associated with the measurement, describing the measurement range around the base result (GONÇALVES; SOUSA, 2008). The measurement uncertainties were calculated according to the procedure described in INMETRO (2012). For the measurements in the dynamometric bench were determined the combined standard uncertainties constituted by standard uncertainties type A and type B.

The standard uncertainties type A are to uncertainties calculated from a group of observations or replications of the measurements. The standard uncertainties type B are not obtained from observations replicated, they are based on the available information about the measured variables. This information can include previous measurements, the manufacturer's specifications, data supplied in calibration certificates, experience or knowledge of the behavior of the measurement instruments.

In the tests on the dynamometric bench were made several readings in each experimental point (load condition) of the variables of interest. In addition, there were replications of the tests. In this condition, there are two random components of the variance of the measured data of a variable, an intraday component and a component among days. According to Annex H of INMETRO (2012), the experimental standard deviation can be calculated as

$$s^2(\bar{x}) = \frac{1}{J(J-1)} \sum_{j=1}^J (\bar{x}_j - \bar{x})^2 \quad (\text{C.1})$$

where $s^2(\bar{x})$ represents the variance of the global mean of a variable x , \bar{x} the overall mean of all data, \bar{x}_j the mean of the observations of each test and J the number of replications. This is the uncertainty type A, $u_A(x)$, calculated for a variable x .

The uncertainty type B, $u_B(x)$, of a variable x , is estimated according to the equipment measurement chain. The calculation is considered as the combination of all sources of uncertainty $u_i(x)$ (repeatability and equipment resolution, acquisition system, etc.)

as shown in equation (C.2). For the evaluation of this uncertainty, it was used the information available in the equipment manuals.

$$u_B^2(x) = u_1^2(x) + u_2^2(x) + \dots + u_i^2(x) \quad (\text{C.2})$$

Combining the standard uncertainties type A and type B, it is obtained the combined standard uncertainty $u_C(x)$ of variable x .

$$u_C^2(x) = u_A^2(x) + u_B^2(x) \quad (\text{C.3})$$

The procedures described to calculate the combined standard uncertainty was used with variables that were measured directly as torque, rotation, fuel mass flow, exhaust gas temperature, cylinder pressure and air-mass flow. In the case of parameters measured indirectly, obtained from relations of other variables such as power, specific fuel consumption, heat release rate and physico-chemical properties calculated for the blends, the combined standard uncertainty was determined as,

$$u_C^2(f) = \sum_{i=1}^N \left[\frac{\partial f}{\partial x_i} \right]^2 u_C^2(x_i) \quad (\text{C.4})$$

where f represents a variable defined as a function of variables x_i , each $u_C(x_i)$ corresponds to the combined standard uncertainty of the variable x , estimated as explained above.

The combined standard uncertainty of each variable must be multiplied by the coverage factor k_p to obtain the expanded uncertainty of the respective variable. This uncertainty is the interval, for a defined probability, one expects to find the random component of the errors of the measurement process (GONÇALVES; SOUSA, 2008). The factor k_p represents an expansion interval of the combined uncertainty according to a probability level of the t-student distribution. In this work, a 95 % probability was chosen. Therefore, the expanded uncertainty was calculated as

$$U(x) = k_p u_C(x) \quad (\text{C.5})$$

The factor k_p is determined from degrees of freedom of the combined uncertainty of the variable. To calculate the degrees of freedom was used the following equation,

$$\frac{u_C^4(x)}{l_{ef}} = \frac{u_A^4(x)}{l_{ef,A}} + \frac{u_B^4(x)}{l_{ef,B}} \quad (\text{C.6})$$

where l_{ef} represents the number of degrees of freedom of the combined uncertainty of a variable x , $l_{ef,A}$ and $l_{ef,B}$ are the degrees of freedom of uncertainties type A and type B of the variable x , respectively.

The expanded uncertainties calculated for the measurements on the dynamometric bench with each fuel tested are shown of Table C1 to Table C4.

Table C1. Expanded measurement uncertainties of the engine operating with 100D(25).

<i>N</i> tested (rpm)	Expanded uncertainty					
	2210	2194	2156	2102	1918	1801
<i>N</i> (rpm)	8.839	8.776	8.623	8.409	7.673	7.203
T_b (N·m)	0.857	0.936	1.005	1.047	1.088	1.125
P_b (kW)	0.198	0.215	0.227	0.230	0.219	0.212
\dot{m}_f (g/s)	0.0281	0.0311	0.0370	0.0372	0.0345	0.0327
m_f (mg/cycle)	1.53	1.70	2.06	2.12	2.16	2.18
\dot{m}_a (kg/h)	3.350	3.346	3.293	3.223	2.956	2.789
η_v	0.036	0.036	0.036	0.036	0.036	0.036
η	0.011	0.011	0.010	0.010	0.010	0.010
<i>sfc</i> (g/(kW·h))	9.76	9.98	11.21	11.12	10.86	10.61
T_e (°C)	4.92	5.40	6.01	6.01	5.75	5.62

Table C2. Expanded measurement uncertainties of the engine operating with 50S/50D(25).

	Expanded uncertainty					
N tested (rpm)	2226	2210	2190	2112	1888	1802
N (rpm)	8.905	8.838	8.759	8.447	7.553	7.208
T_b (N·m)	0.765	0.845	0.921	1.024	1.082	1.106
P_b (kW)	0.178	0.195	0.211	0.226	0.214	0.209
\dot{m}_f (g/s)	0.0263	0.0298	0.0343	0.0388	0.0359	0.0340
m_f (mg/cycle)	1.42	1.62	1.88	2.20	2.28	2.26
\dot{m}_a (kg/h)	3.484	3.361	3.336	3.262	2.962	2.838
η_v	0.037	0.036	0.036	0.036	0.037	0.037
η	0.012	0.011	0.011	0.010	0.010	0.011
sfc (g/(kW·h))	10.17	10.49	11.19	11.79	11.55	11.21
T_e (°C)	4.348	4.975	5.578	6.091	5.777	5.670

Table C3. Expanded measurement uncertainties of the engine operating with 50S/50D(85).

	Expanded uncertainty					
N tested (rpm)	2209	2190	2160	2107	1936	1797
N (rpm)	8.838	8.761	8.641	8.429	7.743	7.186
T_b (N·m)	0.797	0.877	0.957	1.009	1.056	1.093
P_b (kW)	0.184	0.201	0.216	0.223	0.214	0.206
\dot{m}_f (g/s)	0.0278	0.0323	0.0358	0.0373	0.0348	0.0330
m_f (mg/cycle)	1.51	1.77	1.99	2.12	2.16	2.21
\dot{m}_a (kg/h)	3.419	3.336	3.320	3.249	3.012	2.847
η_v	0.037	0.036	0.036	0.036	0.037	0.037
η	0.011	0.011	0.010	0.010	0.010	0.011
sfc (g/(kW·h))	10.36	11.04	11.38	11.53	11.21	11.06
T_e (°C)	4.683	5.332	5.828	6.027	5.840	5.662

Table C4. Expanded measurement uncertainties of the engine operating with 80S/20D(85).

<i>N</i> tested (rpm)	Expanded uncertainty					
	2208	2192	2165	2108	1851	1806
<i>N</i> (rpm)	8.83	8.77	8.66	8.43	7.40	7.22
T_b (N·m)	0.81	0.87	0.95	1.00	1.00	1.04
P_b (kW)	0.19	0.20	0.22	0.22	0.19	0.20
\dot{m}_f (g/s)	0.0291	0.0323	0.0357	0.0379	0.0348	0.0341
m_f (mg/cycle)	1.58	1.77	1.98	2.16	2.26	2.26
\dot{m}_a (kg/h)	3.55	3.45	3.40	3.34	2.99	2.94
η_v	0.038	0.037	0.037	0.038	0.038	0.039
η	0.011	0.011	0.011	0.010	0.010	0.010
<i>sfc</i> (g/(kW·h))	10.75	11.19	11.42	11.85	12.35	11.89
T_e (°C)	4.59	5.07	5.63	5.99	5.61	5.60

The expanded uncertainty of dynamic viscosity and surface tension measurements are presented in Table C5 and Table C6, respectively. In relation to density measurements, the corresponding expanded uncertainty was calculated as ± 2 kg/m³.

Table C5. Expanded measurement uncertainties of the dynamic viscosity.

T (°C)	Expanded uncertainty of dynamic viscosity (mPa·s)			
	Diesel oil	50 % Soybean oil	80 % Soybean oil	Soybean oil
25	0.195	0.053	0.263	0.500
40	0.164	0.203	0.218	0.177
55	0.171	0.127	0.164	0.044
70	0.057	0.112	0.130	0.176
85	0.060	0.090	0.136	0.619

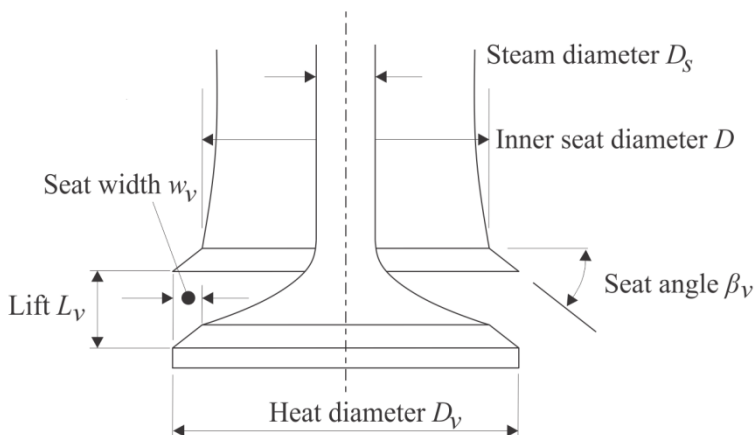
Table C6. Expanded measurement uncertainties of the surface tension.

Expanded uncertainty of surface tension (mN/m)			
T (°C)	Diesel oil	50 % Soybean oil	Soybean oil
25	0.12	0.01	0.61
40	0.15	0.06	0.01
50	0.17	0.06	0.15
70		0.06	0.06
80		0.06	0.07

APPENDIX D. Dimensions of the valves and discharge coefficients

The main geometric parameters of the inlet and exhaust valves are shown in Figure D1 and the specific values for the valves of the engine tested are presented in Table D1.

Figure D1. Geometric parameters of the inlet and exhaust valves.



Source: Adapted from Heywood (1988).

Table D1. Geometric parameters of the inlet and exhaust valves of the engine tested.

Parameter	Inlet valve	Exhaust valve
D_v (mm)	47	41.5
D (mm)	41.04	35.54
D_s (mm)	9	9
D_m (mm)	44.02	38.52
L_v (maximum, mm)	11.43	11.09
w_v (mm)	2.98	2.98
β_v ($^\circ$)	45	45

D_m is the mean seat diameter calculated as $D_m = D_v - w_v$. For measuring each valve lift, the valve camshaft was centralized in a milling machine in order to know the corresponding angular position for each lift reading made on the lobe of the cams. The lift measurements were made using a high precision metric dial comparator. The actual

valve lift was obtained multiplying the lift measurements by the lever ratio of the rocker arm, which was determined as 1.532. Figure D2 shows a picture of the measurement on the valve camshaft. The lift of each valve as a function of crank angle is shown in Figure D3 and Figure D4.

Figure D2. Measurement of the valve lift made on the valve camshaft.

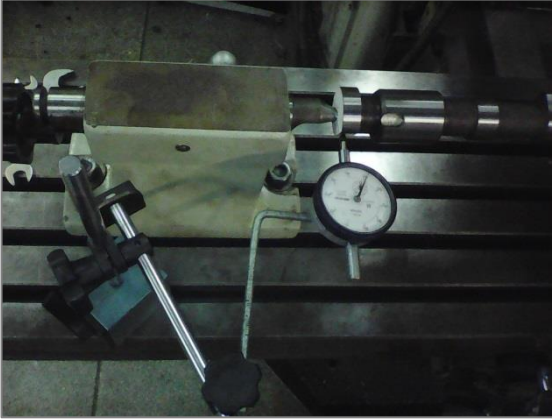


Figure D3. Intake valve lift as a function of crank angle.

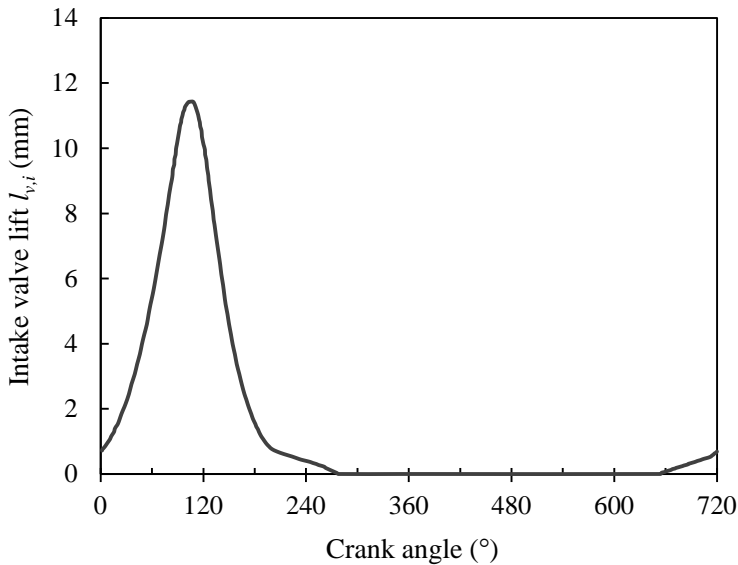
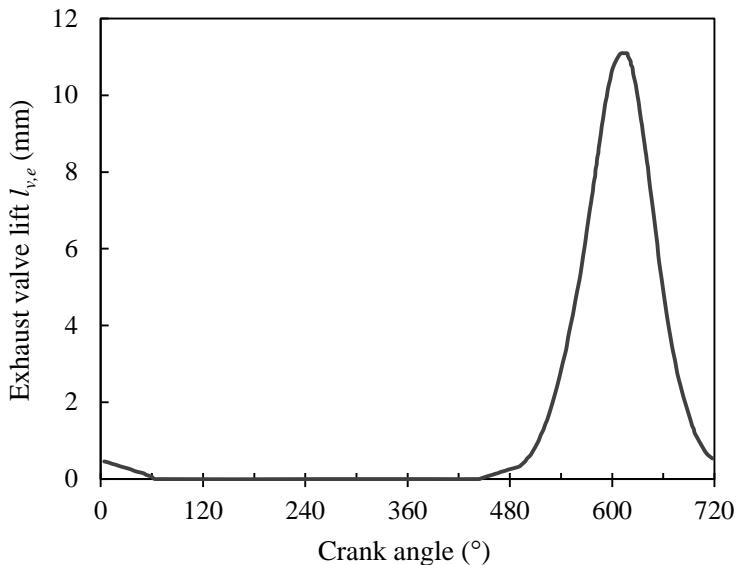


Figure D4. Exhaust valve lift as a function of crank angle.



The coefficients of the polynomial function of degree 10 fitted from experimental data of Kastner, Williams and White (1963) and used to calculate the discharge coefficients of the valves are shown in Table D2.

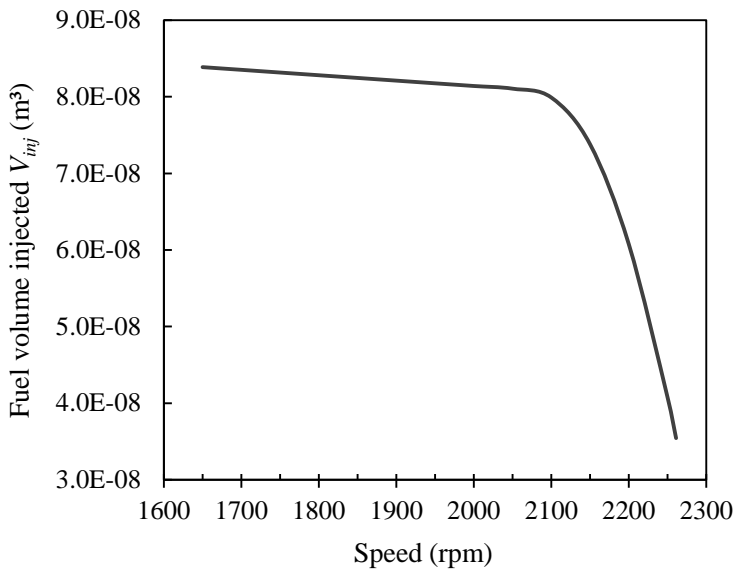
Table D2. Coefficients of the polynomial function of degree 10 used to calculate the discharge coefficients of the valves.

c_0	1.0075
c_1	-5.2890
c_2	265.1480
c_3	-6367.2885
c_4	66984.8679
c_5	-289529.0477
c_6	-98461.1061
c_7	5671407.2080
c_8	-21575870.0714
c_9	34646295.9407
c_{10}	-21117120.8211

APPENDIX E. Injected fuel volume

Figure E1 shows the injected fuel volume as a function of the engine speed.

Figure E1. Injected fuel volume as a function of engine speed tested.



APPENDIX F. Sensibility analysis of the ignition delay correlation

The sensitivity coefficient SC_i is used to determine the ratio of the change in the output variable to the change in each input variable while all other parameters remain constant (HAMBY, 1994). The sensitivity coefficient for the independent variables was calculated from the partial derivatives of the dependent variable with respect to each independent variable, so that

$$SC_i = \frac{\partial Y}{\partial X_i} \quad (F.1)$$

where Y represents the dependent variable and X_i is the independent variable i for a function $Y = f(X_1, X_2, \dots, X_n)$.

For the ignition delay correlation shown in Chapter 5 (equation (5.30)), the sensitive coefficients were calculated for each independent variable, as shown in the following equations:

$$\frac{\partial \tau}{\partial \left(\frac{SMD}{d_o} \right)} = \tau_c b \left(\frac{SMD}{d_o} \right)^{b-1} \text{Re}_D^c \phi_{gl}^d \exp\left(\frac{E_a}{RT}\right) \exp(\chi^e) \quad (F.2)$$

$$\frac{\partial \tau}{\partial \text{Re}_D} = \tau_c c \left(\frac{SMD}{d_o} \right)^b \text{Re}_D^{c-1} \phi_{gl}^d \exp\left(\frac{E_a}{RT}\right) \exp(\chi^e) \quad (F.3)$$

$$\frac{\partial \tau}{\partial \phi} = \tau_c d \left(\frac{SMD}{d_o} \right)^b \text{Re}_D^c \phi_{gl}^{d-1} \exp\left(\frac{E_a}{RT}\right) \exp(\chi^e) \quad (F.4)$$

$$\frac{\partial \tau}{\partial T} = -\tau_c \left(\frac{E_a}{R} \right) \left(\frac{SMD}{d_o} \right)^b \text{Re}_D^c \phi_{gl}^d \frac{\exp\left(\frac{E_a}{RT}\right)}{T^2} \exp(\chi^e) \quad (F.5)$$

$$\frac{\partial \tau}{\partial \gamma} = \tau_c e \left(\frac{SMD}{d_o} \right)^b \text{Re}_D^c \phi_{gl}^d \exp\left(\frac{E_a}{RT}\right) \exp(\chi^e) \chi^{e-1} \quad (F.6)$$

A set of values of the experimental data was selected as a base case, so that the parameters hold constant while each sensitivity coefficient is evaluated in the interval tested. The sensitivity coefficient was normalized to remove the effects of the units. Thus

$$\psi_i = \frac{\partial Y}{\partial X_i} \frac{X_i}{Y} \quad (\text{F.7})$$

The normalized sensitivity coefficients, ψ_i , are shown of the Figure F1 of the Figure F5. These curves show that the parameter SMD/d_o is the least significant on the response of ignition delay. Probably, it is necessary to evaluate this parameter with a larger interval of data to become more significant this parameter. The parameter χ does not influence on the ignition delay for blends with volume fraction lower than 0.5, from this proportion, the influence becomes significant. The parameters Re_D , ϕ_{gl} and T influence significantly on the ignition delay.

Figure F1. Normalized sensitivity coefficient for parameter SMD/d_o .

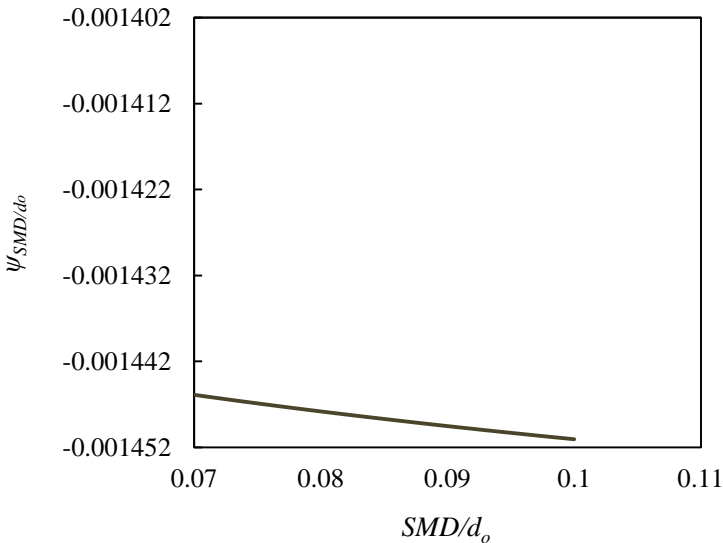


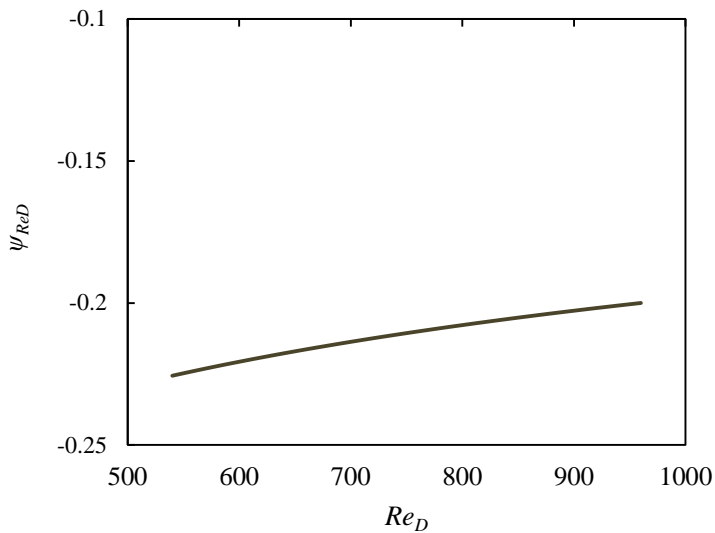
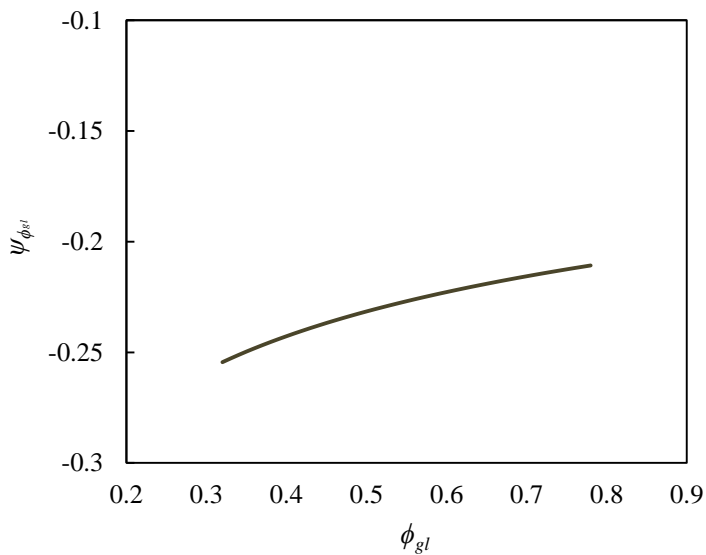
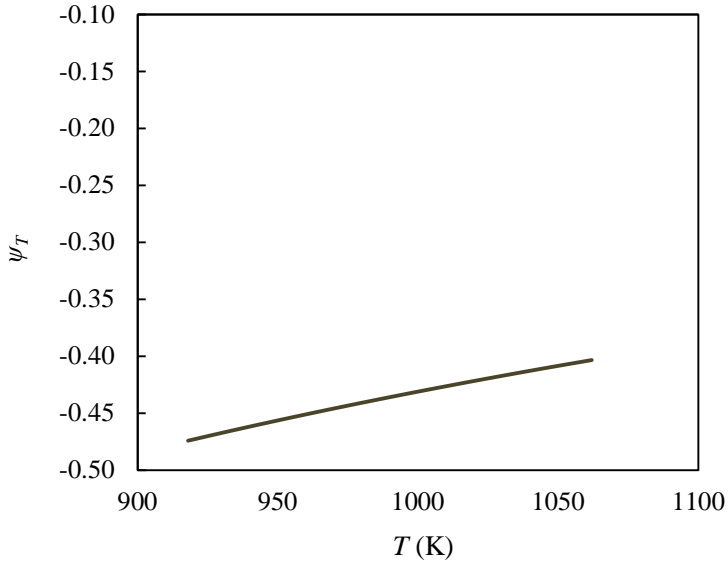
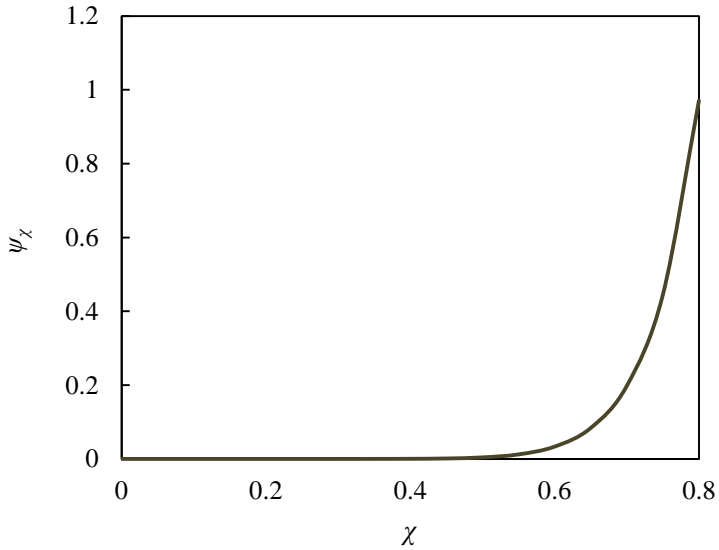
Figure F2. Normalized sensitivity coefficient for parameter Re_D .Figure F3. Normalized sensitivity coefficient for parameter ϕ_{gl} .

Figure F4. Normalized sensitivity coefficient for parameter T .Figure F5. Normalized sensitivity coefficient for parameter χ .

APPENDIX G. Routines performed in MATLAB software

A general algorithm of the routines written in MATLAB software to determine the heat release rate and to simulate the complete cycle of the diesel engine are presented in Table G1 and Table G2, respectively.

Table G1. Routine for obtaining the heat release rate from experimental pressure data.

Initialization

Test conditions:

$$N, T_f, \chi$$

Geometrical and operation characteristics of the diesel engine:

$$B, L, r_c, l, V_d, A_{ch}, A_p, \bar{S}_p, d_o, P_{inj}, \theta_{soi}, \Delta\theta_{inj}, \omega, \Delta t_{CA}$$

Information of valves:

$$\theta_{ivc}, \theta_{evo}$$

Initial conditions in-cylinder gas:

$$p, T, m, \gamma_g, R_g, C_{p,g}$$

Heat transfer conditions:

$$T_{w,ch}, T_{w,p}, T_{w,cyl}$$

Fuel properties:

$$\rho_b, \mu_b, \sigma_b, Oh, LHV, h_f, (AF)_s, C_n, H_m, O_l, N_k, T_{inj}, C_{s,b}$$

Experimental data:

$$m_f, m_a, p, dp$$

Start

$$i = \theta_{ivc}$$

$$i = \theta_{ivc} : \theta_{evo}$$

i corresponds to the crank angle degree. For each i value, the corresponding p and dp experimental data are taken and following variables are calculated:

$$V, dV, A_{cyl}, h_c, Q$$

If $i < \theta_{soi}$ *Compression stroke*

Calculation of gas properties (chemical equilibrium).

Numerical solution of ODE system:

T, m for condition $i+1$

If $i \geq \theta_{soi}$ *Start of injection*

Calculation of gas properties (chemical equilibrium).

Numerical solution of ODE system:

$T, m, m_{f,b}, m_{f,o}, \phi$ for condition $i+1$

End

$i = \theta_{evo}$

Table G2. Routine of complete cycle simulation of diesel engine.

Initialization

Test conditions:

N, T_f, χ

Geometrical and operation characteristics of the diesel engine:

$B, L, r_c, l, V_d, A_{ch}, A_p, \bar{S}_p, d_o, p_{inj}, \theta_{soi}, \Delta\theta_{inj}, \omega, \Delta t_{CA}$

Conditions at intake and exhaust manifolds:

$p_i, T_i, p_e, T_e, h_a, R_a, \gamma_a, \rho_a$

Information of valves:

$D_{v,i}, D_{v,e}, \theta_{ivo}, \theta_{ivc}, \theta_{evo}, \theta_{evc}$

Initial conditions in-cylinder gas:

$p, T, m, \gamma_g, R_g, c_{p,g}$

Heat transfer conditions:

$T_{w,ch}, T_{w,p}, T_{w,cyl}$

Fuel properties:

$\rho_b, \mu_b, \sigma_b, Oh, LHV, h_f, (AF)_s, C_n, H_m, O_l, N_k, T_{inj}, c_{s,b}$

Mass fuel injected:

$m_f = f(V_{inj}, \rho_b)$

Start of simulation

Number of iterations, NIter

$j = 1:NIter$

Start of cycle

$i = 1$

$i = 1:719$

i corresponds to the crank angle degree. For each i value, the following variables are calculated:

$V, dV, A_{cyl}, \rho_g, \mu_g, h_c, Q, l_{v,i}, l_{v,e}, A_i, A_e$

If $i < \theta_{ivc}$ *Intake stroke*

Calculation:

\dot{m}_a, \dot{m}_e , gas properties

Numerical solution of ODE system:

p, T, m for condition $i+1$

If $i < \theta_{evo}$ and $i \geq \theta_{ivc}$

If $i < \theta_{soi}$ *Compression stroke*

Calculation of gas properties:

Numerical solution of ODE system:

p, T, m for condition $i+1$

If $i < \theta_{evo}$ and $i \geq \theta_{ivc}$

If $i \geq \theta_{soi}$ *Start of injection*

If $i = \theta_{soi}$

Calculation of spray parameters:

$S_p, u_{sp}, Re_{sp}, We_{sp}, SMD, We_g, Re_D, \alpha_{sp}$

Calculation of ignition delay and combustion parameters according to correlations proposed:

$\tau, X_p, X_d, X_r, \Delta\theta_p, \Delta\theta_d, \Delta\theta_r, a_p, a_d, m_p, m_d, m_r, \theta_{ig}$

If $i < \theta_{ig}$

No combustion process

If $i \geq \theta_{ig}$ *Start of combustion*

Combustion process based on Wiebe function

Calculation of gas properties (chemical equilibrium).

Numerical solution of ODE system:

$p, T, m, m_{f,b}, m_{f,o}, \phi$ for condition $i+1$

If $i \geq \theta_{evo}$ *Exhaust stroke*

Calculation:

\dot{m}_a, \dot{m}_e , gas properties (chemical equilibrium)

Numerical solution of ODE system:

$p, T, m, m_{f,b}, m_{f,o}, \phi$ for condition $i+1$

End of cycle

$i = 719$

If $j = 1$

$$p(1) = p(720)$$

$$T(1) = T(720)$$

$$m(1) = m(720)$$

Continues to iteration 2

If $j > 1$

Test of convergence:

Analysis of maximum variability of p , T and m between last two cycles.

If the convergence criterion is reached, the simulation stops, else, the simulation continues with the next iteration of the cycle until to reach the convergence or to complete the number of iterations.

End of simulation
